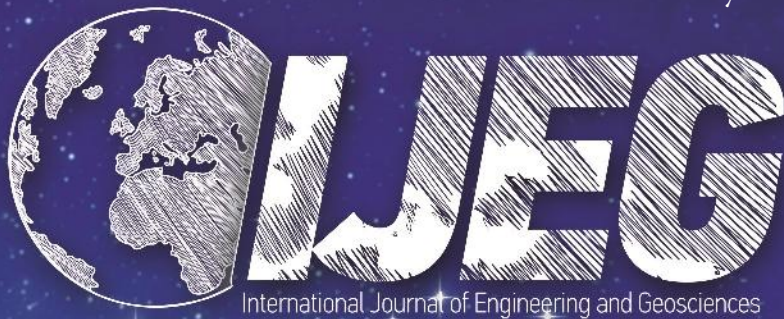


Volume 9 Issue 1 February 2024



IJEG

International Journal of Engineering and Geosciences



e-ISSN 2548-0960

EDITOR IN CHIEF

Prof. Dr. Murat YAKAR
Mersin University Engineering Faculty
Turkey

CO-EDITORS

Prof. Dr. Ekrem TUŞAT
Konya Technical University
Faculty of Engineering and Natural Sciences
Turkey

Prof. Dr. Songnian Li,
Ryerson University
Faculty of Engineering and Architectural Science,
Canada

Assoc. Prof. Dr. Ali ULVI
Mersin University Engineering Faculty
Turkey

ADVISORY BOARD

Prof. Dr. Orhan ALTAN
Honorary Member of ISPRS, ICSU EB Member
Turkey

Prof. Dr. Naser El SHAMY
The University of Calgary Department of Geomatics Engineering,
Canada

Prof. Dr. Armin GRUEN
ETH Zurich University
Switzerland

Prof. Dr. Ferruh YILDIZ
Selcuk University Engineering Faculty
Turkey

Prof. Dr. Artu ELLMANN
Tallinn University of Technology Faculty of Civil Engineering
Estonia

EDITORIAL BOARD

Prof. Dr. Alper YILMAZ
Environmental and Geodetic Engineering, The Ohio State University,
USA

Prof. Dr. Chryssy Potsiou
National Technical University of Athens-Rural and Surveying Engineering,
Greece

Prof. Dr. Cengiz ALYILMAZ
Ataturk University Kazim Karabekir Faculty of Education
Turkey

Prof. Dr. Dieter FRITSCH
University of Stuttgart Institute for Photogrammetry
Germany

Prof. Dr. Edward H. WAITHAKA
Jomo Kenyatta University of Agriculture & Technology
Kenya

Prof.Dr. Halil SEZEN
Environmental and Geodetic Engineering, The Ohio State University
USA

Prof.Dr. Huiming TANG
China University of Geoscience..., Faculty of Engineering,
China

Prof.Dr. Laramie Vance POTTS
New Jersey Institute of Technology, Department of Engineering Technology
USA

Prof.Dr. Lia MATCHAVARIANI
Iv. Javakishvili Tbilisi State University Faculty of Geography
Georgia

Prof.Dr. Məqsəd Hüseyn QOCAMANOV
Baku State University Faculty of Geography
Azerbaijan

Prof.Dr. Muzaffer KAHVECI
Selcuk University Faculty of Engineering
Turkey

Prof.Dr. Nikolai PATYKA
National University of Life and Environmental Sciences of Ukraine
Ukraine

Prof.Dr. Petros PATIAS
The Aristotle University of Thessaloniki, Faculty of Rural & Surveying Engineering
Greece

Prof.Dr. Pierre GRUSSENMEYER
National Institute of Applied Science, Department of Civil Engineering and Surveying
France

Prof.Dr. Rey-Jer You
National Cheng Kung University, Tainan · Department of Geomatics
China

Prof.Dr. Xiaoli DING
The Hong Kong Polytechnic University, Faculty of Construction and Environment
Hong Kong

Assoc.Prof.Dr. Elena SUKHACHEVA
Saint Petersburg State University Institute of Earth Sciences
Russia

Assoc.Prof.Dr. Semra ALYILMAZ
Ataturk University Kazim Karabekir Faculty of Education
Turkey

Assoc.Prof.Dr. Fariz MIKAILSOY
Igdir University Faculty of Agriculture
Turkey

Assoc.Prof.Dr. Lena HALOUNOVA
Czech Technical University Faculty of Civil Engineering
Czech Republic

Assoc.Prof.Dr. Medzida MULIC
University of Sarajevo Faculty of Civil Engineering
Bosnia and Herzegovina

Assoc.Prof.Dr. Michael Ajide OYINLOYE
Federal University of Technology, Akure (FUTA)
Nigeria

Assoc.Prof.Dr. Mohd Zulkifli bin MOHD YUNUS
Universiti Teknologi Malaysia, Faculty of Civil Engineering
Malaysia

Assoc.Prof.Dr. Syed Amer MAHMOOD
University of the Punjab, Department of Space Science
Pakistan

Assist. Prof. Dr. Yelda TURKAN
Oregon State University,
USA

Dr. G. Sanka N. PERERA
Sabaragamuwa University Faculty of Geomatics
Sri Lanka

Dr. Hsiu-Wen CHANG
National Cheng Kung University, Department of Geomatics
Taiwan

The International Journal of Engineering and Geosciences (IJEG)

The International Journal of Engineering and Geosciences (IJEG) is a tri-annually published journal. The journal includes a wide scope of information on scientific and technical advances in the geomatics sciences. The International Journal of Engineering and Geosciences aims to publish pure and applied research in geomatics engineering and technologies. IJEG is a double peer-reviewed (blind) OPEN ACCESS JOURNAL that publishes professional level research articles and subject reviews exclusively in English. It allows authors to submit articles online and track his or her progress via its web interface. All manuscripts will undergo a refereeing process; acceptance for publication is based on at least two positive reviews. The journal publishes research and review papers, professional communication, and technical notes. IJEG does not charge for any article submissions or for processing.

CONTENTS

Volume 9 - Issue 1

RESEARCH ARTICLES

Study of the seismic activity of the Almalyk-Angren industrial zone based on lineament analysis	
Lola Sichugova, Dilbarkhon Fazilova	1-11
Semantic segmentation of very-high spatial resolution satellite images: A comparative analysis of 3D-CNN and traditional machine learning algorithms for automatic vineyard detection	
Özlem Akar, Ekrem Saralioğlu, Oğuz Güngör, Halim Ferit Bayata	12-24
Optimization of expropriation costs on the highway projects in Türkiye	
Kemal Çelik	25-33
Python-based evaluation of road network constraints for electric scooters and bicycles: Izmit Example	
Ahmet Şirin, Arzu Erener	34-48
UAV-mounted thermal camera and its analysis on urban surface textures	
Efdal Kaya, Arzu Erener	49-60
The Multi-Disaster risk assessment: A-GIS based approach for Izmir City	
Nur Sinem Partigöç, Ceyhun Dinçer	61-76
Development of a virtual reality application for the Old Harran School	
Fred Ernst, Songül Akdağ, Nizar Polat, Mehmet Önal, Abdullah Ekinci	77-85
Using GIS-supported MCDA method for appropriate site selection of parking lots: The case study of the city of Tetovo, North Macedonia	
Edmond Jonuzi, Tansu Alkan, Süleyman Savaş Durduran, Hüseyin Zahit Selvi	86-98
Production of fuel-based carbon footprint distribution map using spatial interpolation methods based on GIS	
Ebru Çolak, Tuğba Memişoğlu Baykal, Nihal Genç	99-114
GIS based spatial decision-making approach for solar energy site selection, Ardabil, Iran	
Meysam Hasanzadeh, Khalil Valizadeh Kamran, Bakhtiar Feizizadeh, Sanam Hassanzadeh Mollabashi	115-130



Study of the seismic activity of the Almalyk-Angren industrial zone based on lineament analysis

Lola Sichugova ^{*1}, Dilbarkhon Fazilova ^{1,2,3}

¹ Astronomical Institute of Uzbek Academy of Sciences, Uzbekistan, slola988@gmail.com

² National University of Uzbekistan named after Mirzo Ulugbek, Geodesy and Geoinformatics Department, Uzbekistan, dil_faz@yahoo.com

³ Tashkent State Technical University named after Islam Karimov, Mine Surveying and Geodesy Department, Uzbekistan

Cite this study:

Sichugova, L., & Faziova, D. (2024). Study of the seismic activity of the Almalyk-Angren industrial zone based on lineament analysis. *International Journal of Engineering and Geosciences*, 9 (1), 1-11

<https://doi.org/10.26833/ijeg.1192118>

Keywords

Lineaments
Earthquake
Density
Rose-diagram
Landsat 8

Research Article

Received:20.10.2022

Revised: 10.04.2023

Accepted:23.05.2023

Published:02.01.2024



Abstract

In this work, an automated lineament analysis was carried out to search for earthquake precursors for the territory of the Almalyk-Angren industrial zone in Uzbekistan. The seven events with a magnitude of about 3 were selected for analysis. The Landsat 8 satellite images were processed using the automated lineament detection method in the LEFA software. The processing steps included detecting line elements in raster images, calculating the characteristics of the spatial distribution of line elements, and combining collinear linear elements into lineaments. The analyses of the cyclicity of precursors before and after earthquakes were based on the study of the distribution of the lineament trend in the study area using rose diagrams and lineament density maps. The results showed a change in the dynamics of the lineament structure. The statistics of the number of lineaments showed that their increase begins almost 20 days before the event, reaches its maximum about 1 – 2 days before the earthquake, decreases starting from 14 days after the earthquake, and has a minimum value of 1 – 2 months. The main trends observed in the lineament map showed the dominant trend in NS, WE, NW-SE directions.

1. Introduction

Studying seismic activity in industrial areas is of great importance for understanding the impact of industrial activities on the environment and the possibility of predicting earthquakes in such zones. The understanding and prediction of earthquakes require diverse monitoring methods and data analysis. Specialists are developing and researching lineament systems in addition to alternative methods like satellite interferometry, GPS observations, heat flow tracking, and monitoring the environment, such as the ionosphere and ice cover of water bodies [1-3]. Lineament analysis identifies geological faults and cracks that may indicate seismic activity and potential earthquake sources, offering a means of earthquake prediction. Additionally, lineament analysis provides insights into other geological phenomena, such as geothermal and

hydrothermal systems, which may also be associated with seismic activity [4-5]. Therefore, lineament analysis remains the main for understanding earthquakes and other geological phenomena [6-9].

Scientific studies have shown that there are observable anomalies associated with earthquakes that precede seismic activity. One such anomaly is an increased degree of lineament manifestation confirmed by several studies from various authors. This increase is attributed to the widening and elongation of linear tectonic structures, which merge into larger ones and result in a significantly larger number of lineaments being identified on satellite images than in normal conditions. However, the widespread use of this technique is hindered by technical limitations, such as the need for regular acquisition of images taken under identical conditions (including humidity, lighting, and vegetation cover) [10-13]. The data analysis has shown

that there were more earthquakes registered in areas with the highest number of linear structures. The epicenters of earthquakes are not random, but rather associated with lineaments and their connecting segments. According to the modern understanding of seismic processes, high tectonic stresses that cause earthquakes usually concentrate at the intersections or bends of linear boundaries separating blocks of the Earth's crust [14-15]. Research on stress pattern changes around earthquake epicenters has shown significant changes in the lineaments and observable anomalies before impending earthquakes. In the absence of seismic activity, normal behavior is observed. The most important result of these studies is the high level of correlation between the ongoing maximum horizontal compressive stress that there is obtained from the lineament and the earthquake's focal mechanism. It was observed that a considerable number of lineaments emerged approximately a month or two before the earthquake and returned to their original configuration about a month after the event [10, 12, 16-18]. Busygin and Nikulin [19] reports that earthquake epicenters tend to be located closer to areas with more complex geological structures and specific azimuths of lineaments ($22.5\pm 12.5^\circ$, $67.5\pm 12.5^\circ$, $112.5\pm 12.5^\circ$, and $157.5\pm 12.5^\circ$), which are not typical for the entire Earth's surface. The study found that almost 90% of earthquake epicenters are located within areas with high complexity values, based on the spatial relationship between earthquake epicenters and lineament networks identified from satellite imagery. The traditional method of identifying and mapping lineaments involved manual visual interpretation of satellite or aerial imagery. However, the increasing availability of high-resolution satellite imagery and the need for large-scale mapping has led to the development and implementation of automated methods for lineament analysis. The automated analysis enables the processing of large amounts of data quickly and accurately, making it a valuable tool for studying geological structures and tectonic features in various regions [7, 20-22]. Nonetheless, automated lineament analysis also has limitations, as it may not detect all visible lineaments and can produce false positives or negatives. Therefore, it is crucial to validate the results of automated lineament analysis with other data sources, such as geological maps.

This study aims to use an automated method for extracting lineaments from satellite images to investigate seismic activity in the Almalyk-Angren industrial zone of Uzbekistan. The scientific problem that we should be able to solve is to understand the patterns and characteristics of seismic activity in the region that there is caused by its complex tectonic structure. By using the automated lineament extraction method and comparing the results with geological maps, we hope to efficiently and accurately identify linear features that there is related to tectonic activity in a large dataset. It will contribute to a better understanding of the geological and tectonic features of the region. Specifically, we will examine the relationship between lineament density, orientation, and seismic activity in the region and assess the potential of automated lineament analysis as one of the tools for earthquake hazard assessment. Hypotheses can be

formulated regarding the correlation between certain lineaments detected through automated analysis and tectonic lines where stress accumulation in the crust can lead to earthquakes. Additionally, certain lineaments can be associated with specific geological structures that could increase the likelihood of earthquakes in the region. These hypotheses will be tested by analyzing earthquake data and geological structures and comparing them to the distribution of lineaments. It will allow us a better understanding of the underlying geology and tectonic processes that contribute to earthquake activity in the area. In summary, this study seeks to investigate the dynamics of lineaments in the region, examine the localization of earthquake epicenters based on fault locations, compare the results with geological data, and identify zones of anthropogenic impact. The use of automated lineament analysis has the potential to enhance our understanding of seismic activity and its potential hazards in the region.

2. Method

2.1. Study Area

The Angren-Almalyk region is located in the northeast of Uzbekistan and is one of the richest mineral regions in the country. There are the Angren coal mine up to 300 m deep, the Djigiristan quarry, and the Naugarzan and Apartak coal pits. The Almalyk Mining and Metallurgical Complex (AMMC) is the base production of non-ferrous metals in Uzbekistan (Figure 1). The region is located within the Chatkal-Kuramin block, and there are parts of the Tien Shan geological region. One of the most fundamental geological structures in this region is a magmatic formation that covers around 85% of the region with an age range from Proterozoic to Mesozoic. The formation of structures within the Kuramin part Beltau-Kuramin zone occurred during the Caledonian, Hercynian and Alpine tectonic cycles. The modern relief of the Angren Zone was formed in the Neogene. The North and the South of the Angren zone are characterized by tectonic disturbances superimposed by the Chatkal and the Kuramin horst. The tectonics of the region is represented by a complex combination of various structural elements, including folds, troughs, faults, intrusions, and volcanic rocks (Figure 2). The primary deposit in the region is the Almalyk ore belt, which stretches for over 40 km and is rich in copper, gold, silver, and other minerals. Minerals were found in carbonated rocks, and volcanic deposits were formed due to volcanic activity and magmatic processes during the Mesozoic era [23].

The region is located within the Chatkal-Kuramin block, there is a crystalline rock mass, and it was formed due to ancient geological processes that occurred over 2 billion years ago. The block contains a variety of granite, gneisses, shale and quartzite rocks, that have undergone a strong tectonic deformation, leading to the formation of various structural elements, including folds, faults, and fractures. The most intense tectonic processes in this area occurred during the Mesozoic and Cenozoic eras when subduction and collision of lithospheric plates led to the formation of mountain folds, including the Pamir

and Tien Shan ranges. As a result of this formation, various mountainous rocks were formed in the Angren

and Almalyk regions, including granite, gneisses, shale and sandstone.

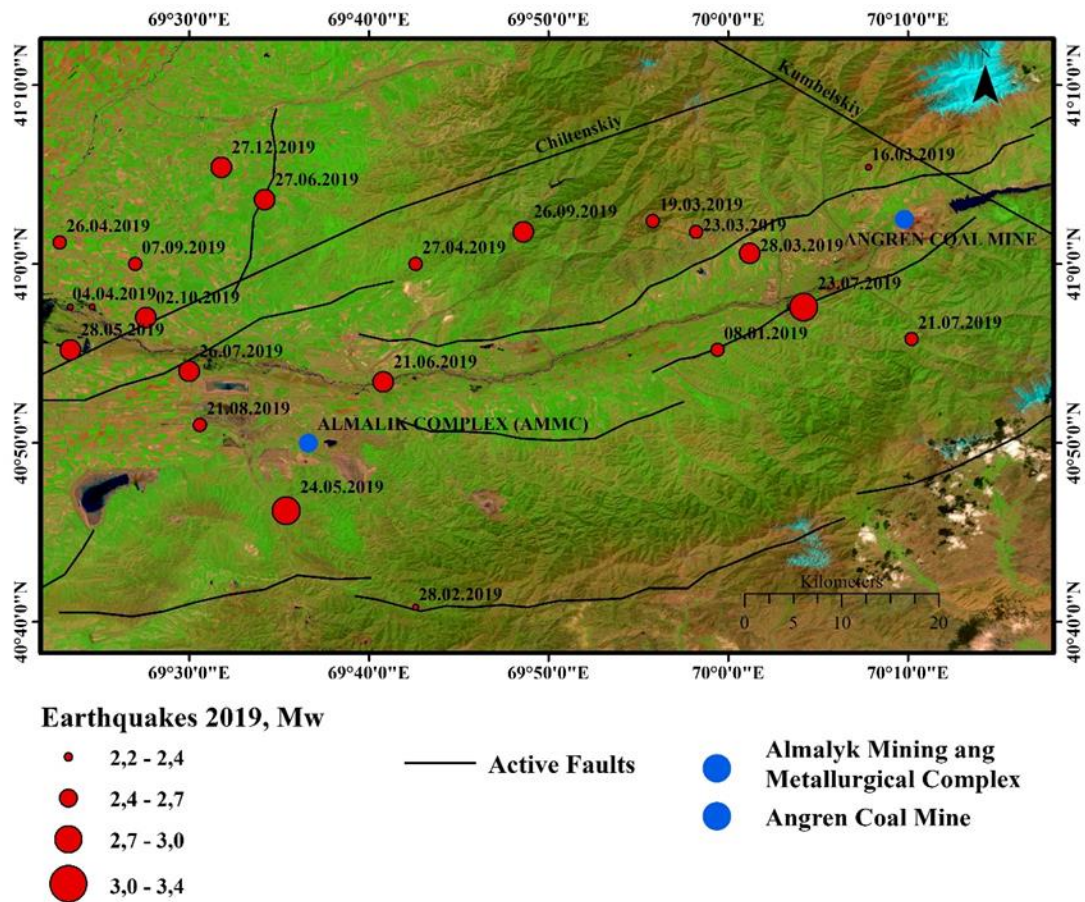


Figure 1. Study area, tectonic faults, and location of the earthquake’s epicentres [24] (Landsat 8) [25].

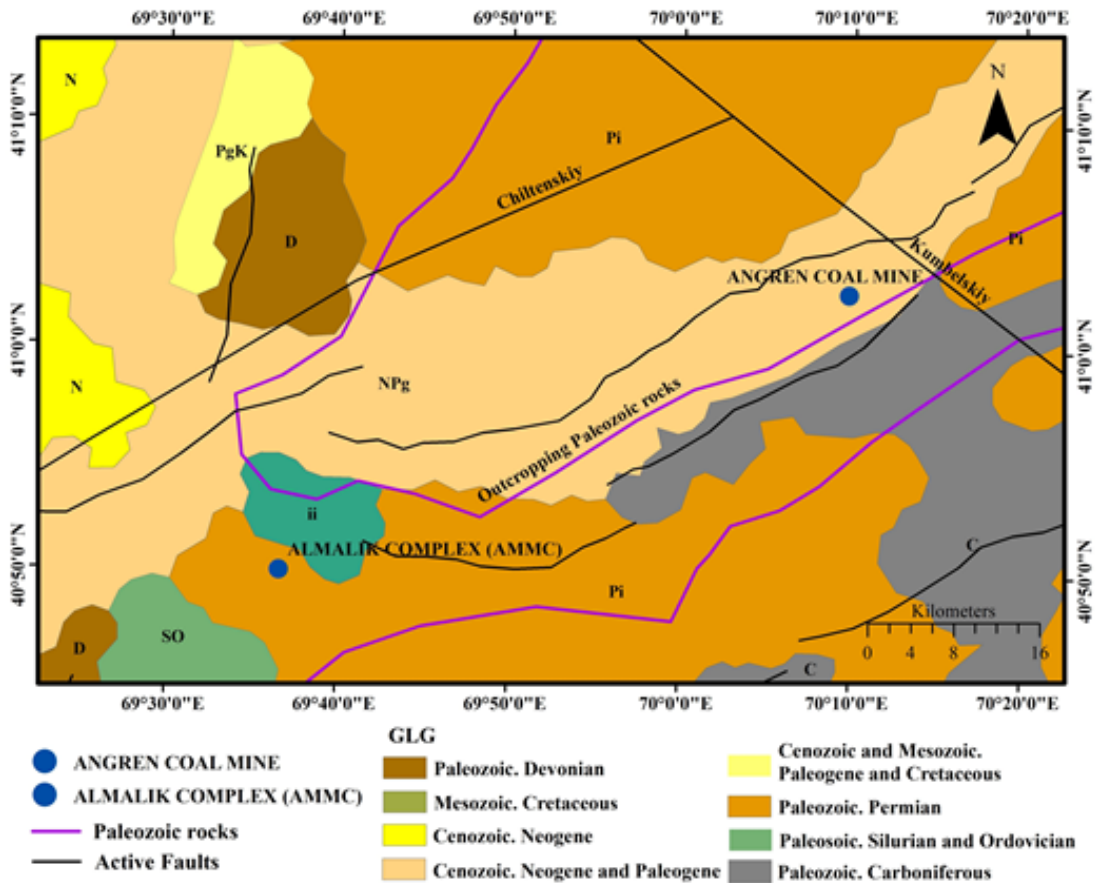


Figure 2. Geology map of the study area [26].

Currently, tectonic processes continue in this area. There are several main faults around the Angren-Almalyk region, which determine the tectonic structure of this region. One of the longest faults is the Chiltensky fault, which runs west of the Angren massif. It is an active fault and can cause earthquakes. Another significant fault is the Almalyk fault, which passes through the Almalyk massif to the north of the city of Almalyk. This fault is also active and can cause strong earthquakes. According to the study of stress distribution and zoning of the western Tien Shan and the adjacent territory based on the excess shear stress calculated by mathematical modelling, compared with data from instrumental measurements in deep wells, this region is identified as an area with the highest values of excess shear stress (>2 MPa) [27].

The Kumbel fault, which runs along the southern edge of the Angren-Almalyk zone, is less active but can still cause earthquakes. The Kumbel fault is a complex thrust fault with north-eastern dipping fault plane angles of 60° - 90° , and the south-western block is uplifted. In recent times, there have strike-slip movements with an amplitude of up to 5 km along this fault [28-30]. The main faults are accompanied by numerous small supporting and accompanying fractures. Due to intensive mining operations and special geological and tectonic conditions, the Almalyk-Angren industrial zone is the region with a high level of seismic activity. The mining industry, which can cause dangerous tremors in the region, is a problem for nearby urban areas. Seismic hazard assessment in mining areas is important for the nearby urban region since local events are located

directly underground and show a high frequency of repeatability.

2.2. Method

The processing of images in the lineament extraction system using various algorithms (Hough transform, Canny, PCI, LESSA, TecLines) allows for obtaining information on the dynamics of the Earth's crust even at depths of tens of kilometers below the surface. Images with lower resolution are required to detect deeper events that spread over large areas. Images with a resolution of 10-30 m are useful for studying earthquakes, as they can integrate information about the presence of faults at depths of tens of kilometers. Although such images cannot detect individual cracks, they can track changes related to the accumulation or weakening of strength caused by the movement of tectonic plates [10]. In our research, we used Landsat 8 OLI images with 30 m resolution of the pre-and post-earthquake that were downloaded from the United States Geological Survey (USGS) Earth Explorer website [31]. Archive images included from May 06, June 23, July 09 and 25, August 10, September 11 and 27, 2019. The catalog of the earthquakes in the region of the Republican Center for Seismic Predictive Monitoring of the Ministry of Emergency Situations of the Republic of Uzbekistan was used for analysis [24]. Data became available in 2018. During 2019, 29 earthquakes ($2.2 < M_w < 4.2$) occurred in Almalyk-Angren industrial zone. In Table 1 are the dates that were selected for analysis ($2.5 < M_w < 3.2$) (Table 1).

Table 1. Catalog of earthquakes in 2019 on the territory of the Almalyk-Angren industrial zone.

Nº	Date	Depth (km)	Magnitude (Mb)	Epicenter region
1	21.06.2019	5	3	Center Uzbekistan
2	27.06.2019	14	3	Center Uzbekistan
3	21.07.2019	5	2,5	Eastern Uzbekistan
4	23.07.2019	15	3,2	Center Uzbekistan
5	26.07.2019	7	2,9	Center Uzbekistan
6	07.09.2019	5	2,6	Center Uzbekistan
7	26.09.2019	30	2,9	Center Uzbekistan

The method of image processing consisted of several stages: selection of suitable satellite images (free of cloud and with the earthquakes), image preprocessing (spatial resolution improvement, brightening satellite image, contour and texture enhancement, resampling), lineament extraction, calculation of the density of lines, estimation their directions. In this analysis, we used the synthesized images of the Landsat 8, which consists of 7 channels (Coastal aerosol, Blue, Green, Red, NIR, SWIR1,2) with a 30 m pixel size [32]. The synthesized image can be useful for studying the Earth's surface. The synthesized images were merged with a higher quality panchromatic channel with a 15 m pixel size using the Create Pan-sharpened tool in ArcGIS ver. 10.8.

To investigate surface variations on Earth, the Lineament Extraction and Fracture Analysis (LEFA) algorithm was selected for this research. It is based on factor analysis and designed for the automatic extraction of the linear features on images, such as a fault or fold boundaries, which are associated with geological

structures. The LEFA algorithm produces more accurate and high-quality results than traditional methods such as Hough processing or Gabor filtering. Additionally, it can automatically adapt to different types of images, including multi-channel and multi-spectral images. The LEFA algorithm uses mathematical morphology and image processing methods to extract linear features from the image. It is based on the observation that linear features on the image usually appear as bright lines on a dark background or vice versa. The algorithm first applies image filtering to reduce noise and improve contrast. Then, it uses the morphological gradient operator to extract edges on the image. LEFA subsequently identifies potential linear features using the skeletonization algorithm. The image skeleton is the thinnest structure representing the central line connecting all object pixels in the image. Finally, the LEFA algorithm conducts feature analysis to identify linear elements. It analyzes the geometric properties of potential linear elements, such as their length,

orientation, and shape, as well as the properties of neighboring pixels to determine whether they are actual linear features or not [22]. The Canny edge detection algorithm with a Gaussian noise filter was selected to study a linear network [21]. To identify and detect the edges of the images needs to reduce the noise of the images, and then the images become smooth. The Canny edge detector uses two filtering thresholds: if the value of the pixel is higher than the upper edge, then it will be in maximum value (the edge is considered reliable), and if the value of the pixel is lower, the pixel is suppressed. Points with a value falling between the thresholds take a fixed average value [33].

The next step of lineament extraction was applying Hough Transform. The most common case is Hough Line Transform. Based on the theory, Hough Transform is any point of a binary image that can be part of some set of possible lines. The Hough Transform is based on the notion that the desired object is in the form of a parametric equation. The parameters of that equation represent the Hough phase space. Then, a binary image is taken (for example, the result of the Canny edge detector). All the points of the edge are sorted through, and a hypothesis is made that point belongs to a line of the desired object. The final step is to traverse the Hough space and selects the maximum values for which the most pixels of the image "voted", which gives us the parameters for the equations of the desired object [34].

3. Results

As we noted earlier, the study area belongs to a seismic zone, but most of the events here have a medium magnitude [Ребецкий]. Therefore, only seven events with a magnitude of about 3, that can be felt, were selected for the study, as indicated in Table 1. In the first stage, the dynamics of the lineaments during these events were investigated based on a statistical analysis of changes in their density. As can be seen from Figure 3, there is a clear trend of an increase in the number of lineaments in the interval before and after 1-3 days from the moment of the earthquake (June 23, July 25,

September 11, and September 27). Moreover, the total number of lineaments sharply decreases 20 days before and approximately 14 days after the earthquake (May 6, July 9, and August 10). It is worth noting that the minimum and maximum length of the lineaments is practically the same for all the events. However, the maximum length of the lineaments of 6 km is observed only on May 6, 2019 (Table 2).

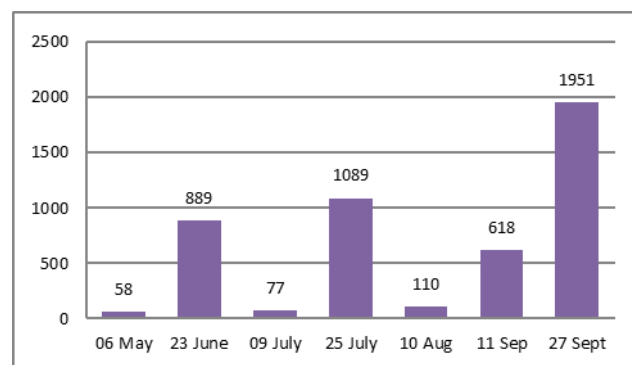


Figure 3. The total number of lineaments.

One of the main statistical indicators used to predict changes in lineaments was rose diagrams and density maps, as shown in Figure 4-10 (right column). The dominant directions obtained were NW, WE, and NW-SE. It was found, that with an increase in the number of lineaments, the length of the north direction also increased. Density maps (Figure 4-10, left column) showed a high density of lineaments near the epicentre of earthquakes that occurred on June 23, 2019, and June 27, 2019. The density of lineaments decreased on May 9, July 9, and August, as indicated by the results with the lowest density observed on July 9, 2019, which was 0.33. A high density of lineaments near the epicentre of the earthquake that occurred on July 26, 2019, was observed on July 25, 2019, with lineaments reaching their maximum one day before the event. The maximum number of lineaments was observed on September 27, 2019, with a density of 1.11.

Table 2. Statistics of lineaments length.

Value	06 May	23 June	09 July	25 July	10 Aug	11 Sep	27 Sept
Minimum, km	1,5	0,75	1,2	0,75	1,35	0,9	0,6
Maximum, km	6,0	2,7	3,0	2,6	3,0	3,7	2,9
Standard Deviation, km	0,7	0,2	0,3	0,2	0,3	0,3	0,2

4. Discussion

The results of the statistical analysis of lineament density during earthquakes are an important contribution to understanding the tectonic processes taking place in the studied region. Changes in the dynamics of lineaments can indicate the influence of complex tectonics on geological processes. A comparison of the geological map and the map of lineament densities shows that the highest density and, therefore, the most stressed and deformed state, even during periods between earthquakes, is observed in the zones around the Chiltin and southern Almalyk faults, particularly in the northwestern part of the territory. At the same time,

the zone around the Kumbel fault can be considered relatively "quiet." These results may indicate the possibility of predicting earthquakes in the future. However, it is worth noting that the results only apply to earthquakes with a magnitude of about 3 and are concentrated in zones near Paleozoic rocks that outcrop on the surface. This can indicate the influence of human activities on the stressed state of the earth's surface in areas of mineral extraction or excavation. Further research can expand this work, including the analysis of earthquakes of higher magnitude and for other geological regions, as well as studying the influence of human activity on tectonic processes. It's also clear from the analysis that there is a tendency for earthquake

epicentres can be located along faults. Regarding the earthquake on September 26th, it is worth noting that it was the deepest of all the events considered, with a depth of about 30 km (Table 1). Despite this, the study shows that it had a significant impact on the lineament dynamics in the region, which indicates that earthquakes with greater depth can influence the geological processes in the region. The results obtained from the analysis of

lineament density during this event were particularly clear and accurate, providing valuable insight into the tectonic processes taking place in the region. The lineaments observed during this event showed a clear correlation with the active faults in the region, highlighting the importance of such studies for understanding the geological and tectonic processes in seismic zones.

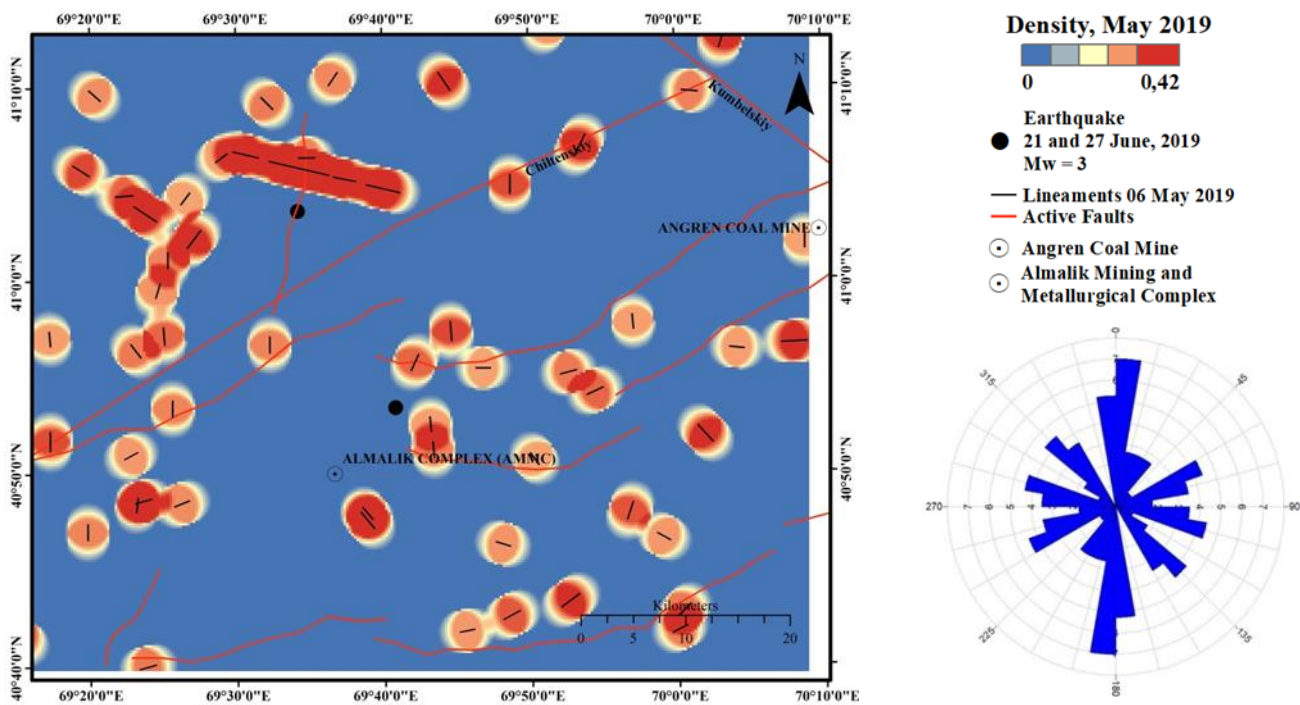


Figure 4. Density map and rose diagrams of lineaments (May 06, 2019).

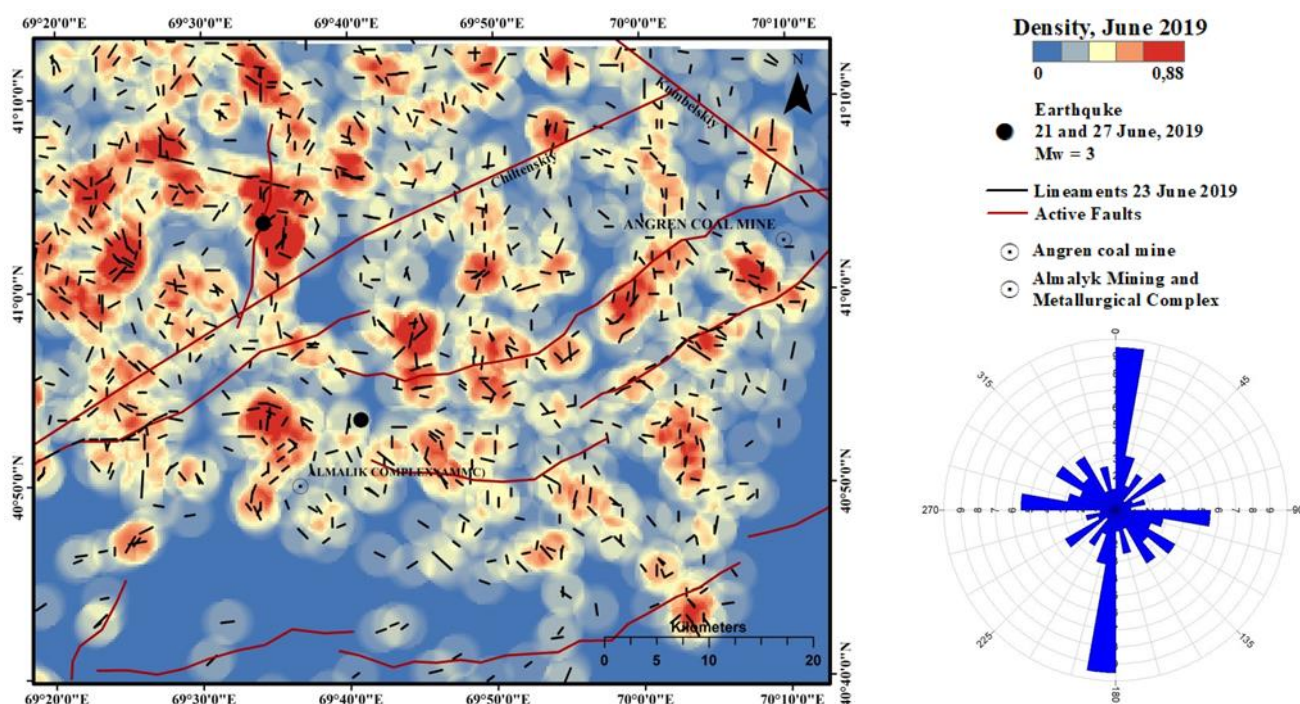


Figure 5. Density map and rose diagrams of lineaments (June 23, 2019).

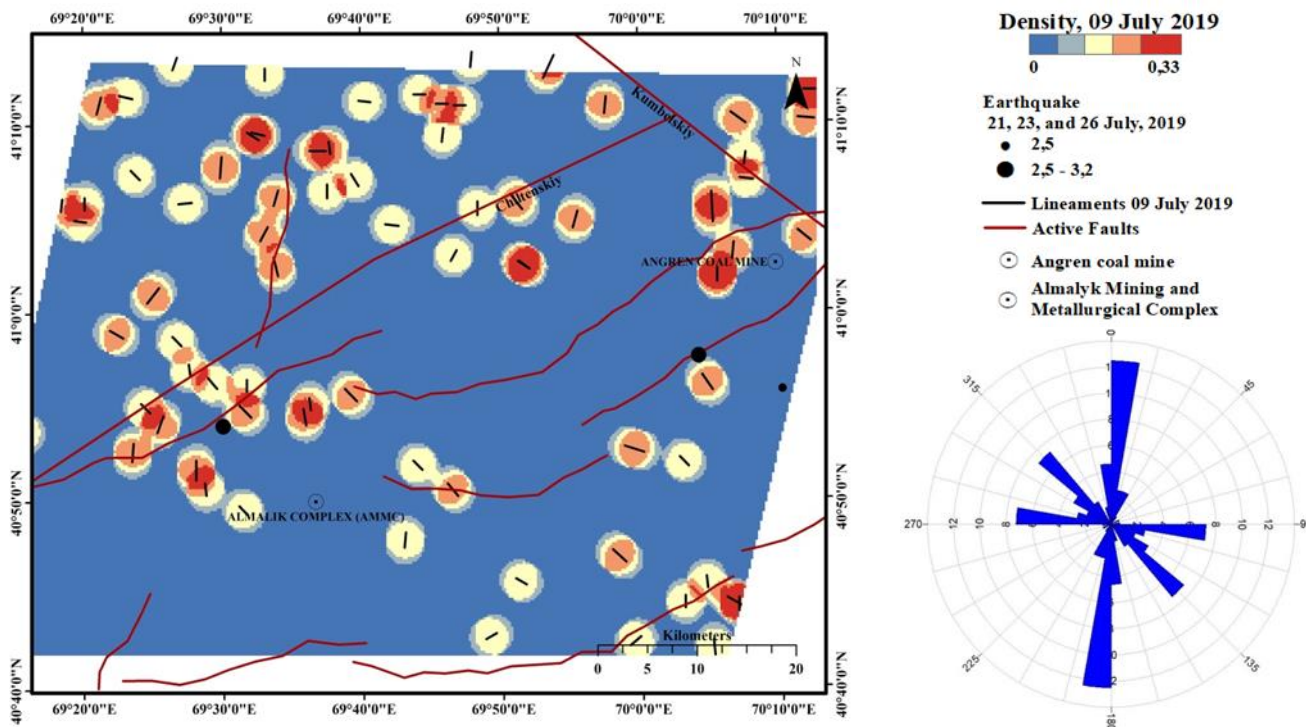


Figure 6. Density map and rose diagrams of lineaments (July 09, 2019).

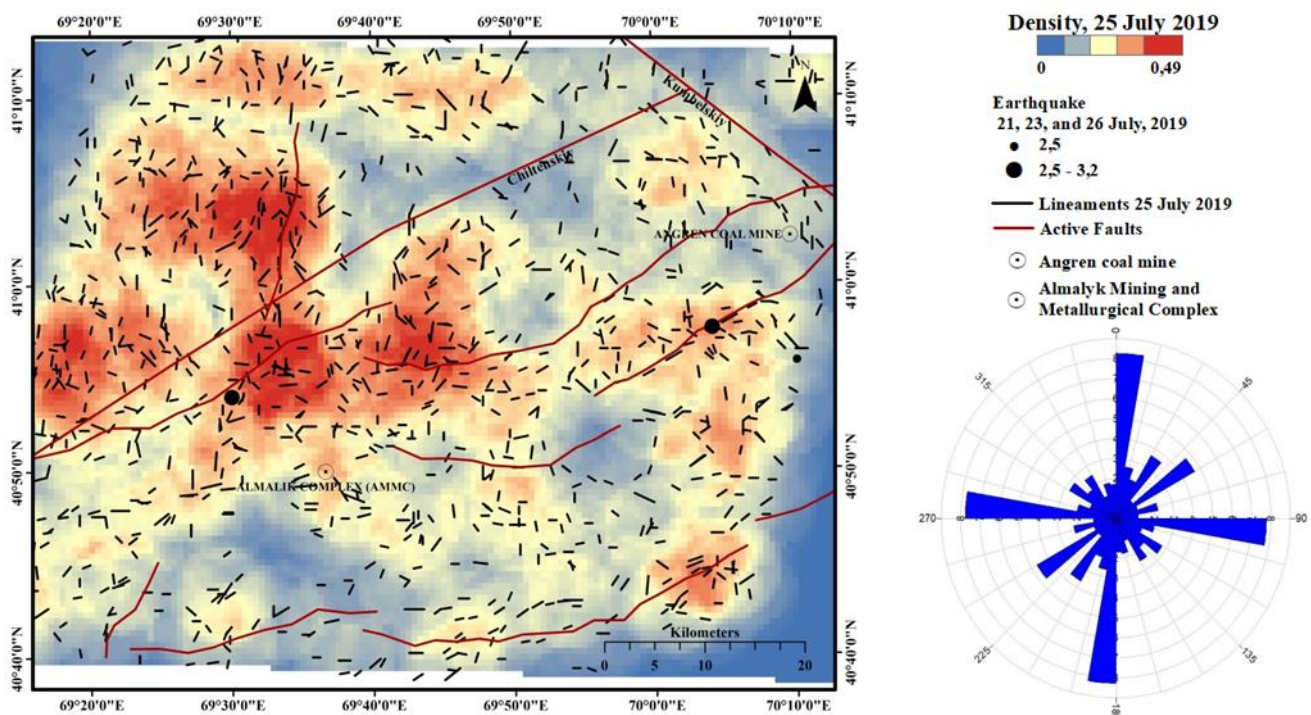


Figure 7. Density map and rose diagrams of lineaments (July 25, 2019).

5. Conclusion

In this work, an automated lineament analysis was carried out to search for earthquake precursors for the territory of the Almalyk-Angren industrial zone. The study area is tectonically and seismically active, but earthquakes typically occur with earthquakes of moderate magnitude. Automatic lineament analysis based on remote sensing data showed high efficiency. The seven events with a magnitude of about 3 were selected for analysis. The statistical analysis was

performed to investigate changes in lineament density before and after the events. The results showed a clear trend of an increase in the number of lineaments in the interval before and after the earthquake, with a sharp decrease in the total number of lineaments 20 days before and approximately 14 days after the earthquake. The rose diagrams and density maps showed dominant directions of NS, WE, and NW-SE, with a high density of lineaments near the epicenter of the earthquakes that occurred on June 23, 2019, June 27, 2019, and September 26, 2019. The results of the statistical analysis of

lineament density during earthquakes provide important insights into the tectonic processes taking place in the studied region and may indicate the possibility of predicting earthquakes in the future. However, the results only apply to earthquakes with a magnitude of about 3 and are concentrated in zones near Paleozoic rocks that outcrop on the surface, indicating the influence of human activities on the stressed state of the

earth's surface in areas of mineral extraction or excavation. Further research can expand this work by including the analysis of earthquakes of higher magnitude and in other geological regions, as well as studying the influence of human activity on tectonic processes. It is also clear from the analysis that there is a tendency for earthquake epicenters to be located along faults.

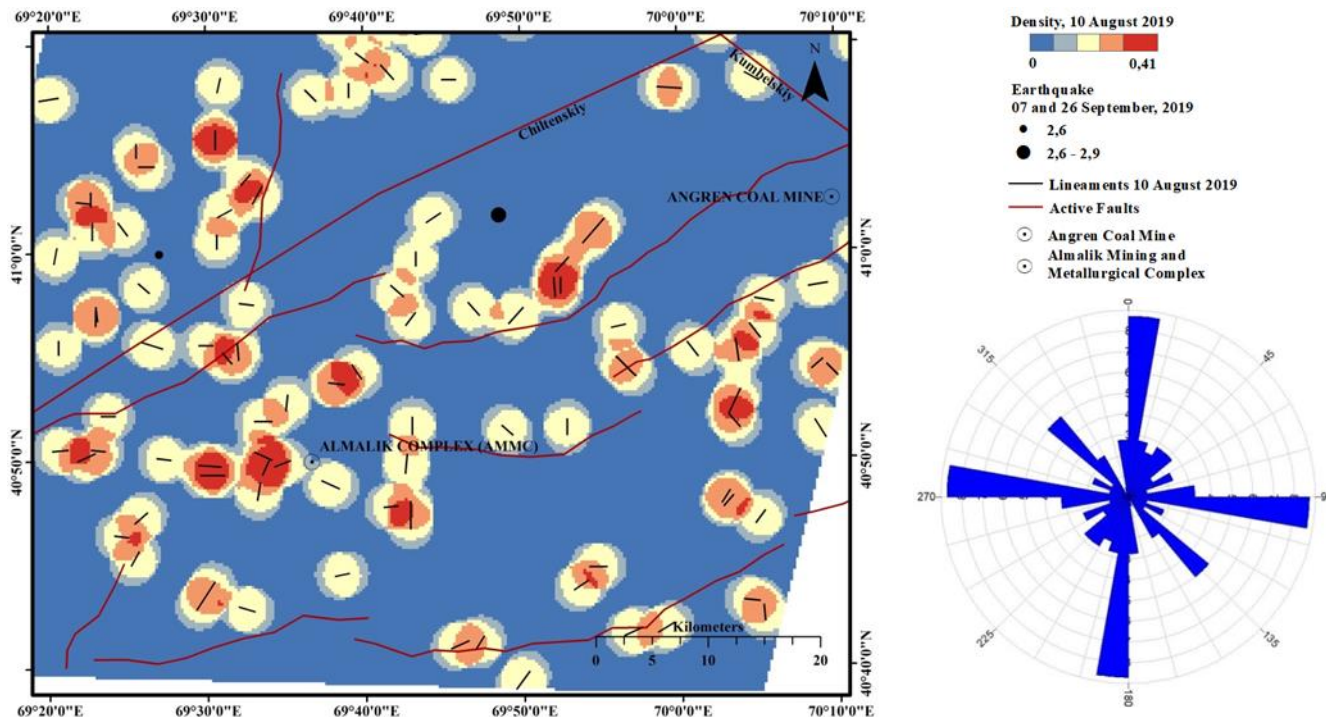


Figure 8. Density map and rose diagrams of lineaments (August 10, 2019).

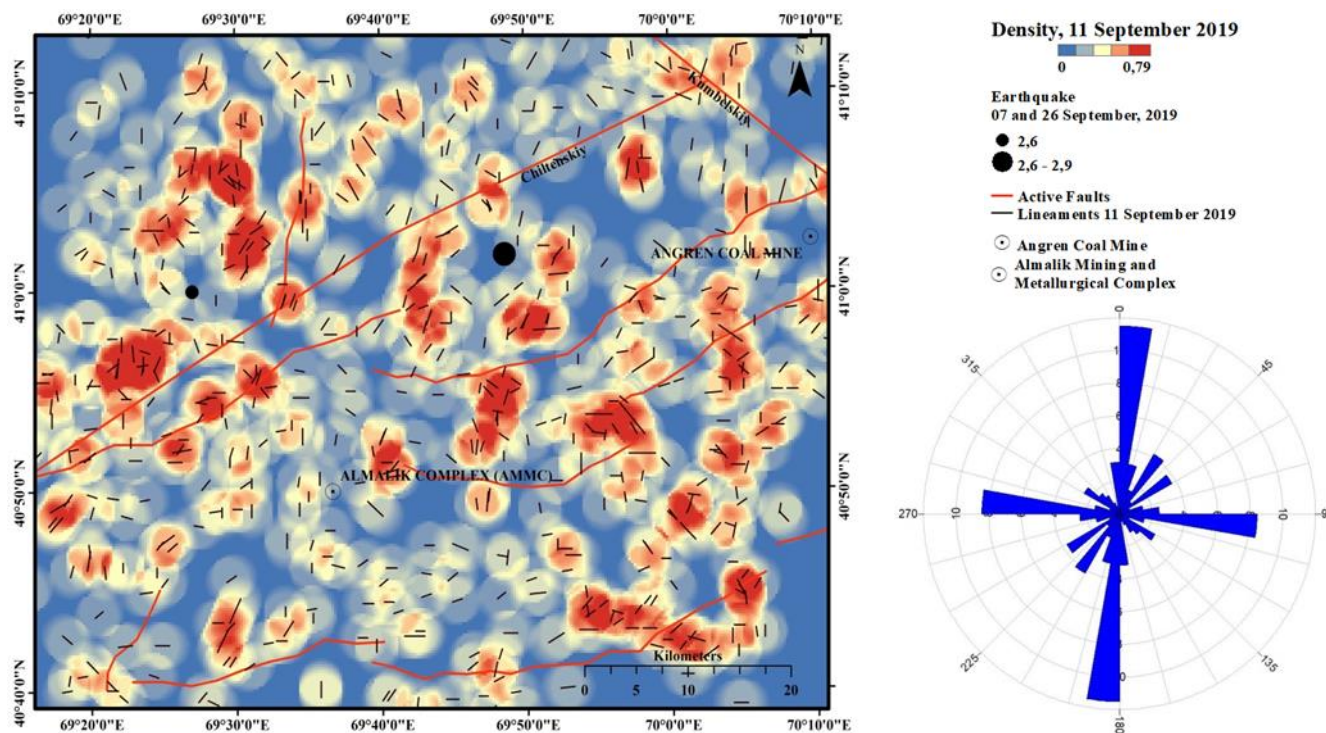


Figure 9. Density map and rose diagrams of lineaments (September 11, 2019).

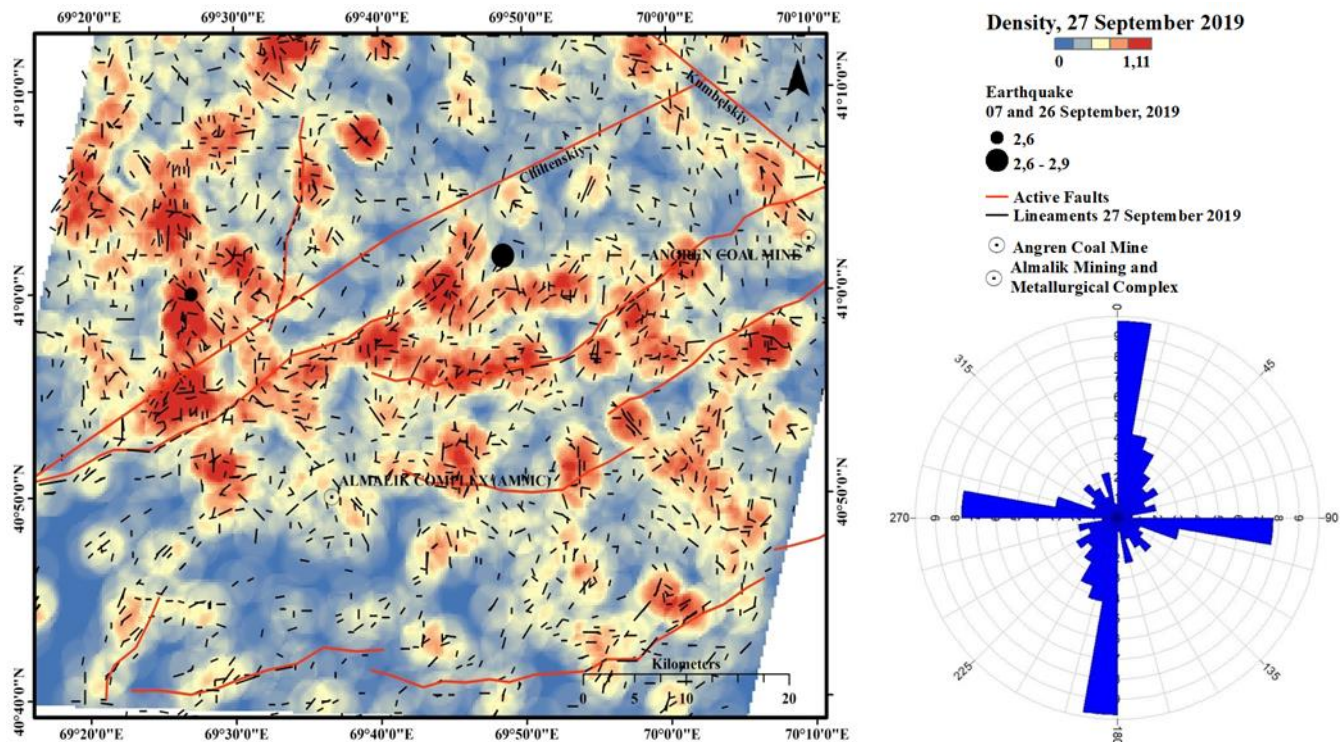


Figure 10. Density map and rose diagrams of lineaments (September 27, 2019).

Automatic lineament analysis based on remote sensing data can be one of the most effective methods with operativeness and effectiveness for geodynamic monitoring of seismically hazardous areas and also industrial zone. The results obtained have shown the possibility of the practical application of such an analysis, especially for the analysis of fracture tectonics, which are zones of high seismic activity and deformations of the earth's surface. The proposed method for studying the dynamics of lineament systems from satellite images, together with other methods, can be used for the operational monitoring of seismic hazards. It should be noted that the automatic method still needs to be improved by mathematical methods and algorithms to make it possible to apply it to territories with different geological conditions.

Acknowledgement

This work was carried out within the scientific project of the Astronomical Institute of Uzbekistan with the financial support of the Academy of Sciences of the Republic of Uzbekistan.

Author contributions

Lola Sichugova: Methodology, Validation, Investigation, Software, Writing-Original draft, Writing – Review and Editing. **Dilbarkhon Fazilova:** Conceptualization, Supervision, Writing-Original draft, Writing – Review and Editing, Project administration, Funding acquisition.

Conflicts of interest

The authors declare no conflicts of interest.

References

- Kalita, S., & Chetia, B. (2020). A novel approach for ionospheric total electron content earthquake precursor and epicenter detection for low-latitude. *International Journal of Engineering and Geosciences*, 5(2), 94-99. <https://doi.org/10.26833/ijeg.614856>
- Konak, H., Nehbit, P. K., Karaöz, A., & Cerit, F. (2020). Interpreting deformation results of geodetic network points using the strain models based on different estimation methods. *International Journal of Engineering and Geosciences*, 5(1), 49-59. <https://doi.org/10.26833/ijeg.581584>
- Nehbit, P. K., & Konak, H. (2020). The global and local robustness analysis in geodetic networks. *International Journal of Engineering and Geosciences*, 5(1), 42-48. <https://doi.org/10.26833/ijeg.581568>
- Al-Nahmi, F., Alami, O. B., Baidder, L., Khanbari, K., Rhinane, H., & Hilali, A. (2016). Using remote sensing for lineament extraction in Al Maghrabah area-Hajjah, Yemen. *The International Archives of the Photogrammetry, Remote Sensing and Spatial Information Sciences*, 42, 137-142. <https://doi.org/10.5194/isprs-archives-XLII-2-W1-137-2016>
- Alshayef, M. S., Mohammed, A. M., Javed, A., & Albaroot, M. A. (2017). Manual and automatic extraction of lineaments from multispectral image in part of Al-Rawdah, Shabwah, Yemen by using remote sensing and GIS technology. *International Journal of New Technology and Research*, 3(2), 67-73.
- Bondur, V.G. & Zverev, A.T. (2006). The physical nature of lineaments recorded on space images

- during monitoring of seismic hazard areas. *Sovremennye problemy distantsionnogo zondirovaniya Zemli iz kosmosa*, 3(2), 177-183. (in Russian)
7. Nath, B., Niu, Z., Acharjee, S., & Qiao, H. (2017). Monitoring the geodynamic behaviour of earthquake using Landsat 8-OLI time series data: case of Gorkha and Imphal. *Natural Hazards and Earth System Sciences Discussions*, 1-26. <https://doi.org/10.5194/nhess-2017-10>
 8. Zakharov, V. N., Zverev, A. V., Zverev, A. T., Malinnikov, V. A., & Malinnikova, O. N. (2017). Application of automated lineament analysis of satellite images in modern geodynamics research: A case study. *Russian Journal of Earth Sciences*, 17(3), 1-15. <https://doi.org/10.2205/2017es000599>
 9. Elmahdy, S. I., & Mohamed, M. M. (2016). Mapping of tecto-lineaments and investigate their association with earthquakes in Egypt: a hybrid approach using remote sensing data. *Geomatics, Natural Hazards and Risk*, 7(2), 600-619. <https://doi.org/10.1080/19475705.2014.996612>
 10. Sharifia, A., Rajabi, M. A., & Moghaddam, N. F. (2008). Studying the Earthquake Effects on Lineament Density Changes by Remote Sensing Technology. *International Proceedings GEOBIA*.
 11. Mogaji, K. A., Aboyeji, O. S., & Omosuyi, G. O. (2011). Mapping of lineaments for groundwater targeting in the basement complex region of Ondo State, Nigeria, using remote sensing and geographic information system (GIS) techniques. *International Journal of Water Resources and Environmental Engineering*, 3(7), 150-160.
 12. Bondur, V. G., Zverev, A. T., & Gaponova, E. V. (2019). Precursor variability of lineament systems detected using satellite images during strong earthquakes. *Izvestiya, Atmospheric and Oceanic Physics*, 55, 1283-1291. <https://doi.org/10.1134/S0001433819090123>
 13. Bondur, V.G., Zverev, A.T., Gaponova, E.V. & Zima, A.L. (2012). Space methods in predictive cyclic dynamics of lineament system before preparation of the earthquakes. *Issledovanie Zemli iz Kosmosa*, 1, 3-20. (in Russian)
 14. Vashchilov, Yu.Ya., Kalinina, L.Yu. (2008). Deep-Seated Faults and Lineaments: The Location of Earthquake Epicenters in the Russian Northeast on Land. *Vulkanologiya i seysmologiya*, 3, 19-31. (in Russian)
 15. Reddy, R. K. T. (1991). Digital analysis of lineaments—a test study on south India. *Computers & Geosciences*, 17(4), 549-559. [https://doi.org/10.1016/0098-3004\(91\)90113-R](https://doi.org/10.1016/0098-3004(91)90113-R)
 16. Sichugova, L., & Fazilova, D. (2021). The lineaments as one of the precursors of earthquakes: A case study of Tashkent geodynamical polygon in Uzbekistan. *Geodesy and Geodynamics*, 12(6), 399-404. <https://doi.org/10.1016/j.geog.2021.08.002>
 17. Singh, V. P., & Singh, R. P. (2005). Changes in stress pattern around epicentral region of Bhuj earthquake of 26 January 2001. *Geophysical Research Letters*, 32(24). <https://doi.org/10.1029/2005GL023912>
 18. Arellano-Baeza, A. A., Zverev, A. T., & Malinnikov, V. A. (2006). Study of changes in the lineament structure, caused by earthquakes in South America by applying the lineament analysis to the Aster (Terra) satellite data. *Advances in Space Research*, 37(4), 690-697. <https://doi.org/10.1016/j.asr.2005.07.068>
 19. Busygin, B. S., & Nikulin, S. L. (2016). The relationships between the lineaments in satellite images and earthquake epicenters within the Baikal Rift Zone. *Sovremennye problemy distantsionnogo zondirovaniya Zemli iz kosmosa*, 13(4), 219-230. <https://doi.org/10.21046/2070-7401-2016-13-15-219-230>
 20. Zlatopolsky, A. A. (1992). Program LESSA (Lineament Extraction and Stripe Statistical Analysis) automated linear image features analysis—experimental results. *Computers & Geosciences*, 18(9), 1121-1126. [https://doi.org/10.1016/0098-3004\(92\)90036-Q](https://doi.org/10.1016/0098-3004(92)90036-Q)
 21. Rahnama, M., & Gloaguen, R. (2014). Teclines: A MATLAB-based toolbox for tectonic lineament analysis from satellite images and DEMs, part 2: Line segments linking and merging. *Remote Sensing*, 6(11), 11468-11493. <https://doi.org/10.3390/rs6111468>
 22. Shevyrev, S.L. (2018). LEFA software: an automatized structural analysis of remote sensing imagery in Matlab environment. *Earth Sciences*, 10, 138-143. (in Russian)
 23. Mamadjanov, Yu., Aminov, J., Hodzhiev, A., Khalimov G. (2017). Late Paleozoic shoshonite – latite – monzonitoid magmatism of the Chatkal-Kurama zone of the Middle Tien Shan: geology, petrogeochemistry and potential ore potential. *International Proceedings, Actual problems of geology, geophysics and metallogeny*, 3, 46-49. (in Russian)
 24. Republican Center for Seismic Predictive Monitoring of the Ministry of Emergency Situations of the Republic of Uzbekistan (2022). https://rcsm.fvv.uz/ru/catalog_col
 25. USGS EROS Archive - Landsat Archives - Landsat 8 OLI (Operational Land Imager) and TIRS (Thermal Infrared Sensor) Level-1 Data Products. By Earth Resources Observation and Science (EROS) Center July 18, 2018. <https://www.usgs.gov/centers/eros/science/usgs-eros-archive-landsat-archives-landsat-8-oli-operational-land-imager-and>
 26. World Geologic Maps (2023). <https://certmapper.cr.usgs.gov/data/apps/world-maps/>
 27. Bakiyev, M. H., Khamidov, L. A., Ibragimov, A. H. (2001). Stress concentration near local crustal inhomogeneities. *Inland Earthquake. China*, 15 (4), 376-384. (in Russian)
 28. Yarmuhamedov, A. R. (1988). Morphostructure of the Middle Tien Shan and Its Relationship with Seismicity, Tashkent “FAN”, p. 163. (in Russian)
 29. Khamidov, L. A. (2010). Study of stresses fields of Chatkal’s mountain zone of West Tien Shan. *Geodinamika*, 1(9), 57-66
 30. Fazilova, D. S., & Sichugova, L. V. (2021). Deformation analysis based on GNSS measurements in Tashkent

- region. In E3S Web of Conferences, 227, 04002. <https://doi.org/10.1051/e3sconf/202122704002>
31. United States Geological Survey (USGS) Earth Explorer (2023). <https://earthexplorer.usgs.gov>
32. Landsat 8-9 Operational Land Imager (OLI) and Thermal Infrared Sensor (TIRS) (2023). <https://www.usgs.gov/faqs/what-are-band-designations-landsat-satellites>
33. Canny, J. (1986). A computational approach to edge detection. *IEEE Transactions on Pattern Analysis and Machine Intelligence*, (6), 679-698.
34. Argialas, D. P., & Mavrantza, O. D. (2004). Comparison of edge detection and Hough transform techniques for the extraction of geologic features. *International Archives of the Photogrammetry, Remote Sensing and Spatial Information Sciences*, 34(Part XXX).



© Author(s) 2024. This work is distributed under <https://creativecommons.org/licenses/by-sa/4.0/>



Semantic segmentation of very-high spatial resolution satellite images: A comparative analysis of 3D-CNN and traditional machine learning algorithms for automatic vineyard detection

Özlem Akar^{*1}, Ekrem Saralioğlu², Oğuz Güngör³, Halim Ferit Bayata⁴

¹Erzincan Binali Yıldırım University, Department of Architecture and City Planning, Türkiye, ozlemerden@gmail.com

²Artvin Coruh University, Department of Geomatics Engineering, Türkiye, ekremsaralioglu@artvin.edu.tr

³Ankara University, Department of Real Estate Development and Management, Türkiye, ogungor@ankara.edu.tr

⁴Erzincan Binali Yıldırım University, Department of Civil Engineering, Türkiye, hfbayata@erzincan.edu.tr

Cite this study:

Akar, Ö, Saralioğlu, E., Güngör, O., & Bayata, H. F. (2024). Semantic segmentation of very-high spatial resolution satellite images: A comparative analysis of 3D-CNN and traditional machine learning algorithms for automatic vineyard detection. *International Journal of Engineering and Geosciences*, 9(1), 12-24

<https://doi.org/10.26833/ijeg.1252298>

Keywords

Machine Learning
Deep Learning
Random Forest
Gabor
Image Classification

Research Article

Received:17.02.2023

Revised: 09.05.2023

Accepted:26.06.2023

Published:02.01.2024



Abstract

The Erzincan (Cimin) grape, which is an endemic product, plays a significant role in the economy of both the region it is cultivated in and the overall country. Therefore, it is crucial to closely monitor and promote this product. The objective of this study was to analyze the spatial distribution of vineyards by utilizing advanced machine learning and deep learning algorithms to classify high-resolution satellite images. A deep learning model based on a 3D Convolutional Neural Network (CNN) was developed for vineyard classification. The proposed model was compared with traditional machine learning algorithms, specifically Support Vector Machine (SVM), Random Forest (RF), and Rotation Forest (ROTF). The accuracy of the classifications was assessed through error matrices, kappa analysis, and McNemar tests. The best overall classification accuracies and kappa values were achieved by the 3D CNN and RF methods, with scores of 86.47% (0.8308) and 70.53% (0.6279) respectively. Notably, when Gabor texture features were incorporated, the accuracy of the RF method increased to 75.94% (0.6364). Nevertheless, the 3D CNN classifier outperformed all others, yielding the highest classification accuracy with an 11% advantage (86.47%). The statistical analysis using McNemar's test confirmed that the χ^2 values for all classification outcomes exceeded 3.84 at the 95% confidence interval, indicating a significant enhancement in classification accuracy provided by the 3D CNN classifier. Additionally, the 3D CNN method demonstrated successful classification performance, as evidenced by the minimum-maximum F1-score (0.79-0.97), specificity (0.95-0.99), and accuracy (0.91-0.99) values.

1. Introduction

Most grape varieties are known to be derived from *vitis vinifera*, the ancient grape often mentioned in the Bible. It was originated in the southern parts of the region between the Caspian and the Black Sea and has been carried all over the world by civilized people [1]. Today this perennial species is cultivated worldwide, including subtropical regions, since it is tolerant of most climates and soil types, and easy to grow. Grapes can be cultivated in the temperate climate zone, generally between 30° and 50° latitudes in both hemispheres. Depending on the latitude, it can be grown up to 1600-

1800 m altitudes [2,3]. According to the Food and Agriculture Organization of the United Nations (FAO), the grape was cultivated on 7.7 million hectares of land worldwide in 2019 and Spain had a 22.7-percent share followed by France, China, Italy, and Türkiye. In 2019, the global export of fresh grapes reached a total of 10 million tons, with Türkiye accounting for 1.7 million tons. South Africa and Spain ranked second and third in fresh grape exports, with 1.3 million tons and 1.2 million tons respectively, following Türkiye. In the same year, global raisin export was 3 million tons and 73 percent (2,1 million tons) was exported by Türkiye alone, followed by the USA and Iran. Fresh grape yield increased by 2.7

percent in 2020 compared to the previous year, reaching 4.2 million tons [4]. According to the statistics of the Erzincan Directorate of Provincial Agriculture and Forestry [5], 5402 tons of fresh grapes were produced in 2021 from the 949.5-hectare vineyard in the province of Erzincan, located in north-eastern Anatolia.

In Erzincan, the "Cimin grape" dominates the grape varieties grown, with its cultivation mainly concentrated in the Üzümlü district, named after its reputation for abundant grape production. After the application of Üzümlü Municipality, the Erzincan Cimin grape was patented by the Turkish Patent Institute in 2001. Since the Cimin grape is the most important endemic agricultural product for Erzincan's economy, conservation, monitoring, and dissemination of this variety is increasingly becoming vital for the region. This can be accomplished with modern agricultural practices powered by remote sensing and geographic information systems, which have become increasingly popular in recent years.

Due to increasing radiometric, spatial, spectral, and temporal resolutions, remote sensing data is used by different disciplines in many different applications including land cover/use mapping, urban and environmental change analysis, object extraction, crop monitoring, disease detection, yield estimation, etc. Furthermore, extracting information classes and determining their spatial distributions in a scene using different multispectral image classification algorithms provide valuable information for various applications needing geo-spatial data.

Multispectral image classification has been used in monitoring tropical forests, which are an important and rich source in terms of biological diversity [6], in determining the spatial distribution of vineyards [7-9], in monitoring coastal changes [10], in monitoring urban development [11], in agriculture [12], designing rangeland information systems [13], in object extraction [14], in land cover classification [15-20], burning area mapping [21], and in classification of different product types [22].

The process of labelling pixels according to their intensity values to transform them into meaningful land cover data is also called image classification or information extraction [23]. Image classification is the process of categorizing pixels in an image using logical decision rules in the spatial domain or statistical decision rules in the spectral domain. The spectral values of the remotely sensed data are used to classify images in the spectral domain. The geometric size, form, texture, and pattern of pixels or objects are at the foreground of spatial domain decision criteria [23]. Various machine learning-based methods such as random forest, artificial neural networks, and support vector machines have been used in recent years to obtain reliable and most accurate information from satellite images efficiently by image classification. There are many studies in which the RF classifier stands out in terms of classification accuracy when it comes to the use of machine learning methods in agriculture [24-29]. In the realm of precision agriculture applications, deep learning algorithms, which are a subset of machine learning techniques, have gained

significant popularity in recent years due to their ability to provide more precise and reliable detection of agricultural products on images [30]. Grinblat et al. were able to detect plant species with high accuracy by using deep learning algorithms to identify plants from their vascular structures [31]. Deep learning algorithms were used by Ferentinos et al. to distinguish diseased plants [32]. Among 25 different plant species, they detected diseased ones with 99.53 percent accuracy. Chlingaryan et al. identified plant species by classifying images with 99.58 percent accuracy using deep learning algorithms [33], and thus made a crop yield estimation [34]. Zhao et al. used deep learning models to produce crop type mapping with sufficient accuracy [35]. Zhong et al. also used RF, SVM, and 1-D Convolutional Neural Network Model (Conv1D) to classify agricultural products and highlighted that the Conv1D yielded satisfactory results [36].

The objective of this study was to identify the cultivation areas of Cimin, an indigenous fruit cultivated in the Üzümlü region, utilizing a deep learning method based on CNN and commonly used machine learning algorithms. The findings demonstrate that by leveraging a pre-trained CNN, vineyards throughout the region can be automatically detected without requiring additional supervised learning. This ability stands as a significant advantage of deep learning architectures over traditional machine learning methods.

2. Study area and data set

In the Üzümlü Town, where the Erzincan grape is cultivated, a pilot study area measuring 25 hectares was designated (Figure 1). This study area is situated at coordinates 39° 41' 00" East and 39° 43' 00" N, within the Upper Euphrates section of Eastern Anatolia, in the province of Erzincan. Around 80% of the administrative boundary of the Üzümlü district is located in the Esence Mountains region to the north of the Erzincan basin, while the remaining 20% lies within the Erzincan plain. With an area of 410 km², Üzümlü is the second smallest district of Erzincan [37].

For this study, the satellite image used was the Worldview-2 (WV-2) image, which covered a significant portion of Cimin vineyards in the Üzümlü region. The WV-2 satellite image consists of 8 multispectral (MS) bands with a spatial resolution of 2 meters, along with a panchromatic band offering a higher spatial resolution of 0.5 meters. The 8 MS bands encompass the following spectral ranges: Coastal, Blue, Green, Yellow, Red, Red Edge, Near-Infrared 1, and Near-Infrared 2. It is worth noting that the satellite image had undergone prior atmospheric, radiometric, and geometric corrections, enabling its direct utilization for classification purposes without requiring any pre-processing steps.

3. Method

This study had two purposes: (a) to determine the locations and distributions of vineyards accurately and robustly by using widely used machine learning algorithms such as SVM, RF, ROTF and CNN-based deep

learning technique (b) to investigate the performance of CNN-based deep learning technique by comparing it aforementioned machine learning algorithms. To better distinguish the vineyards by taking advantage of the sub-meter spatial resolution of PAN image, the WV-2 MS and WV-2 PAN bands were fused with the Hyper Spherical Color Space pan-sharpening method (HCS). The literature contains numerous studies showcasing the efficacy of Padwick's HCS image fusion method [38] in maintaining the spectral and spatial characteristics of both multispectral and panchromatic input images during the fusion process, particularly when applied to Worldview-2 images [38-41].

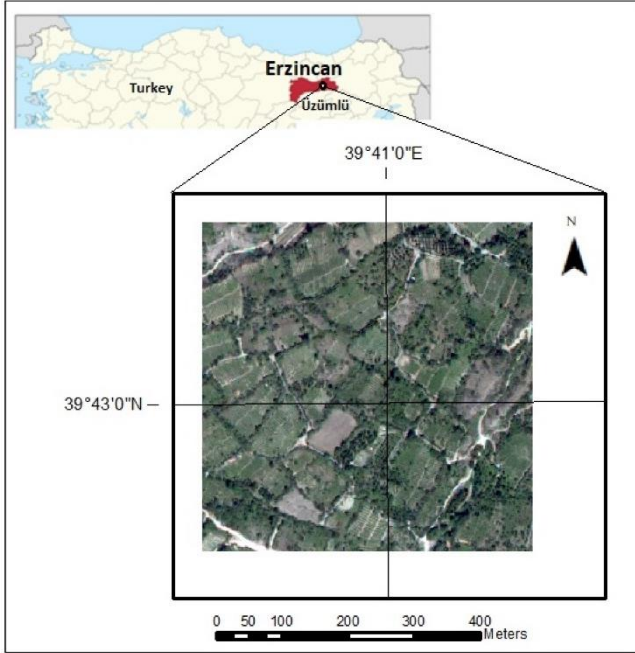


Figure 1. Study area.

The pan-sharpened image (1000x1000 pixels) was categorized into five land cover classes, namely vineyard, forest, soil, road, and shadow. ENVI software was utilized to select a total of 70505 pixels, employing a random feature selection approach in MATLAB, to generate the training and test data. Subsequently, the fused image was subjected to classification using 3D CNN, SVM, RF, and ROTF algorithms. To determine the optimal parameters for classification, a trial-and-error strategy was employed. The optimum parameters for this study were determined as $m=3$, $N=350$ for RF, $K=3$, $L=3$ for ROTF, and $C=100$ for SVM. The 3D CNN model employed in this study utilized both spectral features and texture features, as detailed in [42], to classify the image. Moreover, the

Gabor filter was utilized to extract texture data, which was then integrated into the RF classifier as explained in [26]. Among the machine learning methods employed in the study, the RF classifier exhibited the highest classification accuracy. Consequently, a comparison was conducted to evaluate the performances of these two methods. To identify the optimal parameter values and filter sizes for texture extraction using the Gabor filter, a trial-and-error method was employed to determine the values that most accurately represented the vineyards. Subsequently, the image was classified using these identified parameter values (Figure 2).

3.1. 3D Convolutional neural network model

Deep learning, which is usually defined by neural networks with more than two hidden layers, has been named one of the top ten breakthrough technologies of 2013 [43]. Deep learning model used in this study is created on the structure of CNN. Three-dimensional (3D) convolution is naturally suitable for spatial-temporal studies. Recently, some studies have been conducted on learning spatial-temporal features from video [44, 45], LIDAR point clouds [46], temporal images [47] and hyperspectral images [48]. In general, 3D CNN is not as widely used as 2D CNN because the temporal dimension is typically ignored in machine learning and computer vision applications. Remote sensing images, on the other hand, frequently provide dynamic or temporal information from which more information can be extracted. CNNs, which are widely used in image processing, are also useful for classifying satellite images [49].

High spatial resolution multispectral images with more than three spectral bands contain a lot of spectral information. To extract both spatial and spectral information from a multidimensional image, 3D convolution is preferred. By utilizing 3D convolution, the interaction between various spectral bands can be effectively modeled, encompassing both spatial and spectral information. Unlike 2D convolution, which focuses solely on spatial details, 3D convolution takes into consideration both spatial and spectral aspects, as highlighted in reference [50]. The integration of spatial and spectral information is crucial for improving the accuracy of satellite image classification. In this particular study, 3D convolution layers were employed to capture the spectral relationships among the 8 bands present in the WV-2 image. Consequently, these 8 bands were utilized as input data for the 3DCNN model.

$$v_{ij}^{xyz} = f(b_{ij} + \sum_{p=0}^{P_i-1} \sum_{s=0}^{S_{i-1}} \sum_{q=0}^{Q_{i-1}} \sum_{r=0}^{R_{i-1}} w_{ijp}^{qrs} v_{(i-1)p}^{(x+q)(y+r)(z+s)}) \quad (1)$$

In Equation 1, v represents the output of feature maps, S, Q, R defines spectral and spatial kernel dimensions where (s, q, r) are kernel, and (x, y, z) are feature map indices. While w specifies the kernel parameters, i, j, p represent the input layer, output layer, and feature map indices, respectively. P is the number of

feature maps. P_i represents the feature maps in the i^{th} layer. While the bias term is denoted by b , f represents the activation function of PReLU used in the model. Python programming language on Jupyter notebook and TensorFlow and Keras library in the background were used to create the model and classify the image with this

model. Jupyter Notebooks is an open-source and browser-based tool that combines interpreted languages, libraries, and visualization tools [51]. A Jupyter Notebook can run locally or in the cloud. Typical outputs include text, tables, charts, and graphics. The computer on which the study was conducted has 24 GB of RAM, NDVI GTX 1650 GPU, and an i7 9750h processor. For this study, a model was created using four 3D convolution layers. Each layer had a filter size of 3x3. The first, second, third, and fourth layers were configured with 128, 64, 32, and 16 filters, respectively. Two fully connected layers were used after the convolution layers. The first layer is a dense layer that performs a rough classification of the extracted features from the convolutional layer. The second layer is the model's final layer, and it is used to extract class scores with a Softmax

classifier. Softmax is a technique employed in multi-class classification tasks. It computes probability values for each class in order to classify a given input. The probability value associated with each class falls within the range of 0 to 1, and the sum of all probability values across all classes is equal to 1. Consequently, the Softmax classifier determines the probability values for each class in multi-class classification, ultimately selecting the class with the highest probability as the predicted class. The activation function was the Parametric Rectified Linear Unit (PReLU), the optimization method was Adam, and the subtraction function was categorical cross-entropy. The deep learning model created has 3118405 parameters in total. Figure 3 depicts the 3D CNN model that was used.

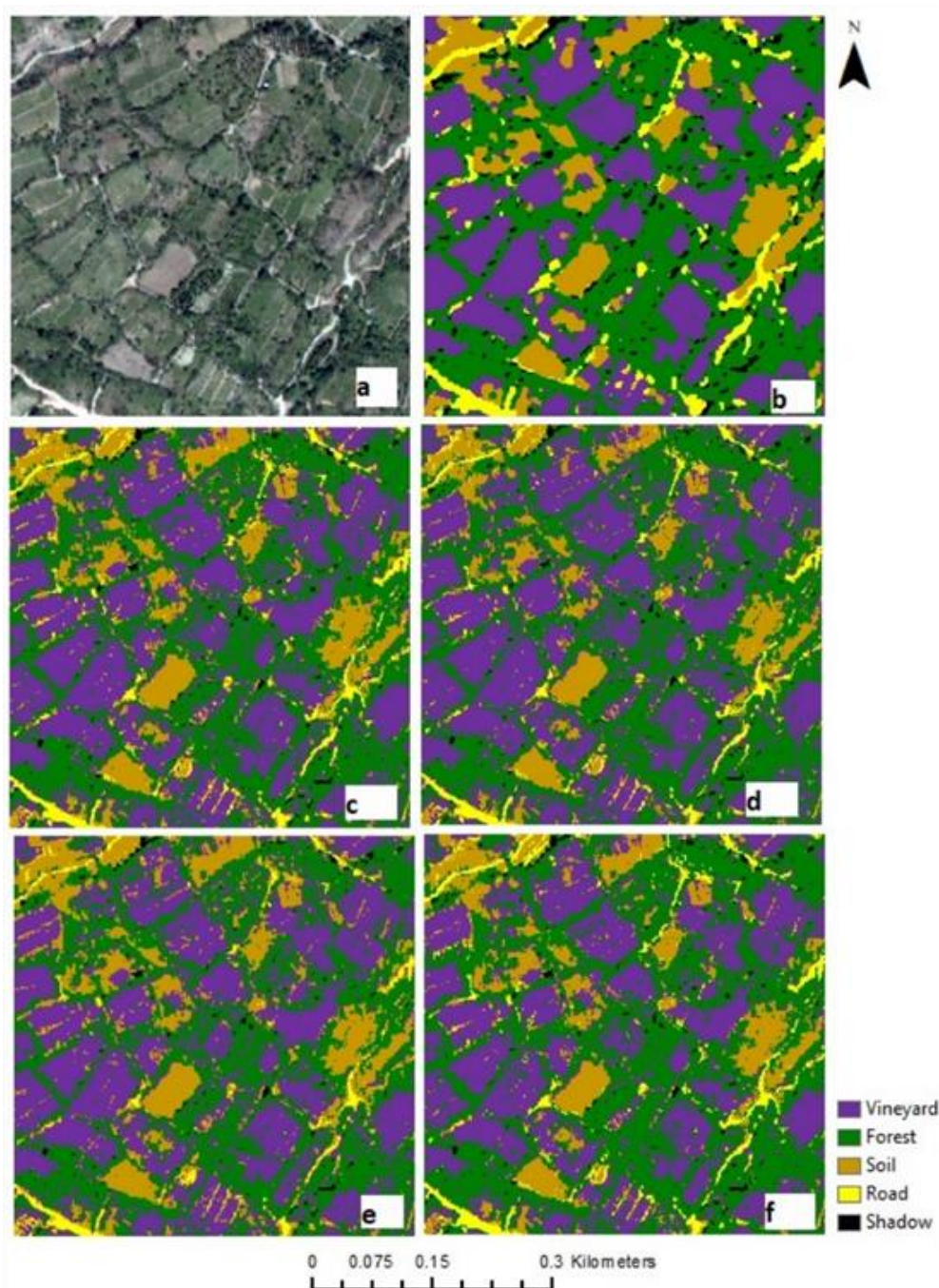


Figure 2. a) Fused image and classified images obtained by classification with b) 3D CNN, c) RF, d) ROTF, e) SVM, f) RF_Gabor.

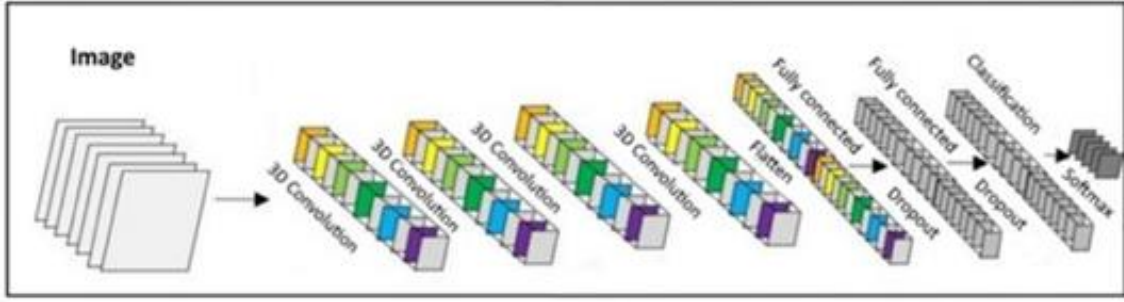


Figure 3. Architecture of 3D CNN model.

3.2. Random Forest

Random Forest is a classifier that can classify multiple variables and classes without the use of complex models or parameters [52]. The RF classifier outperforms many tree-based algorithms [53-56]. RF aims to develop a tree by dividing each node according to the GINI index, basically. Randomly selected variables are used instead of using all variables at each node [26]. Decision trees (DTs) are trained in RF using random bootstrap samples with the replacement of an original dataset [52]. The user defines two parameters: m and N . m (The number of variables) is used to determine the best split at each node. N is the number of DTs to be developed. Bootstrap samples are generated by randomly selecting two-thirds of the training Dataset. Trees are then built from these boot samples without employing pruning. The remaining one-third of the training dataset is reserved for use as the test dataset. The RF algorithm builds a large number of trees to determine the class of each pixel. The labeling of a pixel can vary across different trees, indicating that the total number of trees determines the frequency of the pixel's class assignment. The final class of the pixel is determined based on the class that has the highest occurrence among the candidate pixel's labels.

3.3. Rotation Forest

Rodriguez et al. [57] proposed the Rotation Forest algorithm as an ensemble method for encouraging both individual accuracy and classifier member [58]. The ROTF is a linear transformation method that creates a new performing space within another space [59]. Theoretically, the ROTF algorithm and the RF algorithm share similarities. Both methods aim to grow more than one tree in classification. However, ROTF creates the dataset in the Principle Component Analysis (PCA) feature space. It generates a large number of DTs from training datasets defined within a different feature space. The training dataset is divided into subsets, and feature extraction is performed using the feature space chosen from each subset. The ROTF algorithm has two user-specified parameters, K and L , which are required to determine the dataset used to grow each DT. This approach enables classification by training all classifiers in parallel [59].

3.4. Support Vector Machine

The Support Vector Machine classifier can distinguish linearly and nonlinearly separable data by finding the

best hyperplane for separating the classes [60]. If classes are linearly separable, it finds the planes separating them and uses these planes to construct a linear discriminant function. If classes cannot be separated linearly, the data is transformed to a higher-dimensional space in which the classes can be linearly separated by using a positive C parameter and a kernel function that minimizes classification error while maximizing the distance between planes [51-64]. The Radial basis function is the most commonly used kernel function because it performs well [65, 66]. The radial basis function is widely recognized for its exceptional performance in classification accuracy, making it the preferred choice as the most commonly used kernel function [65, 66].

3.5. Accuracy assessment

Congalton and Green [67] proposed the multinomial distribution to calculate the minimum number of samples needed to statistically calculate the classification accuracy. The minimum number of samples is calculated with the Equation 2 and 3 using the multinomial distribution approach;

$$n = \frac{B\Pi_i(1 - \Pi_i)}{b_i^2} \quad (2)$$

$$B = \left(\frac{\alpha}{k}\right) \times 100th \quad (3)$$

where n represents the number of reference pixels, α represents the confidence interval, k represents the number of classes, Π_i is the ratio of the area of the i th class to the total area, and b_i represents the required accuracy. If no prior information about Π_i is available, the sample number is calculated using Equation 4 [68].

$$n = \frac{B}{4b^2} \quad (4)$$

In the study, the analysis of classification accuracy required determining the minimum number of reference points. For this purpose, a 95% confidence interval was utilized, with the number of classes set at 5. Therefore, in the calculation of the B value, $\alpha/k = 0.05/5 = 0.01$ is used to find the corresponding value at 1 degree of freedom in the χ^2 distribution table as $\chi^2_{(1,0.01)}=6.635$. Accordingly, the minimum number of reference points was calculated as 664 as follows, yet 665 was used instead in the accuracy analysis (Equation 5).

$$n = \frac{B}{4b^2} = \frac{6.635}{4(0.05^2)} = 664 \quad (5)$$

The appropriate number of reference points required to create error matrices that evaluate the accuracy of each classification outcome was determined. The stratified method was utilized to distribute these points evenly across the image. Kappa (κ) analysis is another approach that performs accuracy analysis by determining whether one error matrix is statistically significantly different from another. The κ value, calculated within the range of 0 to 1, provides a statistical assessment of the agreement among the utilized categories or classes. This value serves as a measure of fit and classification accuracy, with higher values indicating better alignment and accuracy (approaching 1) and lower values suggesting poorer fit and lower classification accuracy (approaching 0). Kappa, as pointed out by Pontius and Millones [69], has been criticized for attempting to compare accuracy with a baseline of randomness. As an alternative, they proposed the utilization of allocation and quantity disagreements, which leverage the distinctions between a reference map and a comparison map. The quantity disagreement focuses on disparities in the category proportions between the reference and comparison maps, while the allocation disagreement addresses differences in the spatial distribution of categories between the reference and comparison maps [70]. In light of this suggestion, allocation and quantification values were calculated in addition to the kappa coefficient for each image's post-classification accuracy assessment. Subsequently, the McNemar test was employed to assess the presence of statistically significant differences. The classification results obtained from all algorithms utilized in the study were compared pairwise using the McNemar test. The nonparametric McNemar test can be computed using the Equation 6 [71].

$$\chi^2 = \frac{(|f_{12} - f_{21}| - 1)^2}{f_{12} + f_{21}} \quad (6)$$

Where f_{12} denotes the number of pixels incorrectly classified by the second method but correctly classified by the first one, and f_{21} denotes the number of pixels

incorrectly classified by the first method but correctly classified by the second one.

Furthermore, the performance evaluation of both 3DCNN and the other methods employed in this study was conducted using metrics in Equation 7-11 including F1-Score, specificity, and accuracy.

$$Accuracy = \frac{TN + TP}{TN + TP + FP + FN} \quad (7)$$

$$F1 - Score = \frac{2xPrecisionxRecall}{Precision + Recall} \quad (8)$$

$$Precision = \frac{TP}{TP + FP} \quad (9)$$

$$Recall = \frac{TP}{TP + FN} \quad (10)$$

$$Specificity = \frac{TN}{TN + FP} \quad (11)$$

Where TP and TN represent true positive and true negative observations in the confusion matrix, respectively. FP and FN are false positive and false negative observations [72]. For each class in the confusion matrix of each method, the metrics were computed.

4. Results and Discussion

By analyzing the error matrices, the classification accuracies of the classified images were examined for the SVM, RF, ROTF algorithms, and the 3D CNN model. The overall classification accuracies obtained from the error matrices were 86.47%, 70.53%, 66.92%, and 62.41% for the 3D CNN, RF, ROTF, and SVM, respectively (Table 1). In addition, the Mean IoU value for 3D-CNN, which includes the average of all classes, was found to be 84.93%. These results indicate that the 3D CNN method exhibited superior performance compared to RF by a margin of 16%, ROTF by 20%, and SVM by 24%. This analysis is further supported by the Kappa coefficients presented in Table 1.

Table 1. Overall classification accuracies and kappa analyses.

	3D CNN	RF	ROTF	SVM
Overall Accuracy	86.47	70.53	66.92	62.41
Kallocation	87.35	86.64	81.81	78.86
Kquantity	92.35	57.90	56.58	50.18
Khisto	95.11	72.47	71.09	66.54
Kcongaltion	83.08	62.79	58.16	52.47
Kcohen's	85.91	69.07	65.67	60.10

Upon examining the κ allocation values, it was evident that 3D CNN showcased superiority over RF by 1%, ROTF by 6%, and SVM by 8%. In terms of κ amount values, 3D CNN surpassed RF by 34%, ROTF by 36%, and SVM by 42%. Moreover, the κ histo values indicated that 3D CNN demonstrated a 24% improvement compared to RF, a 24% improvement compared to ROTF, and a 29%

improvement compared to SVM. The κ congaltion and κ cohen values presented in Table 1 further confirm the superiority of 3D CNN over other methods.

In order to enhance the accuracy of RF and assess its performance relative to 3D CNN, the texture features extracted using the Gabor filter were incorporated. The integration of RF texture features resulted in a

classification accuracy of 75.94%, representing a 5% improvement compared to the original RF performance (Table 2).

After comparing the Kappa values, it becomes clear that RF_Gabor exhibits a 3% improvement over RF.

Moreover, Table 3 presents the computed Quantity and Allocation disagreement/agreement values, which were proposed by Pontius and Millones [69] for accuracy assessment.

Table 2. Contribution of texture to classification accuracy for RF.

	Vineyard	Forest	Soil	Road	Shadow	ΣRow	PA (%)	UA(%)	
Vineyard	136	20	5	15	1	177	92.52%	76.84%	
Forest	10	119	3	14	86	232	82.07%	51.29%	
Soil	1	6	120	24	8	159	91.60%	75.47%	
Road	0	0	3	59	0	62	52.68%	95.16%	
Shadow	0	0	0	0	35	35	26.92%	100.00%	
ΣColumn	147	145	131	112	130	665			
Overall accuracy	70.53%								
Khisto	72.47 %								

Table 3. Contribution of texture to classification accuracy for RF_Gabor.

	Vineyard	Forest	Soil	Road	Shadow	ΣRow	PA (%)	UA(%)	
Vineyard	142	8	2	12	0	164	96.60%	86.59%	
Forest	4	135	4	19	88	250	93.10%	54.00%	
Soil	1	2	121	11	5	140	92.37%	86.43%	
Road	0	0	4	70	0	74	62.50%	94.59%	
Shadow	0	0	0	0	37	37	28.46%	100.00%	
ΣColumn	147	145	131	112	130	665			
Overall accuracy	75.94%								
Khisto	75.14%								

Table 4. The agreement and disagreement values.

Agreement/Disagreement (%)	3D CNN	RF_Gabor	RF	ROTF	SVM
Chance agreement	10	10	10	10	10
Quantity agreement	10	11	11	11	11
Allocation agreement	66	55	50	46	41
Allocation disagreement	10	4	8	10	11
Quantity disagreement	4	20	22	23	26

The overall disagreement, sum of both allocation and quantity disagreements, is lowest for 3D CNN at 14%, followed by RF_Gabor at 24%, RF at 30%, ROTF at 33%, and SVM at 37%. This indicates that 3D CNN effectively reduces disagreement and enhances classification

accuracy. Additionally, the incorporation of texture features decreases the disagreement of RF by 6%.

Producer (PA) and User (UA) accuracies that can be obtained from error matrices are also examined (Figure 4).

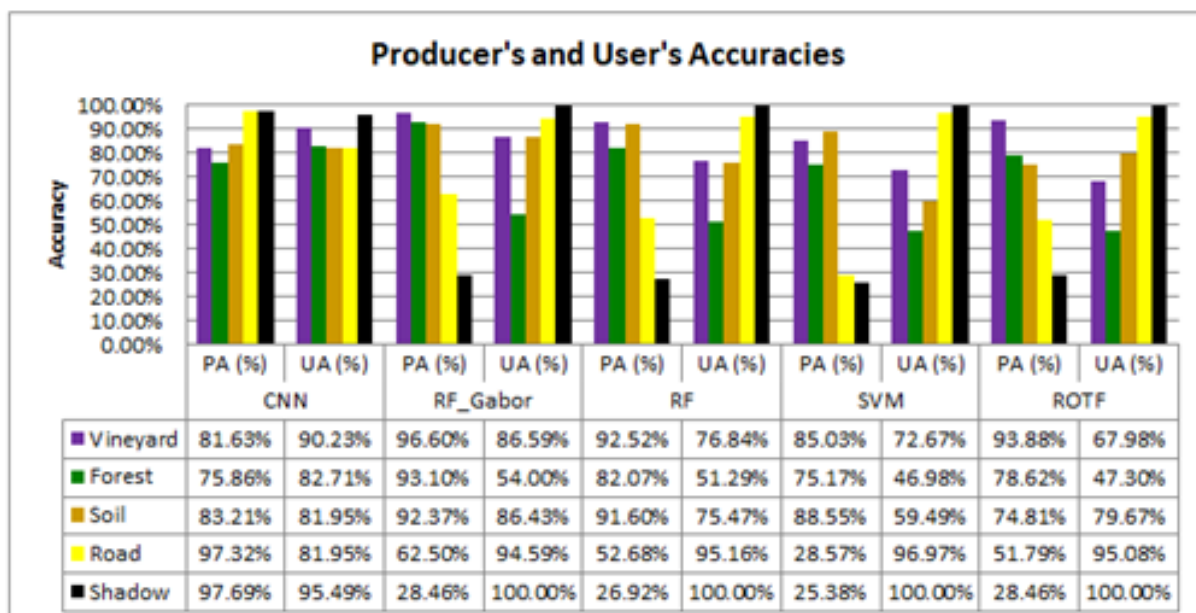


Figure 4. Producer's (PA) and User's (UA) in the error matrices of the classified images obtained with 3DCNN, RF, ROTF, SVM, and RF_Gabor.

Upon comparing the PA (Producer's Accuracy) values, it is evident that RF, ROTF, SVM, and RF_Gabor achieved PA values of 11%, 12%, 3%, and 15% respectively. These results indicate that the other methods demonstrated more accurate classification of the vineyard class compared to 3D CNN. For soil class, RF_Gabor, RF and SVM performed 9%, 8% and 5% better than 3D CNN, respectively, yet 3D CNN performed 8% more successful classification than ROTF. Also, 3D CNN classified road and shadow classes better than other methods. According to UA values (Figure 4), 3D CNN outperforms RF_Gabor by 4%, RF by 13%, SVM by 18%, and ROTF by 22% for the vineyard class. When it comes to the forest class, 3D CNN surpassed RF_Gabor by 29%, RF by 31%, SVM by 36%, and ROTF by 35%. Regarding the soil class, 3D CNN outcompeted RF by 7%, SVM by 23%, and ROTF by 2%, while RF_Gabor outperformed 3D CNN by 5%. Based on the UA results, 3D CNN especially discriminated vineyard, forest and soil classes better than RF, ROTF, and SVM, but was not succeeded as the other methods in road and shadow classes. The high

similarity in spectral properties between the forest and vineyard classes has led to a significant amount of confusion between these classes. Similarly, the spectral properties of very dark pixels in earth roads, soil, and forest classes closely resemble those of the shadow class, resulting in confusion among these classes as well. However, the incorporation of texture information has contributed to improved identification and extraction of vineyards.

In order to evaluate the significance of performance differences between 3D CNN and other classifiers using the McNemar test, χ^2 values were computed for RF_Gabor, RF, ROTF, and SVM as 19.512, 44.100, 63.515, and 90.289, respectively (Table 5).

The χ^2 values exceeding the reference value of 3.84 indicate that the 3D CNN classifier yields a significant improvement in accuracy at the 95% confidence interval. Lastly, Figure 5 presents the land-use map generated from the thematic classified image using the 3D CNN classifier, which demonstrates the highest classification accuracy.

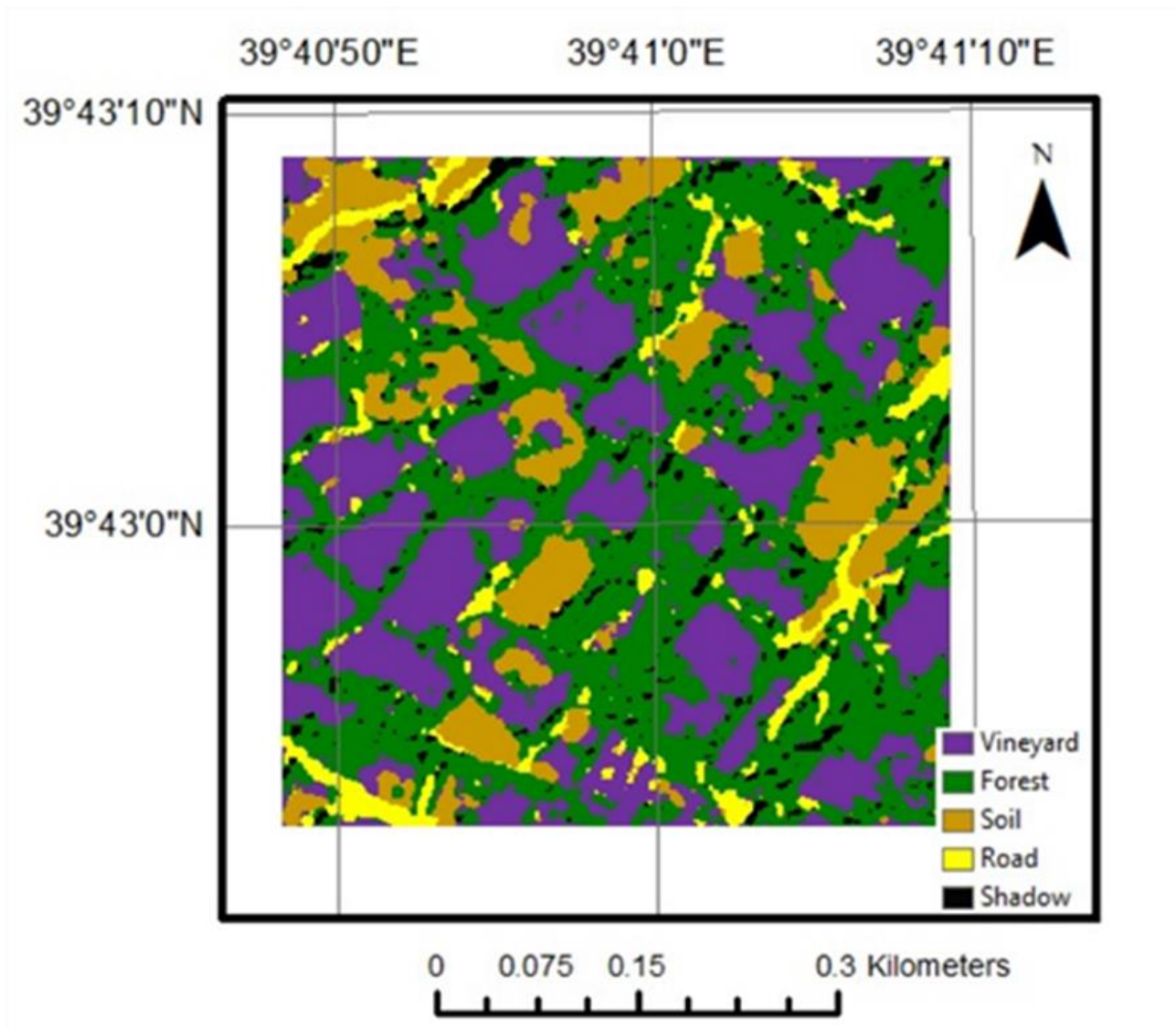


Figure 5. Land-use map was produced from the image classified with the 3D CNN classifier.

Table 5. McNemar test results for 3D CNN and other classifiers.

	f_{11}	f_{12}	f_{21}	f_{22}	Total	χ^2
3D CNN-RF_Gabor	418	157	87	3	665	19.512
3D CNN-RF	397	178	72	18	665	44.100
3D CNN-RTF	379	196	66	24	665	63.515
3D CNN-SVM	355	220	60	30	665	90.289

f_{11} is the number of correctly classified pixels in both cases. f_{22} represents the number of misclassified pixels in both cases. f_{12} represents number of correctly classified pixels with first classifier but misclassified pixels with second classifier. f_{21} is the number of misclassified pixels with second classifier but correctly classified pixels with first classifier

It has been determined that the 3D CNN model, incorporating 3D convolution layers, outperforms RF, ROTF, and SVM, which are commonly utilized in vineyard detection in existing literature. An important aspect to note is that the developed 3D CNN model achieves high accuracy directly from the image data, eliminating the requirement for additional data. For instance, while texture features were added to the WV-2 image using Gabor to enhance the classification accuracy of the RF algorithm, the addition of supplementary textures proved to be less effective compared to the 3D CNN model, which can automatically extract textures from images. However, one drawback of the 3D CNN model, which achieves accurate vineyard detection in WV-2 images without necessitating user intervention, is the significantly longer training time (20 hours) when compared to other machine learning models.

In order to assess the classification performance of the 3DCNN method and other approaches, the metrics presented in Table 5 were analyzed for each method and

class. Upon examining the results in Table 6, it is observed that the 3DCNN method demonstrates successful classification, supported by the minimum and maximum values of F1-score (0.79-0.97), specificity (0.95-0.99), and accuracy (0.91-0.99). The RF_Gabor method exhibits classification performance that closely resembles that of 3DCNN, as indicated by the F1-score (0.44-0.91), specificity (0.76-1.00), and accuracy (0.80-0.95) (Table 7). When averaging the metric values across the classes, the 3DCNN method achieves an F1-score of 0.866, specificity of 0.963, and accuracy of 0.942. For the RF_Gabor method, the corresponding values are an F1-score of 0.737, specificity of 0.930, and accuracy of 0.892. ROTF yields an F1-score of 0.653, specificity of 0.895, and accuracy of 0.839 (Table 8). SVM demonstrates an F1-score of 0.584, specificity of 0.872, and accuracy of 0.809 (Table 9). These results align with the overall classification accuracies obtained from the respective methods.

Table 6. Evaluation the performance of the methods for 3DCNN.

	PRECISION	RECALL	F1-SCORE	SPECIFICITY	ACCURACY
VINEYARD	0.902	0.816	0.857	0.972	0.935
FOREST	0.827	0.759	0.791	0.953	0.908
SOIL	0.820	0.832	0.826	0.951	0.926
ROAD	0.820	0.973	0.890	0.951	0.955
SHADOW	0.955	0.977	0.966	0.987	0.985

Table 7. Evaluation the performance of the methods for RF_Gabor.

	PRECISION	RECALL	F1-SCORE	SPECIFICITY	ACCURACY
VINEYARD	0.866	0.966	0.913	0.943	0.949
FOREST	0.540	0.931	0.684	0.763	0.802
SOIL	0.864	0.924	0.893	0.953	0.946
ROAD	0.946	0.625	0.753	0.991	0.917
SHADOW	1.000	0.285	0.443	1.000	0.844

Table 8. Evaluation the performance of the methods for ROTF.

	PRECISION	RECALL	F1-SCORE	SPECIFICITY	ACCURACY
VINEYARD	0.680	0.939	0.789	0.825	0.857
FOREST	0.473	0.786	0.591	0.723	0.738
SOIL	0.797	0.748	0.772	0.933	0.885
ROAD	0.951	0.518	0.671	0.992	0.886
SHADOW	1.000	0.285	0.443	1.000	0.827

Table 9. Evaluation the performance of the methods for SVM.

	PRECISION	RECALL	F1-SCORE	SPECIFICITY	ACCURACY
VINEYARD	0.727	0.850	0.784	0.861	0.857
FOREST	0.470	0.752	0.578	0.713	0.723
SOIL	0.595	0.885	0.712	0.791	0.815
ROAD	0.970	0.286	0.441	0.997	0.837
SHADOW	1.000	0.254	0.405	1.000	0.811

5. Conclusion

Accurately identifying vineyards is crucial for contributing to the national economy, effectively managing viticulture processes, monitoring crops, and implementing site-specific automated crop management. With this objective in mind, this study aimed to determine the spatial distribution of Cimin grape using high-resolution satellite images. The performance of the developed 3D CNN model was compared to that of the RF, ROTF, and SVM algorithms. The classification accuracies obtained were 86.47%, 75.94%, 70.53%, 66.92%, and 62.41% for the 3D CNN, RF_Gabor, RF, ROTF, and SVM methods, respectively. The 3D CNN method outperformed the RF_Gabor (second-ranked) by 11% and the RF (third-ranked) by 16% in terms of classification performance, resulting in more accurate vineyard classification. The evaluation of metrics such as F1-Score, specificity, accuracy, Kappa analyses, and χ^2 values obtained from the McNemar test further confirm the success of the 3D CNN method. Preliminary results indicate that the proposed 3D CNN-based deep learning model can effectively classify Cimin vineyards and determine their spatial distributions. Future work will focus on evaluating the performance of different CNN-based architectures for the same problem.

Acknowledgement

This work was supported by Erzincan Binali Yıldırım University Scientific Research Project [Grant Number: 636].

Author contributions

Özlem Akar: Processed and classified the images using machine learning methods, and analyzed the results.
Ekrem Saralioğlu: Classified the study area by developing a 3D convolutional neural network model.
Oğuz Güngör: Wrote and reviewed the manuscript.
Halim Ferit Bayata: Wrote and reviewed the manuscript.

Conflicts of interest

The authors declare no conflicts of interest.

References

- Weaver, R. J. (1976). Grape growing. John Wiley & Sons.
- Akpınar, E., & Çelikoğlu, Ş. (2016). Karaerik (Cimin) üzümünün Erzincan ekonomisine ve tanıtımına katkıları. Uluslararası Erzincan Sempozyumu, 2, 15-23.
- Bulut, İ. (2006). Genel tarım bilgileri ve tarımın coğrafi esasları (Ziraat Coğrafyası). Gündüz Eğitim ve Yayıncılık, Ankara, 255.
- Republic of Turkey Ministry of Agriculture and Forestry. (2021). 2021-January Agricultural Products Markets Report: GRAPE, <https://arastirma.tarimorman.gov.tr/tepge/Menu/27/Tarim-Urunleri-Piyasaları>
- Erzincan Directorate of Provincial Agriculture and Forestry (2022). <https://erzincan.tarimorman.gov.tr/Menu/66/Tarimsal-Veriler>
- Christian, B., & Krishnayya, N. S. R. (2009). Classification of tropical trees growing in a sanctuary using Hyperion (EO-1) and SAM algorithm. Current Science, 96(12), 1601-1607.
- Prins, A. J., & Van Niekerk, A. (2020). Regional Mapping of Vineyards Using Machine Learning and LiDAR Data. International Journal of Applied Geospatial Research (IJAGR), 11(4), 1-22. <https://doi.org/10.4018/IJAGR.2020100101>
- Darra, N., Psomiadis, E., Kasimati, A., Anastasiou, A., Anastasiou, E., & Fountas, S. (2021). Remote and proximal sensing-derived spectral indices and biophysical variables for spatial variation determination in vineyards. Agronomy, 11(4), 741. <https://doi.org/10.3390/agronomy11040741>
- Vélez, S., Ariza-Sentís, M., & Valente, J. (2023). Mapping the spatial variability of Botrytis bunch rot risk in vineyards using UAV multispectral imagery. European Journal of Agronomy, 142, 126691. <https://doi.org/10.1016/j.eja.2022.126691>
- Gungor, O., Boz, Y., Gokalp, E., Comert, C., & Akar, A. (2010). Fusion of low and high resolution satellite images to monitor changes on coastal zones. Scientific Research and Essays, 5(7), 654-662.
- Chi, M. V., Thi, L. P., & Si, S. T. (2009, October). Monitoring urban space expansion using Remote sensing data in Ha Long city, Quang Ninh province in Vietnam. In 7th FIG Regional Conference Spatial Data Serving People: Land Governance and the Environment-Building the Capacity Hanoi, Vietnam, 19-22.
- Kaya, Y., & Polat, N. (2023). A linear approach for wheat yield prediction by using different spectral vegetation indices. International Journal of Engineering and Geosciences, 8(1), 52-62. <https://doi.org/10.26833/ijeg.1035037>
- Akar, A., & Gokalp, E. (2018). Designing a sustainable rangeland information system for Turkey. International Journal of Engineering and Geosciences, 3(3), 87-97. <https://doi.org/10.26833/ijeg.412222>
- Zhang, W., Xue, X., Sun, Z., Guo, Y. F., Chi, M., & Lu, H. (2007). Efficient feature extraction for image classification. IEEE 11th International Conference on Computer Vision, 1-8. <https://doi.org/10.1109/ICCV.2007.4409058>
- Huang, Y., Fipps, G., Lacey, R. E., & Thomson, S. J. (2011). Landsat satellite multi-spectral image classification of land cover and land use changes for GIS-based urbanization analysis in irrigation districts of Lower Rio Grande Valley of Texas. Journal of Applied Remote Sensing, 2(1), 27-36.
- Akar, Ö., & Tunç Görmüş, E. (2019). Göktürk-2 ve Hyperion EO-1 uydu görüntülerinden rastgele orman sınıflandırıcısı ve destek vektör makineleri ile arazi kullanım haritalarının üretilmesi. Geomatik, 4(1), 68-81. <https://doi.org/10.29128/geomatik.476668>

17. Ahady, A. B., & Kaplan, G. (2022). Classification comparison of Landsat-8 and Sentinel-2 data in Google Earth Engine, study case of the city of Kabul. *International Journal of Engineering and Geosciences*, 7(1), 24-31. <https://doi.org/10.26833/ijeg.860077>
18. Sefercik, U. G., Kavzoğlu, T., Çölkesen, I., Nazar, M., Öztürk, M. Y., Adalı, S., & Dinç, S. (2023). 3D positioning accuracy and land cover classification performance of multispectral RTK UAVs. *International Journal of Engineering and Geosciences*, 8(2), 119-128. <https://doi.org/10.26833/ijeg.1074791>
19. Cengiz, A. V. C. I., Budak, M., Yağmur, N., & Balçık, F. (2023). Comparison between random forest and support vector machine algorithms for LULC classification. *International Journal of Engineering and Geosciences*, 8(1), 1-10. <https://doi.org/10.26833/ijeg.987605>
20. Tirmanoğlu, B., İsmailoğlu, I., Kokal, A. T., & Musaoğlu, N. (2023). Yeni nesil multispektral ve hiperspektral uydu görüntülerinin arazi örtüsü/arazi kullanımı sınıflandırma performanslarının karşılaştırılması: Sentinel-2 ve PRISMA Uydusu. *Geomatik*, 8(1), 79-90. <https://doi.org/10.29128/geomatik.1126685>
21. Çömert, R., Matci, D. K., & Avdan, U. (2019). Object based burned area mapping with random forest algorithm. *International Journal of Engineering and Geosciences*, 4(2), 78-87. <https://doi.org/10.26833/ijeg.455595>
22. Sun, Z., Di, L., Fang, H., & Burgess, A. (2020). Deep learning classification for crop types in north dakota. *IEEE Journal of Selected Topics in Applied Earth Observations and Remote Sensing*, 13, 2200-2213. <https://doi.org/10.1109/JSTARS.2020.2990104>
23. Gao, J. (2009). *Digital analysis of remotely sensed imagery*. McGraw-Hill Education, New York. ISBN: 9780071604659
24. Jay, S., Lawrence, R., Repasky, K., & Keith, C. (2009). Invasive species mapping using low-cost hyperspectral imagery. In *ASPRS Annual Conference*.
25. Ok, A. O., Akar, O., & Gungor, O. (2012). Evaluation of random forest method for agricultural crop classification. *European Journal of Remote Sensing*, 45(1), 421-432. <https://doi.org/10.5721/EuJRS20124535>
26. Akar, Ö., & Güngör, O. (2015). Integrating multiple texture methods and NDVI to the Random Forest classification algorithm to detect tea and hazelnut plantation areas in northeast Turkey. *International Journal of Remote Sensing*, 36(2), 442-464. <https://doi.org/10.1080/01431161.2014.995276>
27. Ntouros, K. D., Gitas, I. Z., & Silleos, G. N. (2009, August). Mapping agricultural crops with EO-1 Hyperion data. In *2009 First Workshop on Hyperspectral Image and Signal Processing: Evolution in Remote Sensing*, 1-4. <https://doi.org/10.1109/WHISPERS.2009.5289057>
28. Kpienbaareh, D., Sun, X., Wang, J., Luginaah, I., Bezner Kerr, R., Lupafya, E., & Dakishoni, L. (2021). Crop type and land cover mapping in northern Malawi using the integration of sentinel-1, sentinel-2, and planetscope satellite data. *Remote Sensing*, 13(4), 700. <https://doi.org/10.3390/rs13040700>
29. Wang, S., Azzari, G., & Lobell, D. B. (2019). Crop type mapping without field-level labels: Random forest transfer and unsupervised clustering techniques. *Remote sensing of environment*, 222, 303-317. <https://doi.org/10.1016/j.rse.2018.12.026>
30. Akar, Ö., Saralioğlu, E., Güngör, O., & Bayata, H. F. (2021). Determination of vineyards with support vector machine and deep learning-based Image classification. *Intercontinental Geoinformation Days*, 3, 26-29.
31. Grinblat, G. L., Uzal, L. C., Larese, M. G., & Granitto, P. M. (2016). Deep learning for plant identification using vein morphological patterns. *Computers and Electronics in Agriculture*, 127, 418-424. <https://doi.org/10.1016/j.compag.2016.07.003>
32. Ferentinos, K. P. (2018). Deep learning models for plant disease detection and diagnosis. *Computers and electronics in agriculture*, 145, 311-318. <https://doi.org/10.1016/j.compag.2018.01.009>
33. Chlingaryan, A., Sukkarieh, S., & Whelan, B. (2018). Machine learning approaches for crop yield prediction and nitrogen status estimation in precision agriculture: A review. *Computers and Electronics in Agriculture*, 151, 61-69. <https://doi.org/10.1016/j.compag.2018.05.012>
34. Abdullahi, H. S., Sheriff, R., & Mahieddine, F. (2017). Convolution neural network in precision agriculture for plant image recognition and classification. *Seventh International Conference on Innovative Computing Technology (INTECH)*, 10, 256-272.
35. Zhao, H., Duan, S., Liu, J., Sun, L., & Reymondin, L. (2021). Evaluation of five deep learning models for crop type mapping using sentinel-2 time series images with missing information. *Remote Sensing*, 13(14), 2790. <https://doi.org/10.3390/rs13142790>
36. Zhong, L., Hu, L., & Zhou, H. (2019). Deep learning based multi-temporal crop classification. *Remote Sensing of Environment*, 221, 430-443. <https://doi.org/10.1016/j.rse.2018.11.032>
37. TR Erzincan Governorate. (2021). <http://www.erkincan.gov.tr/erkincan-uzumu>
38. Padwick, C., Deskevich, M., Pacifici, F., & Smallwood, S. (2010). WorldView-2 pan-sharpening. In *Proceedings of the ASPRS 2010 Annual Conference*, San Diego, CA, USA, 2630, 1-14.
39. Akar, Ö. (2019). Göktürk-2 ve Worldview-2 Uydu Görüntüleri için Görüntü Keskinleştirme Yöntemlerinin Değerlendirilmesi. *Erzincan University Journal of Science and Technology*, 12(2), 874-885.
40. Li, H., Jing, L., & Tang, Y. (2017). Assessment of pansharpening methods applied to WorldView-2 imagery fusion. *Sensors*, 17(1), 89. <https://doi.org/10.3390/s17010089>
41. Anshu, S. K., Pande, H., Tiwari, P. S., & Shukla, S. (2017). Evaluation of Fusion Techniques for High Resolution Data-A Worldview-2 Imagery.

- International Journal of Applied Remote Sensing and GIS, 4, 10-22.
42. Fu, L., Ma, J., Chen, Y., Larsson, R., & Zhao, J. (2019). Automatic detection of lung nodules using 3D deep convolutional neural networks. *Journal of Shanghai Jiaotong University (Science)*, 24, 517-523. <https://doi.org/10.1007/s12204-019-2084-4>
 43. Zhu, X. X., Tuia, D., Mou, L., Xia, G. S., Zhang, L., Xu, F., & Fraundorfer, F. (2017). Deep learning in remote sensing: A comprehensive review and list of resources. *Geoscience and Remote Sensing Magazine*, 5(4), 8-36. <https://doi.org/10.1109/MGRS.2017.2762307>
 44. Ji, S., Xu, W., Yang, M., & Yu, K. (2012). 3D convolutional neural networks for human action recognition. *Transactions on Pattern Analysis and Machine Intelligence*, 35(1), 221-231. <https://doi.org/10.1109/TPAMI.2012.59>
 45. Tran, D., Bourdev, L., Fergus, R., Torresani, L., & Paluri, M. (2015). Learning spatiotemporal features with 3d convolutional networks. In *Proceedings of the IEEE international conference on computer vision*, 4489-4497.
 46. Xu, Z., Guan, K., Casler, N., Peng, B., & Wang, S. (2018). A 3D convolutional neural network method for land cover classification using LiDAR and multi-temporal Landsat imagery. *ISPRS journal of photogrammetry and remote sensing*, 144, 423-434. <https://doi.org/10.1016/j.isprsjprs.2018.08.005>
 47. Ji, S., Zhang, C., Xu, A., Shi, Y., & Duan, Y. (2018). 3D convolutional neural networks for crop classification with multi-temporal remote sensing images. *Remote Sensing*, 10(1), 75. <https://doi.org/10.3390/rs10010075>
 48. Mei, S., Yuan, X., Ji, J., Zhang, Y., Wan, S., & Du, Q. (2017). Hyperspectral image spatial super-resolution via 3D full convolutional neural network. *Remote Sensing*, 9(11), 1139. <https://doi.org/10.3390/rs9111139>
 49. Saralioglu, E., & Gungor, O. (2022). Semantic segmentation of land cover from high resolution multispectral satellite images by spectral-spatial convolutional neural network. *Geocarto International*, 37(2), 657-677. <https://doi.org/10.1080/10106049.2020.1734871>
 50. Li, Y., Zhang, H., & Shen, Q. (2017). Spectral-spatial classification of hyperspectral imagery with 3D convolutional neural network. *Remote Sensing*, 9(1), 67. <https://doi.org/10.3390/rs9010067>
 51. Pérez, F., & Granger, B. E. (2007). IPython: a system for interactive scientific computing. *Computing in Science & Engineering*, 9(3), 21-29. <https://doi.org/10.1109/MCSE.2007.53>
 52. Breiman, L. (2001). Random forests. *Machine Learning*, 45(1), 5-32.
 53. Watts, J. D., & Lawrence, R. L. (2008). Merging random forest classification with an object-oriented approach for analysis of agricultural lands. *The International Archives of the Photogrammetry, Remote Sensing and Spatial Information Sciences*, 37(B7), 579-582
 54. Waske, B., Heinzl, V., Braun, M., & Menz, G. (2007). Random forests for classifying multi-temporal sar data. *Envisat Symposium*, 2007, 23-27.
 55. Gislason, P. O., Benediktsson, J. A., & Sveinsson, J. R. (2004). Random forest classification of multisource remote sensing and geographic data. In *IGARSS 2004. International Geoscience and Remote Sensing Symposium*, 2, 1049-1052. <https://doi.org/10.1109/IGARSS.2004.1368591>
 56. Pal, M. (2003, July). Random forests for land cover classification. In *IGARSS 2003. 2003 IEEE International Geoscience and Remote Sensing Symposium. Proceedings (IEEE Cat. No. 03CH37477)* 6, 3510-3512. <https://doi.org/10.1109/IGARSS.2003.1294837>
 57. Rodriguez, J. J., Kuncheva, L. I., & Alonso, C. J. (2006). Rotation forest: A new classifier ensemble method. *IEEE transactions on pattern analysis and machine intelligence*, 28(10), 1619-1630. <https://doi.org/10.1109/TPAMI.2006.211>
 58. Xia, J., Du, P., He, X., & Chanussot, J. (2013). Hyperspectral remote sensing image classification based on rotation forest. *IEEE Geoscience and Remote Sensing Letters*, 11(1), 239-243. <https://doi.org/10.1109/LGRS.2013.2254108>
 59. Liu, K. H., & Huang, D. S. (2008). Cancer classification using rotation forest. *Computers in biology and medicine*, 38(5), 601-610. <https://doi.org/10.1016/j.compbiomed.2008.02.007>
 60. Vapnik, V. (1999). *The nature of statistical learning theory*. Springer science and business media.
 61. Özkan, Y. (2008). *Veri Madenciliği Yöntemleri*, Papatya Yayıncılık, İstanbul.
 62. Mather, P., & Tso, B. (2016). *Classification methods for remotely sensed data*. CRC press.
 63. Stephens, D., & Diesing, M. (2014). A comparison of supervised classification methods for the prediction of substrate type using multibeam acoustic and legacy grain-size data. *PloS one*, 9(4), e93950. <https://doi.org/10.1371/journal.pone.0093950>
 64. Çölkesen, İ., & Yomraloğlu, T. (2014). Arazi örtüsü ve kullanımının haritalanmasında WorldView-2 uydu görüntüsü ve yardımcı verilerin kullanımı. *Harita Dergisi*, 152(2), 12-24.
 65. Thanh Noi, P., & Kappas, M. (2018). Comparison of random forest, k-nearest neighbor, and support vector machine classifiers for land cover classification using Sentinel-2 imagery. *Sensors*, 18(1), 18. <https://doi.org/10.3390/s18010018>
 66. Kavzoglu, T., & Colkesen, I. (2009). A kernel functions analysis for support vector machines for land cover classification. *International Journal of Applied Earth Observation and Geoinformation*, 11(5), 352-359. <https://doi.org/10.1016/j.jag.2009.06.002>
 67. Congalton, R. G., & Green, K. (2019). *Assessing the accuracy of remotely sensed data: principles and practices*. CRC Press.
 68. Congalton, R. G., & Green, K. (2019). *Assessing the accuracy of remotely sensed data: principles and practices*. CRC Press.
 69. Pontius Jr, R. G., & Millones, M. (2011). Death to Kappa: birth of quantity disagreement and allocation

- disagreement for accuracy assessment. *International Journal of Remote Sensing*, 32(15), 4407-4429. <https://doi.org/10.1080/01431161.2011.552923>
70. Akar, A. (2022). Improving the accuracy of random forest-based land-use classification using fused images and digital surface models produced via different interpolation methods. *Concurrency and Computation: Practice and Experience*, 34(6), e6787. <https://doi.org/10.1002/cpe.6787>
71. Foody, G. M. (2004). Thematic map comparison. *Photogrammetric Engineering & Remote Sensing*, 70(5), 627-633. <https://doi.org/10.14358/PERS.70.5.627>
72. Amini, S., Saber, M., Rabiei-Dastjerdi, H., & Homayouni, S. (2022). Urban land use and land cover change analysis using random forest classification of landsat time series. *Remote Sensing*, 14(11), 2654. <https://doi.org/10.3390/rs14112654>



© Author(s) 2024. This work is distributed under <https://creativecommons.org/licenses/by-sa/4.0/>



Optimization of expropriation costs on the highway projects in Türkiye

Kemal Çelik *¹ 

¹ Gümüşhane University, Department of Geomatics Engineering, Türkiye, gumuscelik@hotmail.com

Cite this study: Çelik, K. (2024). Optimization of expropriation costs on the highway projects in Türkiye. International Journal of Engineering and Geosciences, 9(1), 25-33

<https://doi.org/10.26833/ijeg.1255727>

Keywords

Highway
Expropriation
Real Estate

Research Article

Received:08.03.2023

Revised: 22.10.2023

Accepted:20.11.2023

Published:02.01.2024



Abstract

Expropriation is widely used to introduce highway projects into the society. Expropriation is the registration process of real estate and equities owned by natural and legal persons on behalf of the administration for public interest, provided that property and easement right amount shall be paid in cash or in advance or by equal installments. In what situations and by which institutions expropriation is carried out are restricted by the law. In accordance with the Article 3 of the Expropriation Law Number 2942 amended by the Law Number 4650, the expropriation process shall not be started without an adequate allowance provided by the administration. The exercise of the right of property shall not be against public interest." Project areas are required to be converted into public property after the development plans for the public projects are prepared. Areas regarded as private property but intersected by highway, railway or waterway routes can only be occupied after expropriation. Without expropriation, projects based on transportation in improvement areas can be opened to public with the application of the provisions of the Development Law Number 3194, while those in areas having no development plan can be opened to public with the application of the relevant provisions of the Agricultural Reform Law Number 3083 on Land Consolidation in Irrigated Areas and Law Number 5403 on Soil Conservation and Land Use. In this article, opening highways, railways, and waterways to public in Türkiye using the implementation of development plans is discussed. For the real estate coinciding with the route of public investments, if land and land lots are arranged in accordance with the Article 18 of the Development Law Number 3194, state withholding up to 45% may be imposed. The objective function in the state withholding can be stated as $f = \text{cost}_{\min} = f(a,b)$. Land acquisition increases as the ratio of state withholding increases, resulting in the minimization of the expropriation costs. Public projects such as highway can be opened to public free of charge with development plan implementation in improvement areas and with land consolidation in rural areas having no development plan.

1. Introduction

According to the amendment made with the Law Number 4709 to the 1982 Constitution Act of Türkiye, "government officials and public legal entities are entitled to expropriate proprietary real estate in whole or in part and constitute administrative easements for public interest as per legal rules and procedures, provided that the actual equivalents are paid in advance". The Law Number 2942 amended by the Law Number 4650 governs transactions to be carried out by government officials and public legal entities to expropriate real estate belonging to real and private legal entities for public interest, calculation of expropriation amount, registration of immovable and easement right

on behalf of the administration, revoking unused immovable, procedures related to the transfer of real estate among administrations, mutual rights and obligations, and resolution procedures and methods of relevant conflicts [1-4].

In any neighborhood, an immovable, its outbuilding and constitution of easement for the immovable may be a subject for expropriation. For expropriation, the authority or the person authorized to initiate the expropriation process should acquire the decision of public utilities. Public institutions and organizations are able to make expropriation on subjects restricted by law. A service that is among the fundamental duties of public institutions can be transferred to another administration to the extent permitted by law [5-6]. In this case, public

interest regarding the expropriation for the realization of the service transferred shall be obtained by the competent authority of the administration that the service is transferred to. Authorities granting the decision of expropriation are entitled to revoke the decision of expropriation as per the principle of formal parallelism. Another administrative authority that is not the one granting the decision of expropriation shall not revoke such decision. In Türkiye, authorities who are entitled to grant and certify the decision of expropriation are explicitly listed under the Articles 5 and 6 of the Expropriation Law Number 2942, respectively. Except for the listed authorities, there are certain institutions granted the duty and authorization of expropriation. Relevant authorities are entitled to make expropriation as per the Law Number 6200 on the Organization and Functions of the General Directorate of State Hydraulic Works (Article 3), the Law Number 6001 on the Services of the General Directorate of Highways (Article 22), the Law Number 3096 on Granting Authorization to Institutions Other Than the Turkish Electricity Authority For the Generation, Transmission, Distribution and Trade of Electricity (Article 11), the Law Number 3154 on the Organization and Duties of the Ministry for Energy and Natural Resources (Article 11/c), the Turkish Mining Law Number 3213 (Article 43), the Free Trade Zones Law Number 3218 (Article 5), the Organized Industrial Zones Law Number 4562 (Article 4), the Natural Gas Market Law Number 4646 (Article 12/a), the Technology Development Zones Law Number 4691 (Article 5), the Petroleum Law Number 6326 (Article 87/1), the Law Number 4753 on Protection Against Flood Waters and Floods (Article 11), the Free Trade Zones Law Number 3218 (Article 2), the Law Number 933 on the Implementation Fundamentals of the Development Plan (Article 2/C), the Law Number 2565 on Military Forbidden Zones and Military Security Zones (Article 7/1), the Law Number 6461 on Liberalization of Railway Transportation in Türkiye (Article 5), the Law Number 6704 on Amending Certain Laws and Decree Laws (Article 8), the Agricultural Reform Law Number 3038 on Land Arrangement in Irrigation Areas. Although

certain authorities are entitled to make expropriation by law, it is often stated in relevant legal regulations that appraisal procedures for the real estate to be expropriated shall be realized as per the provision of the Law Number 2942 [7-13].

Since highways is large public projects, the expropriation of the property needed by a relevant institution costs a lot. Acquisition of land by expropriation is widely used in Türkiye. Although the principle of payment in advance is based on the actual value as per the 1924 Constitution, expropriation is implemented based on tax value using certain laws in some cases. In accordance with the Law Number 2942 amended by the Law Number 4650 in force, expropriation is ensured to be realized based on fair value [14-19].

2. Method

2.1. Optimization of the costs of highway expropriation projects

Türkiye's surface area is 814,578 km² and the projection area is 780,580 km². The difference between the projection area and the actual area is due to the widespread mountainous areas in Türkiye. Of the total surface area of Türkiye, 98.3% is land and 1.3% is water surface (DPT, 2006). According to the summary of agricultural statistics published by the Turkish Statistical Institute (TUIK) in 2009, of the total land size, 35.1% is used as forestland, 27.3% as arable area, 24.2% as meadow and pasture area, 7.1% as fallow land, 4.9% as fruit garden, olive garden and vineyard, and 1.4% as vegetable garden. In Türkiye, the General Directorate of Highways is the investor institution that needs the highest amount of land.

The total expenditure and expropriation amount of the General Directorate of Highways increase each year in proportion. No data is obtained from other institutions with regards to expropriation. Expropriation and total expenditure of the General Directorate of Highways are shown in Figure 1.

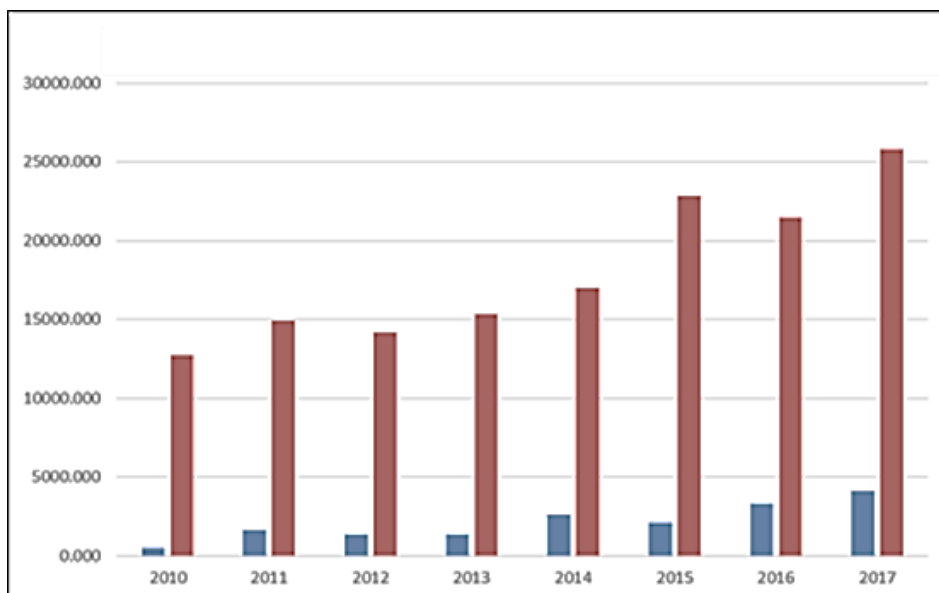


Figure 1. The expropriation costs of the General Directorate of Highways [20].

The expropriation burden of the General Directorate of Highways increases each year. In 2017, the cost of such burden was 4.122.011.000 Turkish Liras. This burden can be opened to the public with development plan implementation and land consolidation, which are among the methods of transfer of land to the public. For the real estate intersected by the routes of public investments, if land and land lots are arranged in accordance with the Article 18 of the Development Law Number 3194, the total area of the cadastral parcel intersected by the implementation area will be [CPA]= 43611.82 m². If the total area of the building blocks in the land arrangement area is [BBA]=26167.09 m², the area reserved for the public will be [ARP]= 17444.73 m². When the Development Readjustment Share (DRP) is calculated for the selected area, DRP is found to be 45% ($DRP=[ARP]/[BBA] = 45\%$). Hence, the expropriated area is maximized and the cost of expropriation is minimized. The related institution bears the costs during the implementation. In a selected readjustment area, there may be areas that are reserved for public services such as roads, squares, parks, public car parks, and green

fields, areas that are not subjected to registration, and areas that are reserved for mosques, police stations, primary and secondary schools under the Ministry of National Education and related facilities. Lands on a route where large public projects are to be carried out can be opened to the public free of charge with development plan implementation in improvement areas other than motorways and with land consolidation in rural areas with no development plan. Withholding up to 10% may be imposed for land consolidation areas. In these areas, it is necessary to make amendments to legislations on land consolidation for opening areas as part of highway projects. In Germany, motorway companies purchase lands in different areas and turn them into land route by implementing land consolidation. It will be possible to transfer areas belonging to the State Treasury in land consolidation areas to the areas planned as a road. As seen in Figure 2, the areas behind the land arrangement are expropriated with minimum cost, i.e. the cost only comprise the cost of the implementation [3, 8,15-19].



Figure 2. Parcel plan on the highway route (red line).

2.2. Public interest in the expropriation process

Expropriation should be made for public interest. The concept of public interest is addressed under a separate title in the 1982 Constitution Act of Türkiye. The purpose of expropriation shall be for the public interest as per the Constitutional Court Decisions. According to the principle highlighting “public interest” as a basic factor, expropriation is defined as “revoking the right of property on an immovable by the administration for

public interest, provided that its equivalent is paid”. As per another definition, expropriation is the dispossession of an immovable for public interest regardless of the owner’s consent, provided that its appraised equivalent is paid. In other words, expropriation is a restriction imposed on the right of private property or abolishing the authorities entitled to the state and the right of private property to protect the public interest and provide public services. However; such authority may be used by the state for the interest of state institutions and

organizations or of private enterprises separately within the framework of conditions and procedures determined by law undoubtedly (decision dated 22.09.1993 (Basis No. 1993/8, Decree No. 1993/31)).

The first paragraph of the Article 46 of the Constitution Act of Türkiye states that government officials and public legal entities are entitled to make expropriation for public interest if applicable. Therefore, the purpose of expropriation is based on the concept of “public interest” [14]. In other words, the administration may only make expropriation for public interest. Unless required for the public interest, it shall be illegal for the administration to carry out an expropriation procedure in terms of its purpose [14].

The decision-making authority that decides where and what the public interest belongs to is the “legislative organ”. In case of conflict, authority to decide “what the public interest is” by interpreting principles and rules belongs to the “judicial organ”. Today, administrations are entitled to make expropriation only “for the public

interest” without any additional condition in accordance with the Article 1 of the Expropriation Law Number 2942 and Article 46 of the Constitution Act of Türkiye. Thus, it can be concluded that the concept of public interest is broadened. It can be said that the Article 3 of the Expropriation Law includes provisions suitable to define the concept of public interest and set its framework. According to this article, public interest as the prerequisite for expropriation shall be a benefit to be obtained by establishing and maintaining public services and enterprises since administrations are able to expropriate real estate required to maintain public services or enterprises that they are legally obliged to provide [20]. Expropriation is not always required for projects for the public interest. Figure 3 shows Google Earth image of the route opened to the public by Trabzon Municipality and the General Directorate of Highways with development plan implementation by signing a protocol and paying implementation expenses only.



Figure 3. Highway route of Çimenli Mahallesi, Ortahisar, Trabzon (Türkiye).

Development plans and projects approved by the relevant ministry are among the documentations that serves to public interest. Plans are listed in the Article 6 of the Development Law Number 3194. These plans start with Spatial Strategic Planning and end with implementation development plans. Spatial planning consists of “Environmental Plans” and “Development Plans” in terms of its purpose and scope in accordance with the Spatial Strategic Planning. Development plans are prepared as a master development plan and an implementation development plan. Each plan is prepared in conformity with the plan of the next stage. In spatial strategic planning, objectives put forth in the development plan and if any, regional planning, regional development strategies, and other strategic documentation are taken into consideration. Implementation of the city development plans upon

acceptance or approval, and land and land lot owners’ power to use and benefit are restricted by the public interest. The Article 6 of the Expropriation Law brings a special arrangement for expropriation implementations to be made as per development plans. Accordingly, it is not necessary to obtain the decision of public interest for services to be provided as per the approved development plan or special plan and project approved by relevant ministries. In such cases, the competent authority makes a decision to prove the expropriation process is commenced. Development plans are for public interest in expropriations to be made by municipalities for the development plan implementation and those to be made for public services to be established and operated by municipalities and other public legal entities. Commitment to development plan is essential to expropriation based on a development plan [21-22]. In

accordance with the Expropriation Law Number 2942, plans and projects approved by ministries are for the public interest by decision. As it is known that when it comes to certain investments of the State and certain state institutions and organizations that are economically and socially significant at the country level, investment decisions are made in accordance with the special plan and projects approved by the relevant ministry. For example, as is in the case of building a dam and irrigation, highway, railway or port.

2.3. Expropriation appraisal and the right of property

Appraisal of real estate; the criteria to be taken into consideration for the expropriation appraisal is listed in the Expropriation Law Number 2942 and Article 11 of the Law on Amending the Expropriation Law. In paragraph (f) under the same article, an appraisal is foreseen to be realized based on the "net income brought by the land, immovable or equity depending on its status and condition on the date of expropriation and in case it is used as is". Since the subject is broad, it is deemed suitable to make a short evaluation here.

Appraisal of lands: land is a building land whose substructure is set up for planning and that is invested with the development right for the superstructure. In accordance with the Real Estate Tax Law Number 1319, land lots that are parceled by the municipality within the municipal boundaries are regarded as land. For land lots that are not parceled regardless whether it is within the municipal boundaries, which ones to be regarded as land is determined by the decision of the Council of Ministers. According to the Decision Number 83/6122 on the Lands That Are Not Parceled to Be Regarded as a Land; lands and land pieces;

a) that are located in the areas assigned as a residential area with development plan within municipal and urban area boundaries,

b) that are not located in the area assigned as a residential area with such development plan but are within municipal and urban area boundaries, occupied,

utilizing municipal services and not parceled, are regarded as a land. However, lands and land pieces in such areas are not regarded as a land if used for agricultural activity.

c) that are parceled by any means for establishing a residential building or a touristic or industrial facility and affixed hereby as an addendum to the title deed but are not within municipal and urban area boundaries,

d) that are located in the areas assigned as a residential area with development plan within the boundaries determined by the decision of the Council of Ministers due to its location near or around the sea, rivers, lakes and transportation, or its industrial or touristic significance or because of fast urbanization activities, and upon the proposal by the Ministry of Development and Housing but are not within municipal and urban area boundaries, are regarded as a land.

According to this decision, lands and land pieces in such areas are basically declared as per their current value. In accordance with the Expropriation Law Number 4650, an immovable can only be regarded as a land if it is in the development plan on the date of expropriation. If it is within the municipal and urban area boundaries but not in the development plan, it shall be utilizing all public services and its surroundings shall be residential [17]. Appraisal of land can often be determined by direct comparison with similar lands whose real sales values are known. For such appraisal, real values of precedent lands that are similar in miscellaneous qualities shall be known and average purchase and sale value shall be calculated based on precedent values. During such comparison, all quality elements affecting the value shall be taken into consideration such as location and type of land, the physical structure of soil and the road it is located on, road and street widths, and restrictive arrangements imposed under the development plan. It is often difficult to find a precedent immovable for the appraisal of an immovable on the route to be expropriated. Sometimes, this becomes a case taken to the European Court of Human Rights (ECHR). Annual distribution of right of property infringement cases taken to the ECHR by years is as follows (Figure 4).

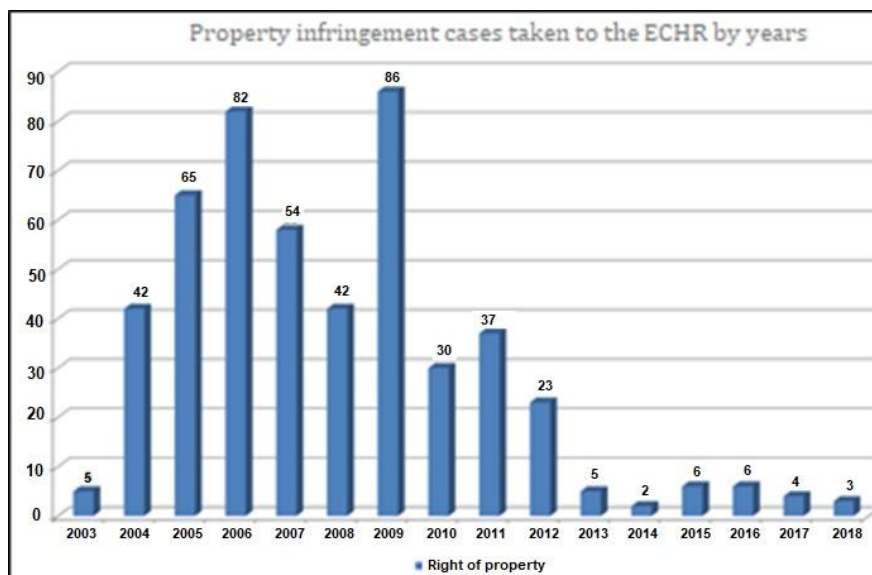


Figure 4. Annual distribution of right of property infringement cases taken to the ECHR by years [22].

Most cases taken to the ECHR are related to the procedure, approach and values determined by the price determination commission. For eliminating these issues caused by the vulnerability within the legal framework of expropriation procedure, amendments were made to the Expropriation Law Number 2942 by the Law Number 4650 in 2001. Amendments made in 2001 is a milestone in terms of broadening the area of freedom given to individuals related to such procedure under the Expropriation Law [10]. Citizens claim their rights by considering the long judicial process taken to the ECHR with the thought that they suffer from forfeiture due to state practices. During this process, citizens confront the state, and such confrontation decreases reliance on the state. The amount of compensation to be paid becomes more of an issue in the expropriation procedure, which is an intervention on the right of property. Since the first paragraph of the Article 1 of Protocol 1 under the European Convention on Human Rights does not mention compensation at all, it is not possible and right to conclude that this provision requires full compensation for expropriation. For the compensation, the superior should be favored as a result of comparing public interest in the expropriation and individual interest related to the protection of the right of property [23]. Since dispossession occurs where expropriation is realized, overburdening the individual should particularly be avoided. Together with the legal regulations made in Türkiye in accordance with the verdicts of conviction by the ECHR, a decrease is observed in the number of cases filed. It is also known that the number of cases filed will be decreased by utilizing alternative land reclamation methods instead of expropriation.

3. Results and Discussion

In accordance with the first paragraph of the Article 18 of the Development Law Number 3194, "for lands and land lots with or without building in the boundaries of development, municipalities are entitled to combine them with each other, road oversupply and areas belonging to public institutions or municipalities, divide them into plots or parcels as per re-development plan, distribute them to beneficiaries as per single, shared or flat ownership basis, and have their registration procedures done ex officio regardless of the consent by owners and other beneficiaries. If such areas are not within municipal and urban area boundaries, above mentioned authorities are exercised by the governorship". The authority belongs to the governorship or municipalities as per the relevant provision. Development readjustment share is deducted as a legal tax or tax in kind from the real estate subjected to the arrangement in reply to the increasing value in development plan implementations. By this way, public spaces mentioned in the law is transferred to the public free of charge. However, it is also a rule that all the parcels subjected to the arrangement are eligible for single building plot as much as possible. During the distribution of lands and land lots subjected to the arrangement by municipalities or governorships,

sufficient area may be deducted from their surfaces as "development readjustment share" in reply to the increasing value due to the arrangement. However, development readjustment shares to be deducted as per this article cannot exceed forty-five percent of the surface of lands and land lots subjected to arrangement (before the arrangement) (Amended paragraph 3: Article 3/12/2003-5006/1). Development readjustment shares cannot be used for purposes other than public services needed to be established in the areas subjected to arrangement such as primary and secondary schools under the Ministry of National Education, roads, access-controlled highways other than motorways, waterways, squares, parks, car parks, playgrounds, green fields, prayer halls, and police stations and facilities for such services (Two additional sentences: Article 19/4/2018-7139/32). It is essential to compensate flood control facility areas within the area subjected to the arrangement from the remaining areas owned by the State Treasury subsequent to deduction of development readjustment share for purposes stated in this paragraph [24-26]. However, if failed to be assign sufficient area for flood control facility, from the surfaces of lands and land lots subjected to arrangement, additional share is assigned for flood control facility up to the percentage stated in the second paragraph after development readjustment share is assigned for purposes stated in this paragraph, provided that the development readjustment share does not exceed the percentage stated in the second paragraph.

Development Readjustment Share is defined in the Article 4 of the Regulation on Principles Related to Land and Land Lot Arrangement to be Made as Per the Article 18 of the Development Law. Accordingly, the value is the amount that can be decreased up to 35% from the surfaces or lands and land lots subjected to arrangement (before the arrangement) and/or the equivalent determined with the consent of the owner in case of unavoidable circumstances, provided that it is to be used for areas assigned to public services needed to be established in the areas subjected to the arrangement such as roads, squares, parks, green fields, and public car parks and not subjected to registration, and mosques, police stations and relevant facilities. The inclusion of real estate subjected to arrangement into public service areas required by the building plots established may be up to 35% at most. However, this percentage was increased to forty-five percent (45%) in accordance with the Article 1 of the "Law on Amending One of the Articles Under the Development Law Number 6785 and Certain Procedures to be Adopted on Structures Incongruent to the Development Law and Development and Anti-squat Law" Dated 03.12.2003 and Number 5006, which was published in the Official Gazette Dated 17.12.2009 and Number 25319.

Works for opening road developments to the public based on the implementation under the Article 18 of the Law Number 3194 are carried out by the General Directorate of Highways under the Ministry of Transportation and Infrastructure. The very first example of such work was the protocol dated 11.07.2006 and Number 10/3015 signed between the General

Directorate of Highways and Datça Municipality. Implementation of the Article 18 on the 80-hectare area within the boundaries of Datça Municipality was given out by contract and the procedure was accomplished with all title deed registrations done. Implementation of the Article 18 of the Development Law Number 3194 and Articles of Annex 1 of the Law Number 2981/3290 was realized for opening the North ring road upon the engagement dated 11.08.2006 and Number 2006/30-3 contracted between Kayseri-Erkilet Municipality and the General Directorate of Highways. Adana-Karataş Double Highway was opened to the public with the implementation of the Article 18 within the framework of the Contingency Plan upon the protocol signed. For opening the road within the region with the implementation of the Article 18 of the Development Law Number 3194, a protocol was signed between the 10th Regional Directorate of Highways and Trabzon Municipality on 10.03.2010. Trabzon Municipality accepted the implementation on the condition that the implementation expenses were paid by the General Directorate of Highways. Due to the protocols signed, the administration was relieved of expropriation expenses. Upon the protocol signed between Antalya Metropolitan Municipality and the 13th Regional Directorate of Highways on 28.08.2015, airport intersection between Antalya and Aksu was opened to the public with the implementation of the Article 18 of the Expropriation Law Number 3194. The General Directorate of Highways under the ministry of Transportation published the Internal Memorandum dated 12.09.2007 and Number 2007/101. This memorandum discusses the importance of development plan implementation. It is highlighted that the internal memorandum should pioneer in solving certain environmental issues. It is stated that favoring development implementation over expropriation for ring roads and city crossings will facilitate the development of infrastructure in the cities easily and properly.

The Article 18 of the Development Law Number 3194 was updated with the Article 9 of the Law Number 6704 by adding the expression “access-controlled highways other than motorways, waterways” following the term “road” in the paragraph. With such amendment, development readjustment share is ensured to be met for the route where the Canal Istanbul (Kanal İstanbul) project passes through. First, development plan works were accomplished within the region. Afterwards, a 45% deduction was made from the real estate. Thus, it was ensured that the rest was assigned as a building plot. It is possible to set up parcels whose agricultural quality is protected by the development plan decision.

In accordance with the Article 6 of the Agricultural Reform Law Number 3083 on Land Consolidation in Irrigated Areas, land consolidation is defined as follows: “To fulfill the objectives stated in this law, land consolidation may be realized by the relevant institution on demand or regardless of the consent by owners”. Supportive measures may be taken by the relevant institution to expand land and to benefit more from credit facilities for encouraging land consolidation provided that priority is given to those on demand.

(Additional paragraph: Article 1 of the Decision Dated 23/02/2001 and Number 4626) In consolidation areas, depending on the project type, a share up to 10% is deducted from the land belonging to real persons and public and private legal entities for the area to be commonly used by the public such as a road or canal. Roads closed due to consolidation and road oversupplies are also used for the same purpose [24-31]. No price is paid for share. However, the land deducted other than the share is compensated from the equivalent area owned by the State Treasury if applicable. If this is not sufficient, then expropriation procedure is implemented for the area required. Transfer of land and land lots to the public is ensured with land consolidation.

4. Conclusion

Expropriation is widely used in Türkiye for introducing highway projects into the society. Public institutions and organizations are able to make expropriation on subjects restricted by law. In what situations and by which institutions the expropriation authority is exercised are restricted by law. In accordance with the Article 3 of the Expropriation Law Number 2942 amended by the Law Number 4650, the expropriation process shall not be started without an adequate allowance provided by the administration. Thus, the land and land lots needed by the public should be obtained by means of different implementations other than expropriation. Restricting the right of property for another public service cannot be against public interest. Expropriation can only be commenced with the decision of public utilities and processing highway projects in the improvement site into 1/5000 scaled Master Development plans and 1/1000 scaled implementation development plan. Road development can be opened to the public free of charge with the application of the provisions in the Article 18 of the Development Law Number 3194 ex officio for the area where the highway would pass in an urban area. In the cost optimization of the highway routes with the selected arrangement areas, maximum area is expropriated with minimum implementation cost. The deduction is lower if the public area in the planned area is small. If land and land lots are arranged in accordance with the Article 18 of the Development Law Number 3194 between the General Directorate of Highways under the Ministry of Transportation and Infrastructure and municipalities, these lands are ensured to be transferred to the public free of charge by imposing state withholding up to 45%.

Expropriation expenses of highway projects for public place excessive burden onto institutions. Necessary lands may be opened to the public by means of development implementations, provided that amendments for the implementation are made to a certain law. The best example to the above-mentioned situation was the inclusion of roads other than motorways under the responsibility of the Institution of Highways into the scope of development readjustment share in accordance with the 6th paragraph of Article 19 of the Law Number 6001 on the Organization and Duties of the General Directorate of Highways. In this sense,

these areas are ensured to be converted into the public property with the implementation of the Article 18 of the Development Law Number 3194 after development plans for the land route are prepared. For project areas intersected by a private property, areas intersected by highway and waterway routes can be transferred to the public with the implementation of the Article 18 of the Development Law Number 3194 and the Agricultural Reform Law Number 3038 on Land Arrangement in Irrigation Areas and relevant provisions. Land acquisition increases as the ratio of state withholding increases, resulting in the minimization of the expropriation costs. Public projects such as highway can be opened to public free of charge with development plan implementation in improvement areas and with land consolidation in rural areas having no development plan.

Conflicts of interest

The authors declare no conflicts of interest.

References

- Pellicani, R., Koç, K., & Özler, V. (2009). Kamulaştırmada Taşınmaz Değerlemesi ve Karayolları Genel Müdürlüğü Uygulamaları, Karayolları Genel Müdürlüğü, Ankara.
- Çelik, K. & Aşık, Y. (2004). Emlak Vergisi Değerinin Piyasa Koşullarına Göre Belirlenmesi, Mülkiyet Dergisi, 52, 15-19
- Cay, T., & Iscan, F. (2006). Optimization in land consolidation. XXIII FIG Congress, Munich, Germany, 1, 11.
- Çelik, K. (2006). Planlama ve imar kanunu uygulaması arazi ve arsa düzenlemesi. Devran Matbaacılık, Ankara.
- Alkan, M., & Polat, Z. A. (2021). Lisans ve lisansüstü düzeyinde verilen taşınmaz değerlendirme eğitiminin değerlendirilmesi. Geomatik, 6(1), 15-30. <https://doi.org/10.29128/geomatik.650766>
- Ünel, F. B., & Yalpir, Ş. (2019). Türkiye’de taşınmazların değerini etkileyen kriterlere yaklaşım. Geomatik, 4(2), 112-133. <https://doi.org/10.29128/geomatik.499681>
- Yomralioğlu, T., Inan, H. I., Aydinoglu, A. C., & Uzun, B. (2009). Evaluation of initiatives for spatial information system to support Turkish agriculture policy. Scientific Research and Essay, 4(12), 1523-1530.
- Dale, P., & McLaughlin, J. (2000). Land administration. Oxford University Press.
- Uzun, B. (2000). Çevre yolu-mülkiyet ilişkilerinin imar hakları açısından incelenmesi ve arazi düzenlemesi yaklaşımıyla bir model önerisi. [Doctoral dissertation, Karadeniz Technical University]
- Evren, N. (2012). Türkiye’de kamulaştırma çalışmaları için alternatif yaklaşımlar. [Doctoral dissertation, Selçuk University].
- Ertaş, M. (2019). Education for real estate valuation in Turkey. International Journal of Engineering and Geosciences, 4(1), 8-15. <https://doi.org/10.26833/ijeg.416336>
- Yalpir, Ş., & Ünel, F. B. (2022). Multivariate statistical analysis application to determine factors affecting the parcel value to be used mass real estate valuation approaches. International Journal of Engineering and Geosciences, 7(1), 32-42. <https://doi.org/10.26833/ijeg.862563>
- Unel, F. B., Yalpir, S., & Gulnar, B. (2017). Preference changes depending on age groups of criteria affecting the real estate value. International Journal of Engineering and Geosciences, 2(2), 41-51. <https://doi.org/10.26833/ijeg.297271>
- Gözler, K. (2003). İdare Hukuku, Ekin Kitabevi, Bursa.
- Haklı, H., 2017, Arazi Toplulaştırma İçin Optimizasyon Tabanlı Yeni Bir Dağıtım Ve Parselasyon Modelinin Geliştirilmesi, [Doctoral dissertation, Selçuk University]
- Hartvigsen, M. (2006). Land Consolidation under the new EU Rural Development Programme 2007-13
- Tanrıvermiş, H. (2004). Arsa-Arazi Ayrımında Kriterler ve Değerleme İşlemleri, ANKÜSEM Kamulaştırma, Değerleme ve Bilirkişilik Eğitim Programı (Sertifikalı), Ocak-Nisan 2004, Ankara
- Yomralioğlu, T. (1992). Arsa ve arazi düzenlemesi için yeni bir uygulama şekli. Harita ve Kadastro Mühendisleri Odası Yayın Organı, (73), 30-43.
- Tüdeş, T. (1992). Türkiye’de imar planı uygulama yöntemleri. İmar Planlarının Uygulanması Semineri, 9-20
- <https://www.kgm.gov.tr/Sayfalar/KGM/SiteTr/Istatistikler/DevletvellYolEnvanteri.aspx>
- Seele, W. (1982). Land readjustment in the Federal Republic of Germany. Land Readjustment, DC Health and Co., Lexingtons, Mass.
- <http://www.inhak.adalet.gov.tr/istatistik/2018/2018istatistikler.html>
- Berberoğlu, A. (2004). Avrupa İnsan Hakları Mahkemesi Kararları Işığında Kamulaştırma Kavramı ve Türkiye Uygulaması. [Master’s thesis, Gazi University]
- Karakayacı, O., & Karakayacı, Z. (2012). Kentsel saçaklanma alanlarında arsa/arazi değerini belirlemeye yönelik yöntem önerisi. The Journal of Academic Social Science Studies, 5(4), 107-120. http://dx.doi.org/10.9761/jass_98
- He, Z., & Asami, Y. (2014). How do landowners price their lands during land expropriation and the motives behind it: An explanation from a WTA/WTP experiment in central Beijing. Urban Studies, 51(2), 412-427. <https://doi.org/10.1177/00420980134922>
- Sert, A. (2005). Kamulaştırma Amaçlı Arazi Toplulaştırma. [Master’s thesis, Yıldız Technical University]
- Yirsaw Alemu, B. (2013). Expropriation, valuation and compensation practice in Ethiopia: The case of Bahir Dar city and surrounding. Property Management, 31(2), 132-158. <https://doi.org/10.1108/02637471311309436>

28. Yomralioglu, T., Uzun, B., & Nisanci, R. (2008). Land valuation issues of expropriation applications in Turkey. *Land Reform*, 1, 80-90.
29. Schnidman, F. (1988). Land readjustment: an alternative to development exactions. *Private supply of public services*, 73-87.
30. Koroğlu, Ö. (1995). *Kamulaştırma*. Seçkin Yayınevi, Ankara.
31. Ayten, T. (2015). *Kamulaştırma amaçlı arazi toplulaştırması*. [Master's thesis, Selçuk University]



© Author(s) 2024. This work is distributed under <https://creativecommons.org/licenses/by-sa/4.0/>



Python-based evaluation of road network constraints for electric scooters and bicycles: Izmit Example

Ahmet Şirin ^{*1}, Arzu Erener ¹

¹ Kocaeli University, Graduate School of Natural and Applied Sciences, Geodesy and Geoinformation Engineering, Türkiye, srnahmet98@gmail.com, arzu.erenner@kocaeli.edu.tr

Cite this study:

Şirin, A., & Erener, A. (2024). Python-based evaluation of road network constraints for electric scooters and bicycles: Izmit Example. *International Journal of Engineering and Geosciences*, 9(1), 34-48

<https://doi.org/10.26833/ijeg.1261677>

Keywords

GIS
Python
Network Analysis
Shortest Path
Electric Scooter

Research Article

Received:07.03.2023
Revised: 21.04.2023
Accepted:26.04.2023
Published:02.01.2024



Abstract

Means of transportation are a large part of our daily life. Along with the development of technology, we encounter different types of vehicles, but we also encounter different problems. For electric scooters, which are one of the new types of vehicles that are seen to be used in vehicle traffic, it seems that there are question marks among the public about the use of vehicles and the rules. It is seen that the legal regulations and rules in this field are not sufficiently standardized in Türkiye yet. Among these question marks, safety, comfort, and vehicle characteristics draw attention to which roads electric scooters should choose during their use. In the research, various applications and examinations were made on the parameters of the slope, road class, length of the road, and land cover, among the parameters considered in the optimal road preferences for electric scooters, where there is a starting point and an ending point. For the research, Dijkstra's Algorithm, QGIS GIS software, python programming language, and various modules were used to use the shortest path problem, cost calculations, and various data processing methods. These applications were compared within the Work titles and the effects of different parameters on the optimal route preferences were compared and discussed. The results of the research were discussed in terms of relevance, and it was determined what improvements could be added and what effects it could have on other research that could be done on this subject. As a result, it has been seen that the parameters in the research directly affect the results in the applications in different works, bringing diversity, and the expected results achieved. It has been determined that the addition of additional parameters such as the maximum distance or time that can be traveled for vehicles such as electric scooters, and the use of more sensitive and various sources will further develop this research and its importance in this type of research.

1. Introduction

The shortest path problems, which have a place in daily life and people often create their own solutions or get solutions through various applications, turn into the optimal path problems as a result of taking into account different environmental parameters. For the solution of the shortest path problem among the roads with different distances, it is a correct solution to choose the path with the shorter distance compared to the others, but this is more complicated for the optimal path problems. For example, considering the traffic density values on the road, the shortest distance road may not be the most suitable way for a vehicle to pass through the

traffic. Such different parameters depend on whether the roads will be covered without vehicles or with which type of vehicles in the problem, but also the importance of the parameters in the optimal path problem may vary according to environmental factors.

With the development of technology, vehicles such as electric scooters and electric bicycles have begun to settle in people's daily lives. In times when the use of motor vehicles using the main roads is increasing day by day, people see electric scooters as an alternative that does not suffer from traffic problems or can be used as an entertainment activity. The most suitable path for a vehicle is always seen as a problem to be solved. For this

reason, the necessity of conducting exemplary research and applications on this problem for these new vehicles of different types that can go into traffic has emerged.

Unfortunate accidents occur because new and technological vehicles such as electric scooters are not fully integrated into daily life and therefore citizens are not used to seeing these vehicles in traffic. Which paths are suitable for these vehicles physically and in terms of security is important for optimal path applications.

Shortest Path problems are one of the most popular problems encountered in Network analysis, which consists of nodes associated with each other through edges and used in decision-making studies, and on which algorithms have been developed. These problems are encountered in many areas such as navigation devices, network systems, and vehicle route calculations [1]. For this reason, various algorithms have been developed for the solutions to these problems, which also take into account special conditions. The most popular among these algorithms is Dijkstra's Algorithm with positively weighted edges. Dijkstra algorithm, which is used to find the shortest (costly) path between two nodes in a network consisting of nodes and edges, reaches the shortest path result by comparing the costs of all possible paths between two nodes. Dijkstra's algorithm can only work on positively weighted edges. Although it gives a fast and precise result compared to algorithms such as Bellman-Ford, which is another shortest path problem solution algorithm that can work with negatively weighted edges, it is more costly in terms of working compared to heuristic algorithms [2].

A road network consists of many nodes connected to each other via edges. Some nodes can play more important roles in the network due to their centrality [3]. Many algorithms have been developed on complex road networks from the past to the present. Reasons such as separating the application according to different types and purposes and considering the time used for problem solving can be given as the reason why there are so many algorithms [4]. Different optimization methods can be followed as a result of additional problems such as data size and branching of the data within itself.

Research and studies are carried out by using spatial information within the scope of Geographic Information Systems (GIS), which deals with spatial information, in various analyzes and models [5]. Many studies such as best fit site analysis, seasonal productivity of agricultural land, disaster risk research, spatial relations, and statistics can be given as examples of these research and studies [6]. In this research, GIS is used to solve the shortest path problems encountered in the use of road networks, road geometries, and attribute information, which are geographical data sources, in the use of electric vehicles such as electric scooters.

Any individual can contribute to the OpenStreetMap (OSM) mapping project, where volunteer-based open-source data is produced [7]. OSM data, which is available completely free of charge, is licensed under the Open Database License [8]. With the update coming in 2022, it now also includes forwarding services. Through this development, it can be seen that a topological relationship (road network) can be created between the

road geometries in the OSM data. While OSM creates the node and edge relations that may be necessary for a network analysis within its own road data, it also includes important information such as the length of the road it represents, the speed and information for the vehicles, and the characteristics of the road into the related road (edge) geometry data [9].

With the development of technology day by day, GIS research and applications are becoming more widespread and their diversity is increasing. Various GIS software and programming languages are used in these studies. Among the popular examples of these software are QGIS and ArcGIS software. As they have a python programming language script, they can be written with plugins [10]. Such features also increase the use of the python programming language on GIS.

Python, an object-oriented programming language, was introduced by Guido van Rossum in 1980 [11]. Today, it is popularly used in many areas such as web applications, artificial intelligence studies, and database software programming. In addition to being easy to use thanks to its simple syntax, one of the reasons for its high usage is that it has many highly functional libraries that can be loaded into it [12]. Libraries such as Pandas, GeoPandas, NetworkX, and OSMnx can be given as examples of important python libraries to be used in the research.

The Pandas module, which allows the data to be used practically, quickly, and efficiently, is used quite frequently today, especially in the field of data science [13]. The GeoPandas module, on the other hand, includes the Pandas module and offers the opportunity to work with spatial data in addition to the capabilities of the Pandas module [14].

NetworkX module is a powerful module that can be used for network analysis and manipulation of network graphs [15]. It has various functions such as shortest path problem algorithms in itself. OSMnx is a python module that enables network analysis like the NetworkX module by using the spatial data provided by OSM. It allows for downloading OSM data, modeling road-street data, creating relationships, analyzing, visualizing, and many other spatial analyzes [16].

In the research, in which the suitability of agricultural crops for land consolidation areas was examined, multi-criteria decision analyses were made by using GIS techniques [17].

In the research where the least cost road algorithm designs for highway route selection were investigated, the effects and results of multiple costs on route calculations were analyzed [18].

In the research using geographic information systems to evaluate accessible forest areas using the Analytic hierarchy process, which is a multi-criteria decision-making method of firefighters, road network and road transportation analyses of firefighters were examined [19].

In the research, that determined the transportation networks that will form the basis of the most appropriate public transportation policy, it was seen that the spatial network analysis techniques of GIS were used [20].

In the research in which Dijkstra and Bellman-Ford shortest path algorithms are compared, it is seen that Dijkstra algorithm gives more precise and invariant results than Bellman-Ford algorithm [21].

In the research in which the GIS-based shortest transportation route is determined, it is seen that the stations on the shortest route are determined with the Dijkstra algorithm using the python programming language [22].

In research, it is seen that Dijkstra's Algorithm is used in the solution of the vehicle routing problem for examining the shortest paths between solid wastes. It was concluded that the Dijkstra algorithm gave a successful result in the shortest path applications made on the graph model created with the topological relations in the road networks [23].

In the research, in which optimal routes for bicycles are examined by considering different attributes other than length, attributes are used in the shortest path algorithm, taking into account different costs. In addition, it has been pointed out that the changes made in the costs with the applications with different combinations and the changes in the optimal cycling routes [24].

In this research, transportation restrictions for two-wheeled vehicles such as electric scooters and bicycles will be examined by using the Dijkstra algorithm, which is one of the most popular shortest path problem solution algorithms, taking into account different costs. Within the scope of the research, besides the python programming language and various modules it contains, GIS software such as QGIS was also used. Obtaining and manipulating the data, associating the data both within themselves and with each other, the shortest path applications on the created topological road network will be mentioned and the results will be discussed. It has been observed that there are not many studies dealing with this issue, especially today when electric vehicles

are becoming more widespread day by day. It is foreseen that the analyzes and examinations to be made within the scope of the research can be handled in other more detailed and comprehensive studies and this research will be beneficial. Since there is no standard weight comparison of the cost indexes among the shortest path applications to be made, it is planned to bring richness to the research with the diversity of the applications made with different cost indices and weight values. The aim of the research is to support the applications that refer to this research with examples and detailed analysis and result comparisons rather than standardizing the cost indices and the weight coefficients of the cost indices on each other in this area. There is not enough research in the literature dealing with these topics. Plynning's research [24] has been one of the rare reference applications for the methodology of the research.

2. Material and Method

2.1. Study Area and Data

Izmit district, which is the central district of Kocaeli province, was chosen as the study area. Due to the importance of slope information in the applications to be made, the rough structure of the land in the Izmit region is taken into account. At the same time, the diversity of land use and the simplicity of road networks in the Izmit region bring convenience to different applications and research. The central coordinates of the İzmit region are known as $40^{\circ} 45' 50''$ N, $29^{\circ} 56' 40''$ E (Figure 1).

Path data is OSM data obtained through OSMnx. During the acquisition of this data, the necessary road network was also established through the module (Table 1). Considering the up-to-dateness and diversity of the datasets for the Izmit district, it has been seen that it can be a suitable dataset for the application.

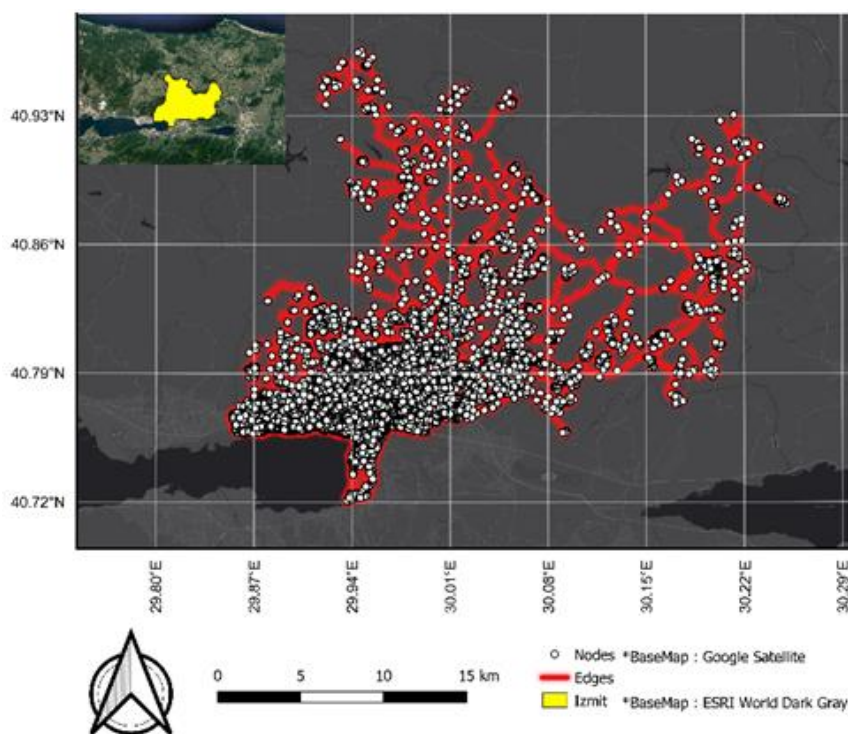


Figure 1. Study area.

Table 1. Data obtained for use in research.

Data	Format	Content	Reason For Use	Source
Road Network Data	Vector (Line)	Path geometry, lengths and classes	Use of road network, path length cost and road class cost	OSM
Elevation	Raster	Elevation values of the area	Generating road slope cost data	[25]
Land Cover	Raster	Land cover in the area	Establishment of land use cost in regions with roads	[26]

2.2. Methodology

With the Dijkstra algorithm, which is a shortest path problem algorithm selected within the scope of the research, applications that provide solutions to optimal road problems based on the shortest path and weight/cost parameters on the road will be made for electric scooter users. In these applications, the main functions for the purpose of the research will be developed with the python programming language and QGIS software will be used for some special cases. During

these applications, OSMnx, NetworkX, Geopandas, and Pandas modules will be used. A topological network will be created with the road geometry data of Izmit, the central district of Kocaeli province. With the created network structure, the effects of different weight/cost parameters on the most appropriate path will be examined within applications, and statistics and reports will be created through applications where different weightings are applied to the parameters in problem solutions and various network analyses.

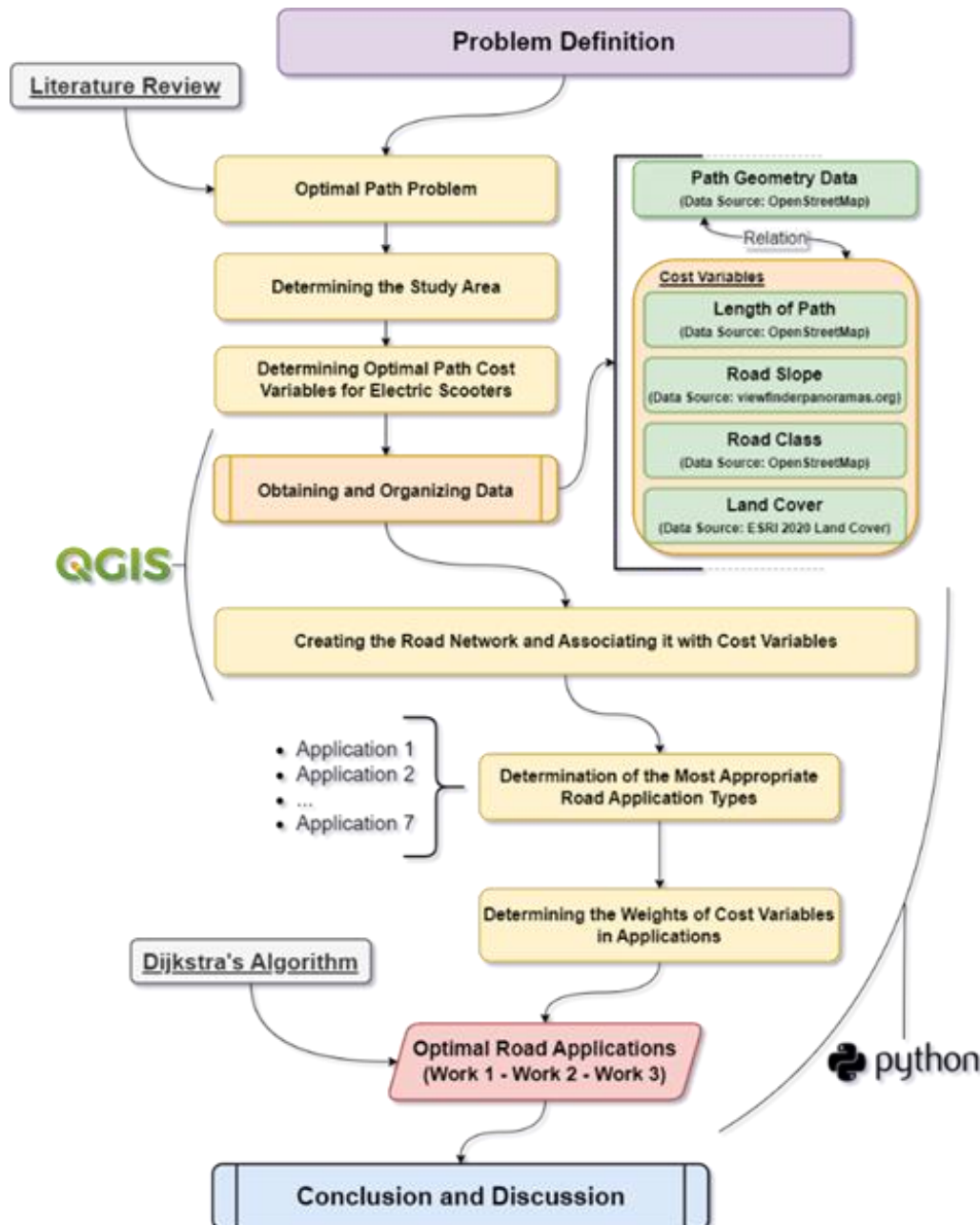


Figure 2. Methodology.

In the first stage, the road data provided by OpenStreetMap was filtered for the Izmit Region. Through the OSMnx module, data can be private with various filters such as pedestrian paths, bicycle paths, and vehicle paths. Within this path data, the necessary topological network is created and prepared in the module. In this way, there is no need to work on the stages of creating a topological network in which the roads will be related to each other. Although the filtering of bicycle paths, which have the closest features to the purpose of the research, was considered appropriate at the beginning, in the examination made on these filtered data, it was determined that some pedestrian bridges where bicycles can use together with pedestrians do not

have road data. With the realization of this detail, the road data in the region were obtained without distinguishing the class, and all the information on the data was classified.

In the analyzes to be made, information such as the length of the road, the class of the road, the slope of the road, and the characteristics of the land where the road is located will be used to calculate the cost of the most suitable road for applications to be made on the road data.

The length values of the road and the road classes (categories) are available as attribute values in the road network obtained from the OSMnx module (Figure 3).

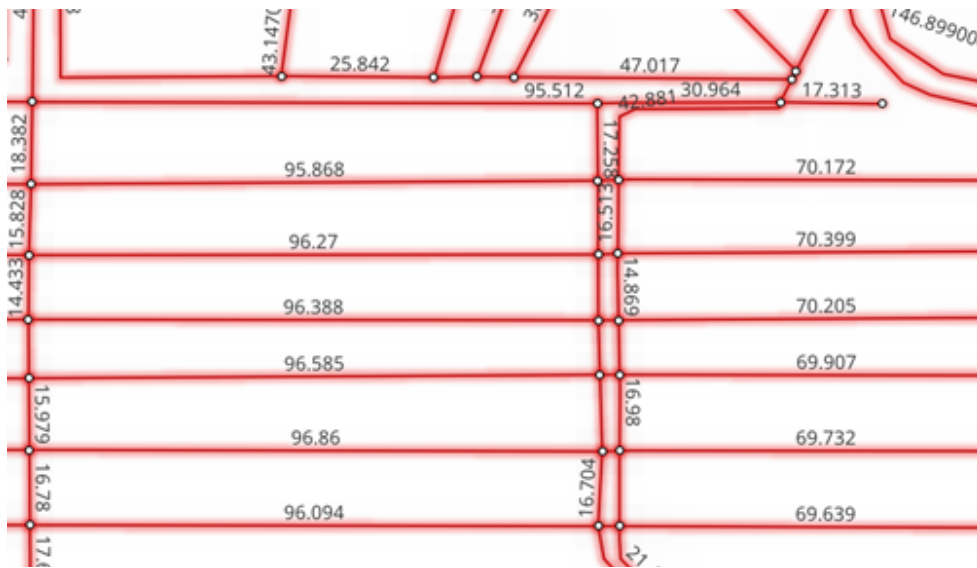


Figure 3. Example region with path length values.

For the slope value of the road, with the help of the raster data obtained from the [25] source, the pixel values of the intersection of the starting and ending node points of the road edges, and the height values — increased through interpolation methods for the resolution of elevation data— were assigned to these nodes. By using these height values and the length data of the road together, the slope value of each road data was calculated. Accuracy sensitivities of the generated slope values are variable. Although the heights at the beginning and end of an edge are helpful in finding the slope between two nodes, they are not helpful in finding the height changes between these two nodes [24]. To increase the accuracy here, more than one point can be

placed on a road line geometry and the slope of the road can be calculated from the height of each point. However, in the sample analyses made on the data, it was observed that the variability in the height changes between two nodes in the road geometries in the Izmit region was mostly unidirectional [26-27]. For this reason, the costs were calculated based on the slope values found only with the heights corresponding to starting points and ending points (Equation 1).

$$slope (\%) = \frac{elevation_2 - elevation_1}{path\ length} * 100 \quad (1)$$

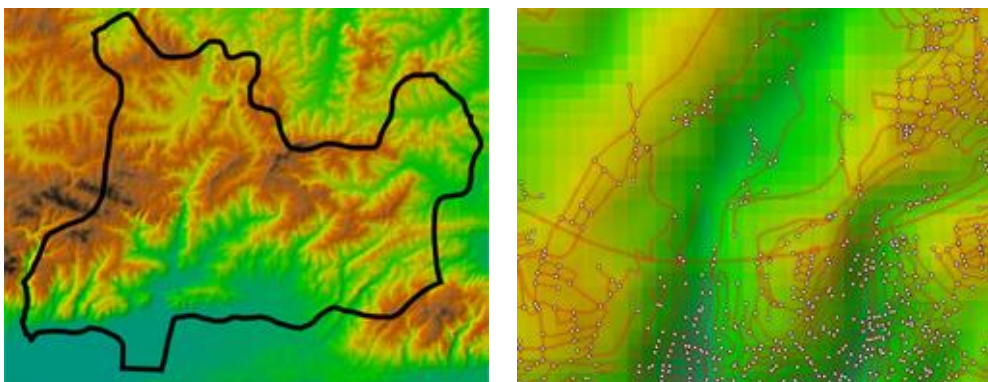


Figure 4. Dem data in Izmit District and road network nodes in a sample region.

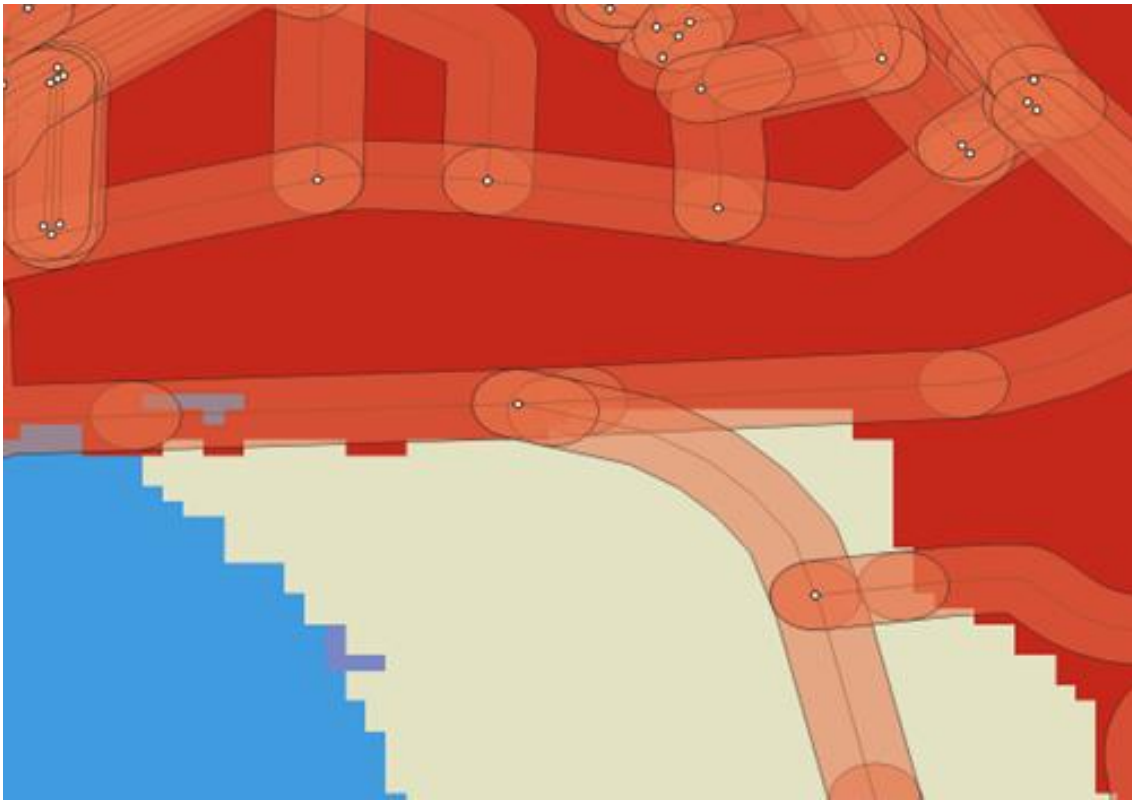


Figure 7. Example study area: Land use raster data and 30-meter buffer zones.

In order for cost indexes to be used in cost calculations, it is necessary to create indexes specific to the applications to be made. The high-cost value of a road in the shortest route application reduces the possibility of that road being preferred over other roads.

The length of the path value is the basic cost index in shortest path applications. It can be used in the application without making any changes to it.

The class of the road cost index plays a role in the drivers' preference for the roads where they can use vehicles such as electric scooters and bicycles more conveniently and safely. In this respect, the costs of road classes such as pedestrian paths and bicycle paths are low in practice. Road classes that represent more neighborhoods and streets are more expensive than pedestrian and bicycle paths. Since the unclassified data in the road data obtained for Izmit are generally similar to the data in this class, this class is also included in the same weight calculation. Main roads used by motor vehicles and considered dangerous for drivers and their derivatives are heavier than other road class weights, except for one exception class. Ladder class road data, which drivers do not have the opportunity to use and which is seen as an exception class, is taken into account as a road class that is almost impossible to be preferred by assigning an extreme value to it. The reason why this road class is not directly removed from the road network is to prevent disconnections within the network. If there is no other choice of road, the driver has to use the stairway by necessity. As a result of the application, it can be noticed whether this road class is used or not, with the extreme value given by the sum of the cost values. Although these calculations are made by considering the research [24], it is aimed to increase the diversity by making some changes to the calculations.

Table 2. Road classes cost indexes.

Road Class Group	Cost Index (NS _i)
Bicycle paths, pedestrian paths, etc.	1
Inner city roads etc.	1.25
Main roads, highway etc.	1.5
Stairs	∞

In the cost index, where the slope of the road is taken into account, the situations where vehicles such as electric scooters and electric bicycles must have a dangerous driving experience on highly inclined ramps, or rough roads or where the vehicle and the driver must rise to a height that they cannot overcome are taken into account. The fact that a road has a high slope both in the down direction and in the up direction reduces the possibility of choosing that road. For this reason, the slope of the road is taken into account by taking its absolute value into the calculation. Since absolute slope values of 10 percent and above are the roads that should not be preferred for an electric scooter/bicycle vehicle, index values are included in the cost calculations as infinity (∞). So, these routes should not be preferred. In absolute slope values of 1 percent or less, the slope difference is ignored and the index values are taken into account as 0. If the 10 percent and 1 percent slope are between the absolute slope values, a normalization is made and the slope is taken into account by taking values between 1 and 0. Although the research [24] is taken into account in this calculation, it is necessary to add an unacceptable limit for electric scooters and bicycles (Equation 2).

$$NE_i = \begin{cases} 0, & |G_i| < 1 \\ \frac{|G_i| - 1}{10 - 1}, & 1 \leq |G_i| \leq 10 \\ \infty, & |G_i| > 10 \end{cases} \quad (2)$$

The use classes of the land where the road is located, namely the land use values, are used for situations where the driver attaches more importance to the lands which are the elements of nature. For example, a forest area may be preferred more than areas where settlements are concentrated, but it may be less preferred than coastal areas. The lack of class diversity and the fact that the resolution of the existing land use data is not high enough can also prevent the application to give high precision results. The land use classes corresponding to the pixel values of the existing land use data were obtained from [35]. Table 3 guidelines were taken to be used in the research and the pixel values in the land use raster data were changed according to this guideline and score values were assigned.

Table 3. Land use classification.

Land use class	Score value
Water	100
Forest	95
Grass	80
Bare Ground	75
Residential area	34

After the processes in which Table 3 is taken into account, the land use index values were calculated by making normalization for the usability of the land use data in the shortest path applications and included in the cost calculations used in the applications. Normalization calculation for land use data can be examined in Equation 3.

$$NA_i = \frac{|A_i - \max(AK)|}{\max(AK) - \min(AK)} \quad (3)$$

Ai =Land Use Index

Cost calculations may vary for each application to be made. Rather than establishing a standard method in this regard, it is planned to investigate the effect of different cost calculations on the diversity of applications. Calculations of cost indexes are kept constant in the applications to be made. Within the works, it is planned to make applications in which the weights of different cost indexes on the cost will vary. The application types classified according to these costs can be examined in Table 4.

Table 4. Applications and cost indices used.

Application	Length of Path index (U _i)	Road Slope Index (NE _i)	Road Class Index (NS _i)	Land Use Index (NA _i)
1	✓	X	X	X
2	✓	✓	X	X
3	✓	✓	✓	X
4	✓	✓	✓	✓
5	✓	X	✓	X
6	✓	X	X	✓
7	✓	X	✓	✓

Table 4 shows which cost indices will be used in which application. These cost indexes can be used in different ways in applications.

In Application 1, the path length index is taken into account as the cost value to be used in the shortest path algorithm. This application provides the shortest path to the result (Equation 4).

$$M1 = U_i \quad (4)$$

M=Cost Value

In Application 2, the road length and the slope of the road are taken into account as cost values. According to this application, if the slope index value of a road is maximum, using that road in the algorithm means that the same distance will be covered twice. Absolute slope value and cost are in a linear relationship. This application elevation gives the desired result when variable paths are not preferred (Equation 5).

$$M2 = U_i + U_i * NE_i \quad (5)$$

The length of the road, the slope of the road, and the class of the road are taken into account for the cost value in Application 3. This practice gives importance to roads where rough roads are not preferred and that the vehicle can drive more safely and healthily (Equation 6).

$$M3 = U_i * NE_i + U_i * NS_i \quad (6)$$

All cost indexes in the research, including the length of the road, the slope of the road, the class of the road, and the land use values, are taken into account in application 4. While this application supports Application 3, It gives results according to the vehicle driver's emphasis on nature excursions (Equation 7).

$$M4 = U_i * NE_i + U_i * NS_i + U_i * NA_i \quad (7)$$

In Application 5, the length of the road and the class of the road are taken into account. This app considers safer routes for the driver while finding the shortest distance to the destination. It does not prefer the roads used by motor vehicles unless it is a necessity according to weight calculations (Equation 8).

$$M5 = U_i * NS_i \quad (8)$$

In application 6, the length of the road and land use are taken into account. This application highlights the nature excursions for the driver and prefers areas such as the coastline more than areas such as the inner city (Equation 9).

$$M6 = U_i * NA_i \quad (9)$$

Compared to Application 4, the slope of the road is not taken into account in Application 7. Care has been taken to ensure that the user has a safe nature drive rather than taking into account the rough areas of the road (Equation 10).

$$M7 = U_i * NS_i + U_i * NA_i \quad (10)$$

3. Results

For the applications to be made, it is planned to make the optimal road problem works in 3 regions where it is foreseen that different and various results will be obtained. These works are also visualized on a special web map application prepared for this research, which also includes the OpenStreetMap basemap. The applications shown on the maps can be examined with the help of Table 5.

Table 5. Application representation colors on the map.

Application	Color (with Hex Code)
1	#20B2AA
2	#FFD700
3	#FF69B4
4	#0000FF
5	#A52A2A
6	#8B008B
7	#FF8C00

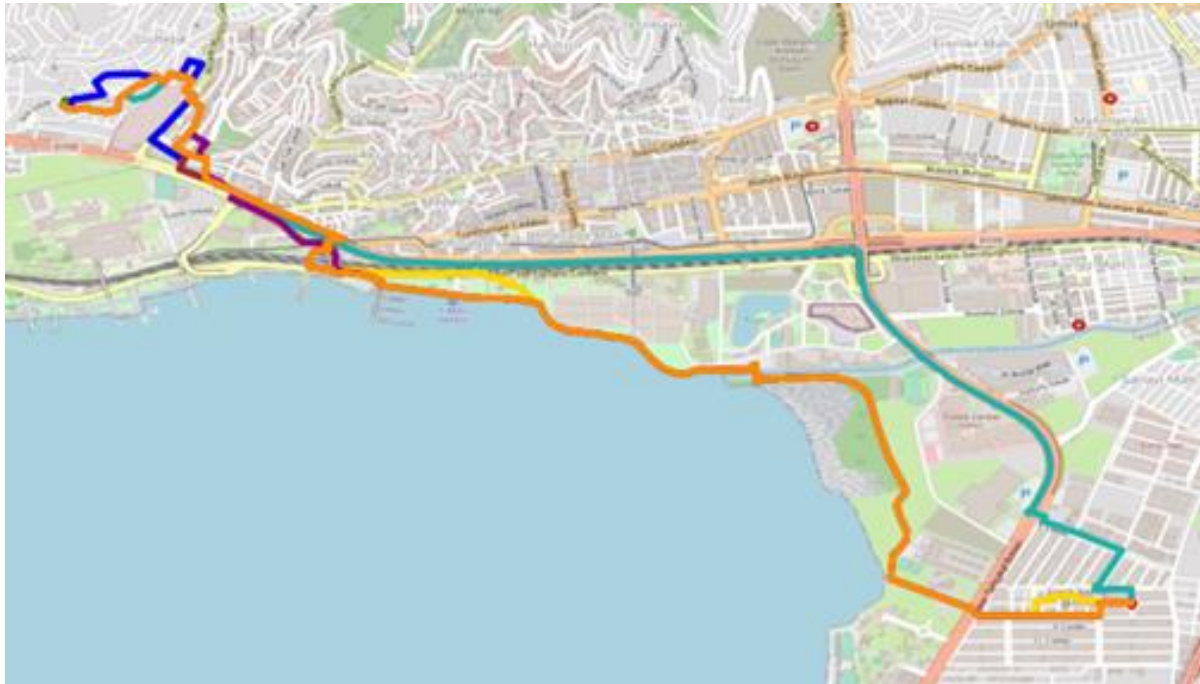


Figure 8. Work 1 map display.

First of all, starting and target points were selected in the coastal areas where pedestrian/bicycle and main roads are dense and the land use class value is the highest, and 7 different applications work were carried out for these points.

Although it is seen that the same roads are preferred in some regions in different applications in the work shown in Figure 8 after the detailed examination made from the work result table in Table 6, road length differences and total cost values emerge more clearly.

When the application results are examined, it can be seen that the applications in which the cost variables are taken into account give results as expected. Especially in applications where road class and land use are taken into account, it is noteworthy that walking/bike paths on the coast side are preferred instead of the main road. In

addition, the total weights of the roads preferred in applications in other applications can be examined in Table 7.

Table 6. Work 1 application results.

Application	Total Path Length	Total Cost Value
1	6194.9	6194.90
2	6541.58	8013.16
3	6676.91	8956.72
4	6676.91	14308.35
5	6447.37	7007.86
6	6268.72	4946.02
7	6432.50	12142.12

Table 7. Work 1 application results comparison.

Application	Cost1	Cost 2	Cost 3	Cost 4	Cost 5	Cost 6	Cost 7
1	6194.90	∞	∞	∞	∞	5913.56	∞
2	6541.58	8013.16	∞	∞	∞	5464.25	∞
3	6676.91	8279.26	8956.72	14308.35	7354.37	5351.63	12706.00
4	6676.91	8279.26	8956.72	14308.35	7354.37	5351.63	12706.00
5	6447.37	∞	∞	∞	7007.86	5151.79	12159.66
6	6268.72	∞	∞	∞	∞	4946.02	∞
7	6432.50	∞	∞	∞	7011.95	5130.17	12142.12

With the examinations made in [Table 7](#), it is noteworthy that the road weights in cases where the cost variable conditions that are not accepted for the most appropriate road in different applications are ignored, the result directly converts the most appropriate road weight to an infinite value in applications where these conditions are considered important.

Additional information such as maximum slope, average slope, and average land use index values encountered in these applications can be examined in [Table 8](#).

According to the examinations made in [Table 8](#), a direct proportion can be established between the cost variables taken into account by the applications with additional information and the application results. [Figure 9](#) can be examined as an example of regions that are mostly preferred due to land use data in Work 1.

For Work 2, care was taken to select two points where the slope cost variable differed greatly. For the starting

point, a central point can be seen almost as sea level, and for the target point, a peak around which the heights vary at different rates was chosen ([Figure 10](#)).

Work 2 application results can be examined in [Table 9](#).

Table 8. Work 1 Applications Results Additional Information.

Applications	Maximum Slope Encountered (%)	Average Slope Encountered (%)	Average Land Use Index
1	12.59	4.94	0.4805
2	5.25	2.84	0.4536
3	5.45	2.88	0.4268
4	5.45	2.88	0.4268
5	12.59	4.69	0.4157
6	12.59	4.58	0.3870
7	12.59	4.38	0.4111



Figure 9. Work 1 sample google street view image.

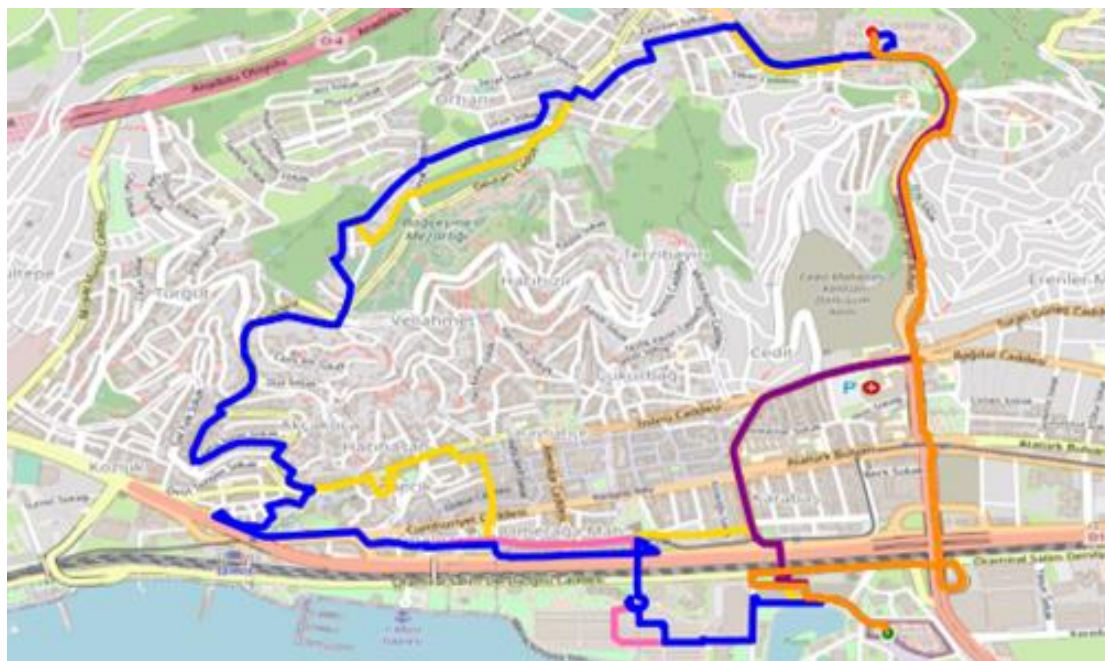


Figure 10. Work 2 map display.

Table 9. Work 2 application results.

Application	Total Path Length	Total Cost Value
1	3064.16	3064.16
2	6510.83	∞
3	7298.74	∞
4	7214.96	∞
5	3593.76	4464.90
6	3073.73	2951.72
7	3593.76	7971.49

As seen in [Table 9](#), it is seen that the slope between these two points necessarily exceeds the unacceptable limits, and therefore the total cost values of application 2, application 3 and application 4 reach infinite values. It is seen that the roads with less total infinite cost are preferred in the applications where the slope is taken into account, due to the desire to reach a result regardless of the map application. Although the result is a road directly on the map in the map application, it is not possible to use this direction under the conditions specified in the applications. Comparisons of application results within Work 2 can be examined in [Table 10](#).

Table 10. Work 2 application results comparison.

Application	Cost1	Cost 2	Cost 3	Cost 4	Cost 5	Cost 6	Cost 7
1	3064.16	∞	∞	∞	∞	2959.66	∞
2	6510.83	∞	∞	∞	∞	6281.32	∞
3	7298.74	∞	∞	∞	∞	7016.53	∞
4	7214.96	∞	∞	∞	∞	6930.40	∞
5	3593.76	∞	∞	∞	4464.90	3506.59	7971.49
6	3073.73	∞	∞	∞	∞	2951.72	∞
7	3593.76	∞	∞	∞	4464.90	3506.59	7971.49

As it can be understood from [Table 10](#), the cost values reach infinite values in all applications where the slope cost variable is included. The reason for this is that the slope values are not below the accepted values in any of the most suitable road preferences in applications. Additional information can be examined in [Table 11](#).

After the examinations made in [Table 11](#), it will be noticed that the average slope value in application 3 is lower than the average slope value in application 2. With the total path length value in [Table 9](#), it will be noticed that the effect of the path length cost variable in the applications should not be ignored even if the slope is taken into account in the work. [Figure 11](#) can be examined as an example of high slope regions in Work 2.

Table 11. Work 2 applications results additional information.

Applications	Maximum Slope Encountered (%)	Average Slope Encountered (%)	Average Land Use Index
1	29.09	5.83	0.542169
2	17.39	3.45	0.500000
3	17.39	3.25	0.536424
4	17.39	3.43	0.510345
5	31.05	6.76	0.542169
6	29.09	5.60	0.506024
7	31.05	6.76	0.542169



Figure 11. Work 2 sample google street view image.

For Work 3, two different points were selected at random in the city where the construction was intense, and it was planned to examine the cost variables of the road class within the applications. It has been taken into account that there are equivalent access roads to different categories such as pedestrian bridges, main roads, avenues, and walking paths between these two selected points. Work 3 application results can be examined in Table 12.

In the examination made in Table 12, it was seen that the conditions that were not accepted in the applications were not encountered. With the result comparison in Table 13, the differences between the applications can be examined in more detail.

Table 13 shows the effects of different road routes on the cost values of the applications in Work 3. It is seen that the values of Application 3, Application 4, Application 5, and Application 7, in which the road classes are examined, have relatively close values on

different roads. With the examinations made in Table 12 and Table 13, it can be interpreted that the roads used in Work 3 are generally the intervals where the road class is suitable for electric scooters and bicycles. Table 14 with additional information for Work 3 can be viewed as an appendix.

Figure 13 can be examined as an example of the most preferred regions due to road class indices in Work 3.

Table 12. Work 3 application results.

Application	Total Path Length	Total Cost Value
1	2175.30	2175.30
2	2273.89	2754.50
3	2244.45	2877.10
4	2225.00	5038.83
5	2227.98	2281.63
6	2202.23	2039.60
7	2231.35	4432.06



Figure 12. Work 3 map display.

Table 13. Work 3 application results comparison.

Application	Cost1	Cost 2	Cost 3	Cost 4	Cost 5	Cost 6	Cost 7
1	2175.3	∞	∞	∞	2884.07	2091.31	4975.38
2	2273.89	2754.5	3188.04	5408.84	2707.44	2220.8	4928.23
3	2244.45	2812.73	2877.1	5054.15	2308.82	2177.04	4485.86
4	2225	2819.61	2883.98	5038.83	2289.37	2154.85	4444.22
5	2227.98	2834.3	2887.95	5044	2281.63	2156.05	4437.68
6	2202.23	∞	∞	∞	3199.5	2039.6	5239.1
7	2231.35	2894.11	2947.76	5094.83	2285	2147.06	4432.06

Table 14. Work 3 applications results additional information.

Applications	Maximum Slope Encountered (%)	Average Slope Encountered (%)	Average Land Use Index
1	11.13	3.50	0.543478
2	5.25	2.61	0.565217
3	6.34	2.98	0.480769
4	5.25	3.13	0.458333
5	6.34	3.19	0.446809
6	12.59	4.39	0.347826
7	6.34	2.96	0.480000

4. Discussion

The results were partially as expected for all three studies, which were planned to yield different results. It can be said that it is positive in terms of the preferred ways and results against the cost variables that the applications have paid attention to in the studies, and partially sufficient in terms of accuracy.

Although the shortest route preferences are close to the city center areas in Work 1 applications, it has been observed that coastal areas are preferred in applications where land use is taken into account. It has been seen that walking and cycling paths are preferred in applications where the road class is taken into account. The applications in Work 1 give the expected results.



Figure 13. Work 3 sample google street view image.

As can be seen in [Figure 11](#), the elevation differences between the two selected points in Work 2 applications are quite large. For this reason, it is seen that in applications where road slopes are taken into account, infinite values and roads that are not preferred for application are encountered. It is planned to examine how road preferences in applications can yield results in different applications. For this reason, an algorithm is designed in which, if there is no path to be preferred in applications, the shortest paths with total infinite cost value will be preferred. Thus, the results of different road preferences in different applications could also be examined.

For Work 3, it is planned to examine the options in the city center. As expected, in applications where road class values are taken into account, it is seen that pedestrian and bicycle paths are preferred.

With the help of results comparison and additional information tables in works, it is possible to observe and discuss whether the application results are reasonable or not. The average and maximum values encountered in applications that consider only the slope may have a lower value in applications that also consider other cost variables other than the slope. It is seen that this situation arises from the fact that the length values of the roads also have an effect on the result. This situation can also be seen in applications where other cost variables are taken into account.

According to the inferences made from the research results, it is seen that both the land use and elevation data resolution are not sensitive enough and diverse data for the study. The height values that vary greatly in the region are vectorially in the same direction. In addition, important conditions such as speed limits on vehicle roads, and battery times for electric scooters/bicycles were not used. Such situations reduce the accuracy of the results of the research and the effect of the inferences to

be made from this research. On the other hand, the usability of the GIS software and software libraries used, the working speed of the Dijkstra algorithm and the effects of the conditions accepted in the study on the result provided a positive impression for this study.

5. Conclusion

In the research, it was examined how different cost variables for electric scooters and bicycles affect the results in applications with various combinations. It was seen that the research gave successful results, but the accuracy of the results was not sensitive enough and the variety in cost variables should be further increased. It has been examined that the results of the research are logical results with the examinations and comparisons made on the results. Thus, it has been concluded that GIS, Dijkstra's Algorithm, used GIS software, programming language, and libraries can be used in research in this area. The materials that can be obtained from open sources for the research can be used in such studies, but these materials should be examined in detail before the research.

The effects of the cost variables found in the research on the weight give positive results. It has been seen that more appropriate and healthy results can be encountered with the optimizations that can be made on the index values of the cost variables in the application and that these applications can also lead to other research.

It is thought that if applications such as bicycle parking points offered by local municipalities are used for electric scooters/bicycles, different results can be seen with different applications and works. Although there are some legal rules for electric scooters/bicycles in various countries today, it is noteworthy that there are no rules in Izmit district (and other nearby

districts/provinces) in this study, which examines the most suitable roads. If some mandatory rules are introduced for electric scooter/bicycle riders, a preliminary research material may be created for such studies.

Acknowledgement

Thanks to the owners of the resources used in the project, to my advisor Arzu Erener, who spent her valuable time, and to Piri1513 Geographical Information Systems Company for their helpfulness when necessary. This article was produced from a master's thesis commissioned by Kocaeli University, Institute of Science and Technology.

Author contributions

Ahmet Şirin: Idea, Design, Literature Review, Data Collection and Processing, Data curation, Visualization, Software, Methodology, Analysis and Interpretation, Writing. **Arzu Erener:** Idea, Design, Writing-Reviewing, Data Collection, Methodology, Thesis and Article Review, Supervision.

Conflicts of interest

The authors declare no conflicts of interest.

References

- Güneri, Ö. İ., & Durmuş, B. (2020). Classical and heuristic algorithms used in solving the shortest path problem and time complexity. *Konuralp Journal of Mathematics*, 8(2), 279-283.
- Arslan, H., & Manguoğlu, M. (2019). A hybrid single-source shortest path algorithm. *Turkish Journal of Electrical Engineering and Computer Sciences*, 27(4), 2636-2647. <https://doi.org/10.3906/elk-1901-23>
- Madkour, A., Aref, W. G., Rehman, F. U., Rahman, M. A., & Basalamah, S. (2017). A survey of shortest-path algorithms. *Data Structures and Algorithms*. <https://doi.org/10.48550/arXiv.1705.02044>
- Park, K., & Yilmaz, A. (2010). A social network analysis approach to analyze road networks. *ASPRS Annual Conference*. San Diego, CA, 1-6.
- Morova, N., Şener, E., & Terzi, S. (2011). Coğrafi bilgi sistemleri ile Isparta İli 112 ambulans istasyonlarının hizmet alanlarının sorgulanması ve optimum yol güzergâhlarının belirlenmesi. *Uluslararası Teknolojik Bilimler Dergisi*, 3(3), 1-13.
- Swapan, P. A. U. L. (2022). Change detection and future change prediction in Habra I and II block using remote sensing and GIS-A case study. *International Journal of Engineering and Geosciences*, 7(2), 191-207. <https://doi.org/10.26833/ijeg.975222>
- Küçük, K., & Anbaroğlu, B. (2019). OpenStreetMap Binalarının Mekansal Doğruluğunun Analiz Edilmesi. *Türkiye Coğrafi Bilgi Sistemleri Dergisi*, 1(1), 5-13.
- OpenStreetMap Data License (2023). <https://blog.openstreetmap.org/2012/09/12/opens-treetmap-data-license-is-odbl>
- OpenStreetMap Routing (2023). <https://wiki.openstreetmap.org/wiki/Routing>
- ArcGIS Pro Python (2023). <https://pro.arcgis.com/en/pro-app/latest/arcpy/main/arcgis-pro-arcpy-reference.htm>
- Python 3.x.x (2023). <https://docs.python.org/3/>
- Ünverdi, A. B., & Şişman, A. (2021). Elektrik Dağıtım Sistemlerinde Kesintilerden Etkilenen Kullanıcıların CBS Entegrasyonu ile Raporlanmasına Yönelik Bir Uygulama Geliştirilmesi. *Türkiye Coğrafi Bilgi Sistemleri Dergisi*, 3(2), 53-59.
- Temiz, H. (2022). Recording Performances of Some File Types for Pandas Data. *Avrupa Bilim ve Teknoloji Dergisi*, (36), 55-60. <https://doi.org/10.31590/ejosat.1103499>
- GeoPandas (2023). <https://geopandas.org>
- Ghen, Q. (2020). The Hotspot Technologies and Cutting-edge Technologies of Organic Solar Cells. *International Journal of Engineering Science and Application*, 4(2), 52-58.
- OSMnx (2023). <https://osmnx.readthedocs.io/>
- Sarı, F., & Koyuncu, F. (2021). Multi criteria decision analysis to determine the suitability of agricultural crops for land consolidation areas. *International Journal of Engineering and Geosciences*, 6(2), 64-73. <https://doi.org/10.26833/ijeg.683754>
- Sarı, F., & Sen, M. (2017). Least cost path algorithm design for highway route selection. *International Journal of Engineering and Geosciences*, 2(1), 1-8. <https://doi.org/10.26833/ijeg.285770>
- Akay, A. E., & İnanç, T. A. Ş. (2021). Using GIS techniques for assessment of accessible forest lands by firefighting teams considering fire risk degrees. *European Journal of Forest Engineering*, 6(2), 87-95. <https://doi.org/10.33904/ejfe.843889>
- Sert, E., Osmanli, N., Eruc, R., & Mevlüt, U. Y. A. N. (2017). Determination of transportation networks base on the optimal public transportation policy using spatial and network analysis methods: a case of the Konya, Turkey. *International Journal of Engineering and Geosciences*, 2(1), 27-34. <https://doi.org/10.26833/ijeg.286034>
- Demirkol, Ö., & Demirkol, A. (2003). Dijkstra ve Bellman-Ford en kısa yol algoritmalarının karşılaştırılması. *Sakarya University Journal of Science*, 7(3), 55-62.
- Özdemir, S., Sacar, Ö., & Özcan, E. (2021). Dijkstra algoritması kullanılarak ipek yolu koridorları arasında en kısa ulaştırma güzergâhının belirlenmesi. *Demiryolu Mühendisliği*, (13), 97-105. <https://doi.org/10.47072/demiryolu.811572>
- Gökcan, A. O., Çöteli, R., & Tanyıldızı, E. (2020). The shortest road algorithm approach in determining the route of solid waste collection vehicles: The case of Manisa 75. Yıl Neighborhood. *Turkish Journal of Science and Technology*, 15(1), 29-35.
- Plynnig, E. (2016). Route planning using multiple attributes: Finding routes other than the shortest for

- bicycles. [Student thesis, KTH, School of Architecture and the Built Environment (ABE), Urban Planning and Environment, Geoinformatics].
25. Digital Elevation Data (2023). <http://viewfinderpanoramas.org/dem3.html>
26. Yakar, M., Kuşak, L., Ünel, F. B., & İban, M. C. (2020). *Surveying: A Comprehensive Guide to Geomatics Engineering Applications*. Mersin Üniversitesi Harita Mühendisliği Kitapları.
27. Yakar, M. (2009). Digital elevation model generation by robotic total station instrument. *Experimental Techniques*, 33, 52-59. <https://doi.org/10.1111/j.1747-1567.2008.00375.x>
28. ESRI Sentinel-2 10m Land Use/Land Cover Timeseries Downloader (2023). <https://www.arcgis.com/apps/instant/media/index.html?appid=fc92d38533d440078f17678ebc20e8e2>
29. Efe, E., & Alganci, U. (2023). Çok zamanlı Sentinel 2 uydu görüntüleri ve makine öğrenmesi tabanlı algoritmalar ile arazi örtüsü değişiminin belirlenmesi. *Geomatik*, 8(1), 27-34. <https://doi.org/10.29128/geomatik.1092838>
30. Türk, S. T., & Balçık, F. (2023). Rastgele orman algoritması ve Sentinel-2 MSI ile fındık ekili alanların belirlenmesi: Piraziz Örneği. *Geomatik*, 8(2), 91-98. <https://doi.org/10.29128/geomatik.1127925>
31. Tirmanoğlu, B., İsmailoğlu, I., Kokal, A. T., & Musaoğlu, N. (2023). Yeni nesil multispektral ve hiperspektral uydu görüntülerinin arazi örtüsü/arazi kullanımı sınıflandırma performanslarının karşılaştırılması: Sentinel-2 ve PRISMA Uydusu. *Geomatik*, 8(1), 79-90. <https://doi.org/10.29128/geomatik.1126685>
32. Yakup, A. E., & Ayazlı, I. E. (2022). Investigating changes in land cover in high-density settlement areas by protected scenario. *International Journal of Engineering and Geosciences*, 7(1), 1-8. <https://doi.org/10.26833/ijeg.850247>
33. Sefercik, U. G., Kavzoğlu, T., Çölkesen, I., Nazar, M., Öztürk, M. Y., Adalı, S., & Dinç, S. (2023). 3D positioning accuracy and land cover classification performance of multispectral RTK UAVs. *International Journal of Engineering and Geosciences*, 8(2), 119-128. <https://doi.org/10.26833/ijeg.1074791>
34. Soysal, Ö. M., Schneider, H., Shrestha, A., Guempel, C. D., Li, P., Donepudi, H., ... & Sekeroglu, K. (2012). Zonal statistics to identify hot-regions of traffic accidents. In *Proceedings of the International Conference on Modeling, Simulation and Visualization Methods (MSV)* (p. 1). The Steering Committee of The World Congress in Computer Science, Computer Engineering and Applied Computing (WorldComp).
35. Esri 2020 Land Cover (Mature Support) (2023). <https://www.arcgis.com/home/item.html?id=d6642f8a4f6d4685a24ae2dc0c73d4ac>



© Author(s) 2024. This work is distributed under <https://creativecommons.org/licenses/by-sa/4.0/>



UAV-mounted thermal camera and its analysis on urban surface textures

Efdal Kaya ^{*1} , Arzu Erener ² 

¹ Iskenderun Technical University, City and Region Planning, Türkiye, efdal.kaya@iste.edu.tr

² Kocaeli University, Department of Geomatics Engineering, Türkiye, arzu.erenner@kocaeli.edu.tr

Cite this study:

Kaya, E., & Erener, A. (2024). UAV-mounted thermal camera and its analysis on urban surface textures. *International Journal of Engineering and Geosciences*, 9 (1), 49-60

<https://doi.org/10.26833/ijeg.1288990>

Keywords

Thermal UAV
Remote Sensing
Pearson Correlation
Urban heat
Surface temperature

Research Article

Received:28.04.2023

Revised: 22.05.2023

Accepted:06.06.2023

Published:02.01.2024



Abstract

Temperature increase, especially global warming, can be observed depending on various factors which led to several severe environmental problems. Urban areas are the most effected places by this temperature increase. Urban heat concentration, the so-called heat island effect, is high in structural areas. This situation causes human life to be adversely affected. Therefore, constant measurement and analyses are required to assess outdoor thermal comfort and thermal stress in urban areas. Today, unmanned aerial vehicle (UAV) systems are used as a rapid data production technique in Earth observation activities. Thermal cameras integrated into UAV systems can monitor the temperature values in urban areas precisely and constantly. This study focuses on the potential application of a UAV-mounted thermal camera system at a local scale due to its rapid response to surface temperature variables. A thermal camera UAV system to measure the energy fluxes and temperatures from the earth's surface, which are integral to understanding landscape processes and responses. Thus, UAV thermal sensors were used directly for different land cover types in and around the Faculty of Engineering building of Kocaeli University in Türkiye. Derived UAV surface temperatures were compared with simultaneously acquired in situ temperature measurements. Simultaneous terrestrial temperature measurements were obtained by using TFA ScanTemp 410 model surface temperature meter. A high correlation between UAV surface temperatures and terrestrial measurements was utilized by Pearson correlation with a 0.94 coefficient. It was concluded that the UAV-mounted thermal camera system is a promising tool that has increased opportunities to understand surface temperature variability at high spatial and temporal resolution.

1. Introduction

Increasing impermeable surfaces, destruction of forest areas, urbanization and industrialization contributed to climate change and global warming. Investigating these climate changes and global warming, and creating climate models takes an important place in the estimation and prevention of future environmental damages. The most important soil parameter in these scientific studies is the land surface temperature (LST). The LST is the most important parameter in calculating the energy transfer between the surface and the atmosphere [1]. It can be used in scientific studies related to evapotranspiration, hydrology, climate change, and geothermal energy [2-7].

Generally, the LST is derived from satellite-based thermal infrared (TIR) measurements. Optical remote

sensing, however, is limited due to high acquisition costs [8]. Given recent developments in UAVs, thermal images offer the opportunity to measure surfaces in high spatial and temporal resolution at a low cost and this has been explored in recent years by different disciplines for the spatial analysis of surface temperatures [9-15].

They have been compared and analyzed LST data generated by a TIR camera mounted on an UAV and LST data from the Landsat 8 satellite for seven specific periods. They investigated LSTs in green spaces, specifically those of different land cover types in an urban park in Korea [10]. Zengin et al. [16] analyzed thermal camera images and spatial thermal comfort at Ataturk Campus, Türkiye. As a result of the analyzes and evaluations, it was emphasized that the use of natural herbaceous plants is important in terms of providing thermal comfort in urban planning. Gülten and Aksoy

[17] was investigated the heat distribution by the thermal imaging method in a pilot study area of Elazığ, Türkiye. In the study, the thermal behaviors of the building, street, roof, and pavement were evaluated by making surface temperature measurements to investigate the urban heat island (UHI) effect. Yalçiner et al. [18] were examined the structural destructions using thermal imaging, microwave moisture measurements, and building radar systems in the Hagia Sophia Museum, Türkiye. In this way, it was determined whether there was any deterioration on the walls of the Museum. Aerobic stability was evaluated by Ünal et al. [19] with 3 pieces of 500 kg corn and wheat bale silage each obtained from Tekirdag Namık Kemal University application and research farm. As a result of the research, it was concluded that the thermal camera imaging technique can be used as a practical method to evaluate the aerobic stability of silages in laboratory conditions. In the study conducted by Çamoğlu and Genç [20], water stress was determined in green bean plants using spectral reflection data and thermal imaging techniques. The researchers were concluded that water stress can be better explained with thermal indices, especially at the I-100 level, in the classification and regression tree analysis on the sample data sets. In the study, it was determined that the Structural Independent Pigment Index (SIPI) and Normalized Vegetative Change Index (NDVI) from the spectral indices, the plant water stress index (CWSI_e) calculated based on the thermal indices, and the plant water stress index (CWSI_a) calculated according to the artificial reference surfaces were found in green beans. They have been suggested to be used in the determination of water stress. In the study conducted by Küçüktopcu and Cemek [21], heat loss in poultry houses was monitored with thermal camera data. As a result of the study, it was understood that thermal imaging technology can detect the structural problems that cause heat losses and gains. It was observed that the most heat loss was caused by the gaps in the windows and doors which leads to energy loss in buildings. A solution was sought for the structural problems that cause heat loss in greenhouses by using thermal camera data in Çaylı et al. [22]. It has been observed that the places where the heat loss is the most in the greenhouses are the bottom of the doors, the margins, the openings on the edges of the ventilation windows, the roof-front wall, and the side roof wall junctions of the covering material. In the study by Akçay [23], terrestrial photogrammetric analysis was performed using multispectral and thermal cameras. 3D models were produced using images obtained from cameras. Seven control points were used during model production. The model was produced in the point cloud after the production step. In the study conducted by Durgut and Akçay [24], a 3D model of the graphics card was created using thermal camera data. As a result of the study, it was concluded that thermal photogrammetric 3D models can be used to detect problems that may occur during the production and maintenance of electronic products such as computer hardware. In the study conducted by Gülci and Akay [25], the locations of ecological art structures were evaluated using UAV systems and thermal infrared camera data. In the study

conducted by Wu et al. [26] in the Jiading Campus area of Tongji University, the LST was calculated using the thermal camera integrated into the UAV. A meteorological ground observation station was used for control purposes. It has been observed that there is a difference between -1.73 and 1.45 Kelvin between the surface temperatures obtained from the terrestrial observation station and UAV systems. Feng et al. [27] calculated the evapotranspiration of various vegetation with the thermal data obtained from UAV systems in a small part of the city of Nanjing, China. As a result of the study, it was observed that high-accuracy evapotranspiration values were obtained with the data obtained from the thermal UAV on different vegetation surfaces. Qin et al. [28] conducted a study in the Beijing University Shenzhen campus area, evapotranspiration was calculated for different vegetation with images obtained by thermal UAV systems and thermal remote sensing data. $R^2=0.95$, $RMSE=30.33$ between evapotranspiration obtained from thermal UAV and remote sensing systems. They revealed that thermal UAV systems can be used in the planning of urban areas as a result of statistical analysis. Jiang et al. [29] were taken photographs at different angles with thermal UAV and UAV systems in Nanjing, China. The relationship between the differences between the obtained temperatures and the directions of the buildings has been revealed.

In present study, LSTs of different land cover types were investigated and compared with simultaneous in situ terrestrial temperatures measured by contact thermometers. Surface temperature variability at high spatial and temporal resolution was revealed which could contribute to decision-making for urban spaces and environmental planning in consideration of the thermal environment.

2. Method

2.1. Study Area

Kocaeli city is located in Marmara Region and it is one of the dense industrial provinces of Türkiye through which the D-100 and TEM highways pass through the city. It was mainly a production, storage, and transfer region for more than 1020 industrial institutions in various sectors such as petroleum refineries, automotive, chemistry, textile, machine, food, paper, wood, tanning, coal, etc. Kocaeli's climate constitutes a transition between the Mediterranean and the Black Sea climate. The city center is hot in the summer with low rainfall and mainly rainy and sometimes snowy and cold in winter. The highest temperature measured in the city center is 41.6°C, the lowest temperature is -8.7°C, and the average annual temperature is 14.8°C. The average annual precipitation in Kocaeli exceeds 835 mm. It is the 10th most populous city in Türkiye and the 2nd city in terms of population density. According to 2021 Turkish Statistical Institute (TUIK) data, it has a population of 2.033.441 people. Kocaeli University has its main campus in the borders of Izmit District, in the north-northwest direction of the center of Kocaeli Province. It was established in 1992 with a campus area of 778,466 m². Within the campus area, there are forest green areas and

a lake as well as the buildings belonging to the university units. In addition to administrative buildings, there are sports facilities and social areas on the campus. The

Engineering Faculty building in Kocaeli University's central campus and its surroundings were defined as the test area (Figure 1).

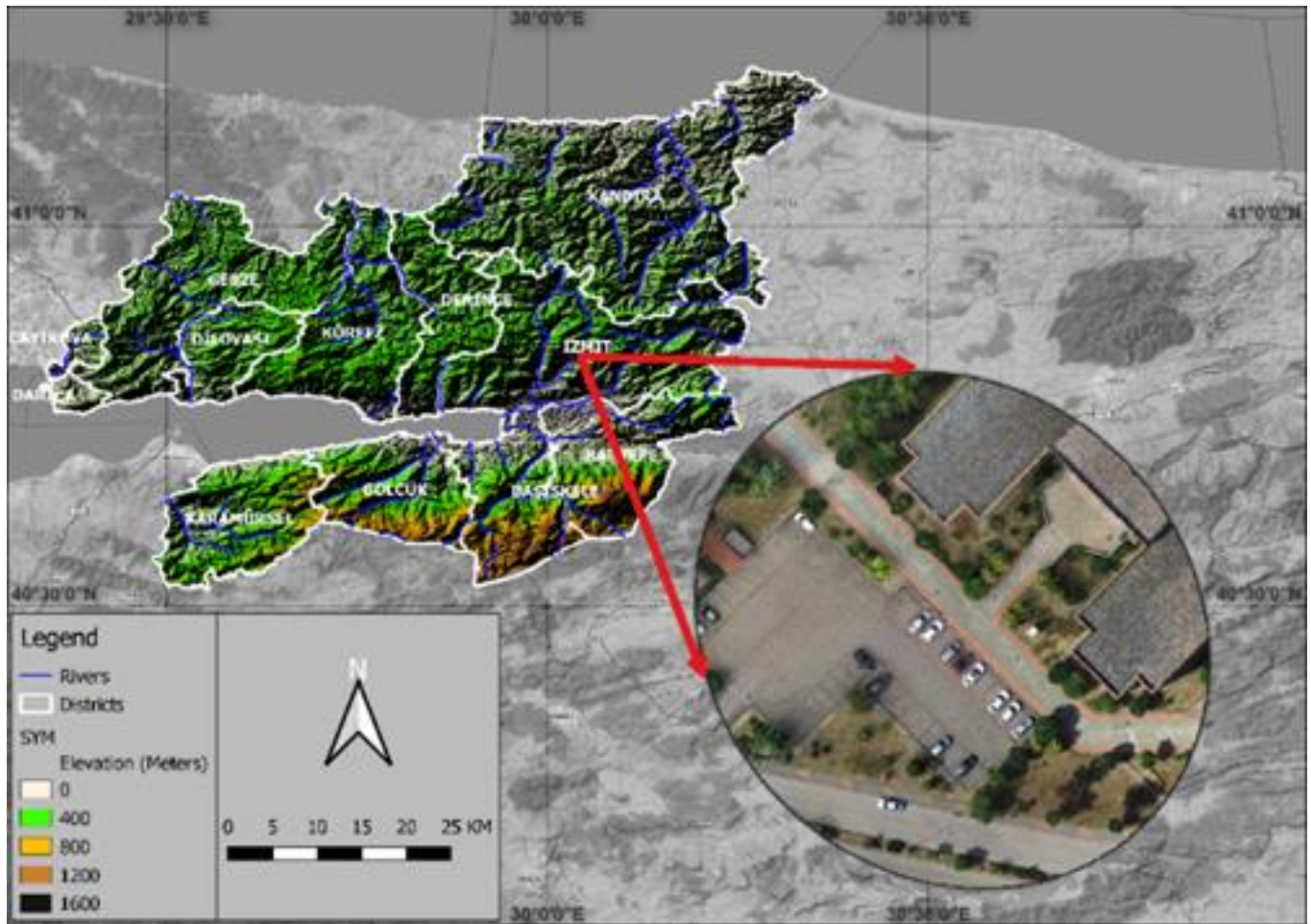


Figure 1. The study area.

The study area is centered at $40^{\circ}49'23.56''$ N and $29^{\circ}55'31.50''$ E. Instant weather conditions were taken into account in the selection of the study area. The flight operation was carried out on 20 August 2021 between 14.00 - 15.30 LT in the afternoon.

The weather data was additionally obtained from the eleven weather stations from Kocaeli districts. Values such as temperature, humidity, and wind speed were determined as presented in Table 1.

Table 1. Weather data in a period of field measurements.

SI	SN	T	RH	WS	SR
18409	Başiskele	25	55	5.9	96.03
18410	Darıca	26.5	47	6.5	82.25
18411	Dilovası	26.6	56	5.8	100.64
17639	Gebze	25.7	55	5.1	96.38
17067	Gölcük	28.3	50	3.9	0
18104	Kandıra	26.7	55	3.6	91.95
18412	Karamürsel	26.7	46	7.5	92.62
18413	Kartepe	25	56	3.2	96.04
17066	Kocaeli	26.7	80	2.6	0
18414	Körfez	28.5	45	5.1	101.15
19116	Derince	27.4	44	3.6	98.36

SI: Station number, SN: Station name, T: Temperature ($^{\circ}$ C), RH: Relative humidity (%), WS: Wind speed (m/s), SR: Solar radiation (WH/m^2)

2.2. Material

The UAV TIR LST data acquisition process can be divided into LST data collection through UAV TIR image capture and ortho mosaic matching stage, and a survey of ground control points (GCPs) for accurate georeferencing of the LST data [30-39].

Using the Remote Sensing Method to Simulate the Land Change in the Year 2030. Evaluation from Rural to Urban Scale for the Effect of NDVI-NDBI Indices on Land Surface Temperature, in Samsun, Türkiye [40]. The assessment of the thermal behavior of an urban park surface in a dense urban area for planning decisions. Using GIS analysis to assess urban green space in terms of accessibility: case study in Kütahya [41]. Determining the bioclimatic comfort in Kastamonu City. Sustainability of urban coastal area management: A case study on Cide [42]. A geographic information systems and remote sensing-based approach to assess urban micro-climate change and its impact on human health in Bartın, Türkiye [43]. The effects of climate on land use/cover: a case study in Türkiye by using remote sensing data. Investigation of the relationship between bioclimatic comfort and land use by using GIS and RS techniques in Trabzon. Integrating of settlement area in urban and

forest area of Bartın with climatic condition decision for managements.

UAV TIR cameras have lower resolutions compared to red, green, and blue (RGB) and multispectral cameras and single-band images [26]. This study used the Parrot Anafi brand UAV system with the thermal sensor to obtain the surface terminal. The characteristics of UAV with thermal sensors are given in Table 2.

The sample points were collected from the field to control the surface temperature map obtained from the thermal UAV. During the data generation with the UAV simultaneous in situ temperature measurements were applied with the TFA ScanTemp 410 infrared thermometer measuring device (Figure 2 and Figure 3).

The specifications of the TFA ScanTemp 410 Infrared Thermometer surface temperature measuring device are given in Table 3.

Table 2. Parrot Anafi model UAV specifications [44].

Properties	Technical Features
Weight	315 g
Maximum flight time	26 minutes
Maximum horizontal/vertical speed	34 mph / 4 m/s
Maximum wind resistance	31 mph
Max working height	4500 m
Operating temperature	-10 ° C with 40 ° C
Folded size	218x69x64mm
Sensor	CMOS 1 / 2.4 ", 21MP
HDR	4K UHD, 2.7K and 1080p videos, JPEG photos
Photo formats	JPEG, DNG (RAW)
Photo modes	Single, burst, bracketing, timer, and panorama
Maximum video sampling rate	100Mbps
Diaphragm open	f / 2,4
Sensor	FLIR Lepton 3.5 microbolometer (radiometric)
Sensor resolution	160x120
Spectral band	8-14µm
Photo format	JPEG
Photo resolution	3264x2448 (4/3)
Video format	MP4
Video recording resolution	1440x1080, 9fps
Sensibility	±5% max. (High gain) or ±10% max. (Low gain)

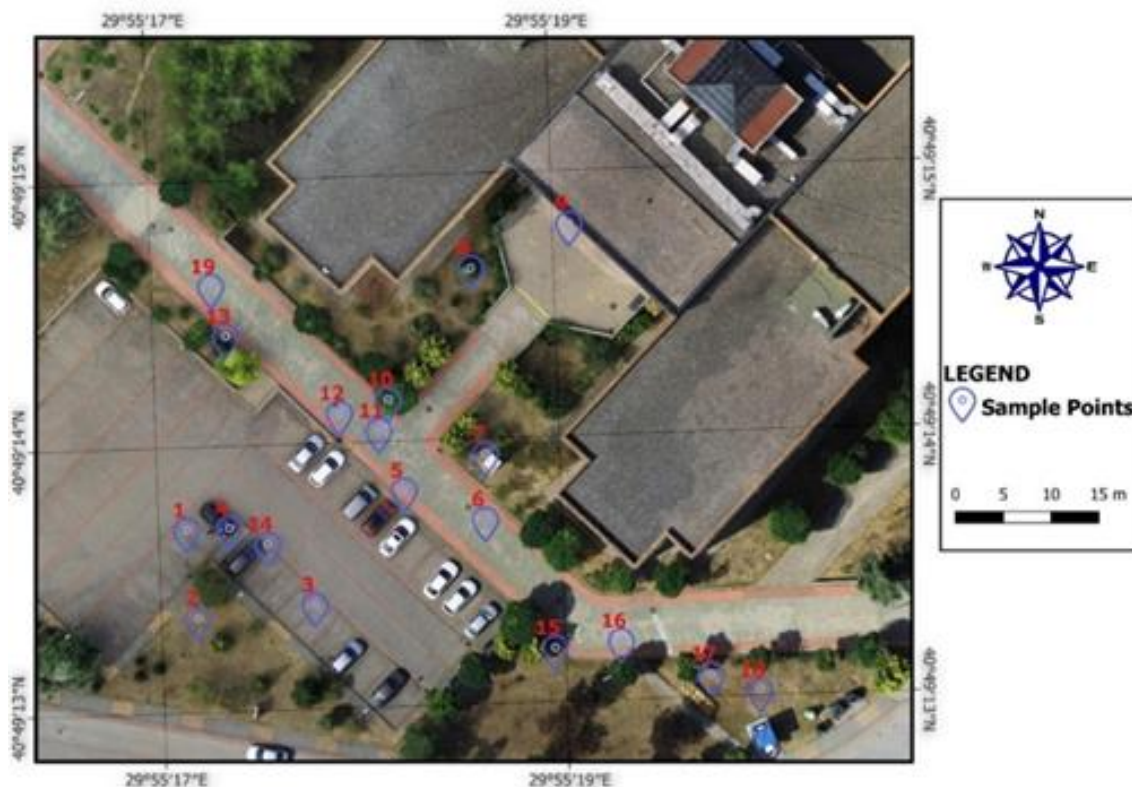


Figure 2. Sample points in the study area.



Figure 3. Measurement at sample points with the TFA ScanTemp 410 Infrared Thermometer.

Table 3. TFA ScanTemp 410 infrared thermometer surface temperature gauge specifications [45].

Properties	Technical Features
Laser temperature measuring range	-60°C +500°C
Laser temperature accuracy	±2°C
°C/°F Ability to choose units	Available
Screen resolution	0,1°C
Target rate	11:1
Weight	180 grams
Dimensions	175 x 39 x 80 m
Power source	2 pieces AAA batteries

Using the TFA ScanTemp 410 Infrared Thermometer, temperature measurements were applied to different surface textures in the field. These measurements were accepted as ground truth and the temperature values obtained from the UAV systems were compared with this collected ground in situ database.

2.3. Method

Initially, flight planning was defined to obtain data from the thermal UAV. A flight plan was prepared in Pix4D Capture software and the flight altitude was determined 40 meters. Two different photos were obtained with the RGB camera and the thermal camera on the Anafi Thermal UAV. During the flight, 562 pictures were obtained. In the project, the transverse and longitudinal overlap rate was entered as 90%. The ground sampling interval is 1.34 centimeters. The pictures collected during the flight were stored on the memory card of the aircraft in the Joint Photographic

Expert Group (JPEG) format. The images were transferred to the trial version of Pix4D Mapper software. The projection of the project was entered as UTM Zone 35. The photos were initially matched by mounting points through the images. Approximately 25000 anchor points are assigned per image. After the matching process, the exact coordinates of the photographs were calculated.

In order to create the point cloud, the point cloud setting section was used. In this step, the image scale $\frac{1}{2}$ was chosen to generate the point cloud. The point density was chosen high and the minimum number of image matching was chosen as 3. The point cloud is saved in .las, .laz, .ply, .xyz formats. As a result of the operations, a total of 55503698 points clouds were created (Figure 7). Pix4D Mapper software was also used to create the orthophoto (Figure 4) and DSM (Figure 5). During the orthophoto production, the information from the thermal camera was processed and the surface temperature map of the area was created (Figure 6).

Figure 6 showed that the Engineering Faculty building was in the temperature range of 30-40 °C in general, and some regions in the roof section have a

temperature of 40-50 °C. Green areas were in the range of 20-30 °C. Additionally, building shadows have the lowest temperature ranges between 0-20 °C.



Figure 4. Orthophoto.

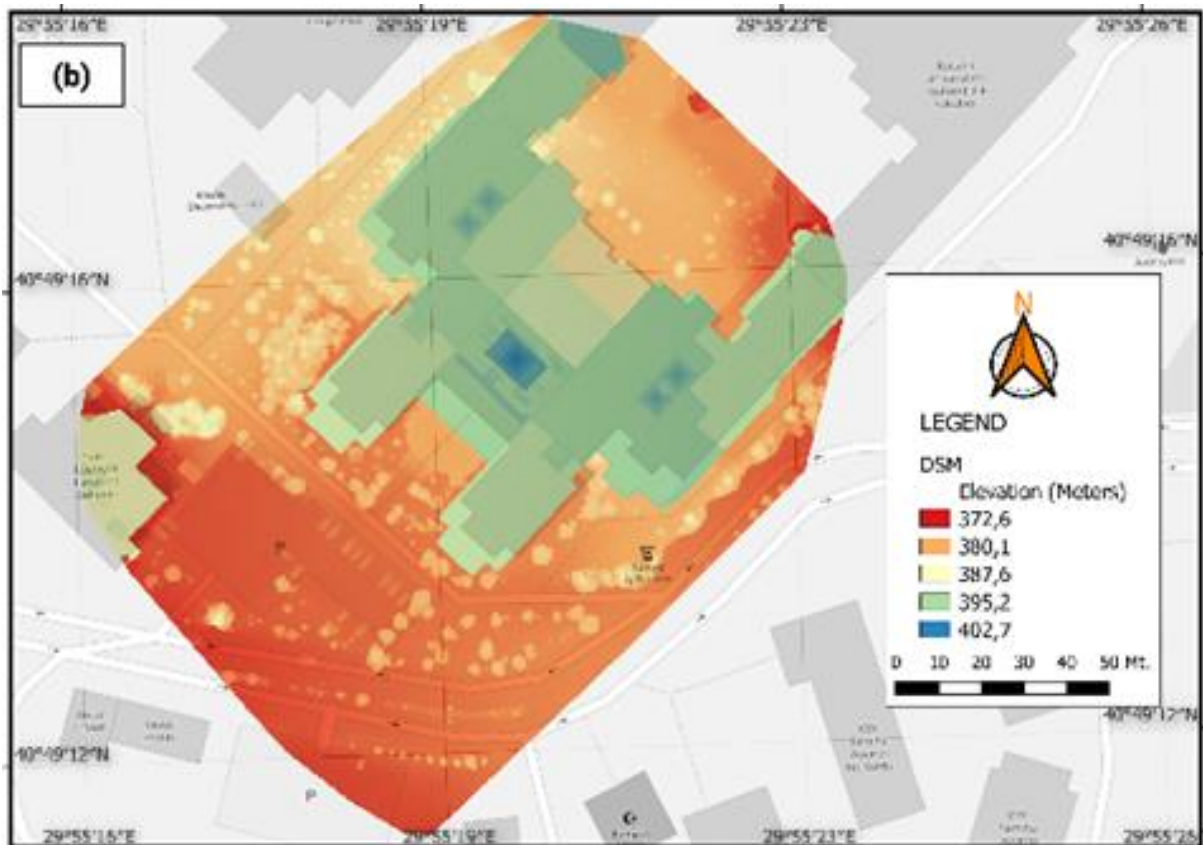


Figure 5. Digital surface model.

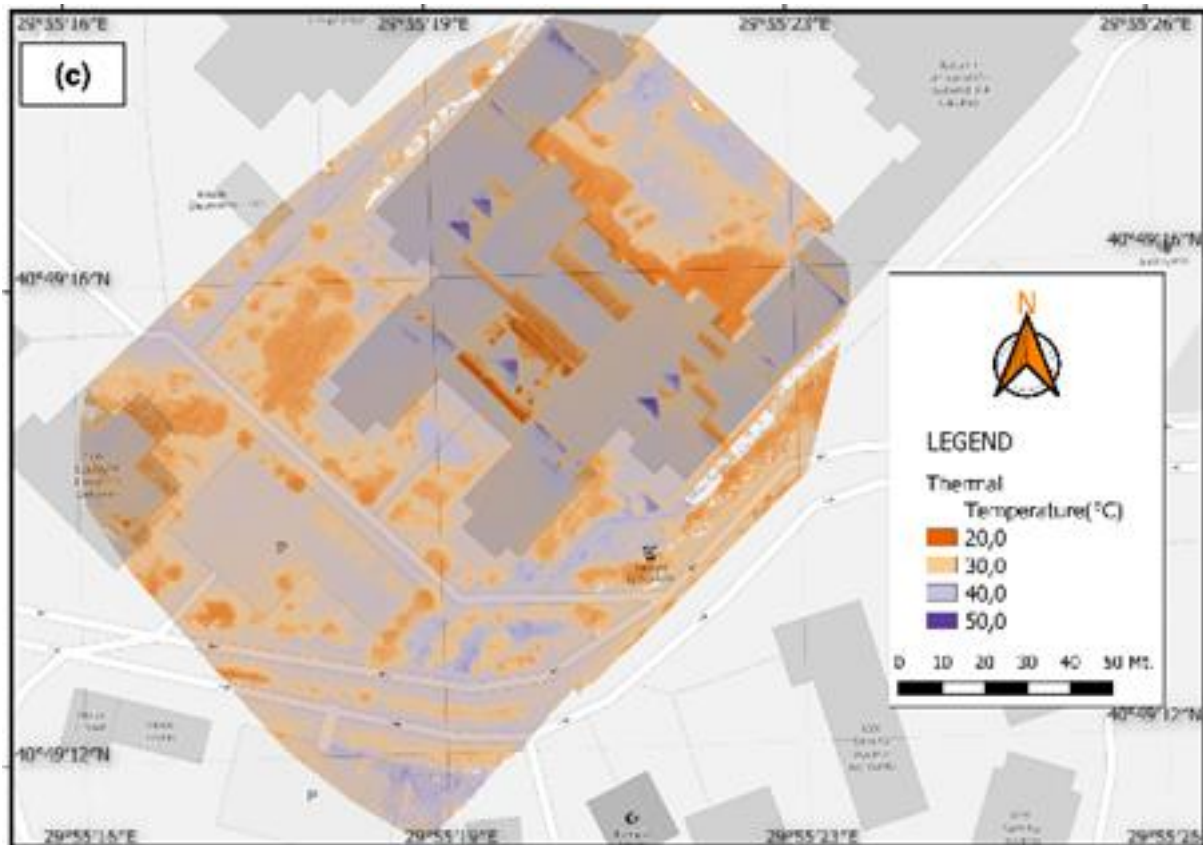


Figure 6. Surface temperature map of the area.



Figure 7. Point cloud.

3. Results

In this study high resolution thermal drone measurements were evaluated in different land cover types and results indicate that there is a wide variability in surface temperature behavior across urban land use types. Additionally, the surface temperatures obtained from the terrestrial observations and UAV systems were compared in order to obtain the performance of UAV thermal measurement performances. In order to evaluate the accuracy of LST data, nineteen LST control points (CP) were selected in the field by considering the land cover type of the study area. The data obtained as a

result of the ground measurements and the data obtained from the thermal band are given in Table 4.

The measurement was observed in front of Kocaeli University Engineering Faculty Building on different textures such as key cobblestone, wood, plastic material covered area, and marble area. As a result of the measurements obtained, the differences were examined. The graph of the differences was shown in Figure 8 and Figure 9. It was observed in Table 4 that the difference between values was mostly low and changed between -0.7 to 0.9 °C. There is only one location that indicates a high difference with 5.6 °C due to its location. The flights in this study were obtained from the nadir view.

Therefore, terrestrial measurements coincide to the shadow of any object regions such as building or tree provides higher differences. In this study this measurement was deliberately obtained to represent these differences.

When the points on the soil areas as key cobblestone and marble floor classes are examined, there was not an important difference between the local measurement and the temperature values obtained from the UAV systems. So, when averages of different surfaces are examined for ground measurement, surface temperatures are low in soil areas, while on other surfaces, they are found to be approximately 34,5 °C. While surface temperatures are expected to be low in green areas, at some points the surface temperature is high. This is due to the different surface coverings within the green area surface class. For example, green grass, dry vegetation etc. An average of the data obtained using thermal band is shown to produce results similar to a ground measurement.

The correlation between the temperatures obtained by the Terrestrial measurement method and the Thermal band was shown in Figure 8.

In Figure 9, triangle, circle, and square shapes were used according to the land use types of the points. Gray square-shaped areas indicate green areas. Blue triangles show land areas. Yellow triangles show key cobblestones. The dot with the red square indicates the marble area. The regression line between the points was presented in red. There is a positive correlation between the terrestrial measurement and the temperature values obtained from the thermal band. The correlation coefficient between them was 0.94. This value indicates

that there is a high degree of correlation between ground-based and UAV-based measurements.

Table 4. Obtained data and differences between.

TS	SN	GM	TB	D
Green Area	1	32,0	37,6	-5,6
	2	25,3	25,5	-0,2
	3	37,2	37,3	-0,1
	4	38,8	38,0	0,8
Soil Area	5	31,3	31,8	-0,5
	6	27,7	27,4	0,3
	7	35,0	35,1	-0,1
	8	36,3	36,4	-0,1
Paving Stone Area	9	35,2	35,9	-0,7
	10	35,2	35,6	-0,4
	11	37,0	36,2	0,8
	12	33,2	33,5	-0,3
	13	26,0	25,1	0,9
	14	36,5	36,8	-0,3
	15	36,2	35,9	0,3
	16	33,6	33,2	0,4
	17	35,5	35,3	0,2
	18	32,3	32,1	0,2
Marble Ground	19	35,0	34,5	0,5

TS: Texture Surface, SN: Sample Number, GM: Ground Measurement Value (°C), TB: Thermal Band Value (°C), D: Difference (°C)

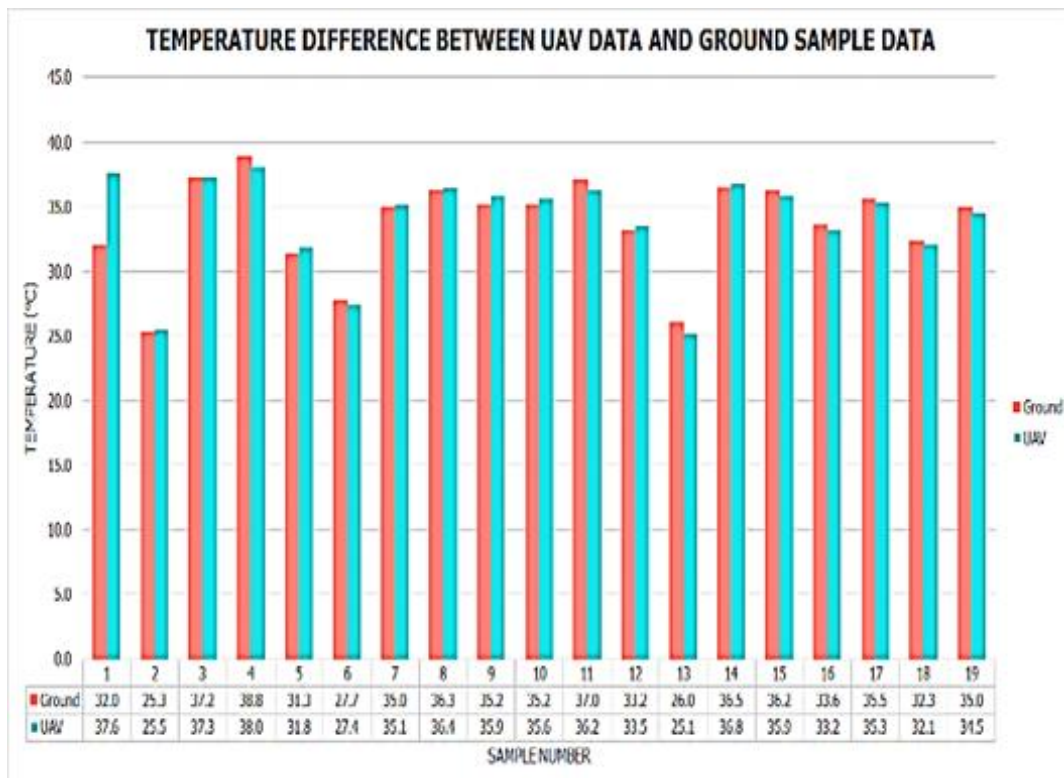


Figure 8. Differences between two different temperature measurements.

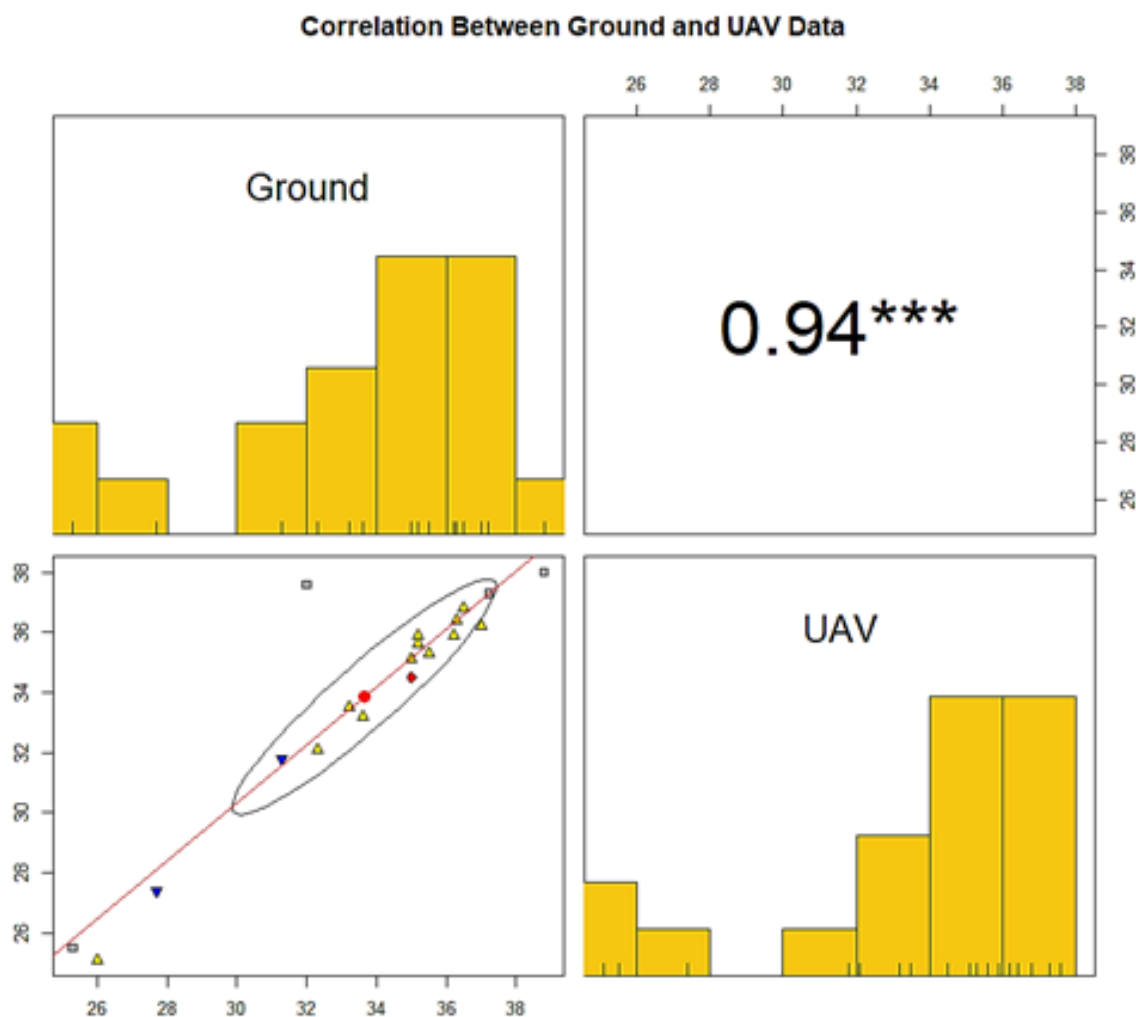


Figure 9. Correlation graph between the temperatures obtained by terrestrial measurement and thermal method.

4. Discussion and Conclusion

The main objectives of this study were to apply drone imagery to capture land surface temperature variability for different surface materials. A thermal camera-integrated UAV system was utilized in this study to evaluate urban surface temperatures. A surface temperature map of approximately 4 ha within the Kocaeli University campus area was monitored. Thermal behaviors of different land surface texture were investigated in the study region. A wide variability between temperature behavior across land use types was obtained. The results indicate that LSTs in different land cover types provide different thermal behaviors such as paving stone area and marble ground temperature were much higher than different vegetation surface types and soil area. This result can lead to the temperatures of different surface textures in urban areas can be easily distinguished by using UAV data.

Additionally, the results indicate that there is a high correlation between UAV-based surface temperatures and simultaneous terrestrial temperature measurements by Pearson correlation with a 0.94 coefficient. There is a difference between -0.7 and 0.9 degrees between the surface temperatures obtained from the terrestrial observation station and UAV systems.

UAVs can cover large areas very quickly, and they can be equipped with tools that can generate RGB, thermal or 3D images. In local areas, UAV systems that can produce fast and instant data compared to the alternative methods. Although UAV systems are fast and instant data generation technique, the most important disadvantage is that they are quickly affected by signal jammers and air conditions such as wind velocity and rain. Especially in city areas, attention should be paid to the UAV during the flight. UAVs can crash due to signal jammers. Since the widespread use of unmanned aerial vehicles is relatively new, legislation related to commercial and recreational use, is still catching up. Despite the disadvantages, it is a technology that can find wide application in many fields.

Acknowledgement

This research was funded by the Scientific Research Project through Kocaeli University, Project No: FDK-2021-2183. Project ID: 2183.

*This article is derived from the Doctoral dissertation titled "Modelling of Bioclimatic Comfort Area Using Artificial Intelligence" conducted under the supervision of Efdal Kaya's Prof. Dr. Arzu Erener.

Thank you for supporting my Doctoral dissertation of Kocaeli University, Scientific Research Projects Office.

Author contributions

Efdal Kaya: Conceptualization, Methodology, Software, Field study Software, Validation **Arzu Erener:** Visualization, Investigation, Writing-Reviewing and Editing.

Conflicts of interest

The authors declare no conflicts of interest.

References

- Li, Z. L., Tang, B. H., Wu, H., Ren, H., Yan, G., Wan, Z., ... & Sobrino, J. A. (2013). Satellite-derived land surface temperature: Current status and perspectives. *Remote Sensing of Environment*, 131, 14-37. <https://doi.org/10.1016/j.rse.2012.12.008>
- Al Kafy, A., Al Rakib, A., Akter, K. S., Rahaman, Z. A., Jahir, D. M. A., Subramanyam, G., ... & Bhatt, A. (2021). The operational role of remote sensing in assessing and predicting land use/land cover and seasonal land surface temperature using machine learning algorithms in Rajshahi, Bangladesh. *Applied Geomatics*, 13(4), 793-816. <https://doi.org/10.1007/s12518-021-00390-3>
- Aneesha Satya, B., Shashi, M., & Deva, P. (2020). Future land use land cover scenario simulation using open source GIS for the city of Warangal, Telangana, India. *Applied Geomatics*, 12, 281-290. <https://doi.org/10.1007/s12518-020-00298-4>
- Gabriele, M., Brumana, R., Previtali, M., & Cazzani, A. (2023). A combined GIS and remote sensing approach for monitoring climate change-related land degradation to support landscape preservation and planning tools: The Basilicata case study. *Applied Geomatics*, 15(3), 497-532. <https://doi.org/10.1007/s12518-022-00437-z>
- Hoque, I., & Lepcha, S. K. (2020). A geospatial analysis of land use dynamics and its impact on land surface temperature in Siliguri Jalpaiguri development region, West Bengal. *Applied Geomatics*, 12(2), 163-178. <https://doi.org/10.1007/s12518-019-00288-1>
- Moisa, M. B., & Gameda, D. O. (2021). Analysis of urban expansion and land use/land cover changes using geospatial techniques: a case of Addis Ababa City, Ethiopia. *Applied Geomatics*, 13(4), 853-861. <https://doi.org/10.1007/s12518-021-00397-w>
- Ndossi, M. I., & Avdan, U. (2016). Inversion of land surface temperature (LST) using Terra ASTER data: a comparison of three algorithms. *Remote Sensing*, 8(12), 993. <https://doi.org/10.3390/rs8120993>
- Khanal, S., Fulton, J., & Shearer, S. (2017). An overview of current and potential applications of thermal remote sensing in precision agriculture. *Computers and Electronics in Agriculture*, 139, 22-32. <https://doi.org/10.1016/j.compag.2017.05.001>
- Kraaijenbrink, P. D. A., Shea, J. M., Pellicciotti, F., De Jong, S. M., & Immerzeel, W. W. (2016). Object-based analysis of unmanned aerial vehicle imagery to map and characterise surface features on a debris-covered glacier. *Remote Sensing of Environment*, 186, 581-595. <https://doi.org/10.1016/j.rse.2016.09.013>
- Kim, D., Yu, J., Yoon, J., Jeon, S., & Son, S. (2021). Comparison of accuracy of surface temperature images from unmanned aerial vehicle and satellite for precise thermal environment monitoring of urban parks using in situ data. *Remote Sensing*, 13(10), 1977. <https://doi.org/10.3390/rs13101977>
- Tiwari, A., Sharma, S. K., Dixit, A., & Mishra, V. (2021). UAV remote sensing for campus monitoring: a comparative evaluation of nearest neighbor and rule-based classification. *Journal of the Indian Society of Remote Sensing*, 49, 527-539. <https://doi.org/10.1007/s12524-020-01268-4>
- Polat, N., & Uysal, M. (2018). An experimental analysis of digital elevation models generated with Lidar Data and UAV photogrammetry. *Journal of the Indian Society of Remote Sensing*, 46(7), 1135-1142. <https://doi.org/10.1007/s12524-018-0760-8>
- Sharma, M., Raghavendra, S., & Agrawal, S. (2021). Development of an open-source tool for UAV photogrammetric data processing. *Journal of the Indian Society of Remote Sensing*, 49, 659-664. <https://doi.org/10.1007/s12524-020-01237-x>
- Das, S., & Jain, G. V. (2022). Assessment and prediction of urban expansion using CA-based SLEUTH urban growth model: A case study of Kolkata Metropolitan area (KMA), West Bengal, India. *Journal of the Indian Society of Remote Sensing*, 50(12), 2277-2302. <https://doi.org/10.1007/s12524-022-01602-y>
- Vinod, P. V., Trivedi, S., Hebbar, R., & Jha, C. S. (2023). Assessment of Trees Outside Forest (TOF) in Urban Landscape Using High-Resolution Satellite Images and Deep Learning Techniques. *Journal of the Indian Society of Remote Sensing*, 51(3), 549-564. <https://doi.org/10.1007/s12524-022-01646-0>
- Zengin, M., Yilmaz, S., & Mutlu, B. E. (2019). Atatürk University Campus in terms of spatial thermal comfort analysis of thermal camera images. *Atatürk Üniversitesi Ziraat Fakültesi Dergisi/Atatürk University Journal of Agricultural Faculty*, 50(3), 239-247. <https://doi.org/10.17097/ataunizfd.535209>
- Gülten, A. A., & Aksoy, U. T. (2011). Kentsel bir alanda ısı dağılımının termal görüntüleme yöntemiyle incelenmesi. *Engineering Sciences*, 6(4), 1582-1589.
- Yalçın, C. Ç., Gündoğdu, E., Kurban, Y. C., & Altunel, E. (2017). Eski Eserlerdeki Yapısal Tahribatların Termal Görüntüleme ve Mikrodalga Nem Ölçümleri ile Belirlenmesi: Ayasofya Müzesi Örnek Çalışması. *Çanakkale Onsekiz Mart Üniversitesi Fen Bilimleri Enstitüsü Dergisi*, 3(2), 34-47. <https://doi.org/10.28979/comufbed.346240>
- Ünal, Ö., Koc, F., Okur, A. A., Okur, E., & Özdüven, M. L. (2018). Using thermal imaging camera technique to evaluation of the aerobic stability of corn and wheat silage. *Alınteri Journal of Agriculture Science*, 33(1), 55-63.
- Çamoğlu, G., & Genç, L. (2013). Taze Fasulyede Su Stresinin Belirlenmesinde Termal Görüntülerin ve Spektral Verilerin Kullanımı. *COMU Journal of Agriculture Faculty*, 1(1), 15-27.

21. Küçüktopcu, E., & Cemek, B. (2020). Kumeslerdeki ısı kayıplarının termal kamerayla izlenmesi. *Anadolu Tarım Bilimleri Dergisi*, 35(3), 404-409. <https://doi.org/10.7161/omuanajas.758342>
22. Çaylı, A., Akyüz, A. D. İ. L., Baytorun, A. N., Üstün, S., & Boyacı, S. (2016). Determination of structural problems causing heat loss with the thermal camera in greenhouses. *Kahramanmaraş Sütçü İmam Üniversitesi Doğa Bilimleri Dergisi*, 19(1), 5-14.
23. Akçay, Ö. (2021). Photogrammetric analysis of multispectral and thermal close-range images. *Mersin Photogrammetry Journal*, 3(1), 29-36.
24. Durgut, A., & Akçay, Ö. (2016). Termal kamera ile ekran kartının 3 boyutlu modelinin oluşturulması. *Anadolu University Journal of Science and Technology A-Applied Sciences and Engineering*, 17(1), 51-63. <https://doi.org/10.18038/btda.72883>
25. Gulci, S., & Akay, A. E. (2016). Using thermal infrared imagery produced by unmanned air vehicles to evaluate locations of ecological road structures. *Journal of the Faculty of Forestry-Istanbul University*. 66(2), 698-709. <http://dx.doi.org/10.17099/jffiu.76461>
26. Wu, Y., Shan, Y., Lai, Y., & Zhou, S. (2022). Method of calculating land surface temperatures based on the low-altitude UAV thermal infrared remote sensing data and the near-ground meteorological data. *Sustainable Cities and Society*, 78, 103615. <https://doi.org/10.1016/j.scs.2021.103615>
27. Feng, L., Liu, Y., Zhou, Y., & Yang, S. (2022). A UAV-derived thermal infrared remote sensing three-temperature model and estimation of various vegetation evapotranspiration in urban micro-environments. *Urban Forestry & Urban Greening*, 69, 127495. <https://doi.org/10.1016/j.ufug.2022.127495>
28. Qin, L., Yan, C., Yu, L., Chai, M., Wang, B., Hayat, M., ... & Qiu, G. Y. (2022). High-resolution spatio-temporal characteristics of urban evapotranspiration measured by unmanned aerial vehicle and infrared remote sensing. *Building and Environment*, 222, 109389. <https://doi.org/10.1016/j.buildenv.2022.109389>
29. Jiang, L., Zhan, W., Tu, L., Dong, P., Wang, S., Li, L., ... & Wang, C. (2022). Diurnal variations in directional brightness temperature over urban areas through a multi-angle UAV experiment. *Building and Environment*, 222, 109408. <https://doi.org/10.1016/j.buildenv.2022.109408>
30. Kim, D., Yu, J., Yoon, J., Jeon, S., & Son, S. (2021). Comparison of accuracy of surface temperature images from unmanned aerial vehicle and satellite for precise thermal environment monitoring of urban parks using in situ data. *Remote Sensing*, 13(10), 1977. <https://doi.org/10.3390/rs13101977>
31. Ağca, M., Gültekin, N., & Kaya, E. (2020). İnsansız hava aracından elde edilen veriler ile kaya düşme potansiyelinin değerlendirilmesi: Adam Kayalar örneği, *Mersin. Geomatik*, 5(2), 134-145. <https://doi.org/10.29128/geomatik.595574>
32. Ulvi, A. (2018). Analysis of the utility of the unmanned aerial vehicle (UAV) in volume calculation by using photogrammetric techniques. *International Journal of Engineering and Geosciences*, 3(2), 43-49. <https://doi.org/10.26833/ijeg.377080>
33. Ulvi, A., & Toprak, A. S. (2016). Investigation of three-dimensional modelling availability taken photograph of the unmanned aerial vehicle; sample of kanlidivane church. *International Journal of Engineering and Geosciences*, 1(1), 1-7. <https://doi.org/10.26833/ijeg.285216>
34. Yakar, M., & Doğan, Y. (2017). Mersin Silifke Mezgit Kale Anıt Mezarı fotogrametrik röleve alımı ve üç boyutlu modelleme çalışması. *Geomatik*, 2(1), 11-17. <https://doi.org/10.29128/geomatik.296763>
35. Şasi, A., & Yakar, M. (2018). Photogrammetric modelling of hasbey dar'ülhuffaz (masjid) using an unmanned aerial vehicle. *International Journal of Engineering and Geosciences*, 3(1), 6-11. <https://doi.org/10.26833/ijeg.328919>
36. Kusak, L., Unel, F. B., Alptekin, A., Celik, M. O., & Yakar, M. (2021). Apriori association rule and K-means clustering algorithms for interpretation of pre-event landslide areas and landslide inventory mapping. *Open Geosciences*, 13(1), 1226-1244. <https://doi.org/10.1515/geo-2020-0299>
37. Alptekin, A., & Yakar, M. (2021). 3D model of Üçayak Ruins obtained from point clouds. *Mersin Photogrammetry Journal*, 3(2), 37-40. <https://doi.org/10.53093/mephoj.939079>
38. Mirdan, O., & Yakar, M. (2017). Tarihi eserlerin İnsansız Hava Aracı ile modellenmesinde karşılaşılan sorunlar. *Geomatik*, 2(3), 118-125. <https://doi.org/10.29128/geomatik.306914>
39. Ulvi, A., Yakar, M., Yiğit, A. Y., & Kaya, Y. (2020). İha ve Yersel Fotogrametrik Teknikler Kullanarak Aksaray Kızıl Kilisenin 3B Modelinin ve Nokta Bulutunun Elde Edilmesi. *Geomatik*, 5(1), 19-26. <https://doi.org/10.29128/geomatik.560179>
40. Degerli, B., & Çetin, M. (2022). Evaluation from rural to urban scale for the effect of NDVI-NDBI indices on land surface temperature, in Samsun, Türkiye. *Turkish Journal of Agriculture-Food Science and Technology*, 10(12), 2446-2452. <https://doi.org/10.24925/turjaf.v10i12.2446-2452.5535>
41. Cetin, M. (2015). Using GIS analysis to assess urban green space in terms of accessibility: case study in Kutahya. *International Journal of Sustainable Development & World Ecology*, 22(5), 420-424. <https://doi.org/10.1080/13504509.2015.1061066>
42. Cetin, M. (2016). Sustainability of urban coastal area management: A case study on Cide. *Journal of Sustainable Forestry*, 35(7), 527-541. <https://doi.org/10.1080/10549811.2016.1228072>
43. Zeren Cetin, I., Varol, T., & Ozel, H. B. (2023). A geographic information systems and remote sensing-based approach to assess urban micro-climate change and its impact on human health in Bartın, Turkey. *Environmental Monitoring and Assessment*, 195(5), 540. <https://doi.org/10.1007/s10661-023-11105-z>

44. Zeren Cetin, I., & Sevik, H. (2020). Investigation of the relationship between bioclimatic comfort and land use by using GIS and RS techniques in Trabzon. *Environmental Monitoring and Assessment* 192, 1-14.
<https://doi.org/10.1007/s10661-019-8029-4>

45. <https://www.paksoyteknik.com.tr/paksoy-topcon/iha/parrot-anafi-thermal.html>



© Author(s) 2024. This work is distributed under <https://creativecommons.org/licenses/by-sa/4.0/>



The Multi-Disaster risk assessment: A-GIS based approach for Izmir City

Nur Sinem Partigöç*¹, Ceyhan Dinçer¹

¹ Pamukkale University, Department of City and Regional Planning, Türkiye, spartigoc@gmail.com, cdincer20@posta.pau.edu.tr

Cite this study: Partigöç, N. S., & Dinçer, C. (2024). The Multi-Disaster risk assessment: A-GIS based approach for Izmir City. International Journal of Engineering and Geosciences, 9 (1), 61-76

<https://doi.org/10.26833/ijeg.1295657>

Keywords

Disaster Risk
Resilient Cities
Geographic Information Systems
Risk Management

Research Article

Received:11.05.2023
Revised: 25.08.2023
Accepted:31.08.2023
Published:02.01.2024



Abstract

Urban settlements currently face many disasters that are increasing in number and frequency every day such as floods, landslides, sea level rise, storms, drought, forest fires, etc. due to the negative consequences of global climate change caused by significantly exceeding the carrying capacity of nature. Cities are currently becoming less resistant to disaster risks because of the unhealthy settlements. These settlements are becoming widespread in terms of physical, economic and social conditions as a natural result of the urbanization in which planning processes are carried out in an uncontrolled and unsupervised manner. This situation makes it a necessity to develop strategies and policies aimed at reducing and/or eliminating possible disaster damages which are defined as high risk. From this viewpoint, the study aims to reveal the current disaster risks in urban areas with a dense population and building stock. Izmir city is determined as the study area. Spatial analyses are performed for disaster risk by using Geographical Information Systems (GIS) tools and Weighted Overlay method considering the natural and built environment elements that significantly affect the disaster risk. The findings obtained from the study and the determinations made within the scope of the Izmir Provincial Disaster Risk Reduction Plan (IRAP) prepared by the Disaster and Emergency Management Presidency (AFAD) are evaluated comparatively. As a result, it has been seen that the determinations put forward for disaster risks have shown consistency throughout Izmir city and the studies carried out at the local level have been prioritized in such a way as to be aimed at risk management and prevention planning by the time.

1. Introduction

Urban growth and rapid urbanization are among the most interesting issues on a global scale. According to the UNHABITAT report [1], 52% of the world's population (3.6 billion people) lives in cities currently and the urbanization rate is projected to increase to 67% in the year 2050. Moreover, it is reported in the same report that the urban population ratio will reach 64% in less developed and developing regions. While considering that Türkiye is one of the developing regions, it is obvious that urbanization will gradually increase and the concept of urban sprawl will pose a problem in the country. In the report published by the United Nations [2], the population density has been increased from 27.6 people/km² to 102.2 people/km² per 1 km² between the years 1950 - 2020 and also the population of urban areas has quadrupled in the period of about 70 years in Türkiye.

Disasters are among the most important social and environmental problems in the urbanization processes [3, 4]. The main common feature of disaster can be shown as the leading motive. Disasters affect negatively the urban life and citizens suddenly and the hemorrhage may occur within the loss of life and property as well as large-scale economic and social losses. Disasters have occurred throughout the human history and have formed an important agenda in every period. Therefore, they have led to serious destruction due to rapid urbanization and negative outputs of urban facilities since the beginning of 20th century. Definite natural disaster examples can be listed as the famine occurred in India in 1900 and the USSR in 1921, the floods occurred in China between the years 1928 - 1939, the volcano eruption occurred in Colombia in 1985, the Kobe earthquake occurred in 1995. Besides, the poisoning of thousands of people by chemicals in India in 1984, the tsunami occurred after the Tōhoku earthquake in 2011, and the leak at the

Fukushima nuclear power plant are anthropogenic disaster examples [5, 6].

Urban settlements currently face many disasters that are increasing in number and frequency every day such as floods, landslides, sea level rise, storms, drought, forest fires, etc. due to the negative consequences of global climate change caused by significantly exceeding the carrying capacity of nature. The flood risk differs due to the local characteristics and dynamics of each city and also its frequency and impact are increasing. Actually, the floods occur and negatively affect the hydrological balance in the river basins because of the intensive building stock and land use decisions taken to meet the needs of the growing population with the acceleration of urbanization and industrialization. The interventions to natural areas referring to the built environment applications are made without considering the conservation-use balance and this situation significantly increases the disaster risk especially in urban settlements.

From this viewpoint, the study aims to reveal the current disaster risks in urban areas with a dense population and building stock. Izmir city is determined as the study area. Spatial analyses are performed for disaster risk by using Geographical Information Systems (GIS) tools and Weighted Overlay method considering the natural and built environment elements that significantly affect the disaster risk. The findings obtained from the study and the determinations made within the scope of the Izmir Provincial Disaster Risk Reduction Plan (IRAP) prepared by the Disaster and Emergency Management Presidency (AFAD) are evaluated comparatively. As a result, it has been seen that the determinations put forward for disaster risks have shown consistency throughout Izmir city and the studies carried out at the local level have been prioritized in such a way as to be aimed at risk management and prevention planning by the time.

2. The National and International Studies to Reduce Disaster Risks

Türkiye has a in a strategic position that is often exposed to natural disasters due to its geological, meteorological and topographical features. Among many disasters, earthquakes, landslides, floods, rock falls and avalanches are disaster types that the country has to cope with and take precautions. When the disasters are examined that occurred between the years 1980 - 2021, it is observed that an average of 6-25 people per one million people lost their lives due to natural disasters in each year in Türkiye. The country ranks fourth with 77 earthquakes in terms of major earthquakes that have occurred since the 1900s [7]. As it is known, Türkiye is one of the 'high-risk' countries of the world. The main reason for this determination is that disasters lead to extensive loss of life and property every five years on average.

The unhealthy settlements are becoming widespread in terms of physical, economic and social conditions as a natural result of the urbanization in which planning processes are carried out in an uncontrolled and

unsupervised manner. Therefore, cities are currently becoming less resistant to disaster risks [8]. This situation makes it a necessity to develop strategies and policies aimed at reducing and/or eliminating possible disaster damages. Although the policies will differ in different scales (country, region, city, local, etc.), the priority should always be given to ensuring that the safety of life and property of citizens for reducing disaster risks.

Balamir [9] explains the concept of resilient city as "it is a city or society that can minimize the losses suffered without losing its efficiency and productivity in the face of disasters and also maintain normal life". The disaster culture is explained as "a social environment in which characteristics such as having a comprehensive level of knowledge about disasters, behavioral habits to prevent losses caused by vulnerabilities and dangers, giving a wide place to protection methods in educational processes and communication techniques are learned."

While the documents including strategies and policies for disaster risk reduction at the international level are examined, it is obvious that the concept of disaster risk reduction is widely adopted by non-governmental organizations, government agencies and international organizations. Many organizations consider the climate change as a direct impact on the prevalence of disasters, as well as having a much greater impact in the future. In accordance with this, efforts to recognize that disaster risk reduction and climate change are closely linked are increasing both politically and practically. The tsunami that occurred in the Indian Ocean in 2004 dramatically reminded us of the fact that residential areas are under threat of disaster risks. This awareness led to an international conference on disaster risk reduction by the United Nations in Kobe, Japan in the year 2005. This conference has initiated the process of efforts by national and international organizations to define appropriate steps for disaster risk reduction [10].

The Hyogo Framework Action Plan is the first accepted internationally for disaster risk reduction studies. It has been emphasized that information, innovation and education should be used for the culture-making process of security and resilience in this plan at all scales. Five priority action plans have been identified within the scope of the Hyogo Framework Action Plan: (1) the determination of national and local priorities for disaster risk reduction, (2) the identification, assessment, monitoring of disaster risks and the development of early warning systems, (3) the usage of information, innovation and education in the process of designing a responsive society, (4) the reduction of key risk factors and (5) the preparation for effective response to disasters [4].

The Sendai Disaster Risk Reduction Framework, as a second international policy guide, is prepared by the United Nations Disaster Risk Reduction Office and includes the basic issues regarding the disaster risk management between the years 2015 - 2030. This document emphasizes that the urban investments for disaster risk reduction should come to the fore as a priority step in order to increase residential areas' resilience. Besides this, there exist other important

issues highlighted by this report such as determining the guidelines for disaster risk reduction, setting action priorities, defining the roles of stakeholders with different levels of authority and responsibility, strengthening international cooperation and global partnership, providing financial support to financial institutions, etc. [2].

In addition to international policy guides, significant reports and applications are examined which contain strategies and policies for disaster risk reduction at the national level. Among many reports and applications, 8th Development Plan (2001-2005), 9th Development Plan (2007-2013), Integrated Urban Development Strategy and Action Plan (KENTGES), Law No. 6306 and Spatial Plans Construction Regulation emphasize not only the disaster risks posing a threat to residential areas, but the concept of resilience is not discussed. However, the importance of the resilient city concept has been emphasized and a wide area has been devoted to disaster risk in the National Earthquake Strategy and Action Plan (UDSEP) (2012-2023) and 10th Development Plan (2014-2018).

The mentioned reports are comparatively analyzed. In accordance with this comparison, it is seen that the 8th Development Plan is a plan that makes a full self-assessment in the closest period to the Düzce earthquake and emphasizes the effort to produce solutions. Although the concept of resilient city is not included in this plan report [11]. It is only emphasized that the decoupling of interagency authority and responsibility should be rationalized and priority will be given to the planning of regions with high disaster risk in 9th Development Plan [12]. The KENTGES Project is prepared in between the years 2007-2013 and Law No. 6306 is decertified [13]. However, the concept of a resilient city is not included and there is no emphasis on participation which indicates the development of social consciousness related disaster risks in the Law No. 6306 and Spatial Plans Construction Regulation. According to Law No. 6306, only high risky areas are identified and zoning plans for urban regeneration projects are implemented for these areas in order to reduce the disaster risk.

The concept of a resilient city has been expressed firstly in the UDSEP report (2012-2023) which has been published in the year 2011. The UDSEP report and 10th Development Plan (2014-2018) are important and strategic plans for guiding strategies in urban planning discipline. The urban planning as a tool and its role are defined in the disaster risk reduction and management processes in both documents [14, 15]. It is generally aimed to realize the earthquake-resistant, healthy and safe settlements for urban areas with these studies. The disaster volunteer system is established in the process of the participation of citizens and private sector and insurance will be encouraged for a resilient city where the earthquake problem is intense [16]. Urban planning should also be used as a principal tool in the realization of these mentioned strategies and actions. In the 10th Development Plan, the concept of disaster risk under the title of 'Livable and Sustainable Environment' is given wide publicity by emphasizing the importance of urban development and improvements. In this plan report, it is

stated that studies for the disaster risk reduction are carried out due to the type of threat from micro-zoning applications for safe settlements and this issue is related to zoning planning processes in resilient cities [17]. For effective disaster risk management and resilience, it is emphasized that minimizing the disaster risks in urban generation processes, increasing social awareness and spreading earthquake risk insurance are crucial [17].

In sum, while considering that 52% of the world's population and 93% of the population in Türkiye live in urban areas today, it is clear that the possible loss of life, property and urban areas may be higher than before regarding disasters increasing in number and frequency due to global climate change. When the national and international studies to reduce disaster risks are examined, this result is an expected result. Although the awareness of the built environment's pressure on the natural environment and the implementation of decisions related to the natural environment began in the 1970s, an understanding of the disaster risks caused by the urbanization dynamics has been realized over a period of about 10-15 years. As this determination includes an important change process and opportunity in itself, it also shows the urgency of the practices that need to be implemented regarding disaster risks at the national and international levels.

3. Method

3.1. Study Area

Totally 30 districts are selected as the study areas which are located in Izmir Metropolitan city. These districts can be listed as Aliağa, Balçova, Bayındır, Bayraklı, Bergama, Beydağ, Bornova, Buca, Çeşme, Çiğli, Dikili, Foça, Gaziemir, Güzelbahçe, Karabağlar, Karaburun, Karşıyaka, Kemalpaşa, Kınık, Kiraz, Konak, Menderes, Menemen, Narlıdere, Ödemiş, Seferihisar, Selçuk, Tire, Torbalı and Urla districts. In Figure 1, the location of Izmir city within all districts defined as the study area is presented. Izmir city is located in the west part of Türkiye and is the third largest city in terms of population. The reasons why Izmir Metropolitan city is chosen as the study area are as follows:

- Its location in the earthquake zone,
- The presence of two large and active fault zones within the built environment,
- Its current geological and tectonic characteristics increasing the risk of disasters in the urbanization process,
- Different types of disasters have occurred in the historical process,
- The development of the existing built environment which is limited in a certain area due to natural thresholds within a basin,
- The suitability for settlements from a topographical point of view varies regionally,
- The settlement texture expanding towards natural areas especially the alluvial plains,
- The city is in a rapid and unhealthy urbanization process in terms of population and building density,

3.2. Data

Many disasters happen in Izmir city because of the geological, topographical and climatic characteristics of the city such as earthquakes, landslides, rock falls, floods, meteorological and climatic disasters, fires, industrial accidents, etc. [20]. From the point view that the entire city is at risk in terms of the direct and/or indirect effects of disasters, it is aimed to reveal the current disaster risks in Izmir city where residential settlements are located with high disaster risk. Accordingly, the parameters constituting the disaster risk are generally divided into two groups. Totally 9 parameters which are taken into account during the spatial analysis process and including the elements related to the natural and built environment are listed as:

- a) Parameters related to the natural environment-> Topographic parameters (slope, aspect, elevation), meteorological parameters (temperature, precipitation amount), fault lines, hydrology, geological formation and soil ability.
- b) Parameters related to the built environment-> Current land use pattern.

The thematic maps are prepared for slope (Figure 2), aspect (Figure 3) and elevation (Figure 4) within the scope of the study. These maps related to the natural environment are examined and it is found that the inclined areas with a slope value between 0 - 10%, areas with an elevation value between 0 - 300 meters and the south aspect features are concentrated in central districts of the city. When considered the built environment has been developed on the mountains

perpendicular to the sea, the plains between them and the coastal area, topography is one of the most important determinants of spatial location selection in city. For this reason, it is observed that the spatial development observed around the city is not in compact form, but in the form of linear development. Actually, potential residential areas are quite limited around the central districts because of natural thresholds. In other words, the topography factor allows for very limited development in terms of new residential areas where the slope value is suitable for settlements between 0 - 10% are only 8.6% of the entire city [21]. Due to this, it can be said that the topographic parameters are the basic factors that increase the disaster risk and can affect it negatively in the study area.

The thematic maps are prepared for fault lines (Figure 5), hydrology (Figure 6), soil ability (Figure 7) and geological formation (Figure 8) within the scope of the study. These maps related to the natural environment are examined. It is found that there are totally 21 fault lines in the entire city that cause any earthquake of magnitude 6 that can trigger other disasters like tsunami (Figure 5). Therefore, according to the findings obtained from the hydrological analysis, it is found that there exist rich underground and above-ground water resources in Izmir city, especially the most important rivers (Küçük Menderes, Bakırçay and Gediz rivers). So, it is obvious that about 54% of city is located within the boundaries of the Küçük Menderes basin, 16% is located within the Gediz basin and 25% is located within the Northern Aegean basin [22] (Figure 6). The entire city and its surroundings have important disadvantages in terms of the disaster risks that the presence of water may cause depending on meteorological and climatic conditions.

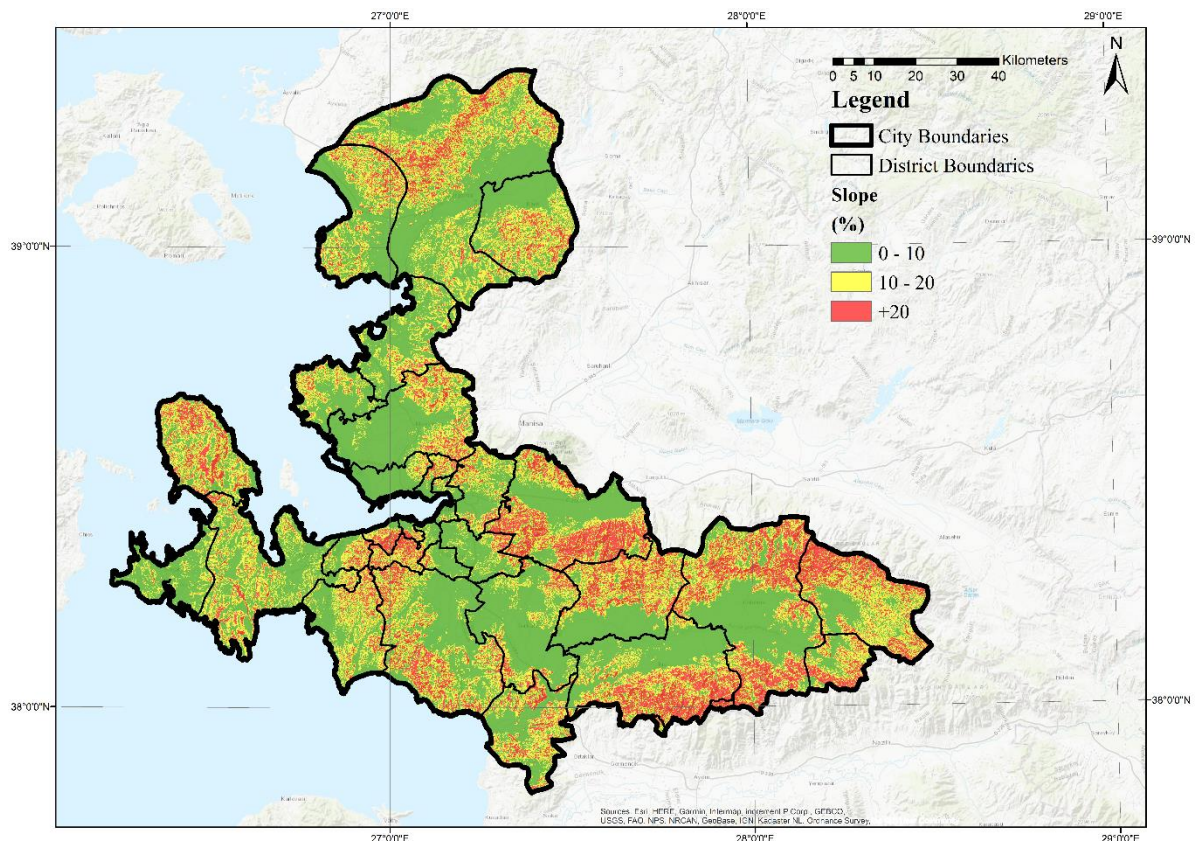


Figure 2. Slope analysis.

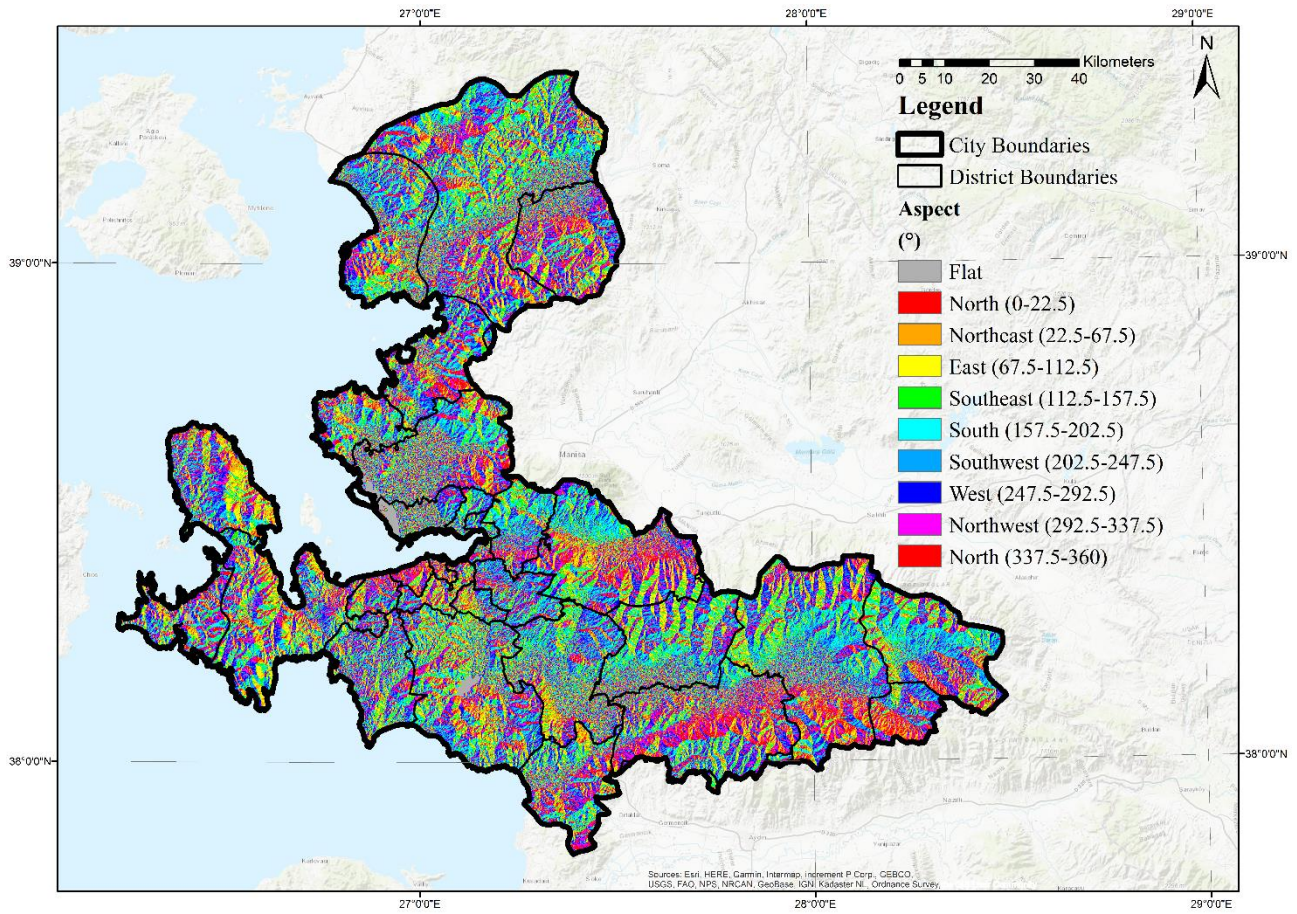


Figure 3. Aspect analysis.

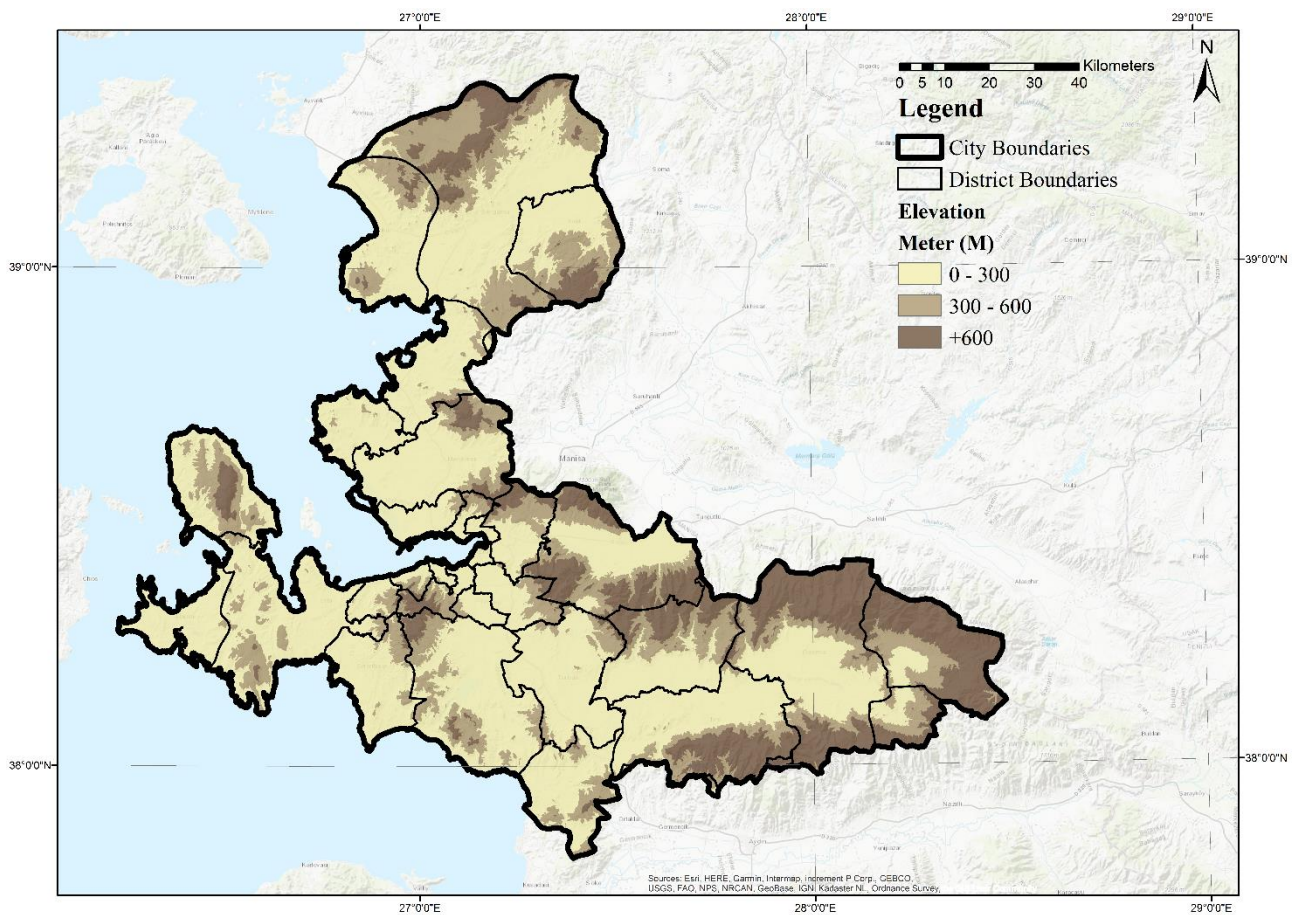


Figure 4. Elevation analysis.

Besides, according to the findings obtained from the analysis of soil ability, it is found that there are large soil groups throughout the city (alluvial soils, brown soils, chestnut-colored soils and red soils) with climatic conditions and topographical effects. The alluvial soils in the north and west parts and the red soils in the south and east parts of the central districts of city are basic factors that increase the disaster risk for landslides and floods (Figure 7). Incidentally, according to the findings

obtained from the geological formation analysis, it is clear that neogene and quaternary sediments, early miocene granitoids, neogene volcanics and Izmir fluxus are mainly located throughout the entire city (Figure 8). All areas except the north-east part of the central districts are not suitable for construction due to the existing soil characteristics while these formation types are examined in terms of suitability for the settlements.

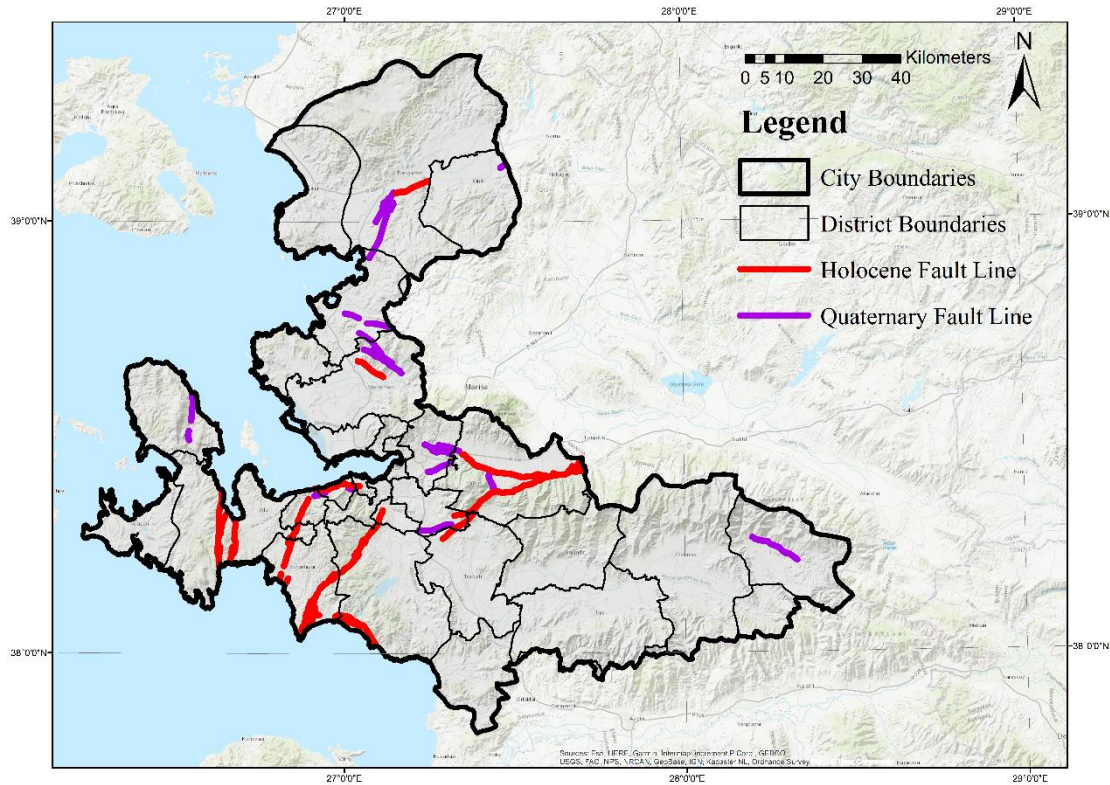


Figure 5. The fault lines' analysis.

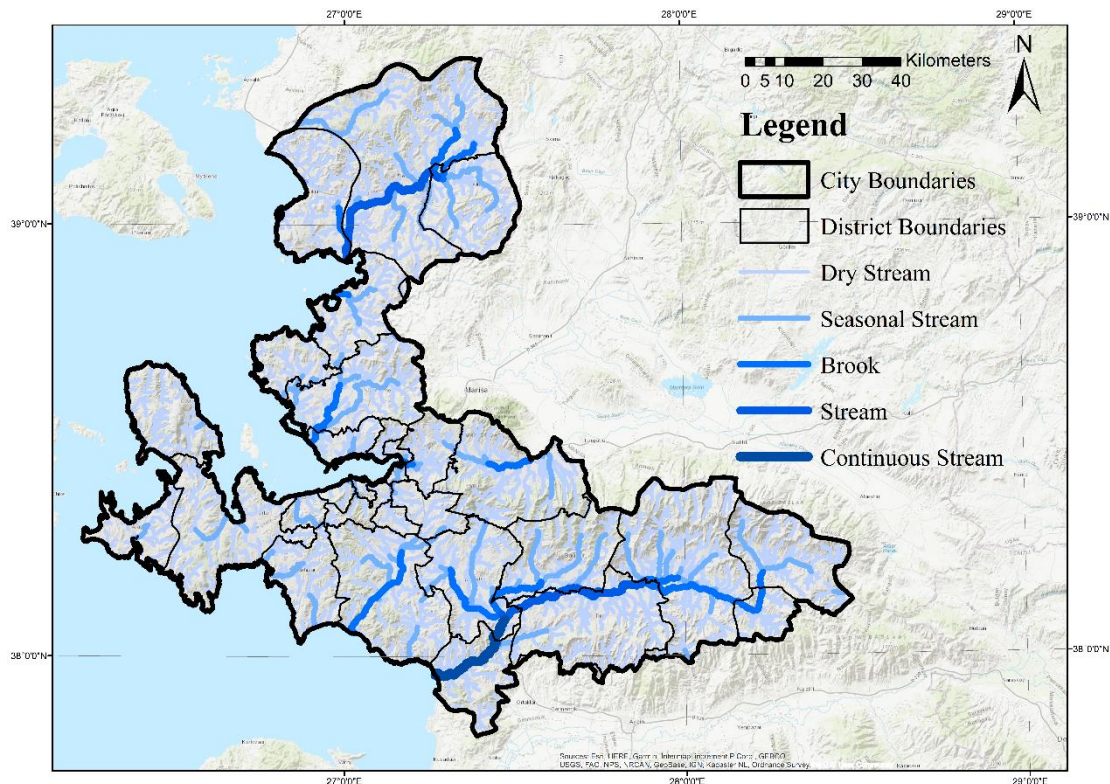


Figure 6. Hydrological analysis.

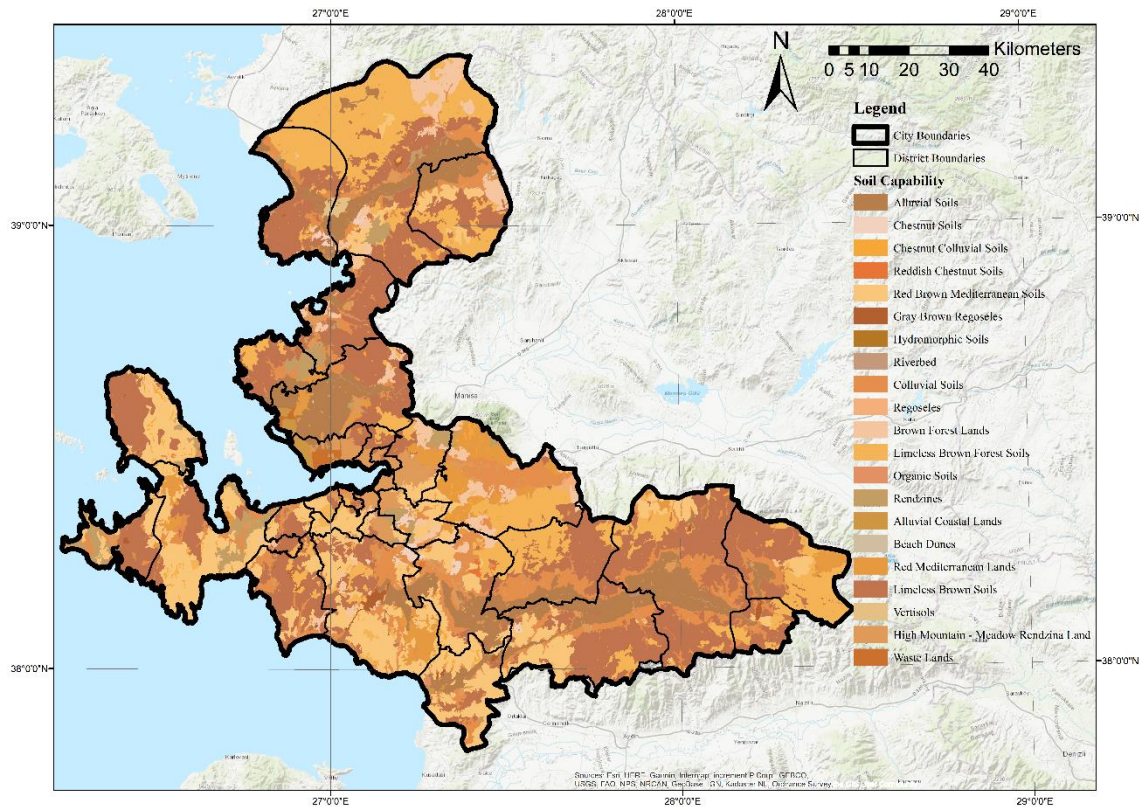


Figure 7. Soil ability analysis.

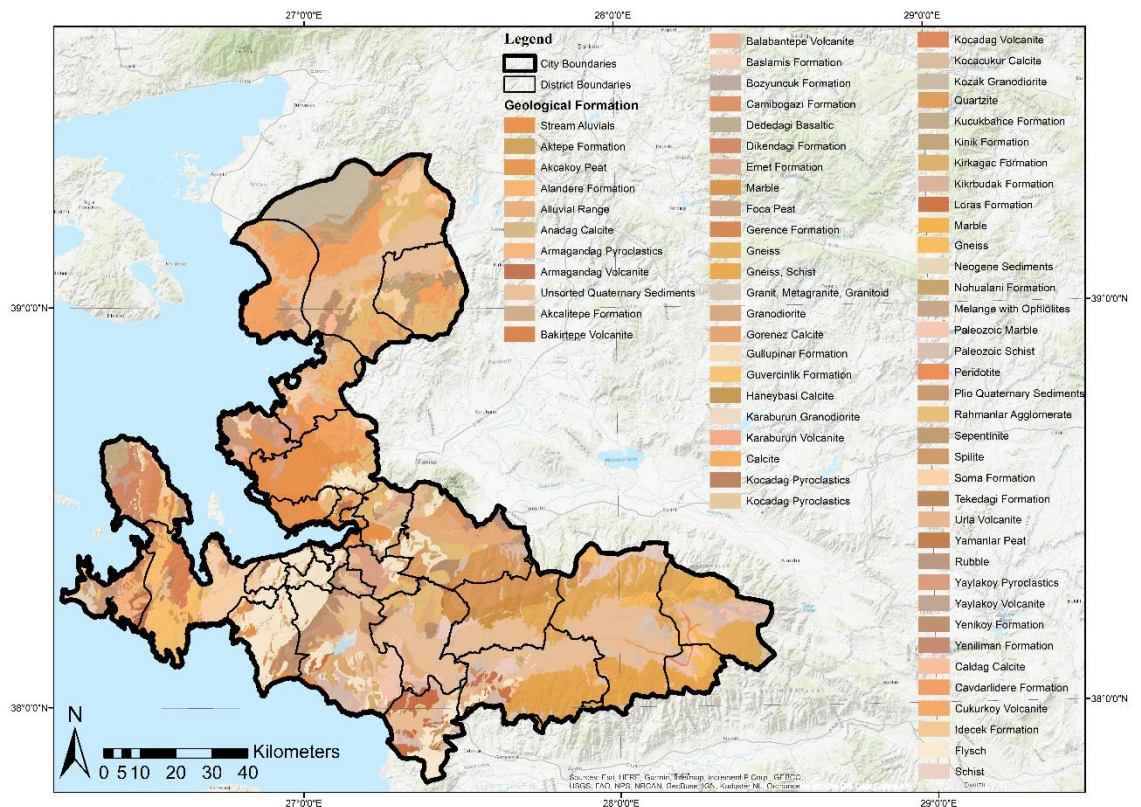


Figure 8. Geological formation analysis.

The current climatic and meteorological features are directly related to the disaster risks in urban areas. Based on this point, the thematic maps are prepared for the temperature (Figure 9) and precipitation amount (Figure 10) within the scope of the study. As well as slope, aspect, elevation, fault lines, hydrology, geological formation and soil ability, these maps related to the natural

environment are examined. It is found related the temperature and precipitation amount that the average annual temperature value is 17°C and the average precipitation amount is 700 mm in the city located in the Mediterranean climate zone. As it is known, the perpendicular position of the mountains to the sea, the sea effect can reach as far inland as the plains. For this

reason, the characteristics of the typical Mediterranean climate (warm and rainy in winter season, dry and hot in summer season) are monitored in the study area. Actually, there exist definite factors which increase disaster risks in urban areas such as the rainy season lasting for about 6 months in a year, significant differences in the precipitation amount between summer

and winter seasons, the excessive precipitation in the winter season and drought caused by low rainfall in summer season, etc. The extreme precipitation events observed outside the seasonal norm cause losses of life and property due to flooding in rural and urban areas and damage to urban infrastructure elements.

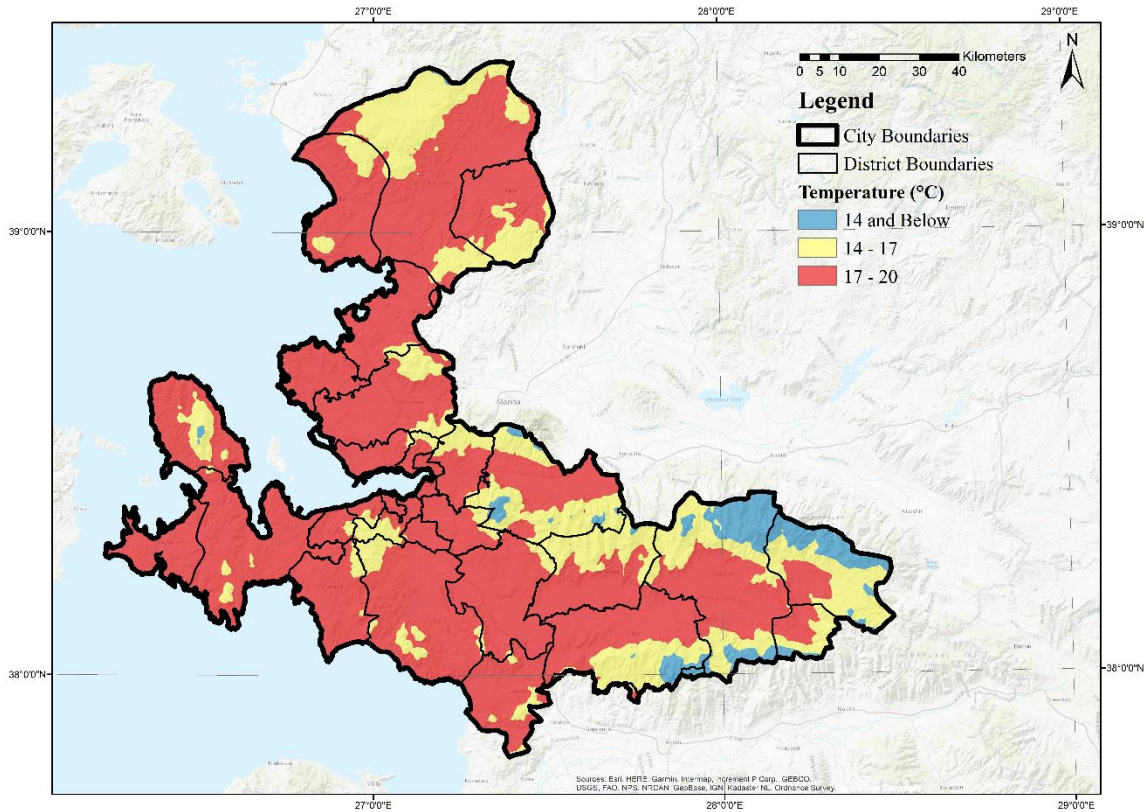


Figure 9. Temperature analysis.

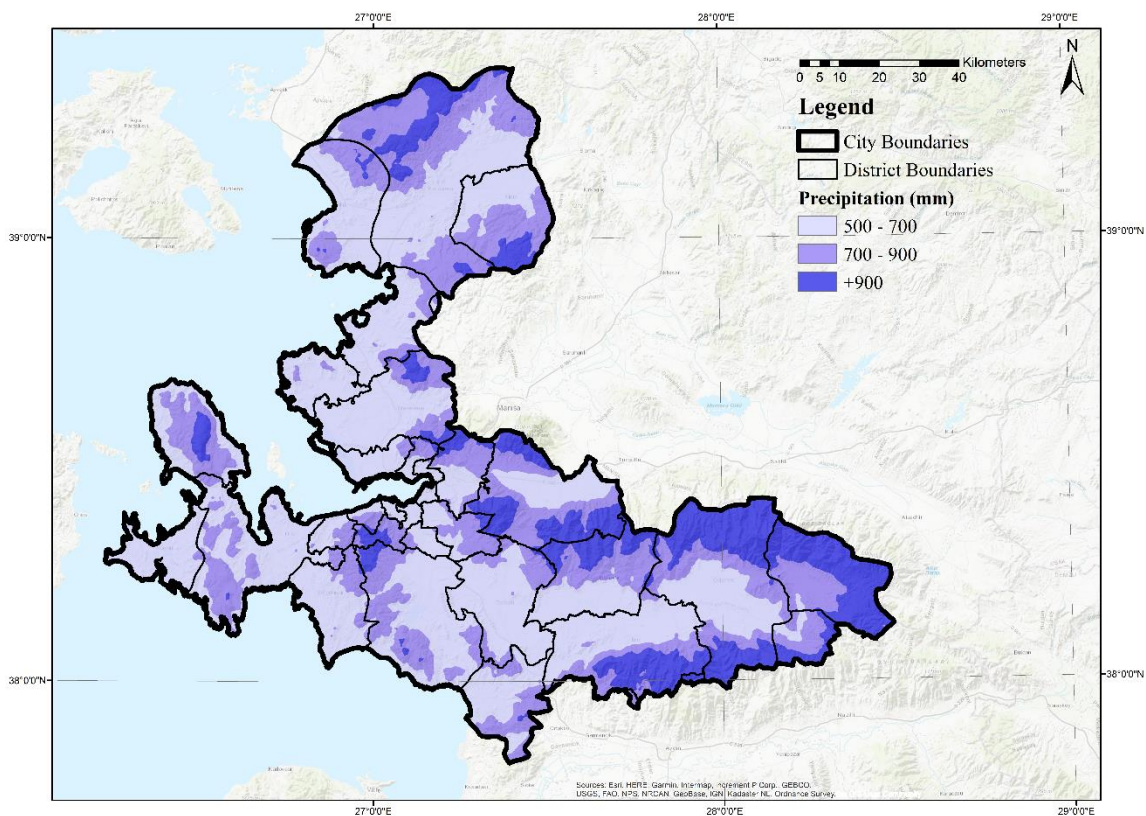


Figure 10. Precipitation amount analysis.

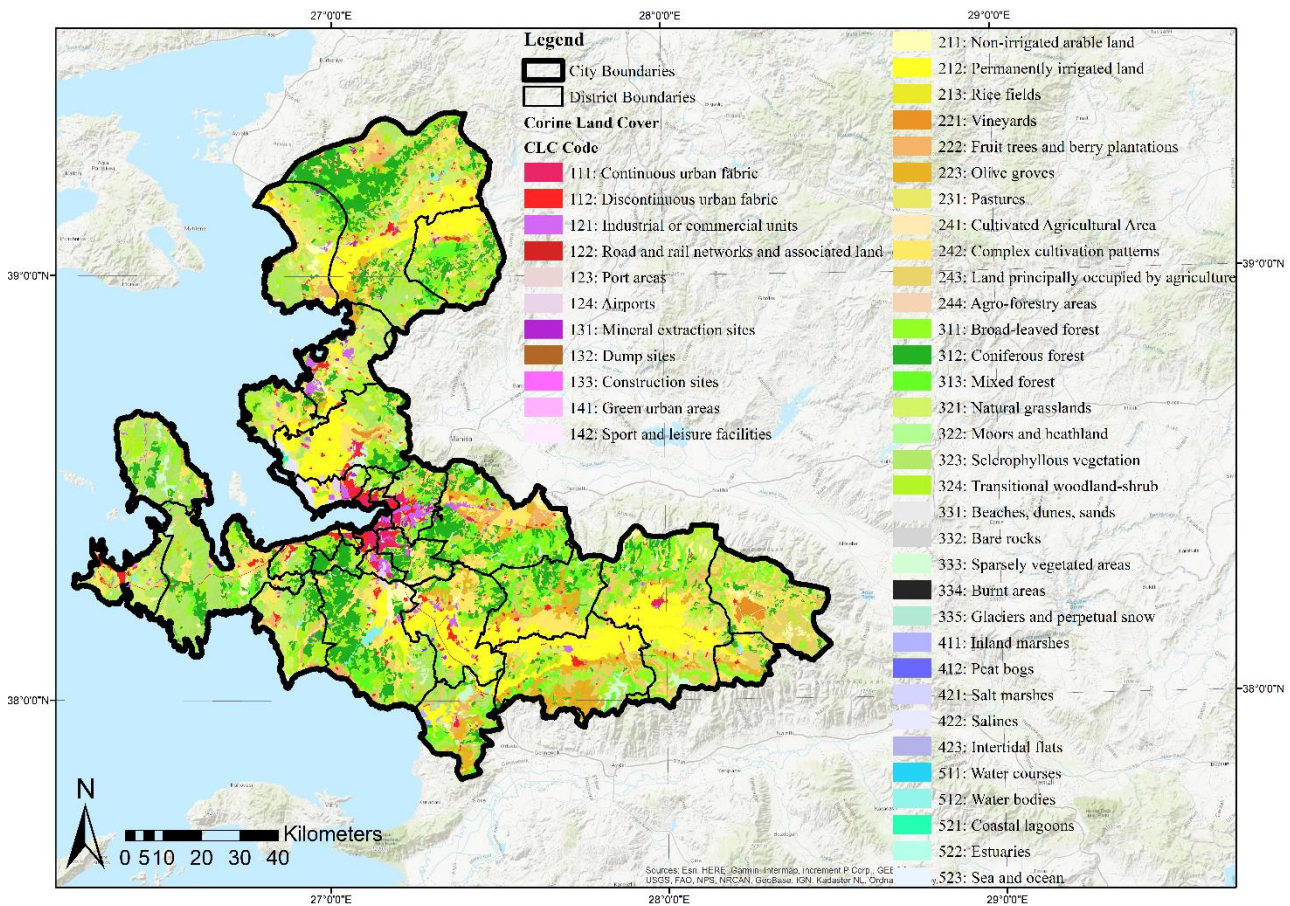


Figure 11. Thematic maps for the built environment parameters (The land use pattern analysis)

According to the results obtained by the General Directorate of Meteorology after analyzing the drought throughout the country for the period March 2022 – March 2023, Izmir city is classified in the class of very severe arid cities [23]. It is estimated that the drought observed is severe throughout the entire city and in its surroundings and the negative effects of drought will increase over time regarding global climate change. So, the study area is in a disadvantaged situation in terms of disaster risks because of facing the threat of drought.

The thematic map is prepared for current land use pattern within the scope of the study and also presented in Figure 11. This map related to the built environment is examined. It is found that forest areas (39%) and agricultural areas (33%) are the largest areas among the land use types in the entire city. As other land use types, there exist residential areas (17%), tourism areas (5.5%) and other land uses (archaeological sites, special environmental protection areas, etc.) (approximately 5.5%). Actually, important advantages are observed for the natural environment parameters such as the large area size of forest areas comparatively in land use types, residential areas constituting about 20% of the entire city, the excess of agricultural production areas providing significant economic returns, etc. Although this determination has significant risks in terms of possible disaster risks (forest fires, earthquakes, floods and drought).

The main objectives of the urban planning process include designing the built environment by considering the protection-use balance, eliminating today's needs

without renouncing the needs of future generations, ensuring sustainability in social, economic and environmental dimensions. In addition, it is crucial that risk management processes are carried out correctly before possible disasters in order for citizens to live in urban areas which are healthy, safe and high quality. It is a necessity to reveal the risk related to the disaster types qualitatively and quantitatively in urban areas where the population is rapidly increasing. The idea of identifying existing risks as a priority in order to develop policies and strategies specific to disaster risk settlements has been successfully put forward with the Provincial Disaster Risk Reduction Plan (IRAP) in the period of September 2021 [20]. A similar content appears in the study named The Disaster Prevention / Mitigation Basic Plan including Seismic Micro-Zoning for the Province of Istanbul prepared by the Japanese International Cooperation Agency (JICA) and Istanbul Metropolitan Municipality (IBB) in the year 2002 [24].

Accordingly, it is aimed to conduct a comprehensive analysis of the disaster risks for the Izmir city within the scope of the study. For this purpose, one of the Geographical Information Systems (GIS) tools named the Weighted Overlay method is used. Spatial analyses are performed for 4 different disaster types (earthquakes, mass movements, floods, industrial accidents, fire, meteorological disaster and climate change, medical geological disasters, infectious diseases, etc.) in the study. These types are identified for Izmir city by the Izmir Provincial Disaster and Emergency Department taking into accounts the natural and built environment

elements that significantly affect the city's resilience. The findings obtained from the study and the determinations made within the scope of the Provincial Disaster Response Plan and the Provincial Disaster Risk Reduction Plan (IRAP) prepared by the Provincial Disaster and Emergency Directorate of the Izmir Governorate is evaluated comparatively.

The Weighted Overlay method as the selected method is has been widely preferred for spatial and non-spatial studies related to disaster risks in which more than one type of disaster related to settlements has been observed. This method is applied in various studies regarding the different disaster risks (flood, landslide, earthquake, rockfall, tsunami, etc.). As examples, researches for Bitlis city [25], Malatya city [26], Istanbul city [27], Manisa city [28], Hatay city [29] and Van city [30] can be given. In addition to these, there exist many researches emphasizing the importance of disaster risk analyses in carrying out urban planning and disaster planning processes together [31-35] in the academic literature.

A database including current data has been constituted via ArcMap software. Using the mentioned database, the following steps are followed in the study:

1. The digitization of the natural and built environment parameters (slope, aspect, elevation, temperature, precipitation amount, fault lines, hydrological structure, soil ability, geological formation and land use pattern),
2. The controlling of coordinate systems of data layers,
3. The classification of parameters according to their features,
4. The transferring spatial and non-spatial features to thematic maps,
5. The determination of the weights of the parameters that pose a risk according to the identified disaster types,
6. The synthesis of data analyzed in separate layers by overlapping,
7. The comparative evaluation of the obtained analysis results with the Provincial Disaster Response Plan and the Provincial Disaster Risk Reduction Plan.

Table 1. The classification of parameters.

Parameter	Values	Classification of Disaster Risk	Class	Weight (%)
Slope (%)	0 - 10	Less risky	1	20
	10 - 20	Medium risky	2	
	20 and above	More risky	3	
Aspect	East - West	Less risky	1	5
	South (South, South-east, South-west)	Medium risky	2	
	North (North, North-east, North-west)	More risky	3	
Elevation (meter)	0 - 300	Less risky	1	5
	300 - 600	Medium risky	2	
	600 and above	More risky	3	
Precipitation amount (mm)	500 - 700	Less risky	1	10
	700 - 900	Medium risky	2	
	900 and above	More risky	3	
Temperature (°C)	14 and below	Less risky	1	5
	14 - 17	Medium risky	2	
	17 and above	More risky	3	
Fault lines	Yes	Less risky	1	10
	No	More risky	3	
Hydrological structure	Day stream	Less risky	1	15
	Seasonal stream	Less risky	1	
	Brook	Medium risky	2	
	Stream	More risky	3	
	Continuous stream	More risky	3	
Soil ability	Brown soils	Less risky	1	5
	Chestnut-colored soils	Medium risky	2	
	Alluvial soils	More risky	3	
	Red soils	More risky	3	
Geological formation	Granitoids	Medium risky	2	15
	Volcanics	Medium risky	2	
	Sediments	More risky	3	
	Flish	More risky	3	
Land use pattern	Agricultural areas	Less risky	1	10
	Meadow-pasture areas	Less risky	1	
	Other land uses	Less risky	1	
	Forests	Medium risky	2	
	Tourism areas	Medium risky	2	
	Industrial areas	Medium risky	2	
	Transportation-infrastructure	More risky	3	
	Settlement areas	More risky	3	

The disaster risk classifications are made using the natural and built environment parameters within the scope of the study in order to make spatial analyses (Table 1). Accordingly, the parameters due to these classifications can be listed as follows: Slope, aspect, elevation, precipitation amount, temperature, fault lines, hydrological structure, geological formation, soil ability and land use pattern.

As natural environment parameters, the slope is an important factor in the formation of floods because it affects the amount of precipitation accumulated and the flow rate. The slope value is high where the water retention ability of the soil is lower in comparison to the slope value is low. In addition, the slope is among the most important factors that increase the erosion risk [36, 37]. Therefore, as the slope increases, the risk for certain types of disasters increases. The aspect is a factor that creates a disaster risk for floods, droughts and erosion. The direction of the topography differs on the northern and southern slopes. On the south-facing slopes, the loss of water in the soil due to evaporation is high, so the potential of drought increases in these areas. On the north-facing slopes, the holding capacity is low because there is too much moisture in the soil, so the risk of flooding and erosion is high in these areas. The riskiest areas are the north-facing slopes in terms of flood risk [30]. The elevation values are high where the slope increases. Streams with high flow accumulation in areas where slope values are high increase the risk of floods and erosion in these areas. In other words, where the river valley expands, the elevation values are low, the slope values and also disaster risks decrease [36].

One of the natural environment parameters given the reference to meteorological and climatic features is the precipitation amount. According to climatic features, the excessive and torrential rainfall increases the risk of erosion, flooding, especially on slopes where the slope is high and vegetation is rare in spring and winter in the semi-arid climate class. The temperature is a climate element that controls geographical conditions and life activities closely [38]. It is the most dynamic parameter that creates the climatic conditions of a place and also plays a decisive role on the living conditions of flora and fauna with its effect on the occurrence and the precipitation amount. The temperature parameter is the primary factor especially in meteorological disasters and climate change. This parameter has a direct or indirect effect on the occurrence of disasters that enable people to perform many activities or interrupt these activities [39]. As another parameter related to the natural environment, the fault lines are one of the geological features of residential areas, the degree of influencing the disaster risk varies according to the fracture length, fracture width, fracture area and surface displacement for a fault line [40]. The residential areas are disadvantaged in terms of earthquake risk while a dense population lives close to fault lines and are located in areas where there is liquefaction of the ground [41].

The hydrological structure is one of the prominent parameters in terms of the presence of underground and above-ground natural resources. Floods are a stage of the hydrological cycle and are a form of surface runoff which

is one of the important types of disasters. Floods may occur from the source in river basins, geological structure of the basin, soil structure, topographical structure, climatic, etc. [42]. As a result of the construction processes into the streams and stream beds and incorrect and unplanned land use decisions, the existing waterbed turns have narrowed and natural cases turn into disasters [43, 44]. The soil ability, as another natural environment parameter, shows different susceptibility states to erosion depending on the slope condition of the land and the lithology on which it develops and the presence of vegetation. Although the soil has a resistant property on slopes where the slope is too high and devoid of vegetation, it may be subject to erosion depending on the severity of precipitation. On the other hand, the non-resistant soil structure that develops in parts where the slope is low and vegetation is frequent may be less susceptible to erosion. Brown soils are young soils that develop in sloping places and are known as steppe soils. This type of soil has a high water-holding capacity which is poor in terms of organic matter content. Chestnut-colored soils are a type of soil with an average annual precipitation of 400 mm and above, formed in meadow and oak forests, containing organic matter and can be seen in pastures in high-slope areas while they are productive enough to be farmed. Alluvial soils and red soils are among the species that increase the risk for landslide and flood-type disaster events due to their less resistant and soft-soil structures [36, 45].

According to the examination related to the geological formation parameter, it is found that neogene and quaternary sediments, early miocene granitoids, neogene volcanics and Izmir fluxus are mainly included in the study area. The formations of sediments and the flash formation are appropriate in terms of suitability for the settlements. The flash formation is very often subject to landslides during different periods and is unsuitable for construction due to the risk factor for disasters. Granitoids with gravel structure and volcanics with fragile mineral structure are partially suitable for construction due to the fact that they do not have a solid ground in terms of structural statics and safety. It can be said that the types of geological formations are a trigger factor for disaster risks for the study area that are not suitable for settlements.

As the built environment parameter, the land use pattern is selected within the scope of the study. It is an important element in the planning processes that the plan decisions developed regarding the existing land use types do not have a nature that increases the disaster risks. There exist definite areas that may cause increased losses of life and property in case of disaster and carry a high risk such as residential areas where there is a dense population and structure, industrial areas where industrial production is carried out and transportation, access, communication in urban areas, etc. Although there is no risk of loss of life and property in forest areas, meadows, pastures and agricultural areas located outside urban centers, the potential economic losses should be taken into account because of drought, fire and flood cases [18, 46-49].

According to the synthesis map reveals the disaster risk status of Izmir city in Figure 12, the districts located in the east and south parts of the city (Bornova, Kemalpaşa, Karabağlar, Gaziemir, Menderes, Bayındır and Karaburun districts) are relatively disadvantaged in terms of disaster risk. In addition, it is found that the districts located in the north, west and south-east parts of the city (Çeşme, Buca, Torbalı, Aliağa, Foça, Dikili, Bergama and Güzelbahçe districts) are more advantageous and the less risky residential areas are

relatively more in these districts. Other districts can be classified as medium risk (Çiğli, Bayraklı, Karşıyaka Menemen, Konak, Balçova, Narlıdere, Seferihisar, Selçuk, Tire, Ödemiş, Kiraz and Beydağ districts). Accordingly, there is a determination for all residential areas with urban and rural characteristics throughout the city are affected by the disaster risks that can be created by 4 different types of disasters identified by the Izmir Provincial Disaster and Emergency Department.

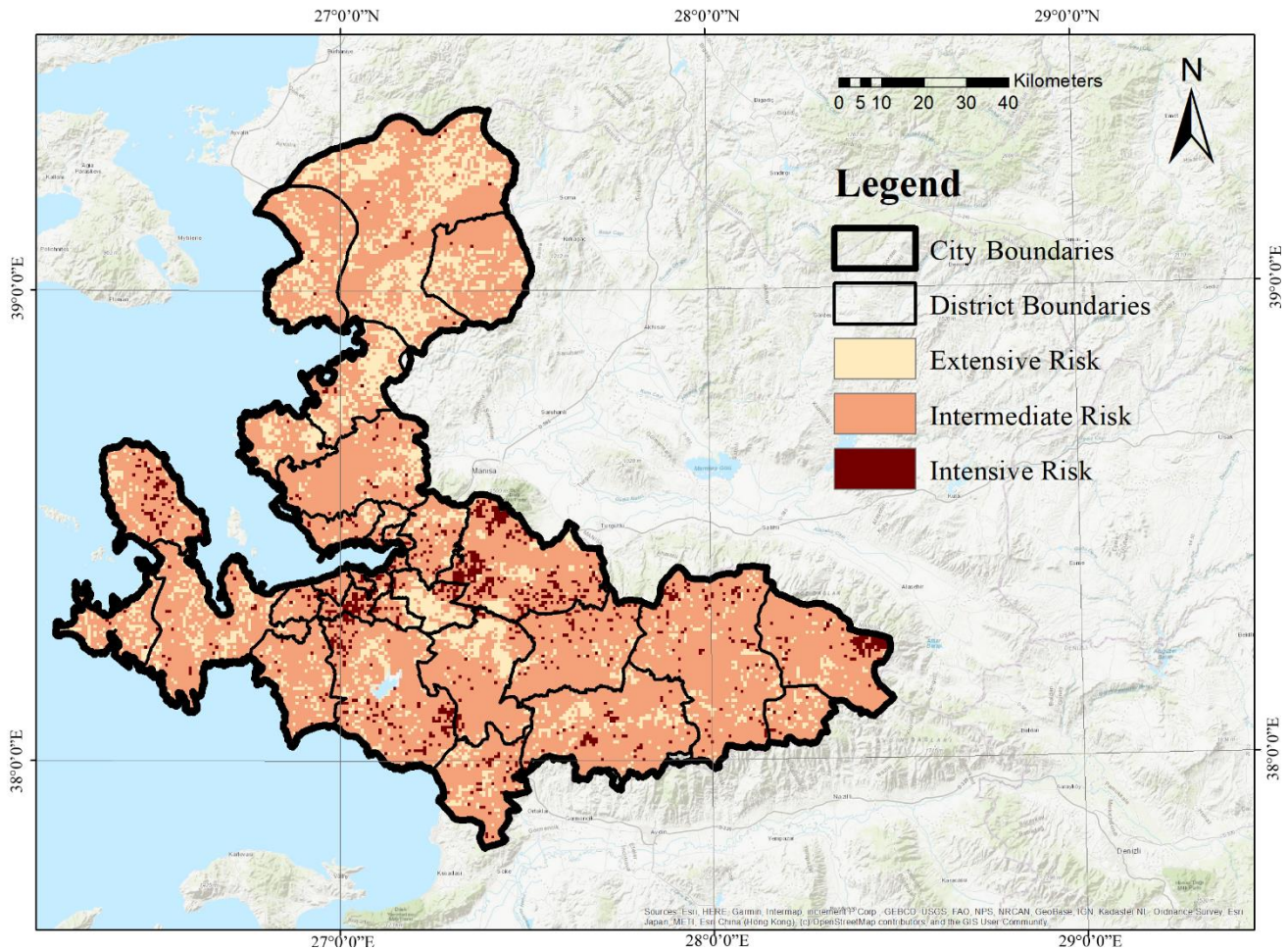


Figure 12. The disaster risk classification of Izmir city.

4. Results and Discussion

The topographic, meteorological and climatic features of the Izmir city are examined comprehensively in this study. The prominent result is that the disaster events that pose a disaster risk throughout the city are similar to the determinations related to these events prepared by the Ministry of Interior Disaster and Emergency Management Directorate. According to the data given from the Turkish Disaster Information Bank (TABB), a total of 27,049 disasters occurred throughout the country between the years 1990 – 2018 and 7616 of these disasters are landslides (28%), 1871 earthquakes (7%) and 17,562 other disasters (65%) [7]. Additionally, a total of 494 disasters occurred in Izmir city between the years 2009 – 2020 and 188 of them are fires (38%), 131 are earthquakes (26.5%), 93 are floods (19%) and 52 are other disasters (16.5%) [20].

The synthesis map is prepared as a result of spatial and non-spatial analyses and reveals the disaster risk situation of Izmir city. It is clear that it is an expected result that urban and rural areas will be affected by the disaster risks that different types of disasters may pose throughout the city. Moreover, due to the spatial analyses made using 10 basic elements related to the natural and built environment, it is determined that the districts located in the east and south parts of Izmir city (Bornova, Kemalpaşa, Karabağlar, Gaziemir, Menderes, Bayındır and Karaburun districts) are relatively disadvantaged in terms of disaster risk. The districts located in the north, west and south-east parts of the province (Çeşme, Buca, Torbalı, Aliağa, Foça, Dikili, Bergama and Güzelbahçe districts) are comparatively more advantageous and the less risky. Other districts (Çiğli, Bayraklı, Karşıyaka, Menemen, Kınık, Konak, Balçova, Narlıdere, Seferihisar, Selçuk, Tire, Ödemiş, Kiraz and Beydağ districts) can be classified as medium risky. In summary, as a result of the

study, it is revealed that almost all residential areas are in a more advantageous situation except for residential areas located in the east and south parts of Izmir city in terms of the disaster risk.

The findings of this study and disaster-oriented planning studies realized for Izmir city are considered comparatively. This comparison is important because the examination related to whether necessary and sufficient steps have been taken is crucial for reducing risks before possible disasters, preventing possible losses of life and property and constituting more resilient urban areas in terms of disaster risks. The report titled the Izmir Provincial Disaster Risk Reduction Plan (IRAP) is one of the documents examined in the study which has been prepared by the Provincial Disaster and Emergency Directorate of Izmir Governorship (AFAD) in the year 2021. This document comes to the fore as the main determination for the correct and effective implementations of Risk Reduction and Prevention Planning processes. Defined determinations are listed as [20]:

a. Totally 494 disasters significantly affected about 1546 houses that occurred in Izmir city between the years 2009 - 2020. In particular, the majority of the structures have been built before the year 1999 and they are not resilient for any disaster risks. In particular, the importance of urban regeneration implementations should be practiced correctly in designing the healthy, safe and resilient built environments especially with the impact of the earthquake that occurred on October 30, 2020.

b. About 6% of the population (253,802 people) is at risk of floods due to the existence of three important river basins. In this context, maps for flood risk and hazard maps have been made according to three different scenarios for 50, 100 and 500 years within the scope of the flood management plans. Various steps have been taken such as prioritizing flood-risk areas and taking the necessary measures to reduce the flood risk regarding the results obtained.

c. Totally 129 integrated disaster risk maps have been prepared within the scale of 1/25,000. These maps include a total of 109 landslide areas, 367 rockfall areas and 20 avalanche areas located throughout the city. In addition, geological – geotechnical survey reports have been prepared which are an important data in the development of plan decisions aimed at reducing disaster risks. Totally 71 survey reports are based on the disaster types throughout the planning area (landslides, rockfalls, floods, liquefaction, high groundwater, etc.). Thus, the precautions have been determined to be taken against the disaster risks and it has been provided to form the basis for land use decisions.

d. About 92% of the total 268 fires that occurred in the last ten-year period are caused by anthropogenic factors and a total area of 1137 hectares is affected. The forestation has been carried out on a total area of 6764 hectares and fire prevention facilities have been planned for the rehabilitation of fire areas within this scope.

In the report of the Izmir Provincial Disaster Risk Reduction Plan (IRAP), there exist SWOT analysis for four disaster types, 1 main goal, 27 goals and 227 action plans for disaster risk reduction have been determined. As stated in this report, the main purposes of these studies are defined to identify risks and possible effects of disasters, to take measures to reduce and/or minimize possible risks and losses of life and property caused by disasters, to identify actions and institutions / organizations responsible for these actions in order to take measures, to make the province a disaster-ready and resilient residential areas, to design healthy and safety residential areas, to make urban areas sustainable and livable by increasing the economic, social and environmental resilience of the city [20]. Therefore, responsible and supportive stakeholders have been identified on the basis of each action, the prescribed timetable for the implementation of actions has been set out and a process based on central and local governments' cooperation has been described in this plan report.

5. Conclusion

The findings obtained from the study are evaluated comparatively with the findings obtained within the scope of the IRAP report due to the studies carried out in Izmir city, it can be seen that the determinations put forward for disaster risks in particular districts showed the consistency. In addition, it has been observed that the studies have been prioritized which are carried out at the local level in terms of disaster risk management and prevention planning.

Although it is known that the crisis management stages for during and after disasters have been successfully applied in both national and local levels, the importance of risk management referring to the pre-disaster period is increasing day by day in coping with the negative effects of disasters. As a result of today's modern understanding of disaster management, risk analysis, search and rescue activities, post-incident recovery and normalization studies have become basic components of modern disaster management within the framework called the Integrated Disaster Management Cycle. It is necessary to disseminate all the studies implemented based on scientific knowledge aimed at reducing the disaster risks and using the findings obtained in a way that contributes to the designing of social disaster awareness. It will be possible to form healthier, safer and more resilient cities in the face of disasters by taking the necessary measures to reduce the risk before disasters occur.

Author contributions

Nur Sinem Partigöç: Literature Review, Spatial Analyses, Writing-Reviewing and Editing.

Ceyhun Dinçer: Visualization, Investigation, Writing-Reviewing and Editing.

Conflicts of interest

The authors declare no conflicts of interest.

References

- Un-Habitat (2012). Developing Local Climate Change Plans a Guide for Cities in Developing Countries. Cities and Climate Change Initiative Tool Series. <https://www.unclearn.org/resources/library/developing-local-climate-change-plans-a-guide-for-cities-in-developing-countries>
- United Nations Office for Disaster Risk Reduction (UNISDR) (2015). 2015 UNISDR final report of the 2014-15 Biennium Work Programme, United Nations Office for Disaster Risk Reduction, Geneva. <https://www.undrr.org/publication/unisdr-annual-report-2015>
- Güler, Ç. & Çobanoğlu, Z. (1994). Çevresel Etkenlere Bağlı Olarak Ortaya Çıkan Hastalıklar. T.C. Sağlık Bakanlığı Yayınları. 1. Edition
- United Nations Office for Disaster Risk Reduction (UNISDR) (2009). 2009 UNISDR Terminology on Disaster Risk Reduction. United Nations International Strategy for Disaster Reduction, United Nations Office for Disaster Risk Reduction, Geneva. <https://www.undrr.org/publication/2009-unisdr-terminology-disaster-risk-reduction>
- Genç, F. N. (2007). Türkiye’de doğal afetler ve doğal afetlerde risk yönetimi. Stratejik Araştırmalar Dergisi, 9(5), 201-226.
- Global Volcanism Program (GVP) (2015). Global Volcanism Program, Smithsonian Institution. <http://volcano.si.edu>
- İçişleri Bakanlığı Afet ve Acil Durum Yönetimi Başkanlığı (AFAD) (2018). Türkiye’de Afet Yönetimi ve Doğa Kaynaklı Afet İstatistikleri. https://www.afad.gov.tr/kurumlar/afad.gov.tr/35429/xfiles/turkiye_de_afetler.pdf
- Nuhoğlu, F. Yapılı çevrenin afet riskinin azaltılması, İstanbul-Küçükçekmece [Master's thesis, Beykent University].
- Balamir, M. (2018). Afetler, Risk Yönetimi ve Sakınım Planlaması Açıklamalı Kavram ve Terimler Dizini. SPO Yayınları
- Altun, A. Ö., & Ögdül, H. G. (2022). Afet Riski Yönetimi Kapsamında Kent Planlama; İstanbul Planları ve Uygulamalar. METU Journal of the Faculty of Architecture, 38(2), 145-172. <http://dx.doi.org/10.4305/metu.jfa.2021.2.7>
- Cumhurbaşkanlığı Strateji ve Bütçe Başkanlığı (SBB) (2000). 8th Development Plan (2001 - 2005). https://www.sbb.gov.tr/wpcontent/uploads/2022/07/Uzun_Vadeli_Strateji_ve_Sekizinci_Bes_Yillik_Kalkinma_Planı-2001-2005.pdf
- Cumhurbaşkanlığı Strateji ve Bütçe Başkanlığı (SBB) (2006). 9th Development Plan (2007 - 2013). https://www.sbb.gov.tr/wp-content/uploads/2022/07/Dokuzuncu_Kalkinma_Planı-2007-2013.pdf
- Ministry of Environment and Urbanisation (2010). Bütünleşik Kentsel Gelişme Stratejisi ve Eylem Planı (KENTGES) (2010 - 2023). <http://www.sp.gov.tr/tr/temel-belge/s/33/KENTGES+Butunlesik+Kentsel+Gelisime+Stratejisi+ve+Eylem+Planı>
- Başbakanlık Afet ve Acil Durum Yönetimi Başkanlığı (AFAD) (2013). Ulusal Deprem Stratejisi ve Eylem Planı (UDSEP 2012-2023). <https://deprem.afad.gov.tr/assets/udsep/UDSEP2023.pdf>
- Cumhurbaşkanlığı Strateji ve Bütçe Başkanlığı (SBB) (2013). 10th Development Plan (2014 - 2018). https://www.sbb.gov.tr/wp-content/uploads/2022/08/Onuncu_Kalkinma_Planı-2014-2018.pdf
- İçişleri Bakanlığı Afet ve Acil Durum Yönetimi Başkanlığı (AFAD) (2011). Ulusal Deprem Stratejisi ve Eylem Planı, <http://www.deprem.gov.tr/tr/kategori/ulusal-deprem-stratejisi-ve-eylem-planı-50009>
- Official Gazette (2012). Afet Riski Altındaki Alanların Dönüştürülmesi Hakkında Kanun (6306 Sayılı Kanun). <https://www.resmigazete.gov.tr/eskiler/2012/05/20120531-1.htm>
- Erdin, H. E., Çelik, H. Z., Aydın, M. B. S., & Partigöç, N. S. (2019). Afet ve Acil Durumlar Sonrası Halkın Toplanma Alanlarına İlişkin Kriterlerin Belirlenmesi ve Değerlendirilmesi Yönteminin Oluşturulması, İzmir Kenti Örneği, AFAD-UDAP Çalışması, Proje No: UDAP-G-16-711 08, Ankara.
- Atay, Ç. (2013). Geçmişten bugüne İzmir Şehir Planı. <https://www.izmirdergisi.com/tr/soylesi/2159-gecmisten-bugune-izmir-sehir-planı>
- İzmir Valiliği İl Afet ve Acil Durum Müdürlüğü (AFAD) (2021). İzmir İl Afet Risk Azaltma Planı, <https://izmir.afad.gov.tr/kurumlar/izmir.afad/E-KUTUPHANE/İl-Planları/İzmir-IRAP.pdf>
- İzmir Büyükşehir Belediyesi (İBB) (2012). 1/25000 Ölçekli İzmir Büyükşehir Bütünü Çevre Düzeni Planı Açıklama Raporu, İzmir.
- Tarım ve Orman Bakanlığı Su Yönetimi Genel Müdürlüğü (SYGM) (2019). Batı Akdeniz Havzası Taşkın Yönetim Planı, Taşkın ve Kuraklık Yönetimi Dairesi Başkanlığı, Ankara.
- General Directorate of Meteorology (2023). Denizli İli İklim Sınıflandırması. <https://www.mgm.gov.tr>
- Japon Uluslararası İşbirliği Ajansı (JICA), İstanbul Büyükşehir Belediyesi (İBB). (2002). Türkiye Cumhuriyeti İstanbul İli Sismik Mikro-Bölgeleme Dâhil Afet Önleme/Azaltma Temel Plan" Çalışması", Son Rapor, Cilt V, Eylül 2002.
- Ariñç, K. (2013). Bitlis'te taşkın ve sel felaketi (01-02 Mayıs 1995). Atatürk Üniversitesi Sosyal Bilimler Dergisi, (25), 101-123
- Karadoğan, S. (2007). Malatya Kenti ve Yakın Çevresi İçin Olası Doğal Riskler ve Afet Yönetimi (GIS ortamında örnek bir uygulama). TMMOB Harita ve Kadastro Mühendisleri Odası Ulusal Coğrafi Bilgi Sistemleri Kongresi, Trabzon, Türkiye.
- Akara, İ., Uysal, C., & Maktav, D. (2008). Determination of natural disaster by integration of remote sensing and GIS: the Yeniçiftlik stream basin model in Istanbul, Turkey. Proceeding of the the XXIIth ISPRS Congress, Beijing, China. 249-253
- Yılmaz, O. S. (2023). Frekans oranı yöntemiyle coğrafi bilgi sistemi ortamında heyelan duyarlılık haritasının

- üretilmesi: Manisa, Demirci, Tekeler Köyü örneği. *Geomatik*, 8(1), 42-54. <https://doi.org/10.29128/geomatik.1108735>
29. Demirkesen, A. C. (2012). Multi-risk interpretation of natural hazards for settlements of the Hatay province in the east Mediterranean region, Turkey using SRTM DEM. *Environmental Earth Sciences*, 65, 1895-1907. <https://doi.org/10.1007/s12665-011-1171-0>
30. Özdemir, H. (2007). Havran çayı havzasının (Balıkesir) CBS ve uzaktan algılama yöntemleriyle taşkın ve heyelan risk analizi. Basılmamış Doktora Tezi, İstanbul Üniversitesi Sosyal Bilimler Enstitüsü, Coğrafya Anabilim Dalı, İstanbul.
31. Erkal, T., & Değerliyurt, M. (2009). Türkiye’de afet yönetimi. *Doğu Coğrafya Dergisi*, 14(22), 147-164.
32. Kadioğlu, M., & Özdamar, E. (2008). Afet zararlarını azaltmanın temel ilkeleri. JICA Türkiye Ofisi, Yayın, (2).
33. Kızıloğlu, F. M., Okuroğlu, M., & Örüng, İ. (2006). Kırsal yerleşimler ve doğal afetler. *Gaziosmanpaşa Üniversitesi Ziraat Fakültesi Dergisi*, 23 (2), 53-58
34. Nurlu, M. (2015). Afet Yönetiminde Bütünleşik Afet Tehlike Haritaları, 3. Türkiye Deprem Mühendisliği ve Sismoloji Konferansı, 14-16 Ekim 2015, Dokuz Eylül Üniversitesi- İzmir, Türkiye.
35. Özşahin, E. (2013). Türkiye’de Yaşanmış (1970-2012) Doğal Afetler Üzerine Bir Değerlendirme. 2. Türkiye Deprem Mühendisliği ve Sismoloji Konferansı, 25-27 Eylül 2013, Hatay, Türkiye.
36. Duman, N., & İrcan, M.R. (2022). Coğrafi Bilgi Sistemleri ve Uzaktan Algılama Tabanında Çankırı Merkez İlçesinin Erozyon Risk Analizi. *Coğrafi Bilimler Dergisi*, 20 (1), 220-245. <https://doi.org/10.33688/aucbd.1074770>
37. Özcan, O., (2008). Sakarya Nehri Alt Havzası’nın Taşkın Riski Analizinin Uzaktan Algılama ve CBS İle Belirlenmesi, Doktora Tezi, Bilişim Enstitüsü, İstanbul Teknik Üniversitesi.
38. Erol, O. (1993). Genel Klimatoloji, Gazi Büro Kitabevi, Ankara.
39. Değerliyurt, M. (2013). Antakya’da Doğal Afet Risk Analizi ve Yönetimi, Doktora Tezi, İstanbul Üniversitesi Sosyal Bilimleri Enstitüsü, İstanbul.
40. Fahjan, Y., Pakdamar, F., Eryılmaz, Y., & Kara, İ. (2015). Afet Planlamasında Deprem Riski Belirsizliklerinin Değerlendirilmesi, Artvin Çoruh Üniversitesi Doğal Afetler Uygulama ve Araştırma Merkezi Doğal Afetler ve Çevre Dergisi, 1 (1-2), 21-39.
41. Demir, A., Kemeç, S., & İlke, F. D. (2022). Afet Riski Değerlendirmelerinde Çoklu Tehlike Analizi ‘Erciş, Van Örneği’. *Resilience*, 6(1), 15-38. <https://doi.org/10.32569/resilience.1013912>
42. Özmen, S. (2010). İstanbul ili yangın riski analizi ve yangın riski haritalarının oluşturulması. [Master’s thesis, Yıldız Teknik Üniversitesi].
43. Demir, V., & Keskin, A. Ü. (2022). Yeterince akım ölçümü olmayan nehirlerde taşkın debisinin hesaplanması ve taşkın modellemesi (Samsun, Mert Irmağı örneği). *Geomatik*, 7(2), 149-162. <https://doi.org/10.29128/geomatik.918502>
44. Oğuz, K., Oğuz, E., & Coşkun, M. (2016). Coğrafi Bilgi Sistemleri İle Taşkın Risk Alanlarının Belirlenmesi: Artvin İli Örneği. 4. Ulusal Taşkın Sempozyumu, 23 – 25 Kasım 2016, Rize, Türkiye
45. Özyavuz, M. (2011). Bitki örtüsünün ekolojik şartlarının Coğrafi Bilgi Sistemleri ve uzaktan algılama teknikleri ile analizi, Ganos (Işıklar) Dağı, Tekirdağ. *Tekirdağ Ziraat Fakültesi Dergisi*, 8(2), 37-47.
46. Coşkun, M., & Toprak, F. (2023). Coğrafi bilgi sistemleri (CBS) tabanlı orman yangını risk analizi: Bartın İli örneği. *Geomatik*, 8(3), 250-263. <https://doi.org/10.29128/geomatik.1192219>
47. Dilekçi, S., Marangoz, A. M., & Ateşoğlu, A. (2021). Zonguldak ve Ereğli Orman İşletme Müdürlükleri orman yangını risk alanlarının belirlenmesi. *Geomatik*, 6(1), 44-53. <https://doi.org/10.29128/geomatik.660623>
48. Kuldeep, T. & Kamlesh, K. (2011). Land Use / Land cover change detection in Doon valley (Dehradun Tehsil), Uttarakhand: using GIS & Remote Sensing Technique. *International Journal of Geomatics and Geosciences*, 2(1), 34-41.
49. Paul, S. (2022). Change detection and future change prediction in Habra I and II block using remote sensing and GIS-A case study. *International Journal of Engineering and Geosciences*, 7(2), 191-207. <https://doi.org/10.26833/ijeg.975222>





Development of a virtual reality application for the Old Harran School

Fred Ernst ^{*1}, Songül Akdağ ¹, Nizar Polat ¹, Dursun Akaslan ¹, Mehmet Önal ¹, Abdullah Ekinci ¹

¹Harran University, Department of Geomatics Engineering, Türkiye, fr_ernst@yahoo.com, songul.akdag1995@gmail.com, nizarpolat@harran.edu.tr, dursunakkaslan@harran.edu.tr, monal@harran.edu.tr, aekinci@harran.edu.tr

Cite this study: Ernst, F., Akdağ, S., Polat, N., Akaslan, D., Önal, M., & Ekinci, A. (2024). Development of a virtual reality application for the Old Harran School. *International Journal of Engineering and Geosciences*, 9 (1), 77-85

<https://doi.org/10.26833/ijeg.1309115>

Keywords

Virtual Reality
Virtual Museum
Harran School

Research Article

Received:02.06.2023
Revised: 25.07.2023
Accepted:02.08.2023
Published:02.01.2024



Abstract

The objective of this project that is described in this paper was to introduce the little-known Harran School of the medieval Islamic period located in Southeast Türkiye to a broader audience using virtual reality technologies. 3D models of the medieval Inner Castle in the Harran archaeological site and one of its saloons were created using photogrammetric methods. In this main saloon, 3D models of artifacts found during excavation works on this site that were used in medieval and earlier times were placed in a museum-like style. Additional objects, illumination and paintings of great Islamic scholars were appended to create a more realistic setting in the saloon. All these 3D models were transferred to the game engine Unity to generate a virtual environment, in which the visitor can immerse. Currently, this virtual museum can be experienced by PC-based head-mounted devices. While different implementations of virtual museums are already available in Türkiye with this project, a museum deploying virtual reality technology has been realized for the first time.

1. Introduction

After the closure of the philosophy schools of Alexandria many philosophers emigrated to Carrhae in Upper Mesopotamia (today, Harran, Türkiye) and there, created the "Harran School". According to some researchers this was the beginning of the golden age of Islam starting in 717 CE with the foundation of the first Islamic university [1]. Jabir Kura, Al-Battani, Jabir Bin-Bayan and Ibn Teymime must be named as the most influential scientists of this school. Al-Battani has been regarded as the greatest astronomer of the medieval Islamic period [2]. His importance is underlined by the fact that he inspired Copernicus in his works that becomes evident from his frequently given references to Al-Battani [3]. The end of the golden age of Islam is usually associated with the Mongol invasions in the Middle East and the Siege of Baghdad in 1258. Again, philosophers and scientists had to flee, and this time found a new residence in Spain and Sicily [4], which eventually contributed to the birth of Renaissance [5].

Anatolia as part of the fertile crescent hosted many civilizations starting with prehistoric times (most famous is Göbeklitepe that is located in the same province a Harran) until the present, houses a big

treasure of artifacts and traces from high cultures like Sumer and Hittite, which are considered as an important part of the cultural heritage of Türkiye.

Until recently, preserving, protecting, storing, and exhibiting of cultural heritage was generally assigned to museums. However, during the last decades the rapid development of information technology especially in the fields of digital photography, laser scanning, computer animation and virtual reality has paved the way for displaying cultural in a virtual way. Therefore, these processes of archaeological documentation have been named digital modelling or digital documentation. Resulting from the multidisciplinary use of these technologies societies have been enabled to create a common cultural heritage. Ultimately, based on these technological evolution "cultural heritage products" of museums that form an essential part of the world's cultural assets can now presented to ordinary users all around the world in an enhanced visual structure. With other words, museums have become universal exhibition saloons that can be regarded as a virtual environment [6].

Due to the fact that the real world exists of three dimensions visualization with the help of computers must be done in a three-dimensional way if it wants to be

realistic. Naturally, such a visualization attracts much more attention as it becomes closer to reality. Using 3D modelling program that support the interaction in an intuitive way creation of 3D models has become much easier today. These programs include options for viewing the objects of interest from different angles by rotating them around different axis and creating animations of their movements [7].

Doğan & Yakar [8] stated that Geographic Information Systems (GIS) and photogrammetry have become commonly used scientific methods for the documentation of cultural heritages. They collected data of 46 historical monuments located in Silifke/Mersin and transferred them to a database. Some of those objects were reconstructed as 3D models using photogrammetric techniques.

Şasi & Yakar [9] carried out a 3D photogrammetric modelling of Hasbey Dar'ülhuffaz at the Karamanids site in Meram District /Konya. They took photographs of the cultural asset with a Nikon D90 camera and captured aerial photographs with a DJI Phantom 4 unmanned aerial vehicle. All data were processed with Agisoft PhotoScan and Nectad software, and a 3D model of the artifact was created.

In 2012, Yıldırım made research on how much the Topkapı Palace Museum currently takes profit of information technologies by taking in consideration virtual applications applied in many of the world's well-known museums. Based on the findings of this research recommendations on the potential future usage of the museums' assets by deploying the state-of-the-art technologies were written [10]. Ünlü [11] carried out a study, in which he described showcases for presenting Turkish museums on web pages that are planned to be hosted by the Ministry of Culture and Tourism. The results of this study found entrance into the homepage that currently consists of a collection of 47 virtual museums.

The "HafenCity University Hamburg" cooperated with the "Museum Alt-Segeberger Bürgerhaus" in developing a Virtual Reality (VR) application that brought to life again the Early Modern Age Early Modern Age of this city in the framework of a virtual museum. This application focused on showing how a house representative for a small town in a North Germany setting changed over time and eventually, becoming a museum. Several digital terrain models and 3D models of the city were created using laser scanning and photogrammetry techniques. After adding information on the city's history and further details of this building this virtual museum could be explored interactively by wearing a 'Head-Mounted-Display' (HMD) of HTC VIVE [12].

According to Yakar & Yılmaz [13] the usage of digital terrestrial photogrammetry offers many advantages for the documentation and preservation of cultural heritage as a result of their practical experience they gained at the Horozlu Han in Konya. With their work it could be demonstrated how restitution and restoration plans and preparation of relief plans can help to transfer cultural heritage to the coming generations. Uysal et al. [14] emphasize the importance of studies for humanity that

deal with the protection of cultural and historical heritage and its transfer to coming generations. This could be realized by deploying different methods to produce three-dimensional models that aim at protecting and promoting archaeological artifacts. In their work it was shown how Unmanned Aerial Vehicles (UAVs) can be used as an efficient carrier of cameras for photogrammetric surveys at archaeological sites.

Buhur et al. [15] created a spatial virtual environment of Istanbul's historical peninsula for touristic purposes. The study consisted of three main stages: During the first phase air-borne Light Detection and Ranging (LIDAR) data were acquired and separated into building, ground and vegetation classes by classifying them with the help of macros. In the second stage, modeling was done using building and ground classes. During the last stage, attribute and address-location information were added to the model giving users the opportunity to get information about the location and structures while navigating in the model.

According to Günen et al. [16] photogrammetry is used as a method now to transfer the physical characteristics of artefacts, objects figures, and spaces from the real world to virtual reality in a fast and cost-effective way. Using photogrammetry, the processing of data acquired optically from the real world can be deployed for creating objects, tools, spaces and even characters on a gaming screen. Models having geometry and covering textures can be produced at a level of detail that is sufficient for the polygonal requirements of a playing environment.

Uslu & Uysal [17] created a 3D model of the Demeter sculpture hosted by the Kütahya Archaeology Museum. For modelling this important antique artefact, they used terrestrial photogrammetric methods. Checkpoints marked on the artefact were measured with a Focus 6 Reflectorless TotalStation and images were taken with a Nikon Coolpix P510 camera. The data was processed with PhotoModeler software, and a 3D model of the Demeter sculpture was created. They concluded that photogrammetric techniques for documentation of cultural heritage provide great advantages in terms of accuracy, speed, cost and product variety.

Kalbani & Rahman [18] investigated issues and challenges arising from the usage of 3D city models for monitoring of flood risks in Oman based on the "City Geography Markup Language" (CityGML) standard. The aim of the study was to reduce time and effort of decision-makers by using a 3D city model to deal with flood risk management.

While being in charge with leading excavation projects at the archaeological site of Harran, Önal et al. [19] could find evidence that ancient Harran played a major role in the region during the Middle Ages. Among others, a traditional bathroom (Çarşı Hamam) located to the east of Harran's Great Mosque (Ulu Mosque) that was unearthed in 2018 and 2019. This hammam that remained largely preserved consisted of rooms with warm water and in some cases with hot water and changing rooms. As part of this work, a detailed restitution plan of the mentioned hammam was created. As these plans already exist in a suitable digital format,

they could be used to make animations displaying the original architecture in detail. At the same site, to the east of Harran's Great Mosque a bazar that included many artifacts could be excavated. These artifacts consisted of different sorts of glass, pottery and metal objects, which were made available in a digital format for the Department of Geomatics Engineering for further processing to produce three-dimensional objects. Within the Inner Castle of medieval Harran, the bathrooms that were unearthed gave evidence that this castle did not only military purposes rather being used as a palace at the same time. A digital documentation of this bath, which has remained in a very good condition, could be easily used to create an animation about the everyday life in the ancient Harran City.

In "Mythology and History of Harran" [20] the history, religious diversity and social structure within the city of Harran has been described in detail. The information contained in this book forms the scientific basis for any museum be it a traditional one or be it in a virtual form to deliver essential information on the different exhibited objects and putting them into the right context for the visitor of the museum.

Building a new museum in the traditional, physical way is a big effort that requires an abundance of resources – not limited to financial ones solely. Walhimer [21] who has been in charge with establishing many museums computed the costs for the construction of the buildings related to such a museum that include the whole furniture and interior architecture and cover a space of about 1000 m² to be at least 2,5 million USD. On top of it, operating costs of almost 360 000 USD per year would have to be added as well.

A commonly used definition of a virtual museum is as follows: "a digital entity that draws on the characteristics of a museum, in order to complement, enhance, or augment the museum experience through personalization, interactivity and richness of content." [22]. The beginning of virtual museums [23] is marked by the first release of an application for a virtual museum tour distributed on CD-ROMs by the company Apple in 1992. These first implementations of a virtual museum applied the broader concept of virtual reality at a very basic level. They did not reach the level of a more advanced form in which the user gets totally emersed in another reality as far as visual and auditory senses are concerned.

Based on these findings, it will be shown how the ancient knowledge of Harran was translated into Arabic and enriched with its own scientific contributions, how it served as a scientific center, and as a result, how knowledge was transferred to Europe and its contribution to the emergence of the Renaissance will be investigated, The findings of the research studies on the importance of the Harran School for the oriental and western world of all relevant working groups will be presented to the academic world and the public by using new technologies such as virtual reality.

If the above-mentioned financial numbers are considered that for the erection of a traditional, physical implementation of a museum are considered it became obvious that a budget with these dimensions could only

be set aside in the far future. Therefore, the idea came up to set a start with the implementation of a virtual form of the envisaged Harran Museum. Such an implementation could trigger events, which ultimately could enable the physical implementation of a museum. Consequently, a project with the title "First Step for the Establishment of a Harran School Museum" with the following purposes was initiated:

1. Recording the current status of the archaeological site of Harran using a high-resolution digital camera and photogrammetry methods,
2. Detailed reconstruction of Haran's medieval city in the form of a 3D model,
3. Data collection and their interpretation for the objects to be included in the Harran School Museum, and
4. Exhibition of components product during steps 1,2 and 3 within a virtual museum to be consumed by visitors using virtual reality devices.

Because of budget constraints works for the second component had to be postponed until additional funding would be available. In this paper, the realization of the fourth purpose will be treated in more detail.

2. Method

This project was implemented within three distinct phases (Figure 1):

- 1) Data Collection and Preparation Phase, in which geomatics engineers, archaeologists and historians worked in their respective field of expertise.
- 2) Virtual Reconstruction, realized by geomatics engineers.
- 3) Building of a Virtual Museum carried out mainly by computer engineers.

2.1. Recording of the current status of the archaeological site of Harran

The Structure from Motion (SfM) method can be used to produce 3D models of image data obtained from different platforms such as terrestrial or aerial. Although the SfM approach has been developed by computer vision scientist especially, to be used as an automatic feature-matching algorithm, it applies the same basic principles that are valid in photogrammetry. In their article "'Structure-from-Motion' photogrammetry: A low-cost, effective tool for geoscience applications" Westoby et al. [24] give a comprehensive description of this relatively new methodology. Photogrammetry can be defined as the technique that makes usage of multiple overlapping photographs for deriving measurements that can be used among others to generate 3D models of complex environments of single objects. SfM determines the geometrical parameters automatically without the necessity to establish a pre-defined number of known ground control points. In this research, SfM has been deployed within photogrammetry to produce realistically textured and scaled models of buildings of parts of an archaeological site and some artefacts

excavated from it. It must be mentioned that the image quality decides the quality of the textured 3d model and in addition, that the availability of images taken from all

sides determines the completeness of the 3D model (Figure 2).

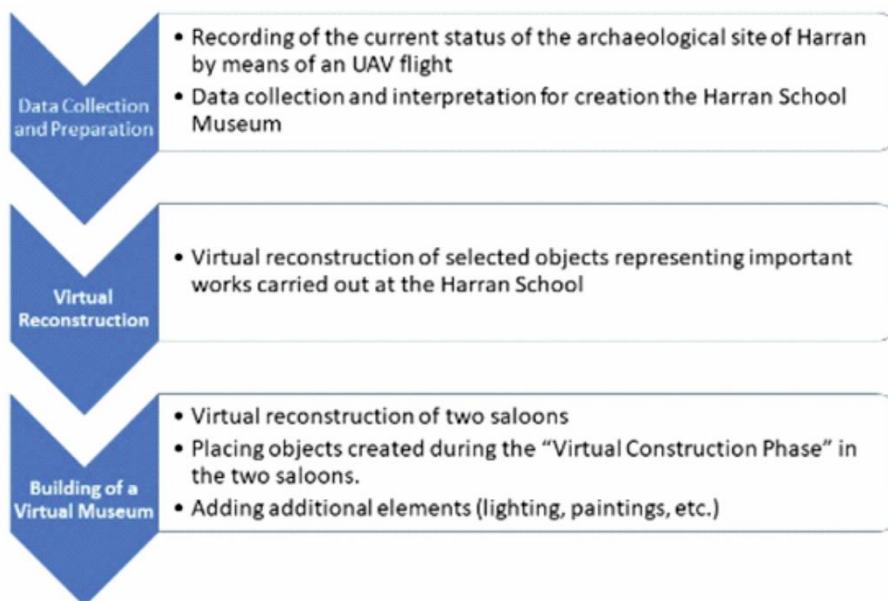


Figure 1. Workflow of the project.

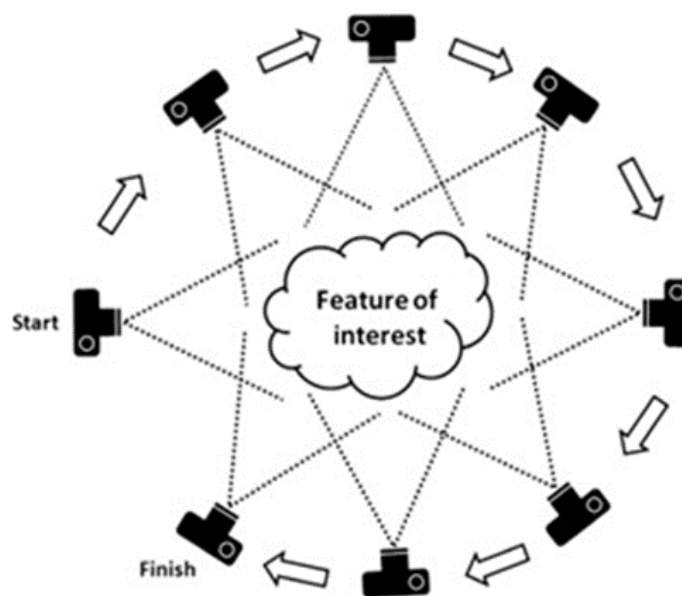


Figure 2. Terrestrial imagery capturing a feature of interest for SfM processing [24].

During the first step, images of the entire Harran Inner Castle were acquired using an Unmanned Aerial Vehicle (UAV), in this case a "Dji Enterprise Phantom 4 RTK" Quadro copter that comes with an integrated 1 inch, 20-megapixel "CMOS" sensor (Figure 3). After a flight plan had been established (Figure 4) the UAV executed the flight mission autonomously. These photographs served as an input for constructing a 3D model with the help of Agisoft software.

During the second step, from a selected set of objects, which had been excavated at the archaeological site of Harran 3D models were created. In total, 9 models have been finished until now. Most of them originate from the Middle Ages but, some data back even to the middle and late stone age period.



Figure 3. DJI Enterprise Phantom 4 RTK.



Figure 4. Flight plan for the “DJI Enterprise Phantom 4 RTK”.

2.2. Data collection and interpretation for creation the Harran School Museum

The search for documents that were directly or indirectly related to the medieval Harran School was conducted in several libraries and archives in the United Kingdom, Türkiye and Iraq. The focus of this step laid in collecting documents from the archives of the “Turkish Historical Society” in Ankara and the Süleymaniye Library located in Istanbul. These collected documents went through a rigorous screening process to determine whether a) they possessed enough significance to be considered for the Harran School Museum and b) whether they were suitable to be used in the setting of a virtual museum. Emphasis was laid on the studies of those scientists that had a proven influence on later scientific developments of the western world especially during the modern epoque. Due to time constraints and travel and visit restrictions during the pandemic the translation only of some selected documents, mostly from Arabic into Turkish could be completed. Notes on studies of relevance for inclusion in the virtual museum have been taken.

2.3. Virtual Reconstruction

Virtual reconstructing falls under the field of digital archaeology, which can be defined as “*the application of information technology and digital media to archaeology*” [25]. Although in a narrower sense works described under “Recording of the current state of the Harran archaeological site” could be considered as Virtual Reconstruction we treat them differently because the applied methodology exhibits important differences. In total 12 models have been finished until now.

In order to explain the works carried out we use a two-beak retort (Figure 5). Considered the father of chemistry in the Islamic and western world Jabir b. Hayyan (who lived in the 8th century) is accepted as the scientist who founded the chemistry laboratory in the modern sense. He conducted many experiments in the

laboratory he founded. This retort had been designed with a double discharge pipe to increase efficiency and speed in distillation.



Figure 5. Two-beak retort from Jabir b. Hayyan's laboratory [26].

The three-dimensional modelling and animation software Blender was used to create the model of the retort. Cylinders were selected from the ready-made meshes offered in Blender and their dimensions were adjusted according to the retort. Then, this cylinder was shaped by changing the size and location of its faces in Edit Mod. Afterwards, a sphere was added to form the hollow cavity part of the retort at the bottom. The empty part of the retort was selected and removed from the circle with the “Extrude Faces” command. The extracted figure was separated from the sphere and then the sphere was deleted. After filling the gaps in this cut part with the “Extrude Region” tool, it was added to the prepared cylinder. In a final step, the upper part of the retort was covered with glass material and the lower part was colored according to the original image (Figure 6).



Figure 6. Virtual reconstruction of two-beak retort shown in Figure 3.

2.4. Building of a virtual museum

During this step, the purpose was to generate an application of a virtual museum, which could be consumed by means of an Android application and a desktop based one and to be viewed by an HMD for virtual reality (Figure 7). The virtual museum consisted of two separate saloons that accommodated all the archaeological artifacts and in addition other related objects. The creation of these saloons was accomplished in the following way:

- The most appropriate room having a sufficient size in the Inner Castle had to be identified.
- During the second step, more than 240 photographs with a handheld high-resolution camera were taken.
- During a last step, using photogrammetric methods described above a 3D model with a precision to reveal the details of the ancient brickwork was processed.

Due to time constraints, a separate 3D model of a second room could not be constructed. Instead, a copy of the first room generated, to which an artificial passage was created.



Figure 7. The Head Mounted Device (HMD) (HTC Vive).

- Placing the exhibition room at the right location within the Inner Castle,
- Duplicating of the 3D model created for the first saloon and placing it parallel to the first room,
- Linking the original room and the duplicated with a passage having a look that is consistent with the architecture of these rooms,
- Adding artificial light sources appropriate for a museum,
- Creating bases for all the objects in the exhibition saloons, and
- Attaching portraits of four important scientists of the Harran School (Câbir bin Hayyân, El-Battani, Farabi, Sabit bin Kurra as displayed in the entrance hall of Harran University's central library) at the rear walls of the saloons.

In addition, when using the MOVE tool of UNITY, the visitor of this virtual museum will have the opportunity to move freely around within the two saloons. However, to be able to do so, the HMD he is using must be equipped with controllers. In our case, we used the HTC Vive HMD with hand controllers.

3. Results

Within this study, two major goals have been achieved:

1) Using different techniques spatial and non-spatial information of the Islamic period related to the Harran School has been collected, compiled and processed. This included the exterior and interior setting of buildings and objects excavated at the archaeological site of Harran and written sources from libraries.

2) Exhibition saloons within a virtual museum that served as a container for displaying objects created in task 1 have been generated.

When the VR application is initialized on a desktop computer, the user has the impression to fly from space to the present-day city of Harran, then to approach the archaeological site and finally to land in the Inner Castle of Harran. Figure 8 shows a 3D model of the castle's state in the year 2018. Only minor modifications due to ongoing restoration works have occurred since then.



Figure 8. 3D model of the Inner Castle of Harran showing the present-day state.

After that, he will find himself at the front side of the first of the two exhibition halls as can be seen in Figure 9. This is the starting point from where with the help of

controllers of the VR system the rooms and the displayed objects can be explored in more detail.

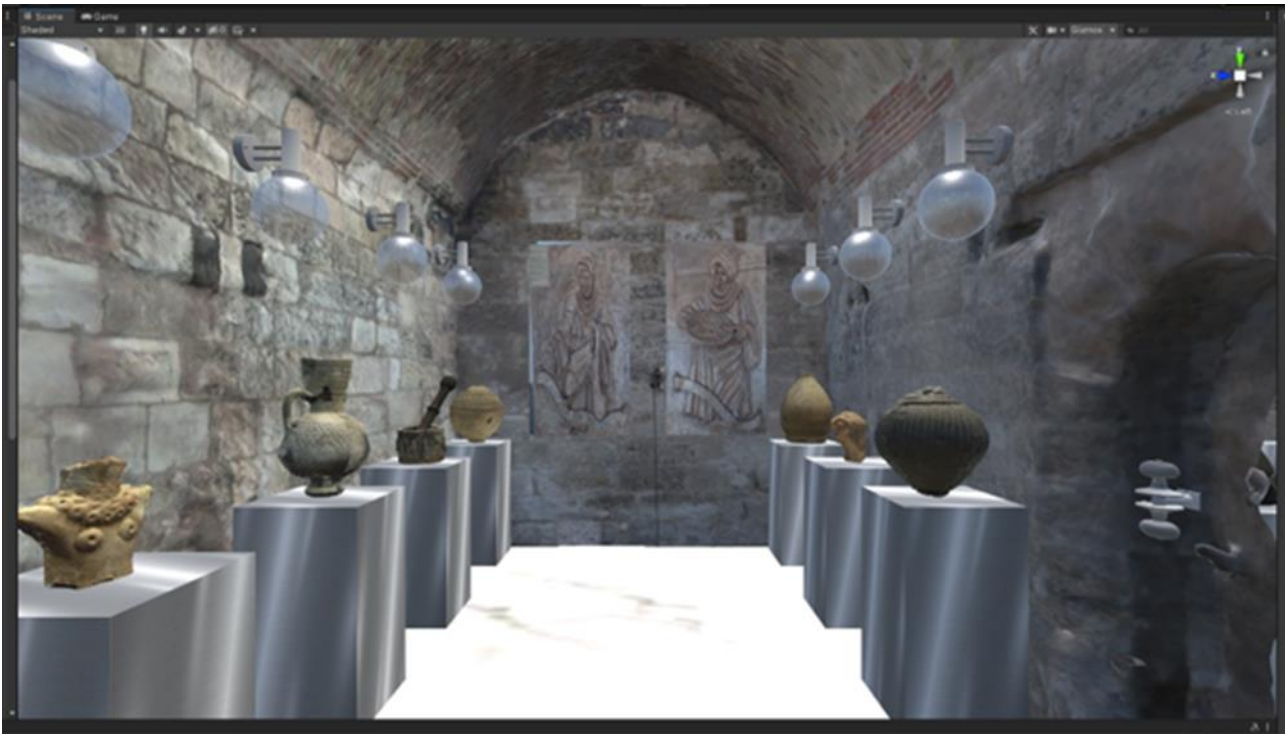


Figure 9. One of the two exhibition saloons of the virtual museum.

Now, he can walk around in two saloons of the virtual museum located within the Inner castle. The walls of the virtual museum have been processed to have a structure that resembles the present-day appearance to deliver a sentiment of authenticity. Here, the user can inspect the exhibits which currently, contains two different kinds of selected objects, in a closer way. First, 3D models created by photogrammetric methods of objects that have been found at the archaeological site of Harran like pottery as shown in Figure 10. Second, 3D models of those tools that could be virtually reconstructed from drawings and pictures found in the related original documents of some of the most important scientist living during this epoque.

purposes and the visitor's expectations could not be satisfied. This general requirement applies to virtual museums as well. Here the latter one can prove its superiority over the classical museums because virtually, no limits exists when it comes to linking other media to a special object.

For this project, the application has been programmed in a way that it is enough to come within a certain proximity of an exhibited object with the HMD someone is wearing. Then, additional information in form of a short text summary will be displayed in red color within the HMD (Figure 11).



Figure 10. 3D model of a terracotta jar used during medieval times for measuring purposes (Islamic period, inventory no. HR.1.77).

Without the provision of information in the form of text, additional pictures and graphics, audio and video clips for the exhibited objects and putting them in their historical content a museum would not reach its

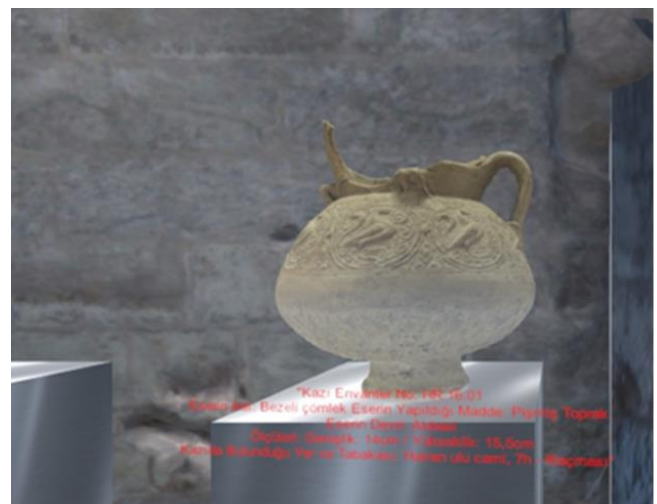


Figure 11. Explanatory text for an exhibited object in the virtual museum.

Currently, Harran School's virtual museum can only be experienced using a PC-connected HMD for virtual reality. However, it is planned to add a version for Android that would offer this application to potentially billions of people having a smartphone that can be connected to an HMD.

4. Discussion

With the goal of promoting the Harran School by spreading knowledge about it to interested people in the entire world, a virtual museum based on virtual reality technology has been built in Türkiye for the first time. Other so-called "Virtual Museums" in Türkiye offer only tours in panoramic view. However, they cannot be viewed with HMDs and therefore do not provide the real feeling of virtuality in the sense of VR [27]. In contrast, the virtual museum described in this paper will be accessible by a PC-connected HMD using channels like YouTube or even a very simple HMD that can be connected to mobile phones running on Android. When such a virtual museum is published on the Internet contrary to a physically implemented one it has the big advantage that virtually anyone in the world who owns a smartphone can be a potential visitor. Although he still must own an HMD, prices for such an Android based device start already at 10 USD. Works for publishing on the Internet are still going on.

The assumption that every owner of a smart phone having an HMD at its disposal would use such an app does not stand up to closer examination. When searching for an Android app and typing "virtual museum" at Google Play 248 results were returned. Most of these results are virtual tours in and around some well-known museums and some lesser-known ones while only a few virtual reality applications are offered. And when a more detailed analysis is conducted it becomes clear that only 13 of them exceed a download rate of more than 5000. Among them, the app of the "Louvre Museum Buddy" displaying the Mona Lisa as a logo is the most prominent one. It can be doubted that Harran School could be able to compete with the most famous painting of the world and therefore, additional effort will be required to attract mobile phone users to this planned app.

One might argue that if someone has visited a virtual museum using virtual reality glasses the incentive to visit a real archaeological site or a physical implementation of a museum related to such a site would no longer exist. Given the current state of technology with its limited image resolution of VR applications especially on mobile phones it can be doubted that virtuality would be preferred to reality. More likely is that a first virtual visit will whet the appetite to see the real physical implementation of a future museum at Harran after the required funding will have been found.

Another issue that needs further attention is the drawback that the content of the virtual museum is very limited. Currently, only thirteen objects and four paintings related to the Harran School are at display, something that cannot be considered to be enough for attracting many visitors. This missing content was caused by some shortcomings of this project. The most important one is the fact that original documents or even

secondary literature related to the Harran School are mostly written in Arabic and therefore, a translation into Turkish and English language is indispensable. According to our experience, many scientific terms that have been used during this epoch are no longer used in modern Arabic. Because of this, sound translations could only be guaranteed through the involvement of Arabic speakers who have a thorough knowledge in the related field of science, which in case of the Harran School covers the fields of mathematics, astronomy and medicine. This can only be achieved by means of adequate funding, something that was not available until now.

A more technical detail that we should mention is the relatively low resolution of the outer walls of Harran's Inner Castle that results in a blurred appearance of the current 3D model. This low resolution originates from the flight height of about 80 m of the UAV, which makes the products of this flight not very suitable for usage in an VR environment. Although this scene of the application lasts only a few seconds, still an enhancement will only be possible after a new flight at a longer altitude will have been realized.

Currently, only text information is available to deliver information on the exhibited objects. In future version, it is planned to add other forms of media that can deliver additional information. For example, in order to understand the implications of some of the most important discoveries at that time in the fields of mathematics and astronomy the option to watch videos on these subjects could be a big advantage.

5. Conclusion

Within the framework of this completed project, the first steps for building a virtual museum of the predecessor of the modern Harran University, the medieval Harran School, have been implemented. This virtual museum includes 3D models of its location, i.e., the Inner Castle within Harran's archaeological site, objects that have been unearthed there, the interior of the museum and display of objects and documents in two museum saloons. These components have been integrated within a virtual reality environment, which can be consumed by visitors wearing a PC connected HMD. Works for developing an Android App and adding more objects for display in the exhibition saloons is continuing. However, adding a greater number of objects that is required for creating the feeling of visiting a real museum can only be achieved with additional funding. Especially, the generation of 3D models of original scientific instruments and translation works of historical scientific documents written in medieval Arabic language into Turkish and English requires very specialized expertise. Such further enhancements are essential to attract enough users to this VR application. And only then, the ultimate goal of our efforts to attract more visitors to the real Harran can be reached.

Acknowledgement

This project has been funded by Harran University's Scientific Research Unit under the Umbrella Group "Harran School" with the project number 20107.

Author contributions

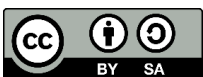
Fred Ernst: Conceptualization, Methodology **Songül Akdağ:** Data Integration, Application Development **Nizar Polat:** Data Acquisition, Photogrammetric Processing **Dursun Akaslan:** Conceptualization, Methodology **Mehmet Önal:** Field Study **Abdullah Ekinci:** Collection and Interpretation of Literature

Conflicts of interest

The authors declare no conflicts of interest.

References

- Frew, D. H. (1999). Harran: Last refuge of classical paganism. *The Pomegranate*, 13(9), 17-29. <https://doi.org/10.1558/pome.v13i9.17>
- Schlager, N., & Lauer, J. (2000). *Science and its times: Understanding the social significance of scientific discovery*. Gale Group
- Hoskin, M. (1999). *The Cambridge concise history of astronomy*. Cambridge University Press.
- Naraghi, E. (1996). The Islamic antecedents of the western renaissance. *Diogenes*, 44(173), 73-106. <https://doi.org/10.1177/0392192196044173>
- Perry, M., Chase, M., Jacob, J., Jacob, M., & Daly, J. W. (2015). *Western civilization: Ideas, politics, and society, Volume I: To 1789*. Cengage Learning.
- Alav, O., Altıngövdü, İ. S., & Kaplan, A. (2006). Sanal müzelerde panoramik ve 3 boyutlu görüntü teknikleri ve içerik sorgulama: Isparta Müzesi örneği.
- Uğur, A. (2002). İnternet üzerinde üç boyut ve Web3D teknolojileri. VIII. Türkiye'de İnternet Konferansı (INET-TR 2002), (54), 1-3.
- Doğan, Y., & Yakar, M. (2018). GIS and three-dimensional modeling for cultural heritages. *International Journal of Engineering and Geosciences*, 3(2), 50-55. <https://doi.org/10.26833/ijeg.378257>
- Şasi, A., & Yakar, M. (2018). Photogrammetric modelling of hasbey dar'ülhuffaz (masjid) using an unmanned aerial vehicle. *International Journal of Engineering and Geosciences*, 3(1), 6-11. <https://doi.org/10.26833/ijeg.328919>
- Yıldırım, A. (2012). Müzecilik faaliyetlerinde bilgi teknolojilerinin kullanılması: Topkapı Sarayı Müzesi Örneği ve dünya müzelerindeki uygulamalar. *Uzmanlık Tezi, Kültür ve Turizm Bakanlığı Topkapı Sarayı Müze Müdürlüğü*.
- Ünlü, H. (2010). Kültür ve Turizm Bakanlığı'na ait web sitelerinin kullanıcı gereksinimleri düzeyinde bilgi mimarisi açısından değerlendirilmesi. *Uzmanlık Tezi. T.C. Kültür ve Turizm Bakanlığı*,
- Degim, S., Kersten, T., Tschirschwitz, F., & Hinrichsen, N. (2017). Segeberg 1600-reconstructing a historic town for virtual reality visualization as an immersive experience. In 5th International Workshop LowCost 3D-Sensors, Algorithms, Applications, 28-29 November 2017, Hamburg, Germany, 87-94.
- Yakar, M., & Yılmaz, H. M. (2008). Kültürel miraslardan tarihi Horozluhan'ın fotogrametrik rölöve çalışması ve 3 boyutlu modellenmesi. *Selçuk Üniversitesi Mühendislik, Bilim ve Teknoloji Dergisi*, 23(2), 25-33.
- Uysal, M., Toprak, A. S., & Polat, N. (2013). Afyon Gedik Ahmet Paşa (İmaret) Camisinin fotogrametrik yöntemle üç boyutlu modellenmesi. *Türkiye Ulusal Fotogrametri ve Uzaktan Algılama Birliği Sempozyumu, Trabzon*.
- Buhur, S., Uluğtekin, N., Gümüşay, M. Ü., & Musaoğlu, N. (2023). Turistik amaçlı mekânsal sanal ortamların oluşturulması: Tarihi Yarımada Örneği. *Geomatik*, 8(2), 99-106. <https://doi.org/10.29128/geomatik.1133484>
- Günen, M. A., Çoruh, L., & Beşdok, E. (2017). Oyun dünyasında model ve doku üretiminde fotogrametri kullanımı. *Geomatik*, 2(2), 86-93. <https://doi.org/10.29128/geomatik.318319>
- Uslu, A., & Uysal, M. (2017). Arkeolojik eserlerin fotogrametri yöntemi ile 3 boyutlu modellenmesi: Demeter Heykeli örneği. *Geomatik*, 2(2), 60-65. <https://doi.org/10.29128/geomatik.319279>
- Al Kalbani, K., & Rahman, A. A. (2022). 3D city model for monitoring flash flood risks in Salalah, Oman. *International Journal of Engineering and Geosciences*, 7(1), 17-23. <https://doi.org/10.26833/ijeg.857971>
- Önal, M., Mutlu, S. İ., & Mutlu, S. (2019). Harran ve çevresi- Arkeoloji.
- Ekinic, A. (2008). Harran mitolojisi ve tarihi - Tarih, mitoloji, inanç ve bilim kenti.
- Walhimer, M. (2015). *Museums 101*. Rowman & Littlefield.
- Virtual museum (2023). https://en.wikipedia.org/wiki/Virtual_museum
- Miller, G., Hoffert, E., Chen, S. E., Patterson, E., Blackletter, D., Rubin, S., ... & Hanan, J. (1992). The virtual museum: Interactive 3d navigation of a multimedia database. *The Journal of visualization and computer animation*, 3(3), 183-197. <https://doi.org/10.1002/vis.4340030305>
- Westoby, M. J., Brasington, J., Glasser, N. F., Hambrey, M. J., & Reynolds, J. M. (2012). Structure-from-Motion photogrammetry: A low-cost, effective tool for geoscience applications. *Geomorphology*, 179, 300-314. <https://doi.org/10.1016/j.geomorph.2012.08.021>
- Daly, P., & Evans, T. L. (2004). *Digital archaeology: bridging method and theory*. Routledge.
- Ganzenmüller, W. (1941). *Liber Florum Geberti: Alchemistische Öfen und Geräte in einer Handschrift des 15. Jahrhunderts*. Von W. Ganzenmüller. Julius Springer.
- Sanal Müze (2023). T.C. Kültür ve Turizm Bakanlığı: <https://sanalmuze.gov.tr/>





Using GIS-supported MCDA method for appropriate site selection of parking lots: The case study of the city of Tetovo, North Macedonia

Edmond Jonuzi ¹, Tansu Alkan ², Süleyman Savaş Durduran ¹, Hüseyin Zahit Selvi ¹

¹ Necmettin Erbakan University, Department of Geomatics Engineering, Türkiye, edmondjonuzi1@gmail.com, durduran2001@gmail.com, hyselvi@erbakan.edu.tr

² Niğde Ömer Halisdemir University, Department of Geomatics Engineering, Türkiye, tansualkan93@gmail.com

Cite this study:

Jonuzi, E., Alkan, T., Durduran, S. S., & Selvi, H. Z. (2024). Using GIS-supported MCDA method for appropriate site selection of parking lots: The case study of the city of Tetovo, North Macedonia. *International Journal of Engineering and Geosciences*, 9 (1), 86-98

<https://doi.org/10.26833/ijeg.1319605>

Keywords

GIS
AHP
MCDA
Parking Lots
Site Selection

Abstract

The provision of adequate parking spaces for vehicles has emerged as a prominent and challenging issue confronted by towns, cities, and municipal authorities in recent years. Addressing this problem necessitates a thorough examination of the prevailing physical conditions in existing parking areas, while simultaneously undertaking analyses to identify suitable locations for new parking areas or parking lots. This study focuses on the city of Tetovo, North Macedonia, investigating and assessing the available parking areas while analyzing potential sites in accordance with the city's needs and requirements. To facilitate decision-making, a Multi-Criteria Decision Analysis (MCDA) approach is employed to address the parking site selection analysis problem. The weightage of criteria utilized in the analysis is estimated, and potential parking solutions or site selections for new parking areas are identified through the combined application of Geographical Information System (GIS) and Analytic Hierarchy Process (AHP) techniques, identifying primary and sub-criteria, with a focus on Land Use and Transportation as the main criteria for selecting parking lots. The integration of GIS and AHP offers an effective and optimal methodology for site selection and identifying suitable parking locations. AHP method, applied to criteria, determined relative weights through expert opinions, while GIS facilitated spatial analysis for identifying suitable parking locations. The study identifies accessibility to main roads as the criterion carrying the greatest weight (0.517), while accessibility to cultural facilities holds the lowest weight (0.117). The study serves as a pivotal resource for sustainable urban management and decision-making, providing insights into future urban planning and the identification of suitable parking lot sites to foster sustainable development within the city.

Research Article

Received:24.06.2023

Revised: 22.11.2023

Accepted:26.11.2023

Published:02.01.2024



1. Introduction

The world continues to show a gradual increase of population. The growing population has a parallel increase in demand. Such a growth and increase indicate growth of cities and towns. With the growth of the population and migration from rural areas to major urban centers [1], the modern world is changing rapidly [2]. Technological advancement and sophistication lead to increased urbanization too. The increased number of citizens into urban areas has principally impacted negatively in different characteristically form. Consequently, people are becoming aware of

environmental issues and urban problems. The rapid growth of the population and development of cities and towns encounter different problems and inevitably results with more limited resources and services, which leads to significant shortages in different fields and different systems [3-5]. In this development, the transport sector is also a rapidly growing field and with this, problems in urban transportation have increased [6]. The growth of the population also affects the growth or the need for increased use of vehicles [7], and with this traffic is presented as one of the main challenges of urban transport [8]. Cities are suffering from the increasing number of vehicles and consequently from the absence of

parking areas. Public parking is one of the main and serious traffic challenges and problems in different cities.

Public parking is one of the biggest challenges facing fast-growing cities, one of the most important urban facilities, and one of the most challenging tasks [9-11]. Parking is a headache for drivers and has become a common problem in all cities [12]. A parking lot is an organized surface or place that is desired for parking vehicles. Finding parking spaces is a major social problem, is stressful and time-consuming [13-15]. Parking areas vary according to location and characteristics. The problem with parking brings traffic congestion, environmental pollution, aggravates different concerns and affects road congestion [16-21]. Providing a parking area is to meet the demand for parking. According to Litman [22] and Demir et al. [9], parking requirements are affected by many circumstances such as location, land use, demographics, the disposability of public transport systems etc. Parking areas are affected by many elements within the transportation system. Easy access to parking facilities and mapping of parking lots comprises complicated techniques and is an excessively significant element in the achievement of urban land uses and transportation systems [6, 9]. Parking spaces enact a significant duty in modern urban transportation.

Planning parking remains one of the most significant components and one of the major intentions for urban planners to consider their work to increase social amenity in the urban ambience [23-25]. Site selection of parking lots is one of the fundamental verdicts in public urban spaces and it requires the attention of many criteria, parameters and factors and generally have a complex nature [3, 4, 26-28]. With the adequate selection of new places for public parking, the efficiency and effectiveness of the parking system is necessarily increased and at the same time it absorbs many traffic problems [7, 29]. The site must be accessible of any ordinary or perimetric invasion [30, 31]. Parking regulations shall be assigned by local governments, and they should not be discriminatory; parking planning shall ensure safety, continuity, and lanes for disabled people [9, 32]. However, this is not enough to solve the problems that offer special solutions [33], especially in the process of selection of public parking spaces. Efficient parking spaces decrease traffic load and reduce marginal parking.

The triage of a parking space is also intended as a Multi-Criteria Decision Analysis (MCDA) problem. Initially, such a process starts with defining and defining the concern and ends as a concluding verdict with many alternatives [23, 34-36]. Although Geographical Information System (GIS) provides wide range in spatial analysis and visualization [37], for solving complex problems such a range is not enough. So, it is hereby mandatory to use a combined GIS and Analytic Hierarchy Process (AHP) method to solve complex tasks of this type [5, 38]. Processes such as globalization, urbanization, climate change, as well as other environmental and technological advancements, necessitate significant attention and consideration, alongside the integration of information systems [39]. The AHP method, introduced by Saaty 1980 [40], is a successful and one of the most

applied methods and measurements operated in diverse site selection concerns for determining the weights of criteria [35, 41-44]. The AHP method and GIS technologies are effective for solving site selection problems and are also operated for selecting suitable parking areas [1, 3]. In addition, GIS supported AHP method is used in site selection analyzes such as wind power plants [45], solar power plants [46], retail market locations [47], shelter areas [48], agricultural crop selection [49]. In decision-making problems, the abundance of evaluation criteria and available options poses a challenge in determining the most optimal choice and becomes crucial to quantify the evaluation criteria and employ mathematical techniques to arrive at the most suitable decision [50].

Numerous studies and research endeavors have investigated the selection of optimal parking lot locations utilizing the AHP in conjunction with GIS methodologies. In their 2021 study, Alkan and Durduran [1] employed the integrated AHP-GIS methodology to identify suitable locations for parking facilities within the city of Konya, Türkiye. In their 2020 study or diploma thesis, Iqbal [51] conducted a comprehensive analysis, focusing particularly on the case study of Pendik, Istanbul. The study utilized a combined approach, employing GIS-based multi-criteria decision analysis for the selection of parking sites. In their 2018 publication, Samani et al. [10] employed the AHP method of MCDA in conjunction with the GIS to identify new locations for public parking in Tehran, Iran. Some other authors used other combined methodologies related to site selection strategic decision. Ozturk and Kılıç-Gul [4], employed the GIS-Ordered Weighted Averaging (OWA) method in their study, which is based on parameters primarily characterized by fuzzy quantifiers. Farzanmanesh et al. [3] and Samani et al., [10] utilized the GIS fuzzy logic and the fuzzy majority method in their study for the selection of parking sites. Numerous works of a similar nature exist globally. While identifying such studies conducted in various countries and regions, it has been observed that there is a gap in similar research and studies within the territory of the Republic of North Macedonia. Some of the aforementioned works, alongside others, have served as foundational sources in shaping the conceptual framework of our study, playing a crucial role in its development.

The primary objective of this study is to perform an analysis to select optimal locations for establishing new parking lots in the central or urban area of the Municipality of Tetovo, with a particular focus on the city of Tetovo. This involves identifying and defining primary criteria and corresponding sub-criteria that significantly influence the decision-making process. For this study, two main criteria, namely Land Use and Transportation, were defined. Under the criterion of Land Use, five sub-criteria were identified, while the criterion of Transportation encompassed three sub-criteria. Each primary criterion was assigned a weight reflecting its relative importance. Density analysis was conducted, and the assigned weights were further distributed among the sub-criteria. Specific density maps were created for each sub-criterion. Utilizing various spatial data processing

and analysis techniques, suitable parking locations were determined based on the assigned criteria weights. Ultimately, a map highlighting suitable areas for the establishment of new parking lots within the central or urban region of the Municipality of Tetovo was generated. To facilitate this process, the AHP method, supported by GIS technology, was employed.

2. Method

2.1. Research area boundaries and main features

Tetovo, situated in the northwestern region of North Macedonia, with a latitude of 42.006191 and a longitude of 20.959682, is a small city that holds significant geographical and strategic importance. Positioned near the Kosovo border, it is nestled amidst the picturesque foothills of Shar Mountain and divided by the flowing Pena (or Shkumbini) River. Tetovo is recognized as one of the prominent cities within the Republic of North Macedonia, forming a crucial part of the Polog Region. It

shares its borders with the cities of Gostivar and the capital of North Macedonia, the city of Skopje, holding an area of 261.89 km² as a municipality, as illustrated also in Figure 1.

Being the sole urban hub in its region, Tetovo attracts a substantial presence of public sector entities, including service industries, diverse state institutions, private sector organizations, two universities, six central municipal high schools, numerous municipal primary schools, and childcare centers, both private and public. Additionally, the city is home to state and private hospitals, various medical clinics, and various professionals such as dentists and veterinarians. It also boasts a vibrant aesthetics and beauty sector, along with shopping centers, cafes, restaurants, and various recreational venues. Furthermore, Tetovo offers some tourist facilities, adding to its appeal for residents in the surrounding areas. Consequently, individuals residing in rural municipalities are compelled to gravitate towards the urban segment of the Tetovo municipality.

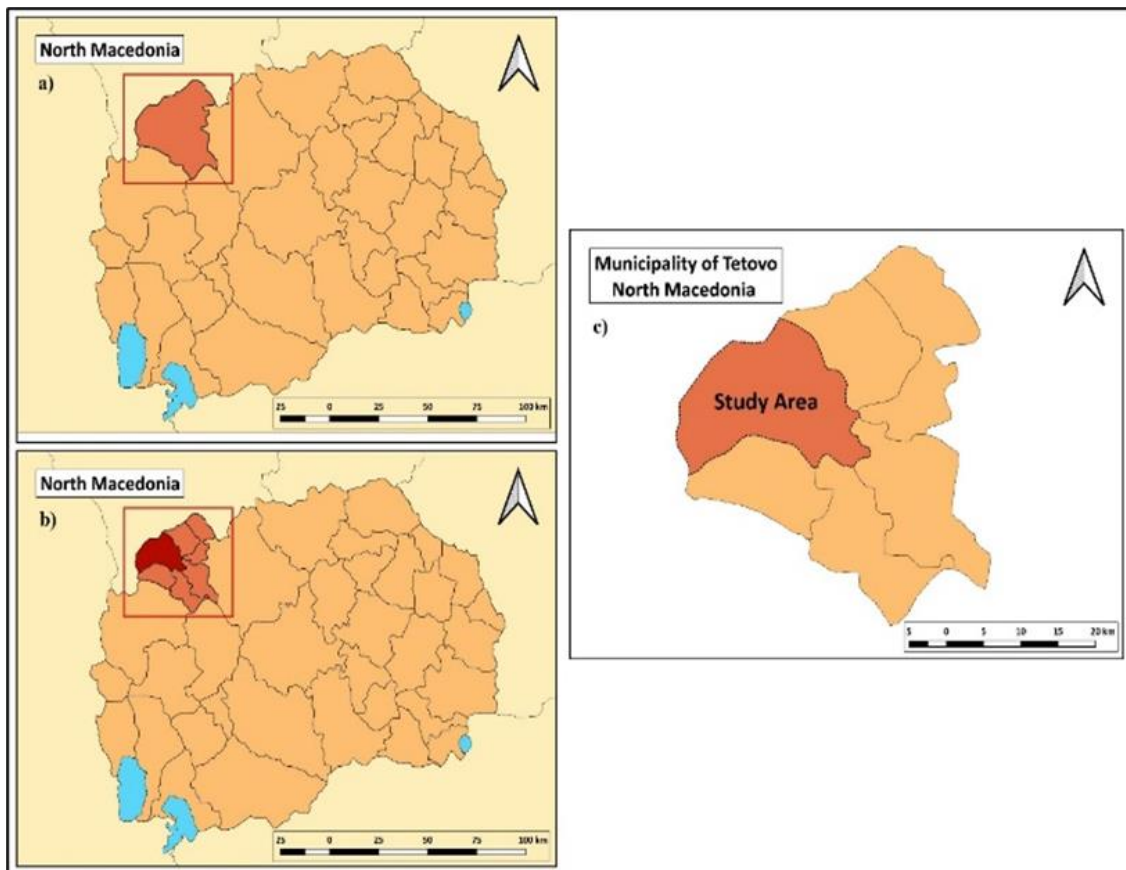


Figure 1. Study area – a) Location of the territory of the city of Tetovo; b) Location of the territory of municipalities located in the territory of the city of Tetovo (both urban municipality and five other rural municipalities); c) Location of the territory of Municipality of Tetovo (urban municipality), Polog Region, Northwest part of Republic of North Macedonia.

2.2. AHP methodology

The adoption of the AHP for decision-making processes is underpinned by its unparalleled capacity to systematically tackle complex, multi-criteria decision problems. AHP empowers decision-makers by providing a structured and prioritized framework through meticulous pairwise comparisons. This method not only

establishes a robust and quantitative foundation but also adeptly integrates subjective judgments and objective data, thereby substantially reinforcing the transparency and rationality intrinsic to the decision-making process. The systematic rigor and comprehensive nature of AHP contribute to its efficacy in navigating intricate decision landscapes, making it an indispensable tool for informed and strategic decision-making.

This study utilized the AHP method to establish suitable parking locations. When employing the AHP method, it is essential to develop a hierarchical structure. Consequently, the identification of primary criteria becomes crucial, followed by the determination of sub-criteria due to their significant importance. In the context of selecting parking lots, two main criteria were defined: Land Use and Transportation. Under the Land Use criterion, the following sub-criteria were established: accessibility to public institutions, accessibility to educational institutions, accessibility to health institutions, accessibility to cultural facilities, and accessibility to shopping centers. Under the Transportation criterion, the following sub-criteria were defined: accessibility to bus stations, accessibility to main roads, and accessibility to existing parking areas.

The meticulous process of selecting criteria for studies involving parking site analysis or analogous urban planning research involves a rigorous integration of expert knowledge, existing literature, and the unique context of the study area. Urban planners, engineers, transportation experts, and local authorities assume a pivotal role in this endeavor, contributing valuable insights derived from practical experience and a nuanced understanding of the local context, crucial for the identification and prioritization of criteria. Drawing inspiration from various foundational studies conducted by different authors, served as a cornerstone for our investigation, the collaborative input of urban planners, engineers, transportation experts, and local authorities was also instrumental in shaping our methodology. Additionally, a comprehensive literature review constitutes another vital dimension of criteria selection, where researchers delve into existing studies and best practices in urban planning, parking analysis, and related fields to ensure a well-informed and robust foundation for the study's criteria framework.

2.2.1. Determining criteria - Developing the hierarchical structure

As a procedure, first the problem is defined and then the definition of basic criteria and sub-criteria follows. As a consequence of this, continues the definition and elaboration or progress of the hierarchical structure of criteria, which are presented in Table 1. Subsequently, a reference table of criteria and sub-criteria presented in Table 2 is also presented.

Table 1. A general framework of the criteria.

Main Criteria	Sub-Criteria
Land Use	1.1. Accessibility to public institutions
	1.2. Accessibility to educational institutions
	1.3. Accessibility to health institutions
	1.4. Accessibility to cultural facilities
	1.5. Accessibility to shopping centers
Transportation	2.1. Accessibility to bus stations
	2.2. Accessibility to main roads
	2.3. Accessibility to existing parking areas

Table 2. A general framework of the criteria definition for determination or selection of parking lot sites based on relevant references

Main Criteria	Sub-Criteria	[1]	[9]	[3]	[7]	[4]	[23]	[10]
C1	1.1	x	x	x	x	x	x	
	1.2	x	x	x			x	
	1.3	x	x	x	x	x		x
	1.4	x	x	x				
	1.5	x	x		x	x	x	x
C2	2.1							
	2.2	x	x		x	x	x	x
	2.3	x	x	x				x

2.2.2. Establishing of binary comparison matrices

For each criterion, are created pairwise comparison matrices and in the same matrices, are evaluated criteria using the comparison scale. In this process and in this course of development, the degree of prominence of the criteria is established, which is represented in Table 3.

Table 4 provides a comprehensive overview of the fundamental data sets, their corresponding sources, and the analytical methods employed in the study. The table is structured to offer a systematic presentation of criteria such as C.1.1 to C.2.3, encompassing diverse aspects ranging from Public Institutions, Schools, Universities, Hospitals, Cultural Facilities, Shopping Centers to Bus Stations, Roadway – Main Roads, and Public Parking. The data, meticulously sourced from the Municipality of Tetovo, is subjected to Kernel Density and Linear Density analyses, ensuring a robust foundation for the subsequent exploration and insights within the study.

Table 3. The 1-9 importance scale table of pairwise comparison presented by Saaty [52]

Prominence Level	Definition	Explanation
1	Equal	Two activities contribute equally to the objective.
3	Moderate	Experience and judgement slightly favor one activity over another.
5	Strong	Experience and judgement strongly favor one activity over another.
7	Very Strong	An activity is favored very strongly over another.
9	Extreme	The evidence favoring one activity over another is of the highest possible order of affirmation.
2, 4, 6, 8	Intermediate values	Values between two consecutive judgments to be used when compromise is needed.

Table 4. Basic data, sources and properties used.

Criteria	Data	Data Source	Analysis
C.1.1	Public Institutions	Municipality of Tetovo	Kernel Density
C.1.2	Schools, Universities	Municipality of Tetovo	Kernel Density
C.1.3	Hospitals	Municipality of Tetovo	Kernel Density
C.1.4	Cultural Facilities	Municipality of Tetovo	Kernel Density
C.1.5	Shopping Centers	Municipality of Tetovo	Kernel Density
C.2.1	Bus Stations	Municipality of Tetovo	Kernel Density
C.2.2	Roadway – Main Roads	Municipality of Tetovo	Linear Density
C.2.3	Public Parking	Municipality of Tetovo	Kernel Density

2.2.3. Assessing Criteria - Weighting process

$$CR = \frac{CI}{RI} \tag{6}$$

The weighting criteria can be calculated and determined in different ways and methods which are presented in various forms. After the paired comparison matrices (Equation 1) are created the procedure of determining the values of importance weights continues.

$$A = \begin{bmatrix} 1 & a_{12} & \dots & a_{1n} \\ 1/a_{12} & 1 & \dots & a_{2n} \\ \vdots & \vdots & \ddots & \vdots \\ 1/a_{1n} & 1/a_{2n} & \dots & 1 \end{bmatrix} \tag{1}$$

After finding the total value of each column separately, each found value is proportionally separated by the total value of the column to which it belongs (Equation 2). Consequently, commanding the average of the values in each row of the received matrix, the column vector W is calculated (Equation 3).

$$c_{ij} = \frac{a_{ij}}{\sum_{i=1}^n a_{ij}} \tag{2}$$

$$w_i = \frac{\sum_{j=1}^n c_{ij}}{n} \tag{3}$$

2.2.4. Estimation of the consistency ratio

The base value (λ) is the first value that must be calculated to arrive at the calculation of the consistency ratio (CR). As a result, the pre-obtained weight vector (W) is multiplied by the pairwise comparison matrix (A). The result of this multiplication is reciprocally divided by the values in the weight vector W, and from this the arithmetic mean is taken (Equation 4). With these actions we calculated the value of λ .

$$\lambda = \frac{1}{n} \sum_{i=1}^n \left(\frac{\sum_{j=1}^n a_{ij} w_j}{w_i} \right) \tag{4}$$

The Consistency Index (CI) is calculated after calculating the base coefficient (Equation 5); while on the other hand the CR is calculated when the Randomness Index (RI) is divided by the CI value (Equation 6). The same is also represented in Table 5.

$$CI = \frac{\lambda - n}{n - 1} \tag{5}$$

Table 5. Randomness index [40]

n	1	2	3	4	5	6	7	8	9
RI	0.00	0.00	0.58	0.90	1.12	1.24	1.32	1.41	1.45

3. Results

The determination of criteria weights in this study was conducted using the AHP method. To gather input from professionals in the field, a questionnaire was prepared and administered to engineers, urban planners, and experts from both the private and public sectors, including municipal employees. The AHP method employed in this research involves the pairwise comparison of criteria to assess their relative importance on a scale from 1 to 9. The questionnaire was distributed to a total of 27 participants, and the results were analyzed using the Expert Choice program. Out of the total sample size of 27 respondents, 13 individuals possessed a bachelor's degree, whereas 14 other respondents had completed a master's degree. Among the participants in the survey, 20 respondents were employed in the public or state sector, whereas the remaining 7 individuals were affiliated with the private sector. The program calculates the weights of the criteria based on the geometric mean of the opinions of experienced professionals, including engineers and urban planners, and generates pairwise comparison matrices. The obtained criteria weights are presented in Table 6, Table 7, and Table 8.

Table 6. Weights of main criteria for determination or selection of parking lot sites.

CR= 0.00	W
Land Use	0.601
Transportation	0.399

Table 7. Weights of land use sub-criteria for determination or selection of parking lot sites.

CR= 0.02	W
Accessibility to public institutions	0.177
Accessibility to educational institutions	0.117
Accessibility to health institutions	0.454
Accessibility to cultural facilities	0.082
Accessibility to shopping centers	0.170

Table 8. Weights of transportation use sub-criteria for determination or selection of parking lot sites.

CR= 0.03	W
Accessibility to bus stations	0.233
Accessibility to main roads	0.517
Accessibility to existing parking areas	0.250

The criterion carrying the greatest weight is the accessibility to main roads with a weight of 0.517. Conversely, the criterion of accessibility to cultural facilities holds the lowest weight of 0.117. The weights assigned to the remaining criteria are as follows: accessibility to health institutions with a weight of 0.454, accessibility to existing parking areas with a weight of 0.250, accessibility to bus stations with a weight of 0.233, accessibility to public institutions with a weight of 0.177, accessibility to shopping centers with a weight of 0.170, and accessibility to educational institutions with a weight of 0.117.

3.1. Land use criteria

Criteria locations were identified, and density

analyses were conducted for each criterion using GIS. Kernel density maps were generated based on the point locations of public institutions, educational institutions, health institutions, cultural facilities, and shopping centers. These maps were then classified according to their density levels. Below, all the sub-criteria are explained and presented with the adequate maps, represented with figures.

3.1.1. Public institutions

A kernel density map was generated employing point location data of public institutions and subsequently categorized based on density levels (Figure 2).

3.1.2. Educational institutions

A kernel density map was generated employing point location data of educational institutions and subsequently categorized based on density levels (Figure 3).

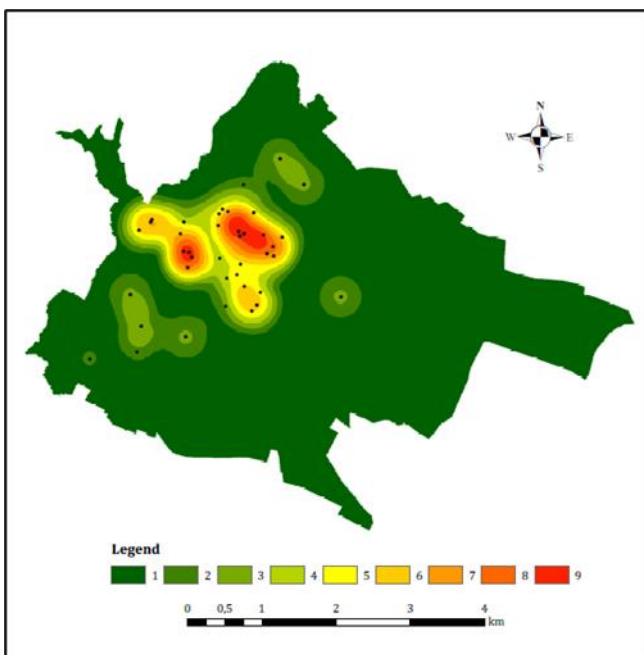


Figure 2. Public institutions density analysis map.

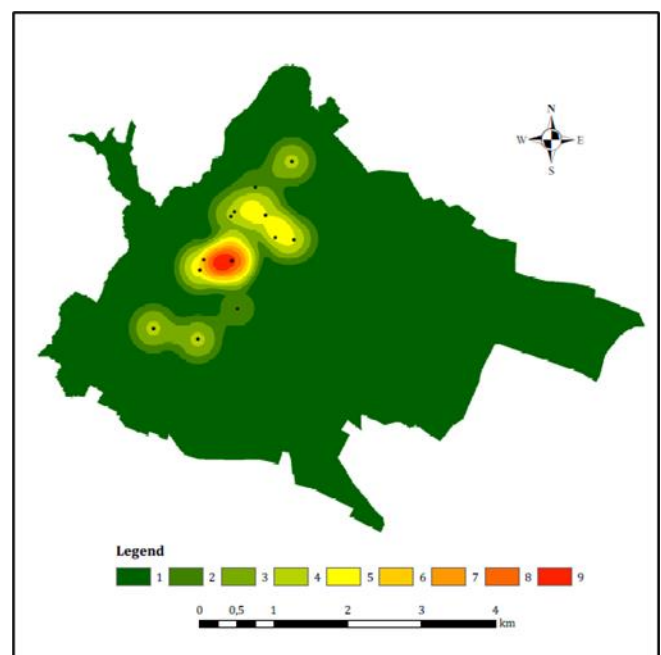


Figure 3. Educational institutions density analysis map.

3.1.3. Health institutions

A kernel density map was generated employing point location data of health institutions and subsequently categorized based on density levels (Figure 4).

3.1.4. Cultural facilities

A kernel density map was generated employing point location data of cultural facilities and subsequently categorized based on density levels (Figure 5).

3.1.5. Shopping centers

A kernel density map was generated employing point

location data of shopping centers and subsequently categorized based on density levels (Figure 6).

3.2. Transportation criteria

Criteria locations were identified, and density analyses were conducted for each criterion using GIS. Kernel density maps were generated based on the point locations of bus stations and existing parking areas, meanwhile line density map was generated based on the line locations of main roads. These maps were then classified according to their density levels. Below, all the sub-criteria are explained and presented with the adequate maps, represented with figures.

3.2.1. Bus stations

A kernel density map was generated employing point location data of bus stations and subsequently categorized based on density levels (Figure 7).

3.2.2. Main roads

A linear density map was generated employing the

linear location data of main roads and subsequently categorized based on density levels (Figure 8).

3.2.3. Existing parking areas

A kernel density map was generated employing point location data of existing parking areas and subsequently categorized based on density levels (Figure 9).

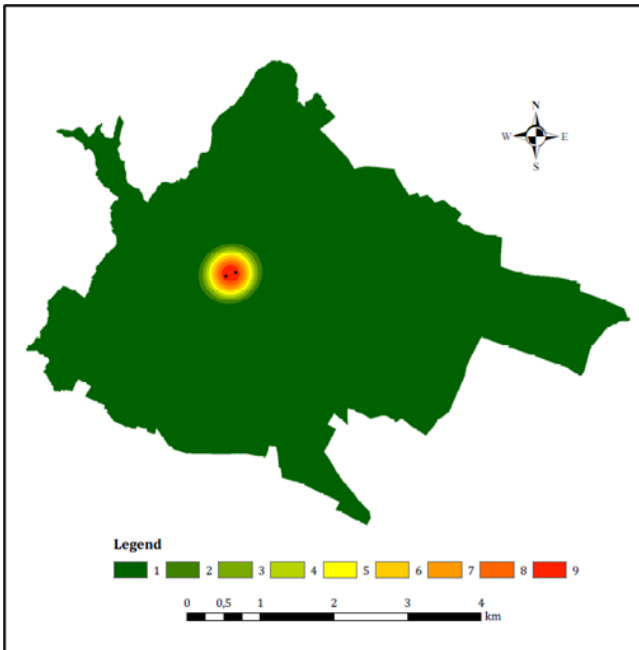


Figure 4. Health institutions density analysis map.

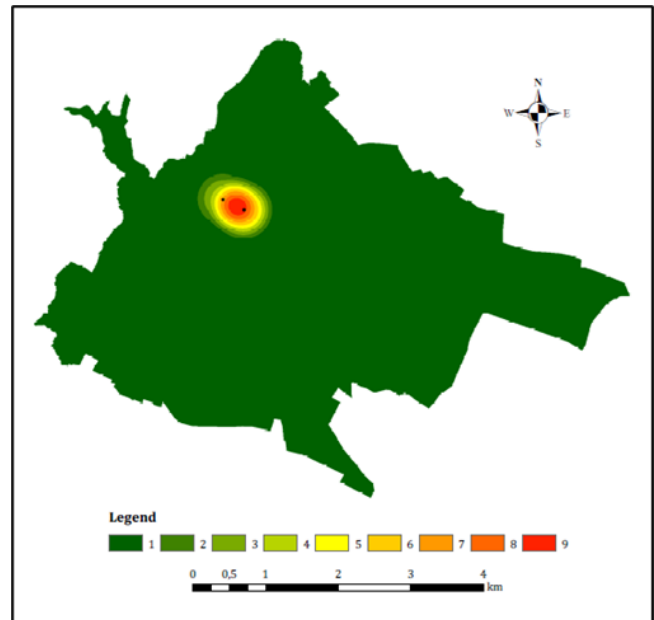


Figure 5. Cultural facilities density analysis map.

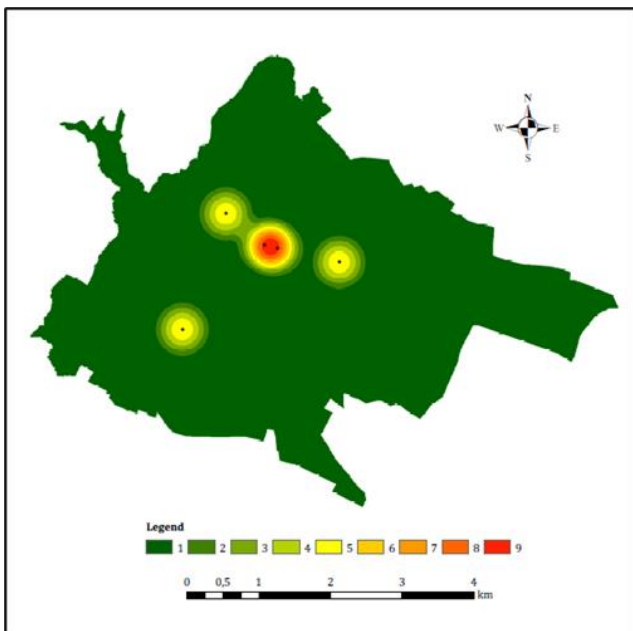


Figure 6. Shopping centers density analysis map.

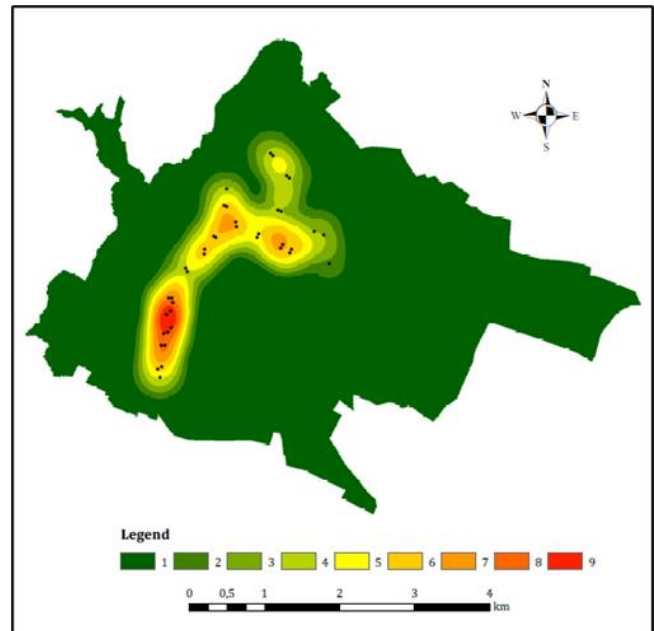


Figure 7. Bus stations density analysis map.

A conversion was made between the main criteria and sub-criteria, and the criteria weights used in the production of the suitable parking lot sites. From the converted weights, the criterion that carries the greatest weight is accessibility to health institutions with a weight of 0.273. In contrast, the criterion of accessibility in cultural facilities holds the lowest weight of 0.049. The weights assigned to the remaining criteria are as follows:

accessibility to main roads with a weight of 0.206, accessibility to public institutions with a weight of 0.107, accessibility to shopping centers with a weight of 0.102, accessibility to existing parking areas with a weight of 0.100, accessibility to bus stations with a weight of 0.093 and access to educational institutions with a weight of 0.070 (Table 8).

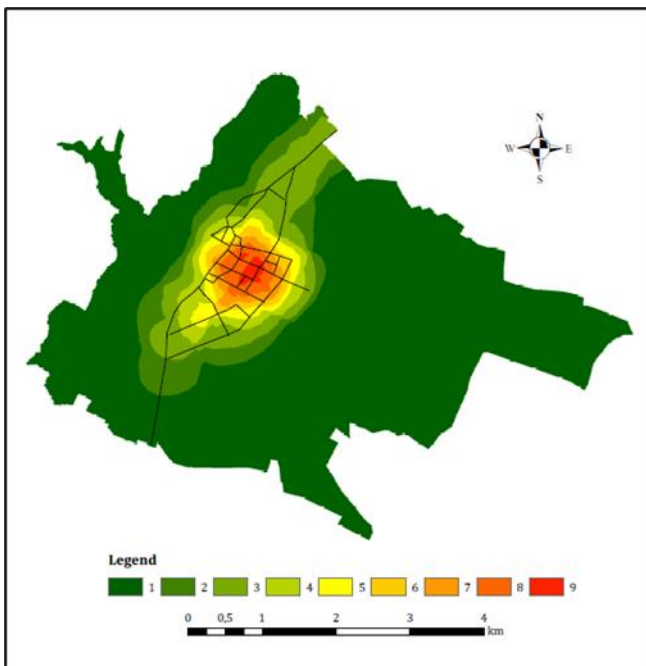


Figure 8. Main roads density analysis map.

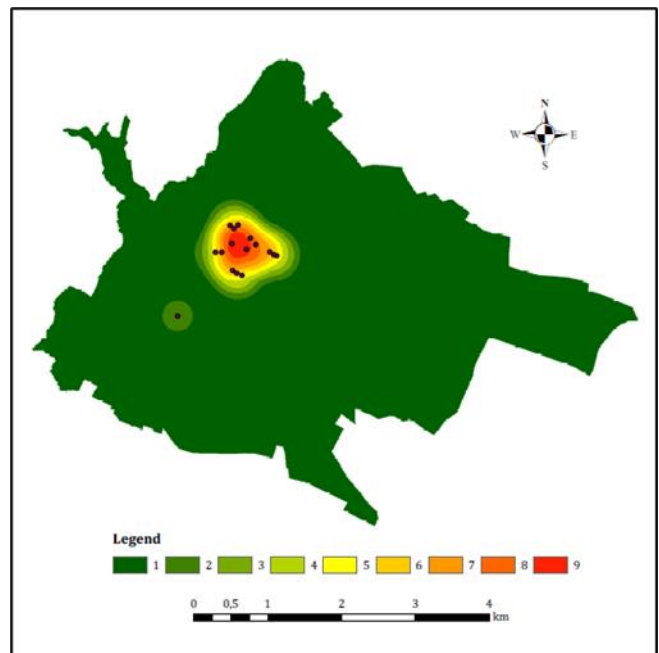


Figure 9. Existing parking areas density analysis map.

Table 9. Converted weights of criteria for determination or selection of parking lot sites.

Main Criteria	Sub-Criteria	Weights	Converted Weights
Land Use (0.601)	1.1	0.177	0.107
	1.2	0.117	0.070
	1.3	0.454	0.273
	1.4	0.082	0.049
	1.5	0.170	0.102
Transportation (0.399)	2.1	0.233	0.093
	2.2	0.517	0.206
	2.3	0.250	0.100

The resulting map was generated using a raster calculator, incorporating the criteria weights provided in Table 9. Criteria locations were identified, and density analyses were conducted for each criterion using GIS. The obtained raster data were classified. This map illustrates the suitable parking lot sites within the central urban area of the Municipality of Tetovo (Figure 10).

Based on the findings presented in Figure 10, the regions encompassing the city square, the vicinity of the two major boulevards within the city (crossed near the city square), the areas surrounding the municipality, the central courthouse, the city hospital, as well as certain primary, secondary, and high schools, are identified as the most favorable areas for establishing new parking lots. These areas exhibit higher suitability grades in terms of their potential for accommodating parking facilities. Results obtained are also presented in a tabular form, in the Table 10.

Table 10. The study findings obtained and presented in the tabular form.

Prominence Level	Area (km ²)	Distribution in percentage (%)
Extremely Suitable	0.590	2.55%
Suitable	0.577	2.49%
Moderately Suitable	1.218	5.26%
Less Suitable	3.457	14.94%
Not Suitable	17.301	74.76%

In the dynamic realm of urban planning and infrastructure development, a nuanced comprehension of suitable parking areas within residential zones assumes paramount significance. Our recent study undertakes a comprehensive exploration, not only to pinpoint areas conducive to parking but also to furnish a geodeterministic rationale for the observed concentration of these areas. The meticulous compilation and tabular presentation of our findings illuminate the diverse degrees of parking suitability across different residential zones. These figures not only quantify the extent of each category but also afford stakeholders a proportional representation, enhancing their understanding of the distribution dynamics. Augmenting our study, a numerical comparison with other crucial infrastructure elements in the residential zone serves as a valuable tool for urban planners and policymakers, facilitating a holistic grasp of spatial resource allocation. This article will delve into the underlying geographical factors influencing the concentration of parking areas. This research strives to be a guiding beacon in the intricacies of urban planning, offering a comprehensive overview of suitable parking areas, thereby fostering sustainable and efficient infrastructure development in residential zones.

4. Discussion

The municipality of Tetovo played a crucial role in providing the essential resources required for the successful execution of this study. The authorities of the municipality facilitated the provision of necessary materials for conducting the research. This included the procurement of relevant data and information essential for the compilation of density maps and the final map depicting suitable parking areas or locations. The municipal authorities were instrumental in supplying the required data and collaborating closely with the research team throughout the study.

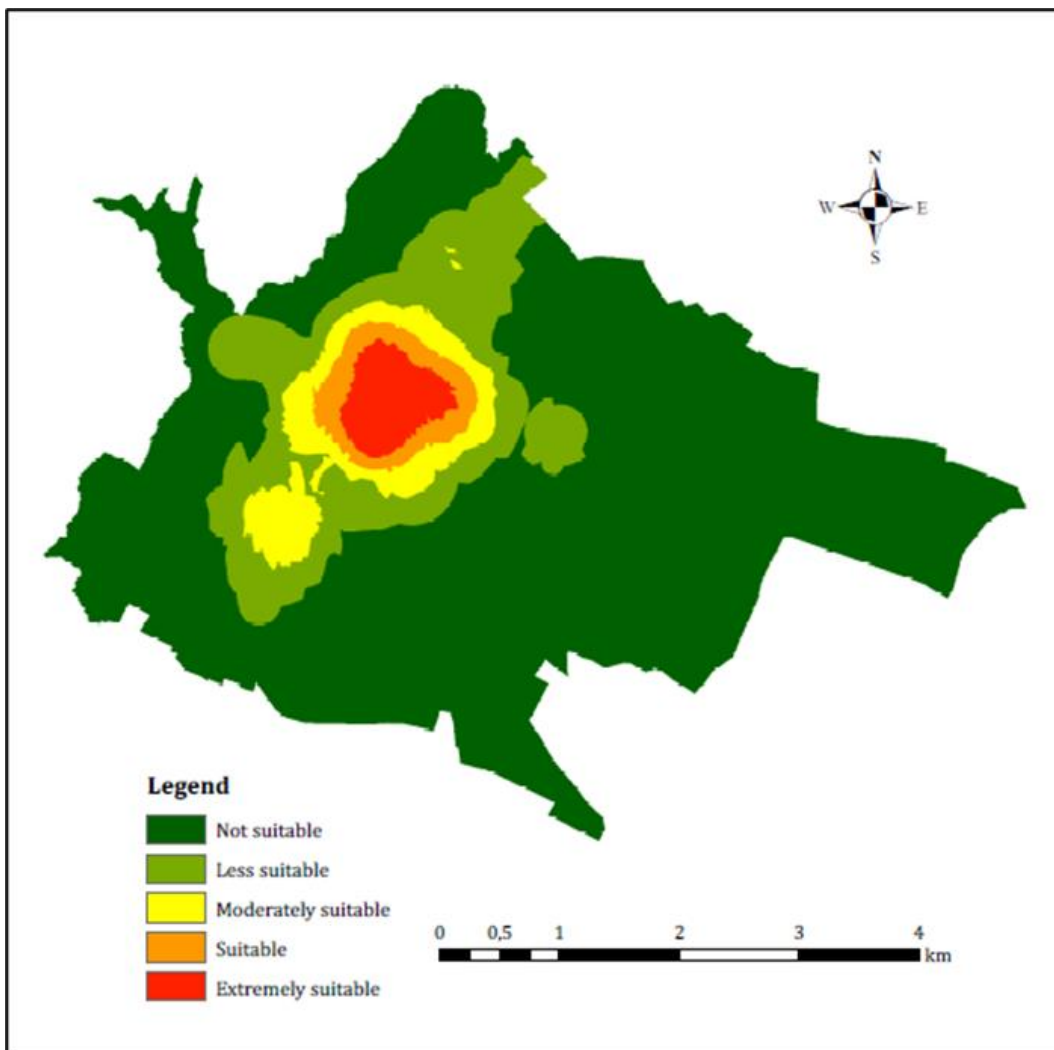


Figure 10. Suitable parking areas map in the central urban territory of Municipality of Tetovo, Polog Region, Northwest part of Republic of North Macedonia.

Employing GIS-based density analyses and kernel density maps significantly enhances the precision in identifying optimal parking lot sites, strategically revealing key areas within Tetovo's central urban zone. The results meticulously pinpoint regions encompassing the city square, major boulevards, municipal and healthcare facilities, and educational institutions, showcasing these locations as exceptionally advantageous for the establishment of new parking lots. This detailed analysis not only provides valuable insights but also furnishes municipal authorities and urban planners with essential data for informed decision-making and strategic urban development initiatives.

The density maps vividly illustrate a significant issue within the city of Tetovo, namely the concentration of public institutions, educational institutions, and health institutions in a confined and closely-knit area. This spatial clustering highlights an anomaly within the city and underscores the challenge of vehicular congestion, leading to an evident shortage of suitable and adequate parking facilities.

Nevertheless, with the implementation of a questionnaire administered to 27 experts, we successfully generated a comprehensive map delineating the appropriate parking zones within the city or

municipality of Tetova. The empirical findings of this study can greatly assist municipal authorities and decision-makers in enhancing the quality of available parking facilities within the jurisdiction. Moreover, urban planners can utilize the study and accompanying materials as valuable resources to streamline the design process.

As part of the discussion in this study, a comparative analysis is conducted, juxtaposing the findings obtained herein with those of previous works by various authors in different countries. The following comparisons are represented as follows:

4.1. Main criteria comparison

Various criteria were considered in this study, as elucidated earlier. In the decision-makers' hierarchy established based on their judgments, the land use criteria held the highest weight (0.601) among the principal criteria, followed by transportation criteria (0.399). Given its direct correlation with the prevalent issue of heavy traffic in the city, decision-makers accorded priority to the land use criteria. This prioritization aligns with findings in other studies; for instance, Alkan and Durduran [1] similarly identified

Land use as the most weighted criterion (0.58), followed by Transportation (0.42). Conversely, in the study conducted by Demir et al. [9], transportation criteria appeared to carry the highest weight (0.55), succeeded by land use criteria (0.33). Iqbal [51] also observed a higher weight for transportation (0.60) compared to land use criteria (0.35) in their study.

4.2. Land use sub-criteria comparison

In the assessment of the land use sub-criterion, in our study the highest weights from pairwise comparison matrices were determined as follows: accessibility to health institutions (0.454), accessibility to public institutions (0.177), accessibility to shopping centres (0.170), accessibility to educational institutions (0.117), and accessibility to cultural facilities (0.082). Alkan and Durduran [1] reported similar weights derived from pairwise comparison matrices, listing accessibility to health institutions (0.357), accessibility to public institutions (0.165), accessibility to educational institutions (0.124), accessibility to shopping centres (0.119), and accessibility to cultural facilities (0.082). Moreover, Demir et al. [9] identified weights from pairwise comparison matrices as accessibility to shopping centres (0.354), accessibility to health institutions (0.261), accessibility to cultural facilities (0.151), accessibility to public institutions (0.107), and accessibility to educational institutions (0.047). In the study by Iqbal [51], weights from pairwise comparison matrices were listed as accessibility to shopping centres (0.197), accessibility to health institutions (0.172), accessibility to public institutions (0.084), accessibility to educational institutions (0.042), and accessibility to cultural facilities (0.024).

4.3. Transportation sub-criteria comparison

In the evaluation of the transportation sub-criterion, our study assigned the highest weights from pairwise comparison matrices as follows: accessibility to main roads (0.517), accessibility to existing parking areas (0.250), and accessibility to bus stations (0.233). Alkan and Durduran [1] reported similar weights derived from pairwise comparison matrices, listing accessibility to main roads (0.442), accessibility to existing parking areas (0.249), and accessibility to bus stations (0.308). Additionally, Demir et al. [9] identified weights from pairwise comparison matrices for accessibility to existing parking areas (0.252), accessibility to main roads (0.151), and accessibility to bus stations (or train, tramway, metro stations) (0.074). In Iqbal's study (2020), weights from pairwise comparison matrices were listed as accessibility to main roads (0.568), accessibility to bus stations (or train, tramway, metro stations) (0.397), and accessibility to existing parking areas (0.347).

5. Conclusion

Urbanization issues and challenges, particularly in the domain of traffic and parking, have emerged as a

consequence of the rapid growth of urban populations and the haphazard development of cities. The model proposed in this paper addresses these concerns by offering a solution for predicting and determining available parking spaces. The approach presented here has distinct advantages as it aims to simplify the process of selecting suitable parking locations. This selection process, which employs the combined AHP method and GIS method, represents a complex decision-making problem for providing a more efficient and effective solution.

The AHP method was utilized to determine the relative weights of the predetermined criteria. Specifically, the selection of suitable parking locations in this study was based on criteria related to Land Use and Transportation. The AHP is a commonly employed method in site selection problems and involves determining the importance levels of criteria that influence site selection through expert opinions. By constructing pairwise comparison matrices, the weights of the predetermined criteria were computed. Subsequently, using the GIS method, the spatial locations of the criteria and sub-criteria were established, and a density analysis was conducted. This analysis resulted in the production of a map that highlights the suitable parking locations within the central territory of the urban area of Municipality of Tetovo, North Macedonia.

This study also serves as a valuable resource for decision makers, providing guidance on two key aspects for the future: sustainable urban management and the identification of suitable parking lot sites. The findings and recommendations of this study can aid decision makers in making informed choices regarding urban planning and the determination of suitable parking lot sites to promote sustainable development.

The research conducted, aimed at tackling urbanization challenges, with a primary focus on traffic and parking issues. The integration of the AHP and GIS not only proposed a model for predicting and determining parking availability but also presented a robust solution for urban planners and decision-makers. Acknowledging the pivotal role of municipality authorities in facilitating data procurement and collaboration, the study advocates for expanding research horizons by exploring additional decision-making methods. To further enhance decision-making processes beyond AHP, it is recommended to consider methodologies such as the Analytic Network Process (ANP), especially in scenarios with intricate interactions and dependencies among criteria and alternatives. ANP's nuanced approach is particularly beneficial for complex urban planning decisions. Additionally, exploring the application of Fuzzy Logic, specifically in handling qualitative and subjective information inherent in urban planning, could prove advantageous. Fuzzy Logic's capacity to represent uncertainty could significantly improve decision-making, especially in situations where data lacks precise values. Given the identified concentration of public institutions in Tetovo, the incorporation of Game Theory is suggested to model strategic interactions among stakeholders in urban planning. Game Theory can offer insights into the

decision choices of various entities, optimizing outcomes and fostering effective collaboration in urban development. This comprehensive and integrative approach, encompassing diverse decision-making methods, is poised to provide a more holistic understanding of decision spaces, effectively addressing the multifaceted challenges associated with sustainable urban management and parking facility identification.

Author contributions

Edmond Jonuzi: Conceptualization, Methodology, Data collecting, Writing-Original draft preparation
Tansu Alkan: Analysis, Visualization, Writing-Reviewing
Süleyman Savaş Durduran: Investigation, Editing
Hüseyin Zahit Selvi: Investigation and Editing.

Conflicts of interest

The authors declare no conflicts of interest.

References

- Alkan, T., & Durduran, S. S. (2021). GIS-supported mapping of suitable parking areas using AHP method: The case of Konya. *The International Archives of the Photogrammetry, Remote Sensing and Spatial Information Sciences*, 46, 51-56. <https://doi.org/10.5194/isprs-archives-XLVI-4-W5-2021-51-2021>
- Fahim, A., Hasan, M., & Chowdhury, M. A. (2021). Smart parking systems: comprehensive review based on various aspects. *Heliyon*, 7(5), e07050. <https://doi.org/10.1016/j.heliyon.2021.e07050>
- Farzanmanesh, R., Naeeni, A. G., & Abdullah, A. M. (2010). Parking site selection management using fuzzy logic and multi criteria decision making. *Environment Asia*, 3(3), 109-116.
- Ozturk, D., & Kılıç-Gul, F. (2020). GIS-based multi-criteria decision analysis for parking site selection. *Kuwait Journal of Science*, 47(3), 2-14
- Jelokhani-Niaraki, M., & Malczewski, J. (2015). A group multicriteria spatial decision support system for parking site selection problem: A case study. *Land Use Policy*, 42, 492-508. <https://doi.org/10.1016/j.landusepol.2014.09.003>
- Alinia, K., Yarahmadi, A., Zarin, J. Z., Yarahmadi, H., & Lak, S. B. (2015). Parking lot site selection: An opening gate towards sustainable GIS-based urban traffic management. *Journal of the Indian Society of Remote Sensing*, 43, 801-813. <https://doi.org/10.1007/s12524-014-0415-3>
- Kazazi Darani, S., Akbari Eslami, A., Jabbari, M., & Asefi, H. (2018). Parking lot site selection using a fuzzy AHP-TOPSIS framework in Tuyserkan, Iran. *Journal of Urban Planning and Development*, 144(3), 04018022. [https://doi.org/10.1061/\(ASCE\)UP.1943-5444.0000456](https://doi.org/10.1061/(ASCE)UP.1943-5444.0000456)
- Hensher, D. A., & King, J. (2001). Parking demand and responsiveness to supply, pricing and location in the Sydney central business district. *Transportation Research Part A: Policy and Practice*, 35(3), 177-196. [https://doi.org/10.1016/S0965-8564\(99\)00054-3](https://doi.org/10.1016/S0965-8564(99)00054-3)
- Demir, S., Basaraner, M., & Gumus, A. T. (2021). Selection of suitable parking lot sites in megacities: A case study for four districts of Istanbul. *Land use policy*, 111, 105731. <https://doi.org/10.1016/j.landusepol.2021.105731>
- Neisani Samani, Z., Karimi, M., & Alesheikh, A. A. (2018). A novel approach to site selection: collaborative multi-criteria decision making through geo-social network (case study: public parking). *ISPRS International Journal of Geo-Information*, 7(3), 82. <https://doi.org/10.3390/ijgi7030082>
- Awan, F. M., Saleem, Y., Minerva, R., & Crespi, N. (2020). A comparative analysis of machine/deep learning models for parking space availability prediction. *Sensors*, 20(1), 322. <https://doi.org/10.3390/s20010322>
- Feng, Y., Xu, Y., Hu, Q., Krishnamoorthy, S., & Tang, Z. (2022). Predicting vacant parking space availability zone-wisely: A hybrid deep learning approach. *Complex & Intelligent Systems*, 8(5), 4145-4161. <https://doi.org/10.1007/s40747-022-00700-1>
- Benenson, I., Martens, K., & Birfir, S. (2008). PARKAGENT: An agent-based model of parking in the city. *Computers, Environment and Urban Systems*, 32(6), 431-439. <https://doi.org/10.1016/j.compenvurbsys.2008.09.011>
- Tian, D., Wang, Y., Lu, G., Yu, G., Duan, X., & Liu, H. (2011). A parking space finding method based on VANETs. In *ICCTP 2011: Towards Sustainable Transportation Systems*, 1511-1520. [https://doi.org/10.1061/41186\(421\)150](https://doi.org/10.1061/41186(421)150)
- Hosseini Lagha, G., Mokhtary Malek Abadi, R., & Gandomkar, A. (2012). Geographical analysis of parking land use in Genaveh applying AHP Model. *Journal of Urban-Regional Studies and Research*, 4(13), 95-114.
- Shoup, D. C. (2006). Cruising for parking. *Transport policy*, 13(6), 479-486. <https://doi.org/10.1016/j.tranpol.2006.05.005>
- Shoup, D. (2018). Free parking or free markets. In *Parking and the City*, 270-275. Routledge.
- Giuffrè, T., Siniscalchi, S. M., & Tesoriere, G. (2012). A novel architecture of parking management for smart cities. *Procedia-Social and Behavioral Sciences*, 53, 16-28. <https://doi.org/10.1016/j.sbspro.2012.09.856>
- Caicedo, F. (2010). Real-time parking information management to reduce search time, vehicle displacement and emissions. *Transportation Research Part D: Transport and Environment*, 15(4), 228-234. <https://doi.org/10.1016/j.trd.2010.02.008>
- Gülhan, G., & Ceylan, H. (2010). Otopark sorununa otopark yönetimi temelinde yaklaşımlar: İzmir Örneği. *Dokuz Eylül Üniversitesi Mühendislik Fakültesi Fen ve Mühendislik Dergisi*, 12(1), 63-73.
- Koster, A., Oliveira, A., Volpato, O., Delvequio, V., & Koch, F. (2014). Recognition and recommendation of

- parking places. In *Ibero-American Conference on Artificial Intelligence*, 675-685. Cham: Springer International Publishing.
https://doi.org/10.1007/978-3-319-12027-0_54
22. Litman, T. (2016). *Parking management: strategies, evaluation and planning* (p. 2). Victoria, BC, Canada: Victoria Transport Policy Institute
 23. Prasertsri, N., & Sangpradid, S. (2020). Parking site selection for light rail stations in Muaeng District, Khon Kaen, Thailand. *Symmetry*, 12(6), 1055. <https://doi.org/10.3390/sym12061055>
 24. Schaffer, F. (1970). *The new town story*. London, UK: Macgibbon and Kee
 25. Lotfi, S., & Koohsari, M. J. (2009). Analyzing accessibility dimension of urban quality of life: Where urban designers face duality between subjective and objective reading of place. *Social Indicators Research*, 94, 417-435. <https://doi.org/10.1007/s11205-009-9438-5>
 26. Kaiser, I., Godschalk, D. & Chapin, F.S. (1995). *Urban land use planning*, University of Illinois Press, Urbana, 61-83
 27. Obot, J. U., Etim, E. E., & Atser, J. (2009). Intra-urban traffic and parking demand in Uyo Urban Area. *Global Journal of Social Sciences*, 8(2), 61-68. <https://doi.org/10.4314/gjss.v8i2.51583>
 28. LaGro Jr, J. A. (2013). *Site analysis: Informing context-sensitive and sustainable site planning and design*. John Wiley & Sons.
 29. Ghaziaskari, N. A. (2005). *Parking lot site selection using GIS*. [Master's thesis, Shahid Beheshti University].
 30. Eldrandaly, K. (2013). Developing a GIS-based MCE site selection tool in ArcGIS using COM technology. *The International Arab Journal of Information Technology*, 10(3), 268-274
 31. Rikalovic, A., Cosic, I., & Lazarevic, D. (2014). GIS based multi-criteria analysis for industrial site selection. *Procedia Engineering*, 69, 1054-1063. <https://doi.org/10.1016/j.proeng.2014.03.090>
 32. Atalay, A., & İçen, Y. (2020). Kentiçi otopark analizi: Elazığ İli Örneği. *Fırat Üniversitesi Mühendislik Bilimleri Dergisi*, 32(2), 403-413. <https://doi.org/10.35234/fumbd.647091>
 33. Öztürk, S., & Işınkaralar, Ö., (2019). Parking problematique in Kastamonu City Center: A critical evaluation. *The Journal of International Social Research*, 12(67), 506-511
 34. Żak, J., & Weğliński, S. (2014). The selection of the logistics center location based on MCDM/A methodology. *Transportation Research Procedia*, 3, 555-564. <https://doi.org/10.1016/j.trpro.2014.10.034>
 35. Guo, S., & Zhao, H. (2015). Optimal site selection of electric vehicle charging station by using fuzzy TOPSIS based on sustainability perspective. *Applied Energy*, 158, 390-402. <https://doi.org/10.1016/j.apenergy.2015.08.082>
 36. Wehmeyer, M. L., Shogren, K. A., Little, T. D., & Lopez, S. J. (2017). *Development of self-determination through the life-course*. Springer.
 37. Butt, A., Ahmad, S. S., Shabbir, R., & Erum, S. (2017). GIS based surveillance of road traffic accidents (RTA) risk for Rawalpindi city: A geo-statistical approach. *Kuwait Journal of Science*, 44(4), 129-134
 38. Sun, C., Wade, M. T., Lee, Y., Orcutt, J. S., Alloatti, L., Georgas, M. S., ... & Stojanović, V. M. (2015). Single-chip microprocessor that communicates directly using light. *Nature*, 528(7583), 534-538. <https://doi.org/10.1038/nature16454>
 39. Jonuzi, E., Durduran, S. S., & Alkan, T. (2022). North Macedonian Cadastre Towards Cadastre 2034. *Necmettin Erbakan Üniversitesi Fen ve Mühendislik Bilimleri Dergisi*, 4(2), 26-44.
 40. Saaty, T. L. (1980). *The Analytic Hierarchy Process*; McGraw-Hill: New York, NY, USA
 41. Sharifi, M. A., & Retsios, V. (2004). Site selection for waste disposal through spatial multiple criteria decision analysis. *Journal of Telecommunications and Information Technology*, 28-38.
 42. Turskis, Z., Zavadskas, E. K., Antucheviciene, J., & Kosareva, N. (2015). A hybrid model based on fuzzy AHP and fuzzy WASPAS for construction site selection. *International Journal of Computers communications & control*, 10(6), 113-128.
 43. Ho, W. (2008). Integrated analytic hierarchy process and its applications—A literature review. *European Journal of Operational Research*, 186(1), 211-228. <https://doi.org/10.1016/j.ejor.2007.01.004>
 44. Wang, J. J., Jing, Y. Y., Zhang, C. F., & Zhao, J. H. (2009). Review on multi-criteria decision analysis aid in sustainable energy decision-making. *Renewable and Sustainable Energy Reviews*, 13(9), 2263-2278. <https://doi.org/10.1016/j.rser.2009.06.021>
 45. Urfali, T., & Eymen, A. (2021). CBS ve AHP yöntemi yardımıyla Kayseri İli örneğinde rüzgâr enerji santrallerinin yer seçimi. *Geomatik*, 6(3), 227-237. <https://doi.org/10.29128/geomatik.772453>
 46. Yalçın, C., & Yüce, M. (2019). Burdur'da güneş enerjisi santrali (GES) yatırımına uygun alanların CBS yöntemiyle tespiti. *Geomatik*, 5(1), 36-46. <https://doi.org/10.29128/geomatik.561962>
 47. Beyhan, H. C., Eren, G., & Aktuğ, B. (2020). Perakende market lokasyonları için CBS tabanlı çok kriterli AHP yöntemi ile optimal yer seçimi analizi: İstanbul Örneği. *Afyon Kocatepe Üniversitesi Fen ve Mühendislik Bilimleri Dergisi*, 20(6), 1032-1050. <https://doi.org/10.35414/akufemubid.803391>
 48. Şentürk, E., & Erener, A. (2017). Determination of temporary shelter areas in natural disasters by GIS: A case study, Gölcük/Turkey. *International Journal of Engineering and Geosciences*, 2(3), 84-90. <https://doi.org/10.26833/ijeg.317314>
 49. Sarı, F., & Koyuncu, F. (2021). Multi criteria decision analysis to determine the suitability of agricultural crops for land consolidation areas. *International Journal of Engineering and Geosciences*, 6(2), 64-73. <https://doi.org/10.26833/ijeg.683754>
 50. Alkan, T., & Durduran, S. S. (2020). Konut seçimi sürecinin AHP temelli TOPSIS yöntemi ile analizi. *Necmettin Erbakan Üniversitesi Fen ve Mühendislik Bilimleri Dergisi*, 2(2), 12-21.

51. Iqbal, A. S. (2020). A GIS-based parking demand analysis and site selection for parking area: Pendik-Istanbul case. [Master's thesis, Gebze Technical University]

52. Saaty, T. L. (2008). Decision making with the analytic hierarchy process. *International Journal of Services Sciences*, 1(1), 83-98.
<https://doi.org/10.1504/IJSSCI.2008.017590>



© Author(s) 2024. This work is distributed under <https://creativecommons.org/licenses/by-sa/4.0/>



Production of fuel-based carbon footprint distribution map using spatial interpolation methods based on GIS

Ebru Çolak¹, Tuğba Memişoğlu Baykal², Nihal Genç³

¹ Karadeniz Technical University, Department of Geomatics Engineering, Türkiye, ecolak@ktu.edu.tr

² Ankara Hacı Bayram Veli University, School of Land Registry and Cadastre, Türkiye, tugbamemisoglu@gmail.com

³ Giresun University, Department of Geomatics Engineering, Türkiye, nhlgn95@hotmail.com

Cite this study:

Çolak, E., Baykal, T. M., & Genç, N. (2024). Production of fuel-based carbon footprint distribution map using spatial interpolation methods based on GIS. *International Journal of Engineering and Geosciences*, 9 (1), 99-114

<https://doi.org/10.26833/ijeg.1330784>

Keywords

Climate Change
Greenhouse gas emissions
Carbon emissions
Carbon footprint
GIS

Research Article

Received: 21.07.2023

Revised: 27.11.2023

Accepted: 30.11.2023

Published: 02.01.2024



Abstract

The Earth is a complex system where living and non-living elements coexist in a delicate balance. Climate change is the primary factor responsible for the degradation of this system over time. The far-reaching consequences of climate change impact various aspects of our lives, including the physical environment, urban settings, human activities, economy, technology, agriculture, food production, access to clean water, and public health, all of which are widely acknowledged. Human-induced greenhouse gas emissions in these areas significantly trigger global climate change. Hence, addressing and mitigating the environmental damage from these emissions and the interconnected climate change phenomena is imperative. This situation is where the concept of "carbon footprint" gains prominence in assessing the extent of this damage. Carbon footprint serves as an essential measure in managing and curbing climate change. This study focused on controlling and mitigating carbon emissions, one of the primary greenhouse gasses responsible for climate change, by implementing spatial interpolation techniques based on Geographic Information Systems (GIS). The investigation targeted the Beşirli neighborhood in the Ortahisar district of Trabzon province. Data concerning electricity and natural gas usage were acquired from relevant institutions to perform carbon footprint calculations. Subsequently, carbon footprint calculations were conducted utilizing the acquired data within the specified region. The resulting outputs were systematically organized, integrated into the GIS environment, and linked to their respective geographical locations. Eventually, region-specific carbon footprint distribution maps were generated using selected spatial interpolation methods. These maps enabled a spatial observation of points exhibiting variability in terms of carbon emissions, thereby highlighting the carbon footprints evident in the region. The ultimate goal of this endeavor is to propose practical measures for minimizing the adverse environmental impacts by suggesting strategies to reduce and prevent carbon footprints associated with carbon emissions in the relevant areas.

1. Introduction

Global warming is characterized by the gradual rise in the Earth's temperature, stemming from various factors and surpassing what is deemed normal. The primary driver of this phenomenon is climate change, which stands as one of the most significant and perilous global challenges [1]. Climate change manifests both through natural occurrences and, more significantly, as a consequence of human activities. In this context, climate change refers to long-term alterations in meteorological parameters, such as temperature, humidity, precipitation, and wind, arising from both natural

conditions and the combustion of fossil fuels [2]. Furthermore, the United Nations Framework Convention on Climate Change (UNFCCC) provides a comprehensive definition, characterizing climate change as "a change of climate which is attributed directly or indirectly to human activity that alters the composition of the global atmosphere and which is in addition to natural climate variability observed over comparable periods." [3].

The main factor in climate change is the greenhouse effect. The greenhouse effect, which provides the temperature balance of the Earth, occurs when the gases and water vapor in the atmosphere retain the heat from the sun to the Earth [4]. The most critical component of

the greenhouse effect is greenhouse gases. Some of the greenhouse gases added to the atmosphere by various human activities are CO, CO₂, H₂O, NO, CH₄, NO₂, and O₃. CO₂, which retains the most heat, significantly impacts climate change. The increase in the need for energy in the world due to increasing industrialization with the industrial revolution has increased the use of fossil fuels, especially carbon-based ones.

On the other hand, changes in land use have occurred, soil structure has deteriorated, and deforestation has emerged. These negativities have increased the emission of CO₂, the most important greenhouse gas. As a result of these activities, the primary source of which is human beings, the amount of CO₂ in the atmosphere has increased and started to accumulate with rapidly increasing CO₂ emissions. This situation has led to the carbon cycle disruption that provides the world's climate balance and temperature changes [5]. This warming of the Earth and the accumulation of gases released into the atmosphere have formed the basic fundamentals of climate change [6].

Climate change has multiple and diverse negative impacts on the earth and people. The severity of these impacts increases over time. In the latest assessment report prepared by the Intergovernmental Panel on Climate Change (IPCC), it is stated that with climate change, there will be sudden changes in the intensity and duration of weather events, and sea levels will rise [7]. When we look at the present day, it is seen that with the impact of human activities, severe increases in temperature values have started, while decreases in cold temperatures have also occurred [8]. On the other hand, many regions face the threat of desertification due to drought caused by decreases in precipitation. On the other hand, the combination of heat and drought conditions increases the risk of forest fires [9]. Rising sea levels cause damage to the structures and arrangements in the coastal zone and the people in this region. Another negative impact of climate change is on seasons. Shifts in the seasons affect agriculture in the first degree, causing the time balance in the growing cycle of crops to be disrupted [10]. In addition, climate change, which affects the ecological balance, jeopardizes the lives of many species and reduces biodiversity [11-13]. Socio-

economic concepts such as human health, migration, tourism, transportation, water resources, forestry, fisheries, energy, agriculture, and animal husbandry are also effective in climate change [14]. The situations that arise from all these situations affecting climate change and being affected by change constitute the main source of carbon emissions into the atmosphere. With the increasing carbon emission and accumulation, the world's stable balance is being damaged. Figure 1 shows the graph of CO₂ emissions in the world between 1990 and 2020, prepared based on World Bank data [15]. According to the graph, CO₂ emissions are generally upward, but entered a downward trend in 2020. The reason for this is thought to be the pandemic experienced that year. On the other hand, Figure 2 shows a map of countries' carbon emissions produced from World Bank data [15]. Looking at the map, it is seen that China, the USA, Canada, Germany, India, and Russia are the countries that stand out with high carbon emissions. The countries with the lowest carbon emissions are located in South Africa.

Many approaches are put forward to reduce CO₂ emissions, which have the largest share in climate change. One of these is economic stagnation and a slowdown in growth. It has been observed that the slowdown in the economy due to the collapse of Soviet Russia, the 2009 crisis in the United States and the pandemic in 2020 reduced carbon emissions. However, this is not a preferred approach as it negatively affects the welfare level [14]. Another approach is to reduce intensive carbon production. Especially in developing countries, carbon emissions from electricity and heat generation are high due to production processes [16]. Therefore, the preference for renewable energy sources in production will reduce carbon production. On the other hand, practices such as improving efficiency, preferring renewable energy sources and imposing a carbon emission tax are considered one of the main approaches to reduce energy consumption using fossil fuels [17, 18]. Finally, the use of carbon capture and sequestration systems to remove carbon emissions from the atmosphere resulting from the combustion of fossil fuels is suggested as a preferable, although complex and costly, approach [2].

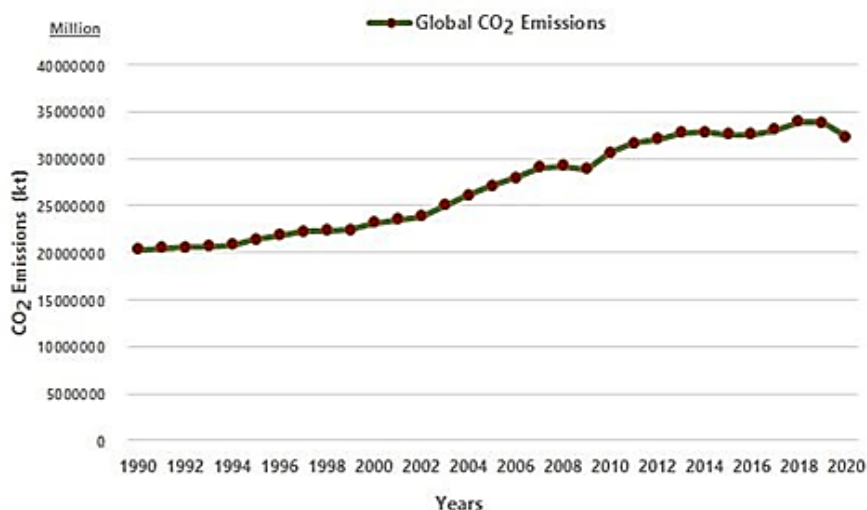


Figure 1. Global CO₂ emissions for the period 1990-2020.

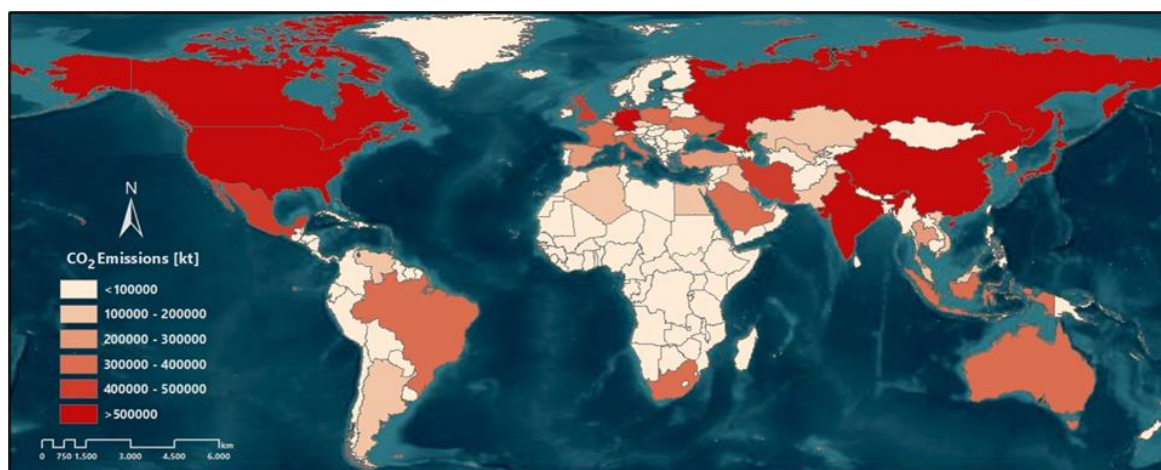


Figure 2. Average CO₂ emissions by country for the period 1990-2020.

A quantitative indicator is used to understand better the adverse effects of carbon emissions that affect the world and people and determine the environmental damage it causes. This indicator, called carbon footprint, is a guiding source for activities to prevent and reduce carbon emissions.

1.1. Carbon footprint

Carbon footprint is the measurement of greenhouse gases emitted into the atmosphere by a person, a specific activity or a country due to transportation, heating activities, energy consumption or every product and service purchased, in CO₂ equivalent [19]. With the concept of carbon footprint, the damage to the environment is defined. The carbon footprint, calculated in units of carbon dioxide, is generally used to measure the trace of the damage left by a person in nature and the environment (Figure 3).

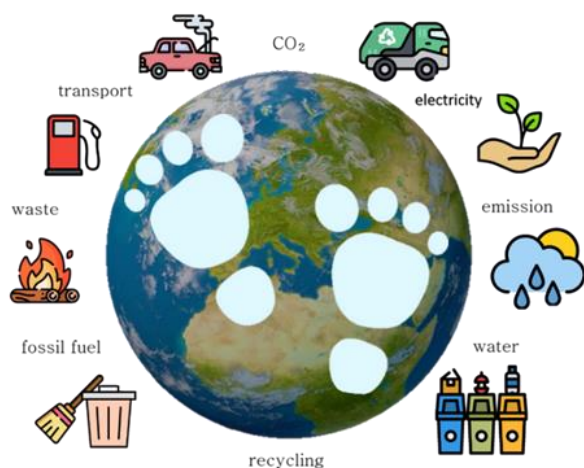


Figure 3. Activities representing carbon footprint.

The concept is generally analyzed under primary and secondary carbon footprint. Primary carbon footprint is the environmental damage directly caused by one's daily habits. It measures the amount of CO₂ generated by activities that use fossil fuels, such as energy consumption through household items and the use of vehicles. The secondary footprint is characterized as the measure of CO₂ emissions from the production phase of

all products used until they are destroyed [20]. For example, vehicles used daily or on vacation fall under the primary carbon footprint status. The damage caused to the atmosphere by the car or airplane is part of the person's carbon footprint [21]. The car used daily also appears as a secondary carbon footprint. All the resources spent for the production of that vehicle and all the resources that vehicle parts will spend until they disappear from the world constitute the person's secondary carbon footprint.

The amount of carbon emissions is obtained by determining the carbon footprint. Therefore, both concepts are interrelated. When we look at the literature, it is seen that there are many studies on carbon footprint from different disciplines. The studies aim to determine the carbon footprint of an individual, community, or organization worldwide, that is, to measure the amount of carbon emissions they emit to nature. Lee [22] aimed to measure carbon footprint left to nature based on direct and indirect consumption in Taiwan. Song et al. [23] investigated the amount of carbon emitted directly and indirectly by individuals in the process of scientific studies. In this context, they concluded that literature review and writing process have a high carbon footprint. Lombardi et al. [24] proposed the concept of urban carbon footprint and revealed its relationship with global climate change. Within the scope of the concept, he evaluated climate strategies and put forward suggestions for their development. Chen et al. [25] evaluated the reflections of the textile industry on climate change by performing carbon footprint and water footprint calculations to evaluate the environmental impacts of cashmere fabric. Huang and Tang [26] produced carbon capacity models by investigating the carbon footprint caused by tourism in the Heilongjiang region of China. As a result of the outputs obtained from the models, they revealed that the environmental impacts of tourism-related carbon footprint are small and acceptable. Uzunali and Yazıcı [27] conducted a comparative study to evaluate the effects of the COVID-19 pandemic on carbon emissions. In this context, the environmental impacts of Turkey's carbon footprint before and after COVID-19 were comprehensively analyzed and social and economic consumption habits were emphasized. Another study was conducted by Islam et al. [28] on the construction sector. The impact and importance of material selection

on the environment are emphasized by evaluating the carbon emissions of different building materials on nature. In addition to these studies, it is possible to come across many studies evaluating the amount and effects of different concepts, materials, and sectors on the carbon footprint in nature [29–37].

1.2. Policies for carbon footprint

Various protocols and standards have been developed internationally for carbon footprint calculation. The Kyoto Protocol, the Paris Agreement, the ISO 14064 standard established by the International Organization for Standardization (ISO) for limiting greenhouse gas emissions [38], The Greenhouse Gas Emission Protocol (GHG) put forward by the World Business Council for Sustainability and the World Resources Institute (WRI) [39, 40], and the assessment reports published by the Intergovernmental Panel on Climate Change (IPCC) guide carbon footprint calculations and mitigation strategies.

The Kyoto Protocol is a part of the United Nations Framework Convention on Climate Change (UNFCCC). This protocol, which serves the same purpose as the UNFCCC, includes obligations set forth depending on the level of development of the industrialized countries that are parties to it. The main purpose of the Kyoto Protocol is to prevent global warming and reduce its effectiveness and negative effects. Within the scope of the measures taken for this purpose, it aims to reduce the carbon footprint by limiting greenhouse gas emissions [41].

The Paris Agreement was also organized as a part of the UNFCCC. With this agreement, which was signed due to the Kyoto Protocol not progressing as expected, new targets were put forward in terms of global warming and climate change. The agreement, which aims to control greenhouse gas emissions and achieve zero emission levels by 2080, also aims to reduce the carbon footprint by providing financial support [42].

The International Organization for Standardization (ISO) is established to conduct studies to determine technical and non-technical standards. ISO gathers standards for environmental management under the umbrella of ISO 14000. The ISO 14064 standard published in this context describes the measurement, monitoring, reporting, and evaluation of greenhouse gas emissions. In line with these objectives, the standard aims to contribute to developing carbon footprint reduction strategies [43].

The Greenhouse Gas Emission Protocol (GHG) provides a framework for calculating, reporting, and managing greenhouse gas emissions resulting from electricity consumption and the activities of organizations. In this context, GHG provides an environment for reducing the carbon footprint [44].

The Intergovernmental Panel on Climate Change (IPCC) was established by the World Meteorological Organization (WMO) and the United Nations Environment Programme (UNEP). The IPCC, whose main purpose is to combat climate change, comprehensively evaluates the global climate change problem worldwide, and expresses the role of the carbon footprint resulting

from greenhouse gas emissions. The reports presented aim to reduce the carbon footprint with recommendations and strategies to reduce greenhouse gas emissions from different sectors such as energy, industry, agriculture, and transportation.

All these protocols and standards aim to make the future sustainable by effectively combating climate change. At the point where these objectives converge is the reduction of the carbon footprint based on carbon emissions.

1.3. Carbon footprint and GIS

Geographic Information System (GIS) is a technology and discipline used to store, manage, analyze and visualize spatial and non-spatial data [45]. The ability of GIS to organize data based on location helps to make more accurate decisions. For this reason, it can be integrated into the studies of many different disciplines. One of the areas where GIS can be used effectively is carbon footprint applications, which play an important role in climate change. Utilizing the effective storage feature of GIS in carbon footprint applications, which include a large number of data and different types of parameters, facilitates the management of complex data.

On the other hand, applying advanced methods based on location with its analysis capability provides a more comprehensive regional understanding of the effects of carbon emissions. In this context, GIS is an effective and powerful tool for monitoring the sources of carbon emissions, observing their distribution, analyzing and calculating carbon footprints, and presenting all of these all these location-based. Another advantage of GIS is its mapping capability. Thanks to its superior visualization power, it enables the production of maps from the outputs obtained from the analysis, helping to better understand and interpret the results. Thanks to the carbon footprint maps produced in the GIS environment after analyzing carbon emissions, the spatial distribution and potentials of emissions can be revealed. On the other hand, easy monitoring of the emission situation by utilizing maps guides decision-makers in implementing policies for reducing and preventing emissions. As a result, the use of GIS in carbon footprinting studies contributes to achieving sustainability goals by helping the implementation of emission reduction strategies.

2. Material and Method

2.1. Method

Analysis for the selected study region was carried out in the following steps (Figure 4):

- Determination of the study area
- Obtaining data from relevant institutions
- Organizing data and associating with the location
- Determination of the carbon footprint for each building in the selected pilot region
- Presentation of maps
- Producing the carbon footprint distribution map in ArcGIS 10.8 using spatial interpolation methods

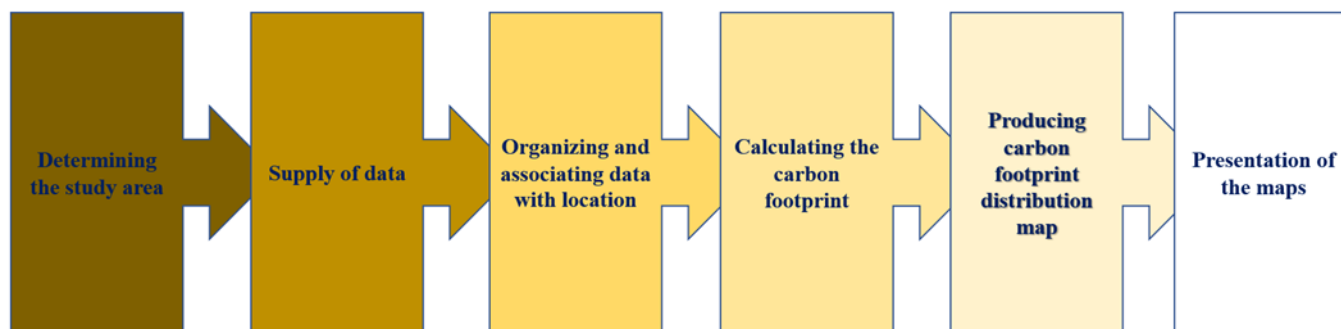


Figure 4. Methodology.

2.2. Study Area

This study was conducted in the Ortahisar district of Trabzon Province, located in the Black Sea Region. Besirli District No. 1, an urban and densely populated neighborhood, is considered the district's application area. 160 buildings were selected as a sample from the region, and data for 2019 on electricity and natural gas consumption were obtained from the relevant institutions. Figure 5 shows the study area.

2.3. Data supply and geographical database creation

In order to calculate the amount of carbon emissions, the data on the electricity consumption of 160 buildings in 2019 were obtained from Çoruh Electricity Distribution Joint Stock Company, and the data on natural gas consumption was obtained from Akşa Karadeniz Natural Gas Distribution Joint Stock Company in Microsoft Excel format. The data were transferred to the GIS environment and matched with the buildings they were related. At this stage, ArcGIS 10.8 software was

used. The matched data were transferred to the geographic database and made ready for application. The edited data is shown in Figure 6.

2.4. Carbon footprint calculation methods

Intergovernmental Panel on climate change (IPCC) shared methodologies that calculate greenhouse gas emissions in 3 different tiers [46]. The stages indicate the complexity of the methodology. The carbon footprint is calculated using Tier 1, Tier 2, or Tier 3 methods, depending on the complexity of the data and methodology required [46]. Tier 2 and Tier 3 are often referred to as higher-tier methods and are considered more accurate than Tier 1 because they value more information and yield more data [46, 47]. The method to calculate the carbon footprint may vary in general. For example, when calculating carbon emissions, the Tier 2 method can be used when electricity consumption is considered, and the Tier 1 method can be used for emissions caused by natural gas consumption [48, 49]. To briefly explain the methods;



Figure 5. Study area.

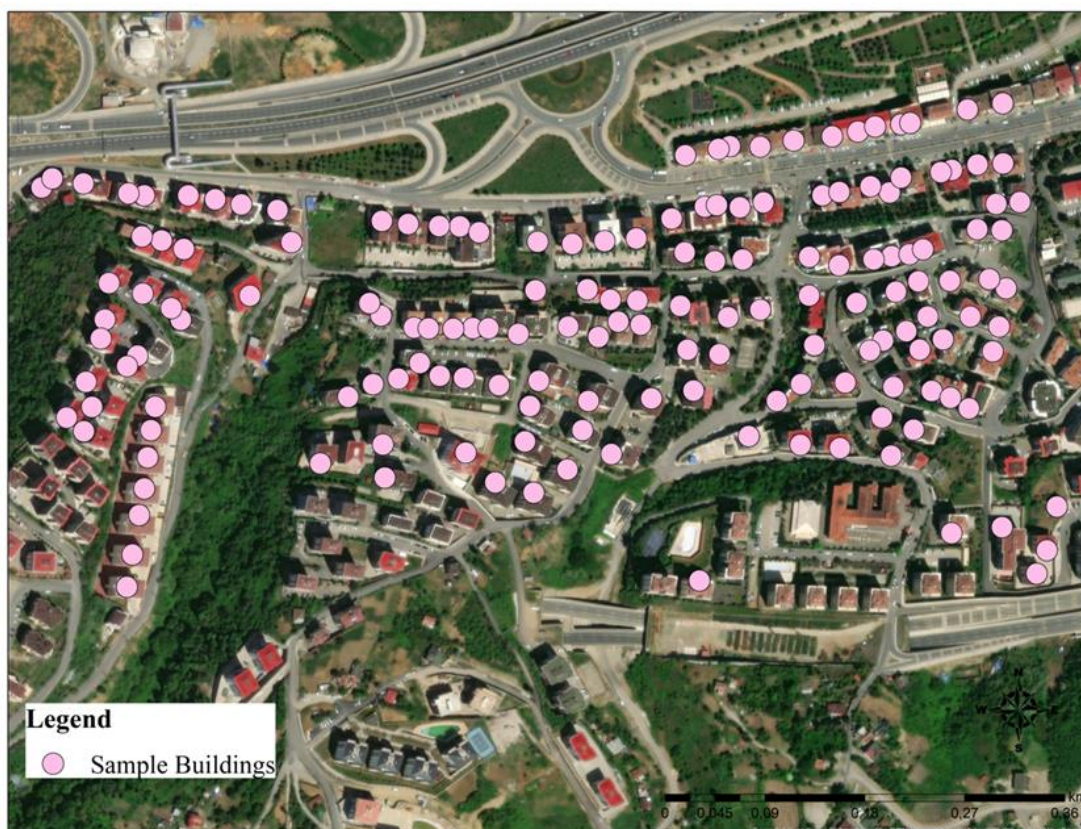


Figure 6. Data that contains electricity and natural gas information associated with location.

Tier 1: Calculations made using the standard emission factor determined according to the amount of fuel consumed and fuel type [46]. It uses emission factors and other parameters described in the IPCC manual. This method has some simplifying assumptions and may

combine some external data with its findings. This method requires two data pieces: the fuel consumed and the standard emission factor. The calculation for Tier 1 is as shown in Equation 1 [46]:

$$\text{Emission GHG, FUEL (kg GHG)} = \text{Fuel Consumption (TJ)} \times \text{Emission Factor (Kg GHG/TJ)} \quad (1)$$

Tier 2: Calculations made using country-specific emission factors determined according to the amount of fuel consumed and combustion technology that varies from country to country, operating conditions, control technology, maintenance quality, and the age of the equipment used while burning fuel [46, 48]. It has the same approach as Tier 1 but uses country-specific emission factors and other parameters. Country-specific

emission factors and parameters are better suited to that country's forests, climate zones, and land use systems. Some of these parameters are the quality of the fuel, its carbon content, and the combustion technology used [47]. This method requires two data. These; the amount of fuel consumed and the country-specific emission factor for each fuel. The calculation for Tier 2 is as shown in Equation 2 [46]:

$$\text{Emission GHG, FUEL (kg GHG)} = \text{Fuel consumption (TJ)} \times \text{Emission Factor (Kg GHG/TJ)} \quad (2)$$

Tier 3: These are calculations that require more detailed data and expertise, such as the thermal power of combustion plants and feeding type. It contains more complex models and requires more data. It was developed to increase the results' transparency and the data's integration with the model. It is generally accepted that it calculates more accurately than the lower stages. The Tier 3 method calculates the fuel consumption and emission factor specific to the facility. For this reason, it is considered that the calculation is close to the truth. The method considers the fuel consumption values and the distance traveled by vehicles or the load carried in ton-km units and calculates with appropriate emission factors [46, 50].

2.5. Calculating carbon footprint

The carbon footprint is revealed by the calculated amounts of greenhouse gas emissions CO₂, N₂O, HFCs, PFCs, and SF₆ based on the CO₂ type. Since carbon dioxide has a 76% share in greenhouse gas emissions and is directly related to fuel combustion, a carbon footprint calculation based on carbon dioxide emissions has been made in this study to make a more precise calculation [33]. When the literature is examined, it is seen that carbon footprint calculations are made based on electricity, natural gas, solid fuel, gasoline, diesel, fuel oil, and LPG data [51, 52]. This study calculated carbon footprint with the Tier 2 method based on natural gas

and electricity consumption data. Table 1 shows the emission factors and net calorific values used in applying the method.

The Equation 3 is used when calculating the carbon footprint based on electricity consumption

Table 1. Emission factors and net calorific values used in carbon footprint calculation.

	Data	Unit	Emission Factor	Net Calorific Value
Tier-2	Electricity	MWh	0,6993 ton CO2e/MWh	-
	Natural Gas	Sm3	0,202 kg CO2e/kWh	9,59 kWh/m ³

$$CO_2 \text{ Emission (t CO}_2\text{e/Year)} = \text{Energy consumption (MWh)} \times \text{Emission factor (tCO}_2\text{e/MWh)} \quad (3)$$

The application used the electricity consumption values obtained from the relevant institution for the energy consumption data contained herein. The value in the Turkish National Electricity Grid Emission Factor report prepared by the Ministry of Energy and Natural

Resources has been taken as the basis for the emission factor that changes specific to countries [52].

The Equation 4 is used when calculating the carbon footprint based on natural gas consumption [46]:

$$\text{Energy Consumption (kWh)} = \text{Fuel consumption (m}^3\text{)} \times \text{Net Calorific Value (kWh/m}^3\text{)} \quad (4)$$

The natural gas consumption data obtained from the relevant institution was used for the fuel consumption data in the formula. In contrast, the value determined by the Ministry of Energy and Natural Resources was used

for the net calorific value. Net calorific value is the unit of heat energy produced by burning fuel. Using the energy consumption data revealed, carbon emissions were calculated with the help of the Equation 5 [46];

$$CO_2 \text{ Emission (kg CO}_2\text{/Yıl)} = \text{Energy consumption (kWh)} \times \text{Emission factor (kgCO}_2\text{e/kWh)} \quad (5)$$

Here, the value in the United Nations Framework Convention on Climate Change (UNFCCC) is used for the emission factor.

Considering the formula; n represents the number of points, the geoid corrugation used to calculate the Ni value Np, the Np the sought corrugation value, and the weight value corresponding to each Ni value used in the calculation of Pi N [54].

2.6. Spatial interpolation methods

2.6.1. Kriging interpolation method

The Kriging interpolation method is a method that allows the values of new points to be estimated by taking the weighted average of the values of known close points. The Kriging interpolation method determines the value of unknown points by calculating a variance value for each point to be estimated. It differs from other interpolation methods because it measures the confidence level of the estimated value with variance. This method achieves more unbiased results than other interpolation techniques; investigates the accuracy of the estimation in terms of the minimum variance and the calculation of the standard deviation of the realized estimation [53–55].

Kriging interpolation calculates the properties of unobserved points by reference to the properties of observed points. The main problem in this method is to determine the weights. The most important feature of the Kriging method that distinguishes it from other methods is that instead of using a standard weight, it performs the estimation by determining a weight, and the estimation made and the error resulting from this estimation can be easily detected. The Equation 6 is used in the application of the Kriging method [54];

$$N_p = \sum_{i=1}^n P_i * N_i \quad (6)$$

2.6.2. Inverse distance weighted interpolation method (IDW)

Inverse Distance Weighted interpolation is a type of deterministic method used for multivariate interpolation with scattered points known as Inverse Distance Weighted (IDW). In this method, the values assigned to the unknown points are calculated by a weighted average of the values available at the known points with a simple algorithm [56]. While calculating, the anchor points close to the cut-off points have a more significant effect on the calculation, while those of the far points are less [53]. In short, the IDW interpolation technique is based on the fact that on the surface to be interpolated, nearby points have more weight than distant points [57]. In addition, this method is used to define constantly changing data belonging to the same field. Shaperd's is the most widely used and well-known IDW method [57, 58]. Shaperd's Equation 7 is as follows:

$$f(x, y) = \sum_i^n w_i f_i \quad (7)$$

In this formula, n is the number of scattered points on the surface, fi is the function that defines the sampling points, and wi is the weights.

3. Results

3.1. Calculating the carbon footprint in the selected pilot region

For the selected pilot region, Beşirli District No. 1, the carbon footprint was calculated using the electricity consumption data as a reference. Since the data obtained belongs to 2019, 0,6993 was taken as the emission factor in the calculations. The energy consumption data for each building is multiplied by this emission factor to obtain the carbon emissions of the buildings and added to the database. An example of the values obtained is shown in Figure 7, and the carbon emission amount map obtained from electricity consumption data is shown in Figure 8. When Figure 8 is examined, the amount of carbon emissions in the study area varies between 565,200 and 235492,82 tons; it is seen that carbon emission is relatively high in some buildings and less than in others some buildings.

Looking at this map, it can be concluded that carbon emissions are high-medium level in this selected region; some buildings emit very high carbon emissions and have a large carbon footprint, as well as buildings that emit less.

For the selected pilot region, Beşirli District No1, the carbon footprint was calculated using the natural gas consumption data as a reference. Since the data obtained belongs to 2019, 0.202 was taken as the emission factor and 9.59 as the net calorific value in the calculations. For each building, natural gas energy consumption was first calculated by multiplying the natural gas fuel consumption with the net calorific values. Then, the carbon emission of the buildings was obtained by multiplying the emission factor with the obtained value and added to the database. An example of the values obtained is shown in Figure 9, and the carbon emission amount map obtained from natural gas consumption data is shown in Figure 10. When Figure 10 is examined, it is seen that the amount of carbon emission in the study area varies between 469,177 and 146208,914 kg; it is seen that carbon emission is relatively high in some buildings and less than others in some buildings. Looking at the map, it can be concluded that carbon emissions in this selected region are at high-medium levels, as in electricity, but are at higher levels than electricity-induced carbon emissions; there are buildings with very high carbon emissions and high carbon footprints, as well as buildings with low emissions.

FID	Shape	OBJECTID	BINA ID	Enerji Tüketim Değerleri	Emisyon Fa	CO2 Salınım Miktarı
0	Point	8	10000020901900	13753,74	0,6993	9617,990382
1	Point	9	10000020924800	29785,99	0,6993	20829,342807
2	Point	10	10000020920100	33968,37	0,6993	23754,081141
3	Point	12	10000020931900	20204,61	0,6993	14129,083773
4	Point	15	10000020943200	48001,31	0,6993	33567,316083
5	Point	21	10000020968800	13689,07	0,6993	9572,766651
6	Point	23	10000020966100	30075,03	0,6993	21031,468479
7	Point	26	10000020984000	26317,06	0,6993	18403,520058
8	Point	27	10000020989200	39348,74	0,6993	27516,573882
9	Point	33	10000021017400	808,25	0,6993	565,209225
10	Point	38	10000021020700	12949	0,6993	9055,2357
11	Point	41	10000021043500	35936,34	0,6993	25130,282562
12	Point	42	10000021046500	266585,86	0,6993	186423,491898
13	Point	45	10000021062500	34608,89	0,6993	24201,996777
14	Point	49	10000021071900	42889,42	0,6993	29992,571406
15	Point	51	10000021084800	24700,42	0,6993	17273,003706
16	Point	54	10000021100900	36912,47	0,6993	25812,890271
17	Point	63	10000021113800	33944,9	0,6993	23737,66857
18	Point	69	10000051938800	24729,42	0,6993	17293,283406
19	Point	70	10000051938800	121572,79	0,6993	85015,852047
20	Point	74	10000053226700	40759,86	0,6993	28503,370098

Figure 7. Example result display of carbon emission amount according to electricity consumption data.

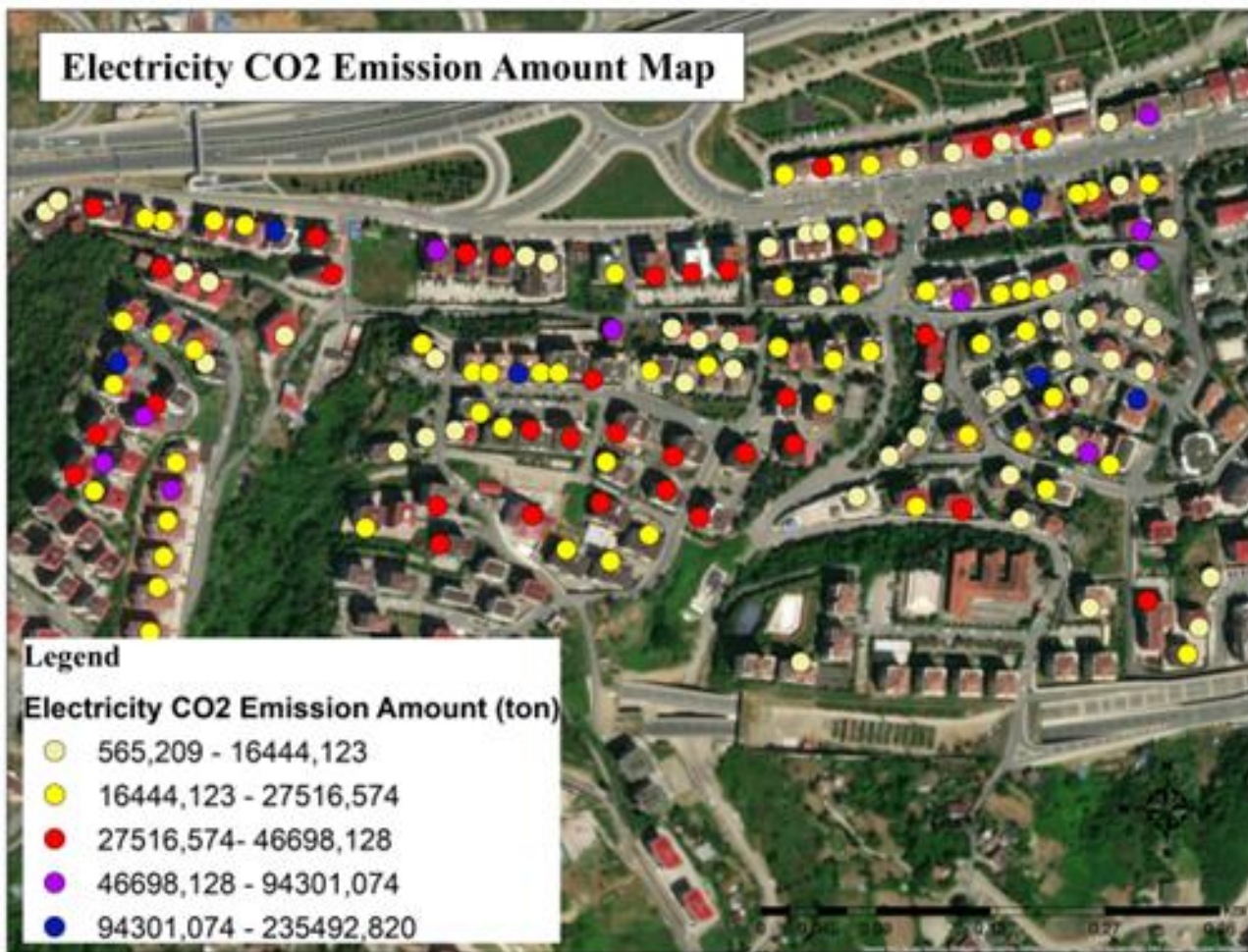


Figure 8. Distribution map of carbon emission amount according to electricity consumption data.

Table

dogalgaz

	KASIM	ARALIK	Y Yakıt T	Net Kal De	Enerji Tü	Emisyon fa	CO2
	1883,619	2551,357	20766,943	9,59	199154,98337	0,202	40229,306641
	1525,827	2383,551	19637,204	9,59	188320,78636	0,202	38040,796845
	1005,31	1713,689	16538,773	9,59	158606,83307	0,202	32038,58028
	606,502	1010,053	8517,735	9,59	81685,07865	0,202	16500,385867
	1396,179	2095,997	16184,618	9,59	155210,48862	0,202	31352,518297
	379,574	821,249	6341,434	9,59	60814,35206	0,202	12284,499116
	694,02	1282,949	8933,368	9,59	85670,99912	0,202	17305,541822
	910,419	1539,539	11979,447	9,59	114882,89673	0,202	23206,34514
	1056,428	1609,291	13054,898	9,59	125196,47182	0,202	25289,687308
	597,345	1007,879	8306,498	9,59	79659,31582	0,202	16091,181796
	634,996	1277,721	7142,057	9,59	68492,32663	0,202	13835,449979
	1030,719	1733,269	13551,217	9,59	129956,17103	0,202	26251,146548
	902,444	1674,153	14982,83	9,59	143685,3397	0,202	29024,438619
	1656,69	2617,284	20726,897	9,59	198769,02423	0,202	40151,342894
	1504,523	2232,205	18044,504	9,59	173046,79336	0,202	34955,452259
	1211,55	1718,429	15243,731	9,59	146187,38029	0,202	29529,850819
	1630,214	2659,671	19898,784	9,59	190829,33856	0,202	38547,526389
	1032,477	1617,524	12723,532	9,59	122018,67188	0,202	24647,77172
	1548,821	2196,266	18368,47	9,59	176153,6273	0,202	35583,032715
	934,178	1338,596	10051,553	9,59	96394,39327	0,202	19471,667441
	690,965	1151,047	8924,96	9,59	85590,3684	0,202	17289,254013
	928,072	1295,314	10819,089	9,59	103755,06351	0,202	20958,522829

Figure 9. Example result display of carbon emission amount according to natural gas consumption data.

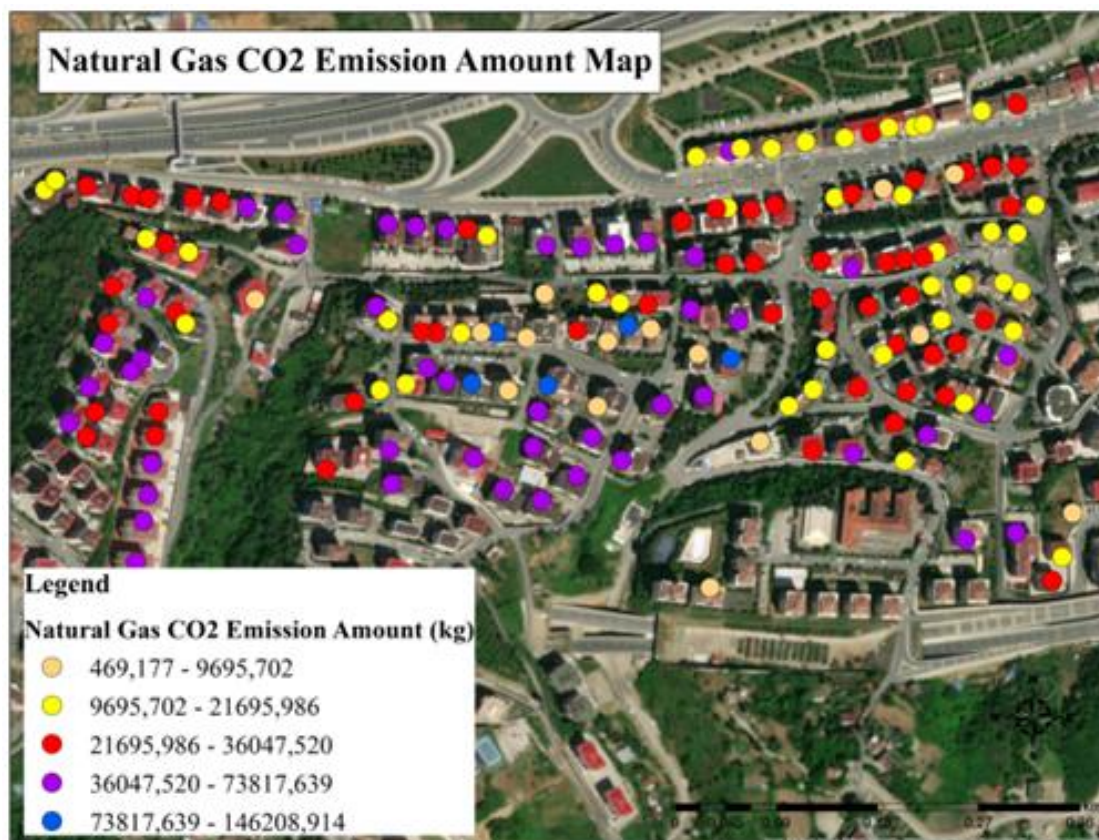


Figure 10. Distribution map of carbon emission amount according to natural gas consumption data.

3.2. Mapping the carbon footprint with spatial interpolation methods

In this study, which was carried out to determine the carbon footprint, set up scenarios accordingly, and increase awareness, the resulting product is maps produced with spatial interpolation analyses based on GIS. At this stage of the study, using the carbon footprint

calculation results, carbon emission distribution maps of the selected region were produced using spatial interpolation analysis.

In the study, first of all, a natural gas carbon footprint distribution map was produced. Kriging (Figure 11) and IDW (Figure 12) analyses were performed separately, and the results were mapped.

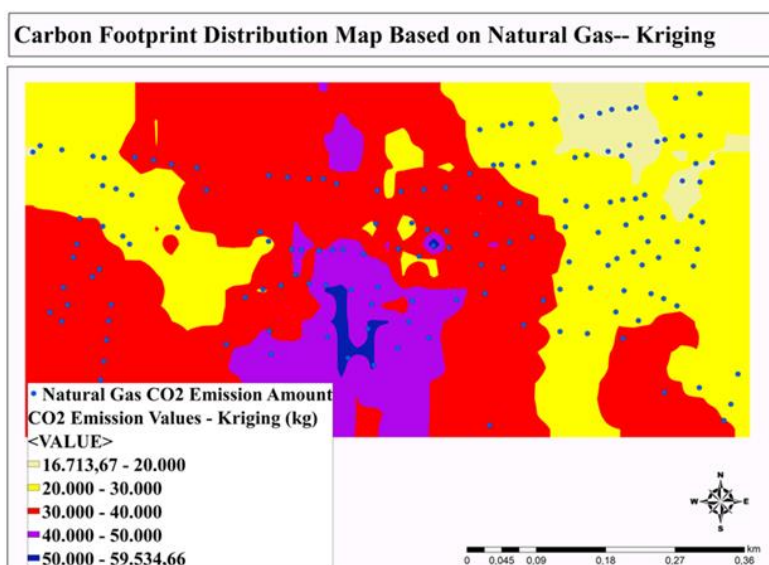


Figure 11. Carbon footprint distribution map based on natural gas according to Kriging analysis.

Looking at Figure 11, it is seen that the carbon emission based on natural gas, according to the Kriging analysis, has increased gradually in the parts corresponding to the south-central part of the selected

pilot region. Especially in the eastern part of the region, there is a lower carbon emission compared to other places; Similarly, in some areas corresponding to the western parts of the region, it can be said that the carbon

footprint is at a better level than in other areas. Generally, there is moderate carbon emission in the middle part of the region. As a result, when an evaluation is carried out in general, it can be concluded that the selected region is in a medium-high risk position regarding carbon footprint.

Figure 12 shows that carbon emission based on natural gas is more intense in the parts corresponding to the south-central part of the selected pilot region, according to the IDW analysis. Especially in the eastern part of the region, there is a lower carbon emission compared to other places; In addition, it is observed that carbon emissions are still at better levels in some parts of the western parts. Generally, there is moderate carbon

emission in the middle part of the region. As a result, when an assessment is carried out in general, it can be concluded that the selected region is in a medium-high risk position regarding carbon footprint, as in the other analysis.

When the analysis results of both methods are compared, it is concluded that the IDW analysis outputs reveal the carbon footprint results more clearly than the kriging analysis outputs. It is more appropriate to consider the IDW method in determining the carbon footprint distribution based on natural gas. This situation is because it gives more precise results in the region, and the mathematical model gives better results in determining the distribution of carbon emissions.

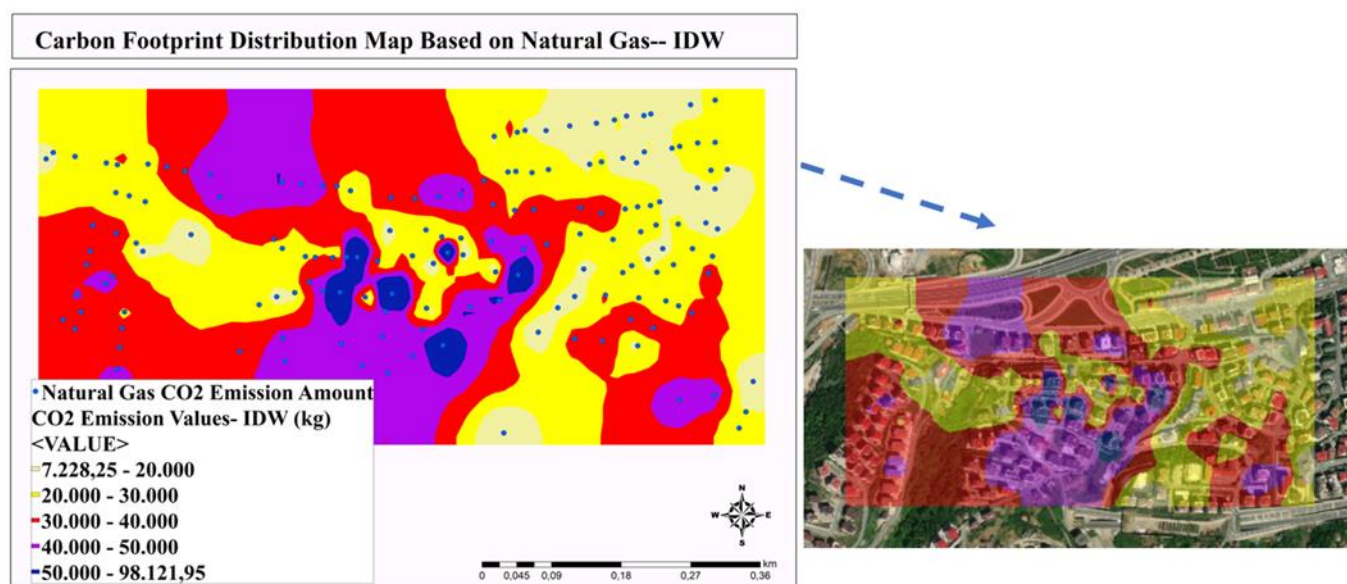


Figure 12. Carbon footprint distribution map based on natural gas according to IDW analysis.

In the study, an electrical carbon footprint distribution map was produced. Kriging (Figure 13) and IDW (Figure 14) analyses were performed separately, and the results were mapped.

Figure 13 shows that carbon emission based on electricity is seen more intensely in the western parts of the selected pilot region, according to the kriging analysis. It is observed that carbon emissions are close to high levels in some parts of the northern, central, and eastern parts of the region.

Especially in the southern parts of the region, in some parts of the central and northern parts, generally much less or moderate carbon emissions were encountered. Therefore, the carbon footprint is at better levels. When an assessment is carried out in general, it can be concluded with this analysis that the selected region is in a medium-high risk position regarding carbon footprint.

Figure 14 shows that electricity-based carbon emissions are at very high levels in small areas in the eastern, western, southern, and central parts of the selected pilot region, according to the IDW analysis. Especially in the southern part of the region, there is a lower carbon emission compared to other places; Similarly, in some parts of the northern parts of the region and the areas corresponding to the middle parts, it can be said that the carbon footprint is at a better level than other areas. As a result, when an evaluation is

carried out in general, it can be concluded that the selected region is in a medium-high risk position regarding carbon footprint.

When the results of both analysis methods are compared, it is concluded that the IDW analysis outputs also reveal the electricity-based carbon footprint results more clearly than the kriging analysis outputs. The result shows that the carbon footprint distribution based on electricity applied, especially in this region, is more prominent. In addition, it has been determined that the mathematical model gives better results in determining the region's carbon emissions distribution. Therefore, preferring the IDW method in the evaluation seems more appropriate.

In the Kriging and IDW analysis results carried out for both factors, it was concluded that both methods produced meaningful results and could be used, but when a comparison is made between each other, IDW analysis results would be better to choose because they gave much better results in distinguishing the outputs. By combining the analysis carried out for both factors in Figure 15 and Figure 16, the areas where the selected region is at risk in terms of both natural gas and electricity have been tried to be shown on a single map. Obtained maps reveal the necessity of taking measures for carbon emissions in this region.

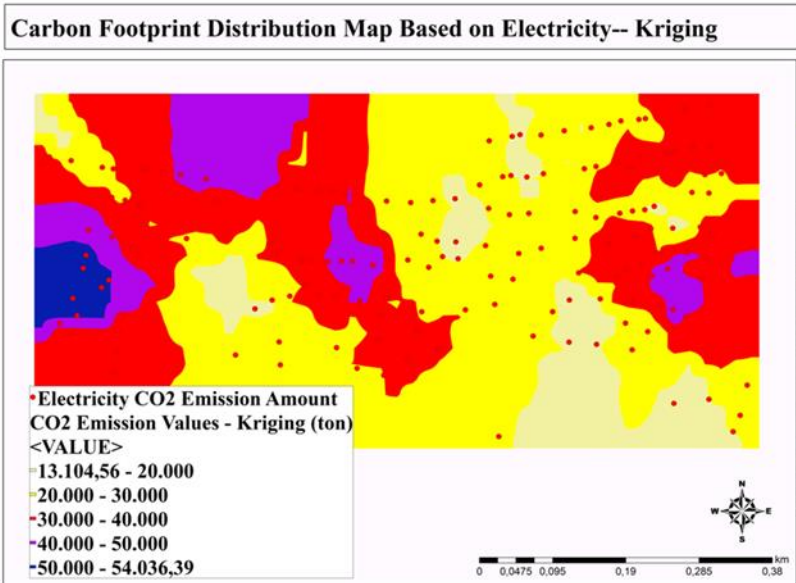


Figure 13. Electricity based carbon footprint distribution map according to Kriging analysis.

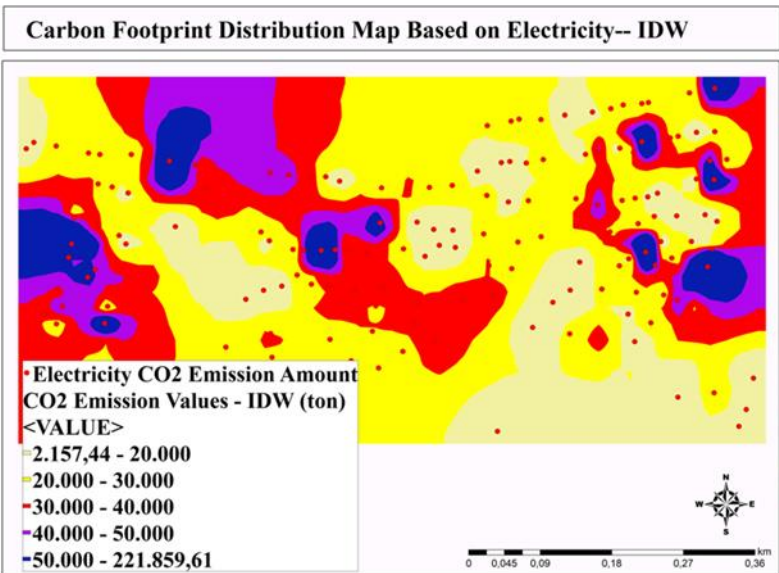
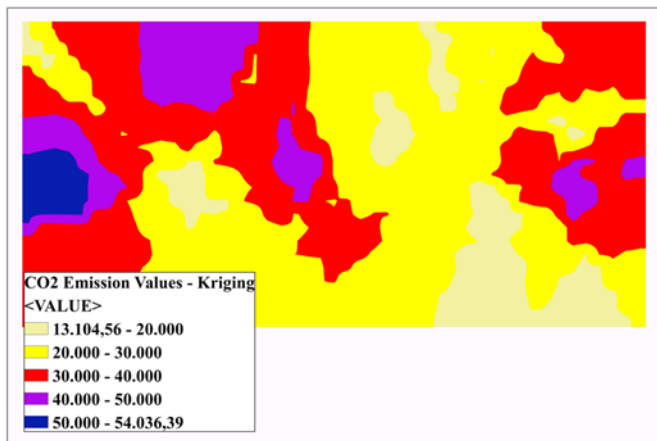
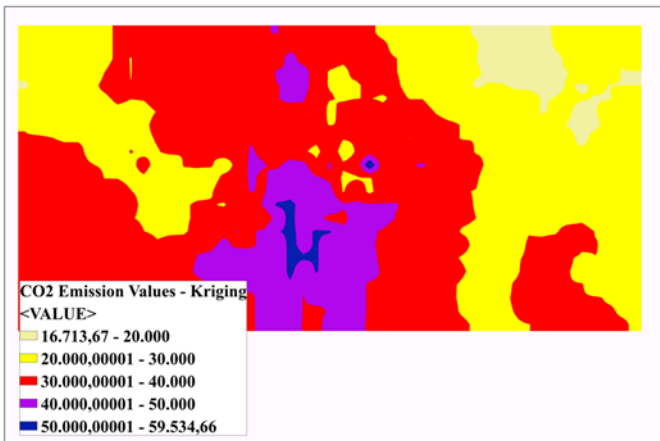
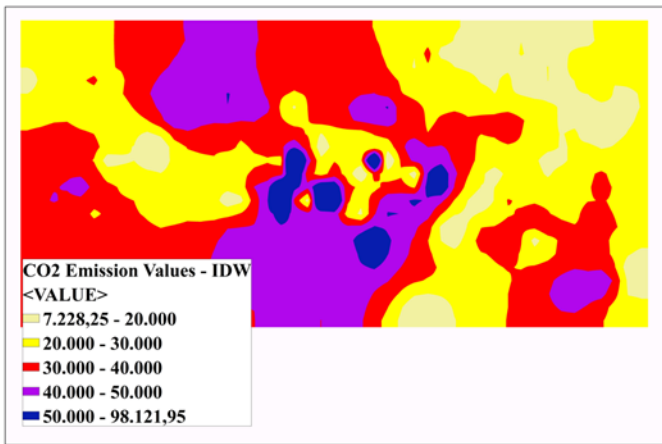


Figure 14. Electricity based carbon footprint distribution map according to IDW analysis.

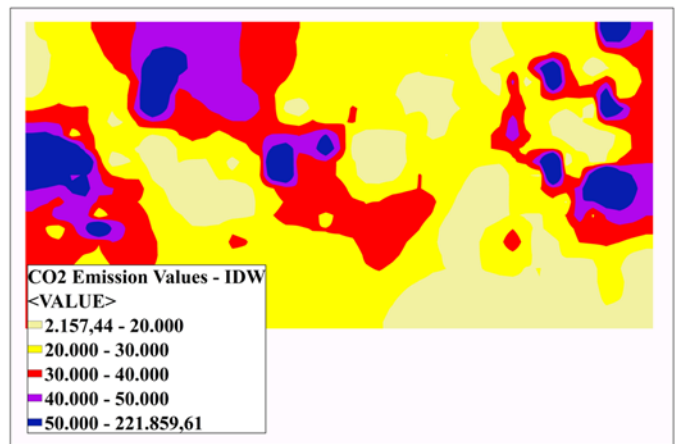


Carbon Footprint Distribution Map Based on Natural Gas-- Kriging Carbon Footprint Distribution Map Based on Electricity-- Kriging

Figure 15. Display of carbon footprint distribution map based on natural gas and electricity according to Kriging analysis.



Carbon Footprint Distribution Map Based on Natural Gas-- IDW



Carbon Footprint Distribution Map Based on Electricity-- IDW

Figure 16. Display of carbon footprint distribution map based on natural gas and electricity according to IDW analysis.

4. Discussion

The world, our living space, is a complex ecosystem with many physical, chemical, and biological features. The atmosphere surrounding the Earth plays a fundamental role in sustaining life. Atmosphere contains various gasses such as nitrogen, oxygen, carbon dioxide, and water vapor. Thanks to these gases, they absorb the rays from the sun and warm the world. The temperature of the Earth is associated with climate and weather events. Therefore, temperature changes cause climate change. One of the primary reasons for these changes is greenhouse gas emissions. The amount of greenhouse gasses released into the atmosphere by the effects of various activities carried out by people and areas, such as industrialization, transportation, and agriculture, has increased and is increasing over time. The fact that this situation disrupts the natural order of the atmosphere negatively affects global warming and prepares the environment for climate change.

The prominent greenhouse gas in climate change is CO₂. In particular, using fossil fuels caused by land changes, deforestation resulting from fires, and the energy demand brought by industrialization has increased carbon emissions. Awareness of carbon emissions will reduce the adverse effects of climate change and ensure that nature is sustainably transferred to the future. In this context, the concept of carbon footprint is used to evaluate the impact of carbon emissions on the environment. A carbon footprint is an indicator that measures the impact of an individual, product, activity, or industry on carbon emissions. Carbon footprint measurement contributes to evaluating the environmental effects of carbon emissions, determining the triggering factors, taking measures against climate change, developing constructive strategies and policies by relevant institutions and organizations, and ensuring sustainability. Therefore, carbon footprint is an important tool for combating climate change.

This study aims to determine the carbon footprint in the selected region by measuring the amount of carbon emissions based on electricity and natural gas. 160 buildings were determined in Beşirli District, No. 1 in Ortahisar district of Trabzon province, and data on

electricity and natural gas consumption were obtained from relevant institutions. In order to determine the carbon footprint in the region, carbon emission amounts based on electricity and natural gas were calculated based on the Tier-2 method. Spatial interpolation analysis was performed to see the region's carbon emissions distribution. Using the ArcGIS program, a GIS software, the distribution of carbon emissions based on the region's electricity and natural gas consumption was analyzed with Kriging and IDW methods, and the outputs were mapped. The results show that the carbon footprint due to natural gas consumption increases in the middle and southern parts of the study area according to both Kriging and IDW analysis. While the carbon footprint due to electricity consumption is on the increase in the western part of the study area in Kriging analysis, it is at high levels in certain areas in IDW analysis, being widespread throughout the study area. When these maps showing the spatial distribution of carbon footprint in the study area are evaluated in general, it is concluded that the region is in a medium-high risk position due to both electricity and natural gas consumption. This situation is likely due to the high population and settlement in the region, the intense use of the transportation network, and the presence of many workplaces. The main action that should be taken to reduce the carbon emissions in the region is to raise people's awareness. For this purpose, encouraging people to use public transportation, promoting recycling and ensuring that renewable energy sources are preferred will be effective in reducing the carbon footprint. On the other hand, as a result of the analyzes based on both consumptions, it was understood that the IDW method produced more precise results than the kriging method. It is thought that this situation arises from the mathematical models of the methods.

Carbon emissions are one of the main drivers of climate change, which is one of the most important problems of the world today. In this study, an application has been realized on such an important issue. With this study, the negative impact of natural gas and electricity consumption on carbon footprint has been proved with the application. In this context, it is thought that the study will contribute to the studies on climate change and emphasize the importance of carbon emissions.

Acknowledgement

Authors would like to thank Çoruh Electricity Distribution Co. and Aksa Karadeniz Natural Gas Distribution Co. for their assistance in the data collection process.

Author contributions

Ebru Colak: Conceptualization, Data Collection, Reviewing and Editing **Tugba Memişoğlu Baykal:** Conceptualization, Data Collection, Methodology, Software, Visualization, Investigation, Writing-Reviewing and Editing **Nihal Genç:** Conceptualization, Data Collection, Methodology, Software, Visualization, Investigation, Writing-Reviewing and Editing

Conflicts of interest

The authors declare no conflicts of interest.

References

- Fang, J., Zhu, J., Wang, S., Yue, C., & Shen, H. (2011). Global warming, human-induced carbon emissions, and their uncertainties. *Science China Earth Sciences*, 54, 1458-1468. <https://doi.org/10.1007/s11430-011-4292-0>
- Nordhaus, W. D. (1993). Rolling the 'DICE': an optimal transition path for controlling greenhouse gases. *Resource and Energy Economics*, 15(1), 27-50. [https://doi.org/10.1016/0928-7655\(93\)90017-0](https://doi.org/10.1016/0928-7655(93)90017-0)
- United Nations (UN). (1992). United Nations Framework Convention on Climate Change.
- NASA. (2023). What is the greenhouse effect? – Climate Change: Vital Signs of the Planet. <https://climate.nasa.gov/faq/19/what-is-the-greenhouse-effect>.
- Tol, R. S. (2021). Europe's climate target for 2050: an assessment. *Intereconomics*, 56(6), 330-335. <https://doi.org/10.1007/s10272-021-1012-7>
- Rörsch, A., Courtney, R. S., & Thoenes, D. (2005). Global warming and the accumulation of carbon dioxide in the atmosphere: A critical consideration of the evidence. *Energy & Environment*, 16(1), 101-125. <https://doi.org/10.1260/0958305053516190>
- Lee, H., Calvin, K., Dasgupta, D., Krinmer, G., Mukherji, A., Thorne, P., ... & Zommers, Z. (2023). Synthesis report of the IPCC Sixth Assessment Report (AR6), Longer report. IPCC.
- Clarke, B., Otto, F., Stuart-Smith, R., & Harrington, L. (2022). Extreme weather impacts of climate change: an attribution perspective. *Environmental Research: Climate*, 1(1), 012001. <https://doi.org/10.1088/2752-5295/ac6e7d>
- Mkorombindo, T., & Balkissoon, R. (2021). Journal Club: Respiratory Impact of Wildfire Smoke. *Chronic Obstructive Pulmonary Diseases: Journal of the COPD Foundation*, 8(3), 408. <https://doi.org/10.15326/jcopdf.2021.0244>
- Maslin, M. (2014). *Climate change: a very short introduction*. OUP Oxford.
- Ripple, W. J., Wolf, C., Newsome, T. M., Galetti, M., Alamgir, M., Crist, E., ... & 15,364 Scientist Signatories from 184 Countries. (2017). World scientists' warning to humanity: a second notice. *BioScience*, 67(12), 1026-1028. <https://doi.org/10.1093/biosci/bix125>
- Pecl, G. T., Araújo, M. B., Bell, J. D., Blanchard, J., Bonebrake, T. C., Chen, I. C., ... & Williams, S. E. (2017). Biodiversity redistribution under climate change: Impacts on ecosystems and human well-being. *Science*, 355(6332), eaai9214. <https://doi.org/10.1126/science.aai9214>
- IPBES. (2019). The global assessment report of the intergovernmental science-policy platform on biodiversity and ecosystem services.
- Aksoy, F. (2023). A framework to improve the modeling of the socioeconomic impacts of climate change [Doctoral dissertation, Bursa Uludağ University].
- World Bank. (2023). CO₂ Emissions (kt), https://data.worldbank.org/indicator/EN.ATM.CO2.E.KT?most_recent_year_desc=true&type=shaded&view=map&year=2020
- Lopes de Sousa Jabbour, A. B., Vazquez-Brust, D., Chiappetta Jabbour, C. J., & Andriani Ribeiro, D. (2020). The interplay between stakeholders, resources and capabilities in climate change strategy: converting barriers into cooperation. *Business Strategy and the Environment*, 29(3), 1362-1386. <https://doi.org/10.1002/bse.2438>
- Akpan, U. F., & Akpan, G. E. (2012). The contribution of energy consumption to climate change: a feasible policy direction. *International Journal of Energy Economics and Policy*, 2(1), 21-33.
- IEA. (2022). World Energy Outlook 2022. www.iea.org/t&c/.
- Plassmann, K., & Edwards-Jones, G. (2010). Carbon foot printing and carbon labelling of food products. *Environmental Assessment and Management in the Food Industry*, 272-296. <https://doi.org/10.1533/9780857090225.3.272>
- Mattila, T., Kujanpää, M., Dahlbo, H., Soukka, R., & Myllymaa, T. (2011). Uncertainty and sensitivity in the carbon footprint of shopping bags. *Journal of Industrial Ecology*, 15(2), 217-227. <https://doi.org/10.1111/j.1530-9290.2010.00326.x>
- Güller, S. (2018). Carbon footprint assesment of Municipal Wastewater Treatment Plant in Muğla [Master's thesis, Muğla Sıtkı Koçman University].
- Lee, Y. J. (2015). Land, carbon and water footprints in Taiwan. *Environmental Impact Assessment Review*, 54, 1-8. <https://doi.org/10.1016/j.eiar.2015.04.004>
- Song, G., Che, L., & Zhang, S. (2016). Carbon footprint of a scientific publication: A case study at Dalian University of Technology, China. *Ecological Indicators*, 60, 275-282. <https://doi.org/10.1016/j.ecolind.2015.06.044>
- Lombardi, M., Laiola, E., Tricase, C., & Rana, R. (2017). Assessing the urban carbon footprint: An overview. *Environmental Impact Assessment Review*, 66, 43-52.

- <https://doi.org/10.1016/j.eiar.2017.06.005>
25. Chen, B., Qian, W., Yang, Y., Liu, H., & Wang, L. (2021). Carbon footprint and water footprint of cashmere fabrics. *Fibres & Textiles in Eastern Europe*, 29, 4(148), 94-99. <https://doi.org/10.5604/01.3001.0014.8235>
 26. Huang, T., & Tang, Z. (2021). Estimation of tourism carbon footprint and carbon capacity. *International Journal of Low-Carbon Technologies*, 16(3), 1040-1046. <https://doi.org/10.1093/ijlct/ctab026>
 27. Uzunali, A., & Yazıcı, T. (2023). Carbon footprint changing with Covid-19 in Turkey. *Environment, Development and Sustainability*, 25(10), 10685-10707. <https://doi.org/10.1007/s10668-022-02500-6>
 28. Islam, R., Chowdhury, S., Jannat, N., & Paul, P. (2022). Carbon footprint evaluation of local dwellings in Bangladesh towards low carbon society. *Built Environment Project and Asset Management*, 12(3), 433-446. <https://doi.org/10.1108/BEPAM-01-2021-0018>
 29. Johnson, E. P. (2012). Carbon footprints of heating oil and LPG heating systems. *Environmental Impact Assessment Review*, 35, 11-22. <https://doi.org/10.1016/j.eiar.2012.01.004>
 30. Melendez, K. (2013). Carbon footprint calculations for Oregon State University and Guadalupe, Cerro Punta, Panama [Master's thesis, Oregon State University].
 31. Chung, C. Y., Miaw, C. L., Huang, Y. C., Chung, C. C., & Lo, T. J. (2014). Investigation of carbon footprint on campus-A case study of Tajen University. *Advanced Materials Research*, 962, 1495-1499. <https://doi.org/10.4028/www.scientific.net/AMR.962-965.1495>
 32. Fitzpatrick, J. J., McCarthy, S., & Byrne, E. P. (2015). Sustainability insights and reflections from a personal carbon footprint study: The need for quantitative and qualitative change. *Sustainable Production and Consumption*, 1, 34-46. <https://doi.org/10.1016/j.spc.2015.05.004>
 33. Binboga, G., & Unal, A. (2018). A research on the calculation of carbon footprint of Manisa Celal Bayar University at sustainability axis. *International Journal of Economic and Administrative Studies*, 21, 187-202.
 34. Okan, B. (2019). Comparison of energy consumption and carbon foot print of wastewater treatment systems through modeling [Master's thesis, Middle East Technical University].
 35. Filimonau, V., Archer, D., Bellamy, L., Smith, N., & Wintrip, R. (2021). The carbon footprint of a UK University during the COVID-19 lockdown. *Science of the Total Environment*, 756, 143964.
 36. Uludağ, P. (2022). Evaluation of Çanakkale Onsekiz Mart University Terzioğlu Campus in terms of energy and carbon footprint [Master's thesis, Giresun University].
 37. Hacı, M. (2020). A rule-based approach for generating urban footprint maps: from road network to urban footprint. *International Journal of Engineering and Geosciences*, 5(2), 100-108. <https://doi.org/10.26833/ijeg.623592>
 38. Bastianoni, S., Marchi, M., Caro, D., Casprini, P., & Pulselli, F. M. (2014). The connection between 2006 IPCC GHG inventory methodology and ISO 14064-1 certification standard-A reference point for the environmental policies at sub-national scale. *Environmental Science & Policy*, 44, 97-107. <https://doi.org/10.1016/j.envsci.2014.07.015>
 39. Hickmann, T. (2017). Voluntary global business initiatives and the international climate negotiations: A case study of the Greenhouse Gas Protocol. *Journal of Cleaner Production*, 169, 94-104. <https://doi.org/10.1016/j.jclepro.2017.06.183>
 40. Bhatia, P., & Ranganathan, J. (2004). The Greenhouse Gas Protocol.
 41. United Nations (UN). (1998). Kyoto Protocol to The United Nations Framework Convention on Climate Change.
 42. Cléménçon, R. (2016). The two sides of the Paris climate agreement: Dismal failure or historic breakthrough?. *The Journal of Environment & Development*, 25(1), 3-24. <https://doi.org/10.1177/1070496516631362>
 43. ISO. (2018). International Standard ISO 14064, Second Edition. Switzerland.
 44. Yañez, P., Sinha, A., & Vásquez, M. (2019). Carbon footprint estimation in a university campus: Evaluation and insights. *Sustainability*, 12(1), 181. <https://doi.org/10.3390/su12010181>
 45. Yomralıoğlu, T. (2000). Coğrafi Bilgi Sistemleri: Temel Kavramlar ve Uygulamalar. 7.Baskı (2015), s.480, ISBN 975-97369-0-X, İber Ofset. İstanbul.
 46. IPCC. (2006). IPCC Guidelines for National Greenhouse Gas Inventories. General Guidance and Reporting. <http://www.ipcc-nggip.iges.or.jp/public/2006gl/vol1.html>
 47. Bıyık, Y. (2018). Calculation of carbon footprint originated from highways in Isparta province [Master's thesis, Süleyman Demirel University].
 48. Jochem, H., & Wolfram, T. (2014). Carbon Footprint. *Environment, Sustainability Report, Volkswagen*, 126-129.
 49. Kılıç, İ., Yaylı, B., & Elekberov, A. (2018). Bursa Bölgesinde Faaliyet Gösteren Üç Adet Broyler İşletmesinin Karbon Ayak İzinin Tahminlenmesi. *Uluslararası Tarım ve Yaban Hayatı Bilimleri Dergisi*, 4(2), 224-230. <https://doi.org/10.24180/ijaws.480796>
 50. IPCC/UNEP/OECD/IEA. (1997). Revised 1996 IPCC Guidelines for National Greenhouse Gas Inventories Volume III: Reference Manual, Chapter 1 pp 4-44, 62-98, Intergovernmental Panel on Climate Change, United Nations Environment Programme, Organization for Economic CoOperation and Development, International Energy Agency, Paris.
 51. T.C. Çevre ve Şehircilik Bakanlığı (2023). İklim Değişikliği ve Sürdürülebilir Kalkınma, T.C. Çevre ve Şehircilik Bakanlığı Yayınları, Ankara.
 52. Enerji ve Tabii Kaynaklar Bakanlığı (2023). https://enerji.gov.tr/Media/Dizin/BHIM/tr/Duyurular/Bilgi_Formu_Web_Sitesi_2019_202110071443.pdf

53. Çolak, H. E. (2010). Spatial analysis of cancer cases by geographical information systems in the Eastern Black Sea region of Turkey [Doctoral dissertation, Karadeniz Technical University].
54. Yaprak, S., & Arslan, E. (2008). Kriging Yöntemi ve Geoit Yüksekliklerin Enterpolasyonu. Jeodezi ve Jeoinformasyon Dergisi, (98), 36-42.
55. Çolak, E., & Memişoğlu, T. (2021). Thornthwaite iklim sınıflandırma yöntemine göre Karadeniz Bölgesi iklim sınır haritasının CBS ile üretilmesi. Geomatik, 6(1), 31-43.
<https://doi.org/10.29128/geomatik.651702>
56. Yılmaz, M., & Kuru, B. (2019). Makro ve Mikro Ölçekteki Lokal Jeoid Tespiti için Enterpolasyon Yöntemlerinin Karşılaştırılması. Geomatik, 4(1), 41-48. <https://doi.org/10.29128/geomatik.465050>
57. Arslanoğlu M., & Özçelik M. (2005). Improvement of Digital Land Elevation Data. TMMOB Chamber of Surveying and Cadastre Engineers 10. Turkish Scientific and Technical Mapping Congress, 28 March-1 April.
58. Uyan, M. (2019). Comparison of different interpolation techniques in determining of agricultural soil index on land consolidation projects. International Journal of Engineering and Geosciences, 4(1), 28-35.
<https://doi.org/10.26833/ijeg.422570>



© Author(s) 2024. This work is distributed under <https://creativecommons.org/licenses/by-sa/4.0/>



GIS based spatial decision-making approach for solar energy site selection, Ardabil, Iran

Meysam Hasanzadeh ^{*1}, Khalil Valizadeh Kamran ¹, Bakhtiar Feizizadeh ¹, Sanam Hassanzadeh Mollabashi ²

¹ University of Tabriz, Department of Remote Sensing and GIS, Iran, meysam.hasanzadeh@yahoo.com, valizadeh@tabrizu.ac.ir, Feizizadeh@tabrizu.ac.ir

² University of Shahid Beheshti, Department of Civil and Environment Engineering, Iran, S_hassanzadeh@sbu.ac.ir

Cite this study:

Hasanzadeh, M., Kamran, K. V., Feizizadeh, B., & Mollabashi, S. H. (2024). GIS based spatial decision-making approach for solar energy site selection, Ardabil, Iran. *International Journal of Engineering and Geosciences*, 9 (1), 115-130

<https://doi.org/10.26833/ijeg.1341451>

Keywords

AHP
Site Selection Analysis
MCDA
Renewable Energy

Research Article

Received:11.08.2023
Revised: 05.11.2023
Accepted:14.11.2023
Published:02.01.2024



Abstract

Fossil fuel emissions have caused immense harm to the environment, making renewable energy sources like solar power essential. However, finding the optimal location for a solar power plant requires multi-criteria decision analysis (MCDA) due to various factors influencing the selection process. This study used the AHP method to weigh criteria such as GHI, Temperature, Elevation, Slope, Land cover, Distance from city, and Distance from road. The layers created from satellite imagery were combined using algebraic sums to produce a final map with 9 classes. The analysis showed that class 9 has the most desirable values for each criterion, indicating the most suitable regions for a solar power plant. The results of the study have identified the southern and some central regions of Ardabil province as being the most suitable location for the construction of a solar power plant. These regions have been found to have favorable values for the criteria studied, indicating a higher potential for solar energy generation. Based on the criteria assigned to class 9, the best lands have been identified, occupying a total area of 3085 hectares. This area represents approximately 0.17% of the total area of Ardabil province. These findings highlight the importance of careful site selection for solar power plants to ensure maximum efficiency and sustainability.

1. Introduction

Environmental pollution and global warming pose a great threat to our planet [1]. The Energy Information Administration (EIA) predicts a 50% increase in global energy consumption between 2018 and 2050 [2], highlighting the need for a shift towards renewable energy sources due to the harmful effects of fossil fuels [3]. Many countries are adopting strategies to transition to low-carbon economies and use clean, environmentally-friendly energy sources [4]. The Paris Agreement, which promotes innovations and solutions for addressing climate change, calls for an increase in renewable energy use [5].

One of the most important sources of renewable energy is solar energy. The main advantages of solar energy systems are reliability, low utilization costs, economic and easy maintenance, free energy source, clean energy, availability, production close to the consumer, low environmental impact, lower emission of

greenhouse gases and silence. In contrast, the main disadvantages include high initial cost, large installation area, high dependence on technological development and weather conditions [6].

Solar energy is the third most important source of renewable energy after hydropower and wind power, and its use is increasing [7]. Iran has a high potential for solar energy production [8], and efforts are being made to increase its use to reduce fossil fuel dependence and air pollution. Solar power plants are large-scale installations covered with solar panels that convert solar radiation into electricity [9]. The benefits of solar technology have exponentially increased the installation capacity of solar energy systems between 1992 and 2020 [10]. Geographic information systems (GIS) are commonly used together with multi-criteria decision analysis (MCDA) to determine the optimal locations for constructing solar power plants and performing spatial analysis [3,11-12]. The Analytical Hierarchy Process (AHP) is a commonly used tool in various MCDA methods

to evaluate the suitability of sites for constructing solar power plants.

Various studies have utilized GIS and AHP methods to determine suitable locations for solar power plants [5, 13-17]. Tair et al. [18] evaluated suitable locations for large-scale solar power plants in Iraq using GIS, hierarchical analysis methods, and TOPSIS. Watson and Hudson [19] used a combination of GIS and AHP to identify the most suitable locations for photovoltaic systems in southern England. Fuzzy logic and AHP have been used in integrated methods to evaluate the suitability of PV systems in Iran [20-21], Türkiye [5], South Korea [22], and Spain [23].

Criteria selection is an important step in any site suitability assessment process for photovoltaic systems. Table 1 shows the criteria considered in some previous studies that have analyzed site suitability for photovoltaic systems.

Table 1. Different criteria considered in previous similar studies on suitability of solar power plant site.

Source	A	B	C	D	E	F	G	H	I
[1]	✓	✓	✓	✓	✓	✓	✓	✓	
[3]	✓		✓	✓	✓	✓	✓	✓	✓
[14]			✓	✓		✓			✓
[19]			✓			✓	✓	✓	✓
[20]			✓	✓	✓		✓	✓	✓
[21]	✓	✓	✓		✓	✓	✓	✓	✓
[22]	✓	✓	✓				✓	✓	✓
[23]	✓	✓	✓			✓	✓	✓	✓

A: Global horizontal irradiance, B: Temperature, C: Slope, D: Aspect, E: Elevation, F: Distance from urban areas, G: Distance from road, H: Distance from power lines, I: Land cover

According to reports published by the International Renewable Energy Agency (IRENA) on March 20th, 2023, the total global installed capacity of renewable energy by 2022 is 3,371,793 MW. Solar power plants are 31% of this capacity with 1,053,115 megawatts. Fourteen Middle Eastern countries have allocated 0.85% of the world's capacity to themselves with a total installed capacity of 28,539 megawatts. Among Middle Eastern countries, Iran has received the first rank with an installed capacity of 12,045 megawatts, followed by Israel with 4,470 megawatts and the United Arab Emirates with 3,058 megawatts. Due to the fact that so far, no published research has investigated the location of solar photovoltaic power plant specifically in Ardabil province, the present research was conducted with the aim of classifying and determining the degree of suitability in each point of the province for placing solar panels. The purpose of determining the best place for the construction of a solar power plant in this province is to increase the annual production of electrical energy, which reduces the investment return time and also reduces investment costs.

In this study, various criteria were considered to assess the suitability of locations for building a solar power plant, and each criterion was prepared as a raster layer. Necessary preprocessing was performed on the layers, and they were normalized. The normalization of

the layers was modified compared to conventional methods such as fuzzy membership by using the Python programming language and the Arcpy package. This was done because different normalization methods in ArcMap software have limitations that can produce undesired and, in some cases, incorrect results, based on defined conditions. MCDA was employed to determine the optimal locations. In this research, certain areas of the province within the studied layers were identified as restricted areas according to predetermined conditions and were therefore excluded from the study.

2. Method

Ardabil province is located in the northwest of Iran with an area of 17799 km². Due to its longitudinal shape (Figure 1), the province experiences significant climate diversity, with relatively cold and dry conditions in the southern and central regions and relatively warm and semi-moist conditions in the northern parts. According to the Meteorological Organization of Ardabil Province, the province receives more than 2,497 hours of sunshine annually [24].

For the purpose of this research, certain areas were excluded and considered as restricted areas. These included all water bodies such as dams, lakes, and rivers, along with a 200-meter buffer. Additionally, areas with ice and snow, flooded vegetation, forest areas, cities with a buffer of 4 kilometers from Ardabil city and 2 kilometers from other cities, areas with a distance of more than 20 kilometers from them, and all other built-up areas, such as rural and industrial towns, airports, military areas, and all other enclosed areas with a 100-meter buffer were also excluded. These areas were extracted from the land cover map, relevant buffers were applied, and during the classification operation of the land cover layer, they were assigned to the zero class. As a result, they received a zero value in the normalization stage using the linear method.

In this research, seven criteria were considered to determine the optimal location for the construction of a solar power plant in Ardabil, based on the availability of relevant data at the provincial scale. These criteria include global horizontal irradiance (GHI), temperature, elevation, slope, distance from road, distance from city, and land cover.

2.1. The criteria examined

2.1.1. Global Horizontal Irradiance (GHI)

Solar radiation is a critical factor in determining the best location for a solar power plant. It is important to choose locations that receive sufficient sunlight throughout the year [25]. In previous studies, by Martins et al. [26], Amillo et al. [27], and Huld [28], solar radiation was related to global horizontal irradiance, which is also used in this study.

Direct solar radiation is the portion of radiation that reaches a surface directly, while diffuse radiation is the portion that is scattered by the atmosphere. Global radiation is the sum of scattered and direct components that reach a surface. The term solar radiation refers to

the total energy per unit area received from the sun over a specific period of time. Figure 2 presents an overview of the estimated solar energy available for electricity

generation and other energy applications. It also displays the long-term average annual/daily total global horizontal irradiance (GHI) [29].



Figure 1. Map of the study area, Ardabil Province.

Based on the report by the National Renewable Energy Laboratory (NREL), areas with solar radiation less than 3.56 kWh/m^2 are not considered economically efficient, and as a result, these areas were not investigated in this research [30]. The GHI value for the Ardabil province ranges from 3.361 kWh/m^2 at the lowest point to 5.012 kWh/m^2 at the highest point. Figure 2 indicates that the northern region of the province has less potential for solar radiation compared to the southern region, and contrary to popular belief, the southern cities of Givi and Khalkhal have significant solar radiation potential.

2.1.2. Temperature

The temperature of photovoltaic cells is a crucial factor in their performance. High-temperature areas can have a negative impact on energy production [31]. The optimal temperature range for solar energy production is below 25°C , and for every 1°C increase in temperature, there is a corresponding decrease in output power of 0.4 to 0.5 percent [32].

The average annual temperature in the Ardabil Province ranges from -9.3°C in the coldest areas to 16.6°C in the hottest regions. The map in Figure 3 indicates that the northern region of the province has a lower potential for temperature compared to the central and southern regions. However, based on the minimum and maximum values associated with the average annual temperature of the province (Figure 3), all parts of the province are suitable in terms of temperature. The value of pixels will increase linearly as the temperature decreases.

2.1.3. Elevation

Higher elevations have the potential to receive more solar radiation compared to lower areas [32]. The elevation of a region above sea level is inversely related to the density of the atmosphere. As the density of the atmosphere increases, the concentration of absorbing or reflecting agents also increases. Since the coarser materials are located in the lower layers, the atmosphere is sparser at the top of mountains. Therefore, high areas have more potential for solar energy production.

However, it should be noted that as the elevation of an area increases, the cost and difficulty of transferring infrastructure and labor also increase [33].

In this research, areas with elevations lower than zero (i.e., below sea level) were removed due to the reduction in solar panel performance. Areas with elevations higher than 2000 meters were also excluded due to the increase in construction costs (Figure 4).

2.1.4. Slope

Increasing the slope of the land can increase the cost of construction and make it more difficult. According to studies conducted by Tahri et al. [33], the maximum acceptable slope for solar power plant construction is 25% or 14 degrees. Therefore, for this research, the maximum allowed slope was set at 15 degrees (Figure 5).

2.1.5. Land cover

In this research, bare ground, pastures, and farms were considered and classified from the most important to the least important land covers, while the rest of the covers, designated as restricted areas, were excluded (Table 2, Figure 6). Built-up areas, flooded vegetation, snow, ice, trees, and water were classified as unsuitable for solar power plant construction, and therefore were assigned a value of zero.

Bare ground was classified as the most suitable

because it is economical and readily available. Farms and pastures were classified between these two classes, based on economic and environmental considerations.

2.1.6. Distance from city

Studies conducted by AlGarni and Awasthi [31] and Al-Shammari et al. [34] have removed areas more than 50 km away from built-up areas to determine the optimal location for a solar power plant. However, in this research, areas with a distance more than 20 km away were removed to reduce transportation and construction costs, and to provide cheaper electricity supply to cities (Figure 7).

2.1.7. Distance from road

In the study conducted by Masoom et al. [35], the maximum distance of 50 km from roads was considered to determine the optimal location for a solar power plant, and a distance of 500 m from the center of roads was designated as the road boundary and excluded as restricted areas. Areas far from roads were deemed unsuitable and uneconomical for construction. In this research, areas with a distance greater than 2 km from roads were excluded, and a distance of 100 m from the center of roads was considered as the road boundary and removed (Figure 8). Table 3 provides specifications for all the mentioned criteria.

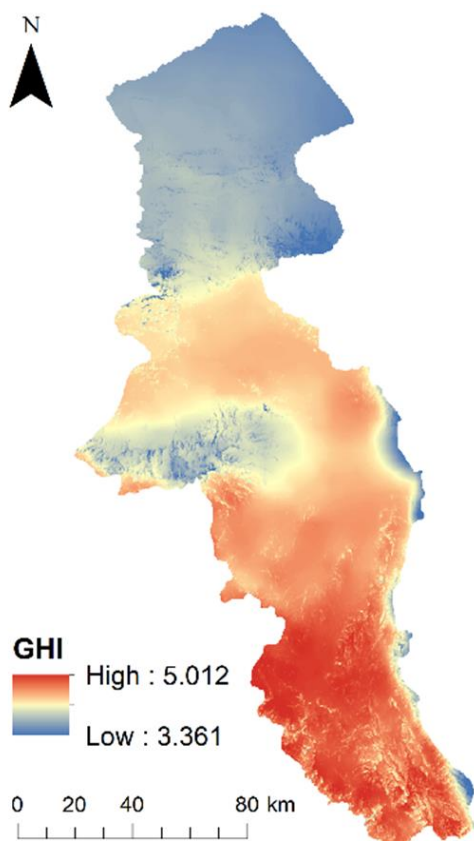


Figure 2. Global horizontal radiation map of Ardabil Province (kwh/m²).

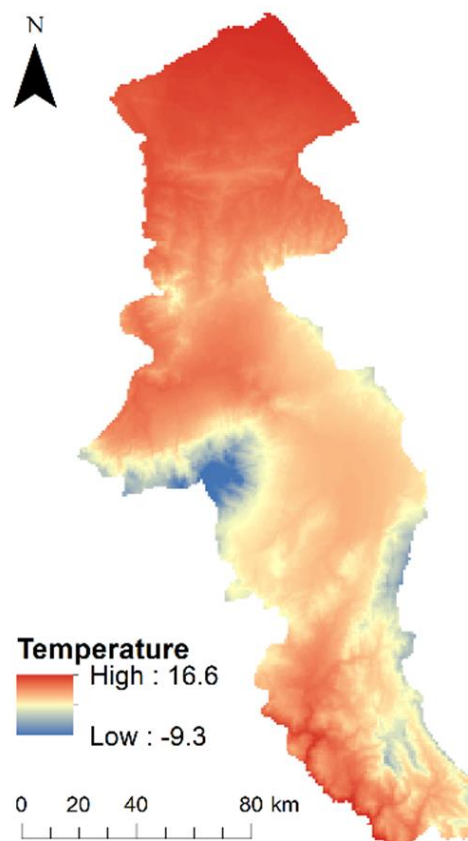


Figure 3. Average annual temperature map of Ardabil Province (°C).

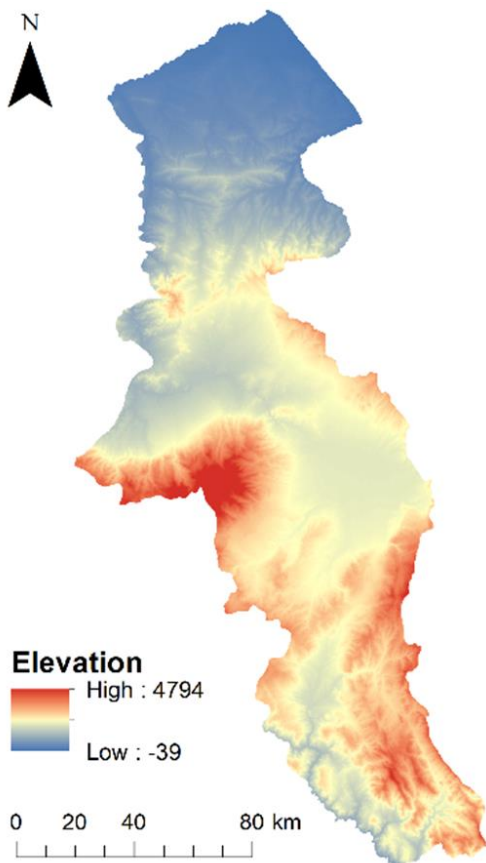


Figure 4. Digital elevation model map of Ardabil Province (m).

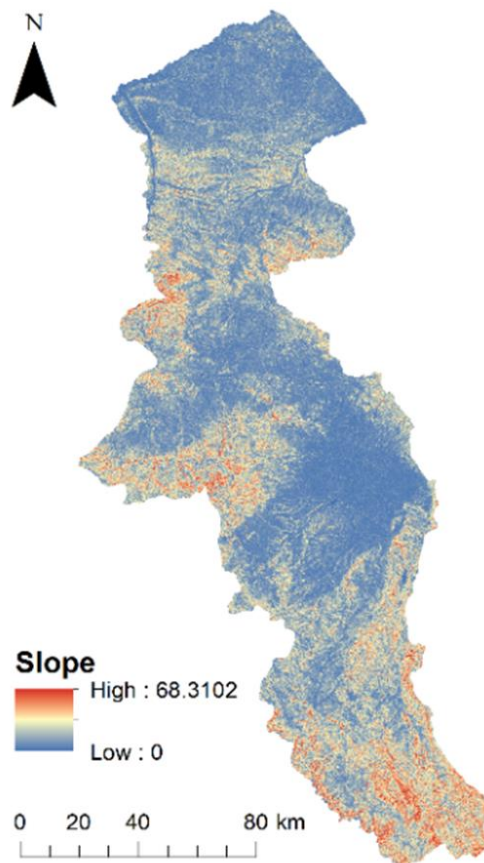


Figure 5. Slope map of Ardabil Province (Degree).

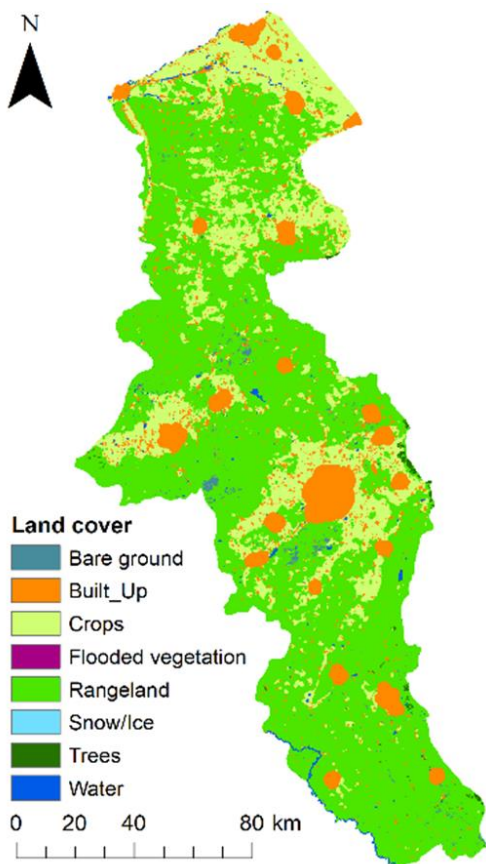


Figure 6. Land cover map of Ardabil Province.

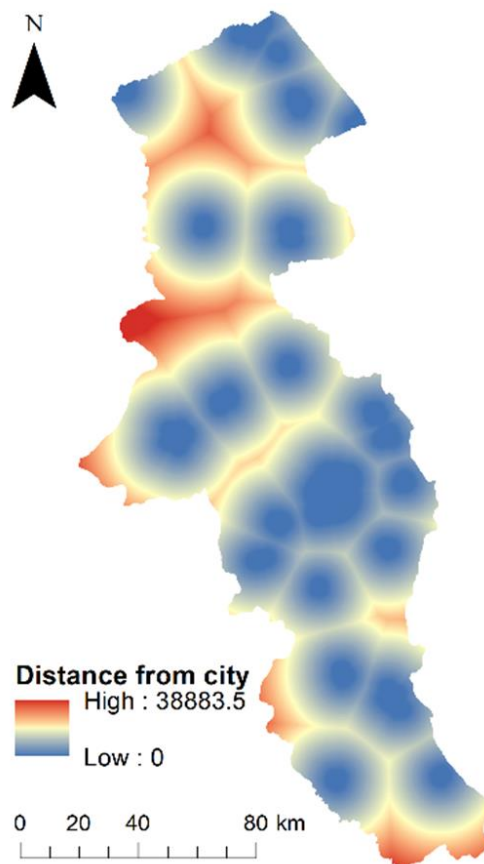


Figure 7. Distance from city map of Ardabil Province (km).



Figure 8. Distance from road map of Ardabil Province (m).

Table 2. Classes related to land cover in Ardabil province.

	0	1	2	3
Built-up areas		Farms	Pastures	Bare ground
Flooded vegetations				
Snow and ice				
Trees				
Water				

This research uses MCDA method. the layers were normalized using a modified linear fuzzy logic, coded using the Arcpy package in ArcMap. This involved assigning a value of one to pixels with the maximum degree of desirability and a value of zero to unsuitable pixels, with the remaining pixels assigned values between these two extremes. The weight of each parameter was determined using the AHP weighting technique, and the normalized layer was multiplied by its respective weight. Pixels with a value of zero were removed, and the final layer was produced by summing the values of the pixels in each investigated layer. The final layer was classified into 9 classes to preserve valuable information and maintain accuracy, while avoiding the creation of empty or useless classes.

To validate the model, two points were selected from classes 9 and 3, and the corresponding values of each layer were extracted. ArcMap 10.2 software (ESRI) was used for data processing and analysis. Maps related to distance from city and road were converted from vector format to raster using the Euclidean distance tool. The spatial resolution of the layers was resampled to 28.40590591 to match the spatial resolution of the Digital Elevation Model (DEM) image, while considering the extent of the studied area.

Table 3. Specifications of the investigated parameters.

	Data	Spatial Resolution	Reference	Format
Climate	GHI	250 m	Global Solar Atlas- Solar GIS [29]	Raster
	Temperature	800 m	Global Solar Atlas- Solar GIS [29]	Raster
Geomorphological	Elevation	28.406 m	Nasa Earth Data [36]	Raster
	Slope	28.406 m	Nasa Earth Data [36]	Raster
Spatial	Distance from city	28.406 m	Esri Global Land Use [37]	Vector
	Distance from road	28.406 m	OSM [38]	Vector
Environmental	Land cover	10 m	Esri Global Land Use [37]	Raster

2.2. Data standardization

Considering that each parameter can have a unique range, normalization should be conducted in order to use them in multi criteria evaluations. Fuzzy normalization

standardizes input layers on a scale of 0 to 1 [22]. To evaluate the degree of membership of a parameter in a fuzzy set, several types of fuzzy functions have been developed and published in scientific literature (Equation 1) [39].

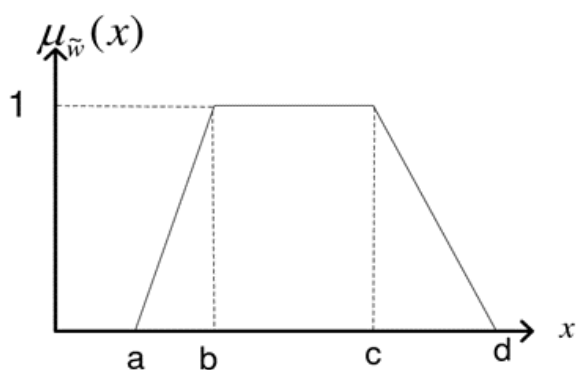


Figure 9. Linear fuzzy logic function (x, parameter; u(x), degree of fuzzy membership) [40].

$$\text{trapezoid}(x; a, b, c, d) = \begin{cases} 0, & x \leq a. \\ \frac{x-a}{b-a}, & a \leq x \leq b. \\ 1, & b \leq x \leq c. \\ \frac{d-x}{d-c}, & c \leq x \leq d. \\ 0, & d \leq x. \end{cases} \quad (1)$$

Due to the limitations in the linear fuzzy logic set of ArcMap, it was decided to code this linear function in Python programming language in this software using Arcpy package. For example, while normalizing the elevation layer of the province, by increasing elevation to 2000m, the value of the pixels increased, where pixels with elevation of 2000 got the value one. Elevations more than 2000 have been excluded from this research, but using the linear fuzzy logic membership set ready in ArcMap software, the areas with elevation more than 2000 are also assigned a value of one, and this issue is contrary to the intended criterion in this study. According to this issue, the normalization of the layers in the GIS environment was coded using the linear fuzzy logic method.

The normalization of the GHI layer of the province is done in order that the pixels that have radiation between 3.56 kwh/m² and 5.012 kwh/m² are assigned values between zero and one, so that with the increase in the amount of radiation, the value of pixels increase and get one. Considering that the maximum amount of global horizontal radiation in the province is 5.012 kwh/m², the pixels with this value are assigned the value of one after applying the normalization functions. Pixels with radiation of 3.56 kwh/m² and less receive zero value.

Also, in the normalization of the temperature layer of the province, the pixels with the temperature between -9.3 and 16.6 °C are assigned values between zero and one, so that with the decrease in temperature, the value of the pixels increases and reaches a value of one. pixels with temperature -9.3°C is assigned a value of one and a pixel with a temperature of 16.6 is assigned a value of zero.

Pixels with an elevation between 0 and 2000 m above sea level are assigned values between 0 and 1. As the elevation increases, the value of the pixels increases and approaches the value of one, so that pixels with a height of zero and less have a value of zero and pixels with a height of 2000 m are assigned a value of 1. Those with an elevation of more than 2000 m are excluded from this

study due to their high elevation and increased construction costs, and are assigned a value of zero.

Pixels with a slope between 0 and 15 degrees received values between zero and one, and as the slope decreases, the value of pixels increases and approaches the value of one. Pixels with a slope of 15 degrees and more have a value of zero, and pixels with a slope of zero degrees have a value of one.

Class 3 land cover layer, which corresponds to rocky or soil areas with very little or no vegetation cover during the year, such as rock or soil, desert and dunes, salt marshes, dry hills and dried lakes, has the highest value in this research and they are assigned a value of one, while the uses of built-up areas, water areas, forest areas, and areas with ice and snow, which are assigned to the zero class, will be taken as zero after normalization and will be removed.

As the distance from cities increases, the value of pixels decreases. Pixels that have a distance of 20 km or more from the considered city (which its boundary is determined using the special mentioned buffer) have a value of zero, and as the distance from city limits decreases, its value gets closer to one.

As the distance from road increases, the value of the pixels decreases. Pixels that have a distance of 2 km or more from the center of the road have a value of zero, and the closer we get to a distance of 100m from the center of the road, the value becomes closer to one. Pixels with distance equal to and less than 100m from the center of the road receive value of zero.

2.3. Using AHP technique in layer weighting

AHP technique was first proposed by Saaty [41] and consists of a system that compares a number of variables by determining the weight of importance of a factor relative to each factor considered. Pairwise comparison refers to the process of comparing several factors or elements in pairs to decide which factor is preferable (relative importance) or whether two factors are equally important in a particular problem. Thus, it simplifies a complex problem and facilitates the determination of reasonable weights for multiple factors. In a pairwise comparison, the sum of the weights of all criteria is 1. For example, in the case of four criteria (i.e., factors A-D), a 4x4 matrix is needed to determine the weights of the four criteria (Equation 2).

Each element of the pairwise comparison matrix represents the relative importance value of one factor to another, assigned using the 1-9 scale of importance intensity described in Table 4. For example, if factor A is more important than factor B in predicting a subsidence event, CAB is assigned a relative intensity value of 5. Since the matrix is symmetric, only the upper triangular half of the pairwise comparison matrix needs to be completed. The remaining elements are reversed of upper half-triangular. The value of the diagonal elements of the matrix is one.

Once all the values of the pairwise comparison matrix elements were determined, a normalized matrix with respect to the number of criteria can be calculated based on Equation 3:

where each element represents the weighted value of each criterion. The relative weight for each factor is determined in the range of 0 to 1. A higher weight

indicates a greater contribution of this factor to PV suitability.

$$\text{Matrix: } \begin{bmatrix} C_{11} & C_{12} & C_{13} & C_{14} \\ C_{21} & C_{22} & C_{23} & C_{24} \\ C_{31} & C_{32} & C_{33} & C_{34} \\ C_{41} & C_{42} & C_{43} & C_{44} \end{bmatrix} = \begin{bmatrix} 1 & C_{AB} & C_{AC} & C_{AD} \\ C_{BA} & 1 & C_{BC} & C_{BD} \\ C_{CA} & C_{CB} & 1 & C_{CD} \\ C_{DA} & C_{DB} & C_{DC} & 1 \end{bmatrix} \quad (2)$$

$$P = \begin{bmatrix} p_1 \\ p_2 \\ p_3 \\ p_4 \end{bmatrix} = \begin{bmatrix} \omega_A \\ \omega_B \\ \omega_C \\ \omega_D \end{bmatrix} = \frac{1}{4} \times \begin{bmatrix} \sum_{j=1}^4 \frac{C_{1j}}{C_{0j}} \\ \sum_{j=1}^4 \frac{C_{2j}}{C_{0j}} \\ \sum_{j=1}^4 \frac{C_{3j}}{C_{0j}} \\ \sum_{j=1}^4 \frac{C_{4j}}{C_{0j}} \end{bmatrix} \quad \text{where } C_{0j} = \sum_{i=1}^4 C_{ij} \quad (3)$$

Table 4. Degree of importance in pairwise comparisons.

Importance	Definition	Explanation
1	Equal importance	The two activities contribute equally to the goal
3	Medium importance	A little experience and judgment prefer one activity over another
5	Strong importance	Experience and judgment strongly prefer one activity over another
7	Very strong or demonstrated importance	One activity is strongly preferred over another. Its domination was demonstrated in practice
9	Too much importance	Evidence that prefers one activity over another has the highest possible degree of confirmation
2,4,6,8	Intermediate values	
The reverse of the above		In the case of inverse comparison of the relationship between elements, the reversed values are assigned a degree of importance

To identify the degree of consistency in the assignment of element values in the pairwise comparison matrix, the consistency ratio (CR) can be used. CR shows the consistency of the participants opinions in scoring the pairwise comparison matrix. CR is defined as the ratio between the consistency index (CI) (Equation 5) of the matrix and a randomness index (RI) shown in Equation 6. As reported by Ishizaka and Labib [42], RI can be assigned based on the number of criteria, using an appropriate value. In general, a CR value of less than 0.1 is considered to indicate a valid comparison.

$$M = C \times P = \begin{bmatrix} m_1 \\ m_2 \\ m_3 \\ m_4 \end{bmatrix} \quad (4)$$

$$CI = \frac{\left(\frac{\sum_{i=1}^4 \frac{m_i}{p_i}}{4} \right) - 4}{4 - 1} \quad (5)$$

$$CR = CI/RI \quad (6)$$

When expert's judgments differed for a particular element of the comparison matrix, geometric mean

values were used to combine the preferences for each element to minimize the multiplicative error in computing the comparison matrix, as suggested by Ishizaka and Labib [42].

2.4. Determining the weights of the criteria using the AHP method

According to the previous studies and researches in the field of solar power plant location [3-4,22], considering the social and economic conditions of Iran and Ardabil province and judgments between criteria gathered from a group of experts related in solar energy, the degree of importance of the criteria was determined in Table 5. By dividing the elements of each column by the sum of the columns, the normal matrix of pairwise comparisons is made according to Table 6. By averaging each row of the normal matrix of pairwise comparisons, the weight of each criterion is acquired, shown in Table 7.

In order to calculate the consistency rate, we first multiply each element of the primary matrix column (Table 5) by the weight of each criterion (Table 7). The sum of each row of the acquired matrix is called the weighted sum of values. Finally, we divide the obtained weighted sum of values by the weight of each criterion, which we name the corresponding as column A (Table 8).

Table 5. Matrix of pairwise comparisons.

AHP	GHI	Slope	Distance from road	Distance from city	Elevation	Land cover	Temperature
GHI	1	2	3	4	5	6	7
Slope	1/2	1	2	3	4	5	6
Distance from road	1/3	1/2	1	2	3	4	5
Distance from city	1/4	1/3	1/2	1	2	3	4
Elevation	1/5	1/4	1/3	1/2	1	2	3
Land cover	1/6	1/5	1/4	1/3	1/2	1	2
Temperature	1/7	1/6	1/5	1/4	1/3	1/2	1

Table 6. Normal matrix of pairwise comparisons.

AHP	GHI	Slope	Distance from road	Distance from city	Elevation	Land cover	Temperature
GHI	0.3857	0.4494	0.4119	0.3609	0.3158	0.2791	0.2500
Slope	0.1928	0.2247	0.2746	0.2707	0.2526	0.2326	0.2143
Distance from road	0.1286	0.1124	0.1373	0.1805	0.1895	0.1860	0.1786
Distance from city	0.0964	0.0749	0.0686	0.0902	0.1263	0.1395	0.1429
Elevation	0.0771	0.0562	0.0458	0.0451	0.0632	0.0930	0.1071
Land cover	0.0643	0.0449	0.0343	0.0301	0.0316	0.0456	0.0714
Temperature	0.0551	0.0375	0.0275	0.0226	0.0211	0.0233	0.0357

Table 7. The weight of each criterion.

GHI	Slope	Distance from road	Distance from city	Elevation	Land cover	Temperature
0.3504	0.2375	0.1590	0.1056	0.0696	0.0462	0.0318

Table 8. Weighted sum of values.

AHP	GHI	Slope	Distance from road	Distance from city	Elevation	Land cover	Temperature	Weighted total values	A
GHI	0.3504	0.4750	0.4770	0.4224	0.3480	0.2772	0.2226	2.5726	7.341894977
Slope	0.1752	0.2375	0.3180	0.3168	0.2784	0.2310	0.1908	1.7477	7.358736842
Distance from road	0.1168	0.1188	0.1590	0.2112	0.2088	0.1848	0.1590	1.1584	7.285220126
Distance from city	0.0876	0.0792	0.0795	0.1056	0.1392	0.1386	0.1272	0.7569	7.16729798
Elevation	0.0701	0.0594	0.0530	0.0528	0.0696	0.0924	0.0954	0.4927	7.078376437
Land cover	0.0584	0.0475	0.0398	0.0352	0.0348	0.0462	0.0636	0.3255	7.044372294
Temperature	0.0501	0.0396	0.0318	0.0264	0.0232	0.0231	0.0318	0.2259	7.105046421

By averaging the values of column, A, λ is acquired:

$$\lambda = 7.1972$$

Then it's time to calculate the C.I consistency index:

$$C.I = (\lambda - 8) / 7$$

$$C.I = 0.0328$$

The consistency rate or C.R is obtained by dividing the

consistency index C.I by R.I, which R.I is determined according to the number of criteria and [Table 9](#):

$$C.R = C.I / R.I$$

$$C.R = 0.0249$$

Considering that the consistency rate is 0.0249 and is less than 0.1, it can be concluded that the acquired weight values are acceptable and the criteria are logically compatible.

Table 9. The value of R.I based on the number of criteria.

n	1	2	3	4	5	6	7	8	9	10
R.I	0	0	0.58	0.9	1.12	1.24	1.32	1.41	1.45	1.49

In order to normalize the layers, Python programming language was used in the GIS environment. The package used is Arcpy and the module used is Arcpy.sa (Spatial Analyst), which is a module for raster and vector data analysis with the capacity provided by the ArcGIS Spatial Analyst extension. This module provides access to all the geoprocessing tools in the Spatial Analyst toolbox, as well as other functions and classes that allow you to automate your raster processing workflows [44]. Codes used for the linear normalization of the layers are presented in Table 10. It should be noted

that if, for example, a pixel has all the appropriate conditions and is inappropriate only in terms of one criterion, meaning its value is zero after normalization, then that pixel is considered inappropriate and is not classified in any of the classes of the final layer. For this purpose, before overlaying the layers, the pixels that received zero value after normalization and weighting will be removed using the Raster Calculator tool and the Set Null command. Table 11 includes the commands used to remove pixels with zero values.

Table 10. The normalization scripts of each layer along with the applied weights.

Elevation	<pre>>>> import arcpy >>> from arcpy.sa import* >>> x = Raster ("Elevation") >>> ElevationNormalizedMap=Con((x>=0) &(x<=2000), ((x-0)/2000.0),0) >>> ElevationWeightedNormalizedMap = ElevationNormalizedMap *0.0696</pre>
Slope	<pre>>>> import arcpy >>> from arcpy.sa import* >>> x=Raster("Slope") >>> SlopeNormalizedMap =Con((x>=0) &(x<=15), ((15-x)/15.0),0) >>> SlopeWeightedNormalizedMap = SlopeNormalizedMap *0.2375</pre>
GHI	<pre>>>> import arcpy >>> from arcpy.sa import* >>> x = Raster ("GHI") >>> GHINormalizedMap =Con((x>=3.560) &(x<=5.012), ((x-3.560)/1.452),0) >>> GHIWeightedNormalizedMap = GHINormalizedMap *0.3504</pre>
Temperature	<pre>>>> import arcpy >>> from arcpy.sa import* >>> x = Raster ("Temperature") >>> TemperatureNormalizedMap =Con((x>=-9.3) &(x<=16.6), ((16.6-x)/25.9),0) >>> TemperatureWeightedNormalizedMap = TemperatureNormalizedMap *0.0318</pre>
Distance From Road	<pre>>>> import arcpy >>> from arcpy.sa import* >>> x = Raster ("DistancefromRoad") >>> DistancefromRoadNormalizedMap =Con((x>100) &(x<=2000.0), (2000.0-x)/1900.0, Con((x<=100) &(x>2000),0,0)) >>> DistancefromRoadWeightedNormalizedMap = DistancefromRoadNormalizedMap *0.1590</pre>
Distance From City	<pre>>>> import arcpy >>> from arcpy.sa import* >>> x = Raster ("DistancefromCity") >>> DistancefromCityNormalizedMap =Con((x>0) &(x<=20000.0), (20000.0-x)/20000.0, Con((x<=0) &(x>20000),0,0)) >>> DistancefromCityWeightedNormalizedMap = DistancefromCityNormalizedMap *0.1056</pre>
Landcover	<pre>>>> import arcpy >>> from arcpy.sa import* >>> x = Raster ("Landcover") >>> LandcoverNormalizedMap =Con((x>=0) &(x<=3), (x)/3.0,0) >>> LandcoverWightedNormalizedMap = LandcoverNormalizedMap *0.0462</pre>

Table 11. Command to remove pixels with zero values in each layer after applying normalization functions.

Elevation	SetNull (" ElevationWeightedNormalizedMap " == 0," ElevationWeightedNormalizedMap ")
Slope	SetNull (" SlopeWeightedNormalizedMap " == 0," SlopeWeightedNormalizedMap ")
GHI	SetNull (" GHIWeightedNormalizedMap " == 0," GHIWeightedNormalizedMap ")
Temperature	SetNull (" TemperatureWeightedNormalizedMap " == 0," TemperatureWeightedNormalizedMap ")
Distance From Road	SetNull (" DistancefromRoadWeightedNormalizedMap " == 0," DistancefromRoadWeightedNormalizedMap ")
Distance From City	SetNull (" DistancefromCityWeightedNormalizedMap " == 0," DistancefromCityWeightedNormalizedMap ")
Landcover	SetNull (" LandcoverWightedNormalizedMap " == 0," LandcoverWightedNormalizedMap ")

2.5. Produce the final map

By using the method of summing the pixel values of the layers related to the investigated criteria that are

$$\text{Suitability index} = \sum (\text{Fuzzy membership index}_i \times \text{Weight}_i) \quad (7)$$

3. Results

Many studies have been conducted to identify suitable sites for solar power plants [45]. The importance of criteria considered in such studies may vary depending on the region's location, environment, climate, geomorphological, economic, and infrastructure conditions, depending on the opinions of specialists and experts. By using multi-criteria decision-making methods, prioritizing criteria using the AHP method, and stacking layers in different ways in the GIS environment, regional location costs for solar power plants can be effectively reduced [1,3-4,22,43, 46]. To increase the use of solar energy, it is essential to achieve cost-effectiveness and reduce the investment return time for investors. Therefore, determining the optimal location for a solar power plant is crucial.

This research uses the algebraic sum method to overlay normalized layers and account for the relative importance of different criteria in determining the suitability of various locations within Ardabil province for the construction of a solar power plant. By normalizing the layers and considering the importance of criteria relative to each other, the research aims to

normalized and multiplied by the weight obtained using the AHP technique, the final layer indicating the degree of suitability of each pixel for the construction of a solar power plant is acquired (Equation 7).

accurately determine the optimal location for a solar power plant in the region. The final map, with pixels divided into nine equal interval classes, is shown in Figure 9. Class 9 refers to the strongest pixels and class 1 refers to the weakest pixels.

The area of each class along with the percentage of its area compared to the total area of the province is shown in the Table 12. This table shows that 59.88% of the area of the province is completely unsuitable for the construction of a solar power plant.

Pixels that are assigned class 9 should be prioritized when planning to build a solar power plant.

As shown in Figure 9, the most suitable areas are located in the south and somehow in the center of the province, which are indicated by classes 9 and 8. This is due to relatively lower temperature and more solar radiation as well as higher altitude. The areas of classes 8 and 9 cover a total area of 78260.3 hectares, equivalent to 4.39% of the total area of the province. Also, the northern regions of the province are mainly allocated to lower classes due to high temperature, lower elevation and lower global horizontal irradiance, which are all three negative factors affecting the location for the construction of a solar power plant.

Table 12. The pixels area of suitability map for Ardabil province, separated by each class, along with the percentage of the area of each class compared to the total area of the province.

Class	9	8	7	6	5	4	3	2	1
Area (Hectares)	3085.81	75174.49	177814.75	183189.32	164937.99	90193.24	19495.24	769.29	1.53
Percentage	0.17	4.22	9.98	10.29	9.26	5.06	1.09	0.0432	0.00008

The solar site suitability analysis performed in this research can be a preventive step to support decision makers in finding and selecting the most suitable locations for the development of PV systems in Ardabil province whether small-scale PV systems or large-scale ones. Large-scale PV systems can be built on certain vacant lands that achieve a high degree of suitability, such as areas assigned to Class 9 as shown in Figure 10.

Table 13 shows the pixel values of each criterion for two points located in classes 9 and 3. Class 9 which represents the best pixels for construction of solar power plant, and land related to this class has higher global horizontal irradiance and elevation, lower slope and temperature and generally shorter distance from road and city. X and Y refer to the coordinates of the desired pixel in UTM (Universal Transverse Mercator) coordinate system, located in zone 39S.

In order to calculate the efficiency of the solar power plant for two points in Table 13, the open-source Global Solar Atlas Energy was used. The type of power plant was selected from the ground mounted large-scale type and

the nominal capacity of the power plant was arbitrarily determined to be 10 MW. Results show that land related to class 9 has higher efficiency than land related to class 3, about 24% (Table 10).

The pixel data in Table 13 and Table 14 shows the importance of using AHP weighting method. Considering that according to the opinion of experts in this field, the amount of solar radiation and the slope of the earth are more important, as a result, they have been given more weight. Figure 11 shows the value of each criterion considering two determination points. These charts obviously present the difference between class 9 and 3 of this study.

As a result of processing the received satellite imageries of Ardabil province, related to the seven criteria examined in the GIS environment and their overlaying, the final map produced was classified into 9 classes. It can be concluded that the best land for the construction of a solar power plant according to criteria and conditions, is located mainly in the south and to some extent in the central areas of the province. The best lands

assigned to class 9 occupy 3085 hectares, which is about 0.17% of the area of the province. In general, suggest to use lands assigned to class 9 and then class 8, when deciding to construct a solar power plant considering sustainable development and economic efficiency for investors. The requirement of any sustainable development is the correct choice of location, using site selection techniques and multi-criteria decision-making methods.

Table 13. Pixel values related to random points determined in the examined raster criteria.

Class	9	3
X	268350	262980
Y	4167506	4321501
Temperature (°C)	10.4	11.8
Slope (degree)	3.35	14.18
Distance from Road (m)	204	779
GHI (kwh/m ²)	4.95	4.03
Elevation (m)	1682	821
Distance from City (m)	4484	95
Land cover	Rangeland	Rangeland

Table 14. Calculated Energy yield for two random points.

Class	9	3
X	268350	262980
Y	4167506	4321501
Energy yield of a 10MW installed capacity power plant (GW per year)	16.777	13.562

After investigating the existing solar power plants in Ardabil province, results were obtained that with two solar power plants, each with a capacity of 1 megawatt, it has allocated 0.01% of the total installed capacity of renewable energy to itself in Iran. The power plant located in the south of the province is in classes 8 and 9, while the power plant located in the north of the province is in classes 7 and 8, according to this study.

4. Conclusion

This study used MCDA method to determine the optimal locations to Construct Solar Power plant in Ardabil Province, Iran. Seven criteria considered to be evaluated in this study: GHI, Temperature, Elevation, Slope, Land cover, Distance from city and Distance from road. AHP was used to weight the criteria and then the linear normalization of the layers was done using python programming in ArcMap software. All the pixels that received zero value after normalization were excluded from this study. The final layer was obtained as an algebraic sum of the weighted criteria. The final map produced was classified into 9 classes and indicates that the best lands that belong to class 9 and 8 which are respectively 0.17 and 4.22 percent of the province area, are located in the south and central regions of the province which show the best lands to build a solar power plant and requires multi-criteria decision making.

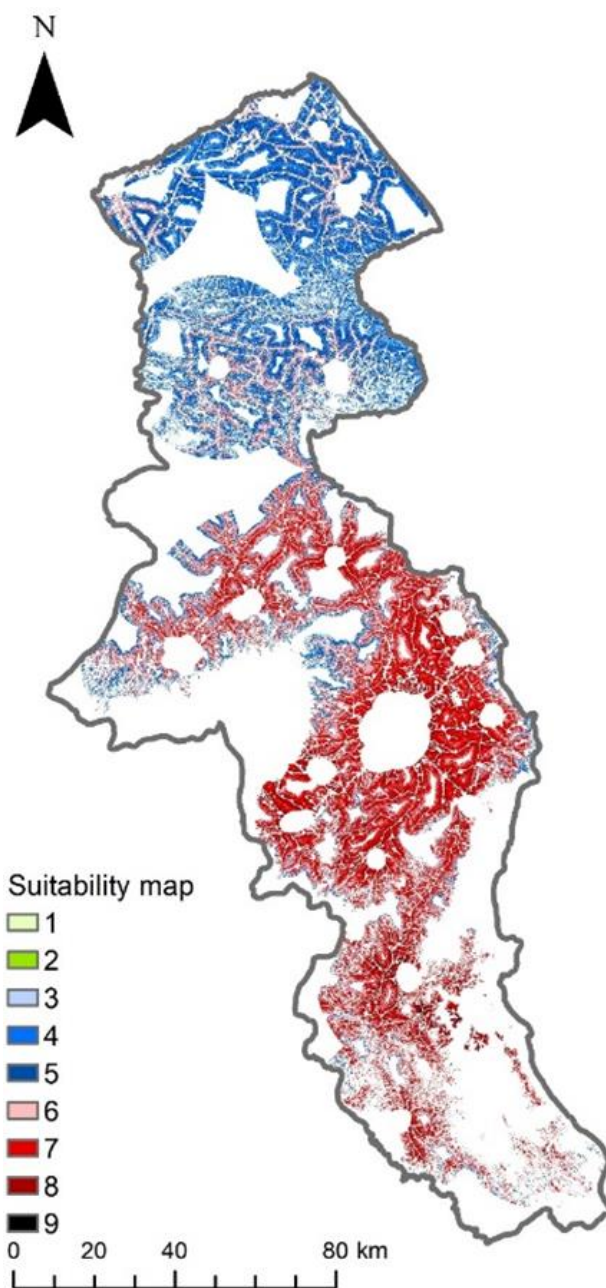


Figure 9. Classified map for the suitability degree of Ardabil province in order to construction of a solar power plant.

Author contributions

Meysam Hasanzadeh: Conducted this research, analyzed results and wrote the manuscript
Khalil Valizadeh Kamran: Analyzed results
Bakhtiar Feizizadeh: Edited Scientific and literary
Sanam Hassanzadeh Mollabashi: Edited Scientific and literary

Conflicts of interest

The authors declare no conflicts of interest.

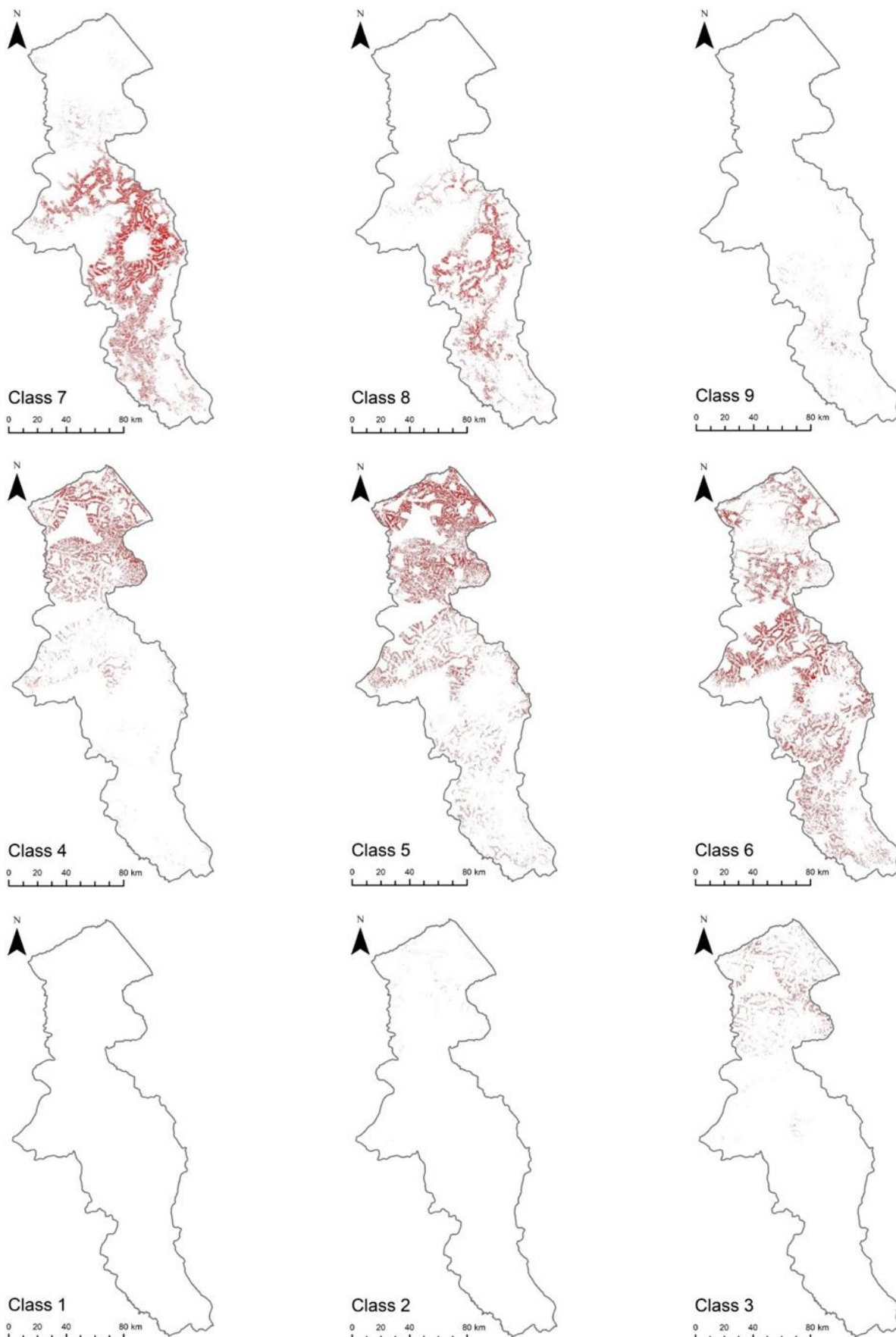


Figure 10. Suitability map of Ardabil province by each class.



Figure 11. Values of each criterion for two random points.

References

- Albraheem, L., & Alabdulkarim, L. (2021). Geospatial analysis of solar energy in riyadh using a GIS-AHP-based technique. *ISPRS International Journal of Geo-Information*, 10(5), 291. <https://doi.org/10.3390/ijgi10050291>
- U. S. (2021). Energy Information Administration. <https://www.eia.gov/todayinenergy/detail.php?id=41433/>
- Gašparović, I., & Gašparović, M. (2019). Determining optimal solar power plant locations based on remote sensing and GIS methods: A case study from Croatia. *Remote Sensing*, 11(12), 1481. <https://doi.org/10.3390/rs11121481>
- Munkhbat, U., & Choi, Y. (2021). GIS-based site suitability analysis for solar power systems in Mongolia. *Applied Sciences*, 11(9), 3748. <https://doi.org/10.3390/app11093748>
- Uyan, M. (2013). GIS-based solar farms site selection using analytic hierarchy process (AHP) in Karapınar region, Konya/Turkey. *Renewable and Sustainable Energy Reviews*, 28, 11-17. <https://doi.org/10.1016/j.rser.2013.07.042>
- Sampaio, P. G. V., & González, M. O. A. (2017). Photovoltaic solar energy: Conceptual framework. *Renewable and Sustainable Energy Reviews*, 74, 590-601. <https://doi.org/10.1016/j.rser.2017.02.081>
- World Energy Outlook (2019). <https://www.iea.org/reports/world-energy-outlook-2019>.
- Weather Data and Software for Solar Power Investments. Available online: http://solargis.info/doc/_pics/freemaps/1000px/ghi/SolarGIS-Solar-map-Iran-en.png
- Shaikh, M. R. S., Waghmare, S. B., Labade, S. S., Fuke, P. V., Tekale, A. (2017). A review paper on electricity generation from solar energy. *International Journal for Research in Applied Science & Technology* 5(9), 1884-1889. <http://dx.doi.org/10.22214/ijraset.2017.9272>
- Rabaia, M. K. H., Abdelkareem, M. A., Sayed, E. T., Elsaid, K., Chae, K. J., Wilberforce, T., & Olabi, A. G.

- (2021). Environmental impacts of solar energy systems: A review. *Science of The Total Environment*, 754, 141989. <https://doi.org/10.1016/j.scitotenv.2020.141989>
11. Choi, Y., Suh, J., & Kim, S. M. (2019). GIS-based solar radiation mapping, site evaluation, and potential assessment: A review. *Applied Sciences*, 9(9), 1960. <https://doi.org/10.3390/app9091960>
 12. Genç, M. S., Karipoğlu, F., Koca, K., & Azgın, Ş. T. (2021). Suitable site selection for offshore wind farms in Turkey's seas: GIS-MCDM based approach. *Earth Science Informatics*, 14(3), 1213-1225. <https://doi.org/10.1007/s12145-021-00632-3>
 13. Doorga, J. R., Rughooputh, S. D., & Boojhawon, R. (2019). Multi-criteria GIS-based modelling technique for identifying potential solar farm sites: A case study in Mauritius. *Renewable energy*, 133, 1201-1219. <https://doi.org/10.1016/j.renene.2018.08.105>
 14. Ziuku, S., Seyitini, L., Mapurisa, B., Chikodzi, D., & van Kuijk, K. (2014). Potential of concentrated solar power (CSP) in Zimbabwe. *Energy for Sustainable Development*, 23, 220-227. <https://doi.org/10.1016/j.esd.2014.07.006>
 15. Neisani Samani, N., & Tahouni, A. (2019). The Evaluation of suitable Sites for Solar Farms by Multi Criteria Decision Making in GIS (Case Study: East Azarbaijan Province). *Human Geography Research*, 51(3), 747-764. <https://doi.org/10.22059/jhgr.2019.279885.1007909>
 16. Piirisaar, I. (2019). A multi criteria GIS analysis for siting of utility-scale photovoltaic solar plants in county Kilkenny, Ireland. [Master's thesis, Lund University].
 17. Ruiz, H. S., Sunarso, A., Ibrahim-Bathis, K., Murti, S. A., & Budiarto, I. (2020). GIS-AHP Multi Criteria Decision Analysis for the optimal location of solar energy plants at Indonesia. *Energy Reports*, 6, 3249-3263. <https://doi.org/10.1016/j.egy.2020.11.198>
 18. Taiar, A., M. Rezvan, & H. Hashemi. (2019). Evaluation of suitable locations for large-scale solar power plants using GIS, Hierarchical Analysis Process (AHP) and TOPSIS (Case Study: Karbala Province, Iraq). *Energy Engineering and Management*, 4, 60-73. <https://doi.org/10.22052/11.4.60>
 19. Watson, J. J., & Hudson, M. D. (2015). Regional Scale wind farm and solar farm suitability assessment using GIS-assisted multi-criteria evaluation. *Landscape and Urban Planning*, 138, 20-31. <https://doi.org/10.1016/j.landurbplan.2015.02.001>
 20. Asakereh, A., Omid, M., Alimardani, R., & Sarmadian, F. (2014). Developing a GIS-based fuzzy AHP model for selecting solar energy sites in Shodirwan region in Iran. *International Journal of Advanced Science and Technology*, 68, 37-48. <http://dx.doi.org/10.14257/ijast.2014.68.04>
 21. Noorollahi, E., Fadai, D., Akbarpour Shirazi, M., & Ghodsipour, S. H. (2016). Land suitability analysis for solar farms exploitation using GIS and fuzzy analytic hierarchy process (FAHP)—a case study of Iran. *Energies*, 9(8), 643. <https://doi.org/10.3390/en9080643>
 22. Suh, J., & Brownson, J. R. (2016). Solar farm suitability using geographic information system fuzzy sets and analytic hierarchy processes: Case study of Ulleung Island, Korea. *Energies*, 9(8), 648. <https://doi.org/10.3390/en9080648>
 23. Sánchez-Lozano, J. M., Teruel-Solano, J., Soto-Elvira, P. L., & García-Cascales, M. S. (2013). Geographical Information Systems (GIS) and Multi-Criteria Decision Making (MCDM) methods for the evaluation of solar farms locations: Case study in south-eastern Spain. *Renewable and sustainable energy reviews*, 24, 544-556. <https://doi.org/10.1016/j.rser.2013.03.019>
 24. <https://ardmet.ir>
 25. Abdelrazek, M. (2017). GIS Approach to Find Suitable Locations for Installing Renewable Energy Production Units in Sinai Peninsula, Egypt. [Master's thesis, University of Salzburg].
 26. Martins, F. R., Pereira, E. B., & Abreu, S. L. (2007). Satellite-derived solar resource maps for Brazil under SWERA project. *Solar Energy*, 81(4), 517-528. <https://doi.org/10.1016/j.solener.2006.07.009>
 27. Amillo, A. G., Huld, T., & Müller, R. (2014). A new database of global and direct solar radiation using the eastern meteosat satellite, models and validation. *Remote sensing*, 6(9), 8165-8189. <https://doi.org/10.3390/rs6098165>
 28. Huld, T. (2017). PVMAPS: Software tools and data for the estimation of solar radiation and photovoltaic module performance over large geographical areas. *Solar Energy*, 142, 171-181. <https://doi.org/10.1016/j.solener.2016.12.014>
 29. <https://globalsolaratlas.info>
 30. Nebey, A. H., Taye, B. Z., & Workineh, T. G. (2020). Site Suitability Analysis of Solar PV Power Generation in South Gondar, Amhara Region. *Journal of Energy*, 3519257. <https://doi.org/10.1155/2020/3519257>
 31. Al Garni, H. Z., & Awasthi, A. (2017). Solar PV power plant site selection using a GIS-AHP based approach with application in Saudi Arabia. *Applied Energy*, 206, 1225-1240. <https://doi.org/10.1016/j.apenergy.2017.10.024>
 32. Li, D. (2013). Using GIS and Remote Sensing Techniques for Solar Panel Installation Site Selection. [Master's thesis, University of Waterloo]. <https://doi.org/10.1016/j.solener.2006.07.009>
 33. Tahri, M., Hakdaoui, M., & Maanan, M. (2015). The evaluation of solar farm locations applying Geographic Information System and Multi-Criteria Decision-Making methods: Case study in southern Morocco. *Renewable and sustainable energy reviews*, 51, 1354-1362. <https://doi.org/10.1016/j.rser.2015.07.054>
 34. Al-Shammari, S., Ko, W., Al Ammar, E. A., Alotaibi, M. A., & Choi, H. J. (2021). Optimal decision-making in photovoltaic system selection in Saudi Arabia. *Energies*, 14(2), 357. <https://doi.org/10.3390/en14020357>
 35. Masoom, A., Kosmopolous, P., & Bansal, A. (2021). Solar Irradiance Assessment and Forecasting in Tropical Climates using Satellite Remote Sensing

- and Physical Modelling (No. EMS2021-352). Copernicus Meetings.
<https://doi.org/10.5194/ems2021-352>
36. <https://www.earthdata.nasa.gov>
37. <https://livingatlas.arcgis.com/landcover>
38. <https://www.openstreetmap.org>
39. Robinson, V. B. (2003). A perspective on the fundamentals of fuzzy sets and their use in geographic information systems. *Transactions in GIS*, 7(1), 3-30. <https://doi.org/10.1111/1467-9671.00127>
40. Corrente, S., Greco, S., & Słowiński, R. (2017). Handling imprecise evaluations in multiple criteria decision aiding and robust ordinal regression by n-point intervals. *Fuzzy Optimization and Decision Making*, 16, 127-157.
<https://doi.org/10.1007/s10700-016-9244-x>
41. Saaty, T. L. (1977). A scaling method for priorities in hierarchical structures. *Journal of mathematical psychology*, 15(3), 234-281.
[https://doi.org/10.1016/0022-2496\(77\)90033-5](https://doi.org/10.1016/0022-2496(77)90033-5)
42. Ishizaka, A., & Labib, A. (2011). Review of the main developments in the analytic hierarchy process. *Expert Systems with Applications*, 38(11), 14336-14345.
<https://doi.org/10.1016/j.eswa.2011.04.143>
43. Alhammad, A., Sun, Q., & Tao, Y. (2022). Optimal solar plant site identification using GIS and remote sensing: framework and case study. *Energies*, 15(1), 312.
44. <https://pro.arcgis.com/en/pro-app/latest/arcpy/spatial-analyst/what-is-the-spatial-analyst-module.htm>
45. Adjiski, V., Kaplan, G., & Mijalkovski, S. (2022). Assessment of the solar energy potential of rooftops using LiDAR datasets and GIS based approach. *International Journal of Engineering and Geosciences*, 8(2), 188-199.
<https://doi.org/10.26833/ijeg.1112274>
46. Senkal, E., Kaplan, G., & Avdan, U. (2021). Accuracy assessment of digital surface models from unmanned aerial vehicles' imagery on archaeological sites. *International Journal of Engineering and Geosciences*, 6(2), 81-89.
<https://doi.org/10.26833/ijeg.696001>



© Author(s) 2024. This work is distributed under <https://creativecommons.org/licenses/by-sa/4.0/>